UNIVERSITÀ DI PARMA

UNIVERSITA' DEGLI STUDI DI PARMA

DOTTORATO DI RICERCA IN
"SCIENZE CHIMICHE"

CICLO XXXI

# Advanced PNA-based sensor systems

Coordinatore:
Chiar.mo Prof. Roberto Corradini

Tutore:
Chiar.mo Prof. Roberto Corradini

Dottorando: Andrea Rozzi

Anni 2015/2018

*All that is gold does not glitter,*

*Not all those who wander are lost;*

*The old that is strong does not wither,*

*Deep roots are not reached by the frost.*

*From the ashes, a fire shall be woken,*

*A light from the shadows shall spring;*

*Renewed shall be blade that was broken,*

*The crownless again shall be king.*

[J. R. R. Tolkien, ”The Lord of the Rings”]

# SUMMARY:

# 1- REVIEW OF NUCLEIC ACIDS DETECTION METHODS


## Abstract:

In this chapter, the state-of-the-art of nucleic acids detection will be discussed. Different transduction systems will be analyzed (Figure 1.1), focusing especially on ultrasensitive-techniques that avoid a pre-amplification of DNA strand by PCR (Polymerase Chain Reaction). Time, cost of analysis and possibility of contamination can diminish, avoiding the amplification process. The selectivity of the sensor, another important key-point, will be specifically discussed, since detection of Single Point Mutations (SPMs) or single nucleotide polymorphisms (SNPs) is very important in both food analysis and in clinical diagnosis, in particular for the latter for the early detection of cancer and for genetic diseases. At the end of the chapter, the emerging approach of novel screening liquid biopsy tests will be described.


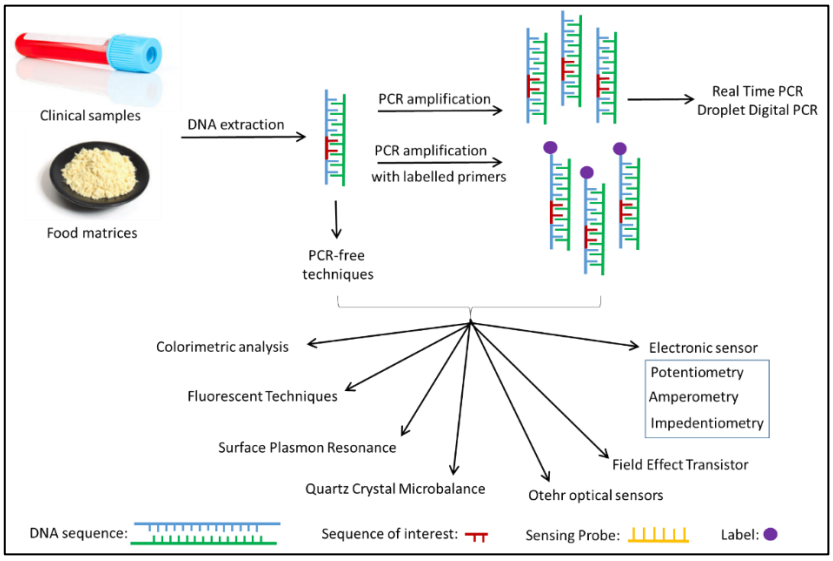


**Figure 1.1: scheme of different type of transduction of the signal. The figure show the possibility to have a pre-amplification of the samples or, for most sensible techniques, a PCR-free approach.**

# 1.0 REAL-TIME PCR

In molecular biology, at present, the most used technique for amplification and quantification of nucleic acids is Real-Time PCR[1] for DNA and RT-qPCR (reverse transcriptase quantitative PCR) for RNA. In the latter, the starting analyte (RNA), is converted in DNA following an enzymatic pathway[2]. This technique have high sensitivity, reproducibility and shows a wide dynamic range of response: several magnitudes of initial number of DNA or RNA molecules[3]. Total amount of amplified DNA is exponentially proportional to the starting quantity of nucleic acid, and the monitoring of the increasing of the signal after each step allows to directly follow the PCR process. Detection of the total DNA amount for quantification can be obtained by adding an intercalating fluorescent dye (see Figure 1.2) or, in a more selective variant, by a specific, fluorescently-labelled switching DNA probe (e.g. by a TaqMan probe or a molecular beacon). A crucial part for reliability in absolute quantification is the identical amplification efficiency both in the calibration and in samples. The starting solution has to be at the proper pH and have to contain sample, enzyme(s), appropriate primers, dyes and bivalent cations like $Mg^{2+}$, and should not contain polymerase inhibitors. The starting step is the denaturation of the dsDNA (double stranded DNA) at 95°C, then at temperatures around 55-65°C the primers are allowed to anneal to the ssDNA (single stranded DNA) and finally the sample is brought at temperatures around 70°C to allow the polymerase reaction to occur. The fluorescent measurement has to be performed at high temperature (e.g. 80°C) for minimizing non-specific fluorescence caused by primer dimers and other unspecific minor products. In this way, the amount of fluorescent noise at the final plateau can be lowered to 2-3%. Usually the analysis is performed in microplate wells of at least 10 µL. The fluorescence signal is measured after every amplification step.

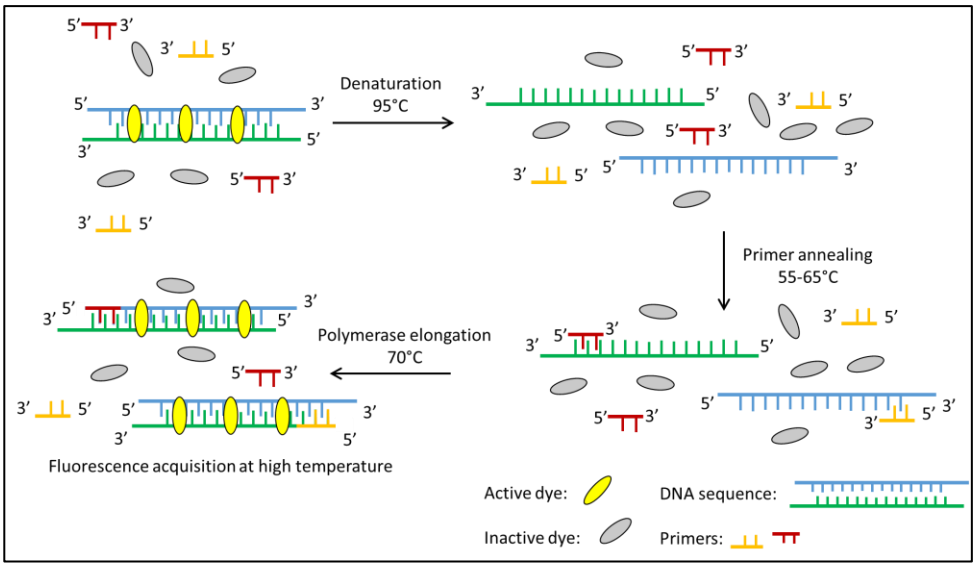


**Figure 1.2: fluorescent dye-based real time PCR.**

Several variants of PCR using molecular beacon probes have been developed for enhancing specificity; all of them use the Föster Resonance Energy Transfer model (briefly described in paragraph 1.2). The most used type of probe in selective real time PCR is hydrolysis probe (TaqMan Probe, Figure 1.3) that consist of a short DNA sequence that hybridizes with one target amplicon and is 3'-end blocked, so it cannot be extended by polymerase[4]. Attached to opposite ends of the probe there are a reporter fluorophore and a quencher. When the probe is intact, the distance between reporter and quencher is short and fluorescence is quenched. During the elongation step, the DNA polymerase (e.g. from bacterium *Thermus aquaticus*) while synthesizing the new DNA strand exert its exonuclease activity on the probe; the reporter is thus cleaved from the quencher and the fluorescence signal, proportional to the amount of amplified DNA, is 'switched on'. TaqMan Probe guarantees sequence-selectivity detection and high fluorescent response maintaining an easy PCR setup. On the other hand, this technique is expensive and if primers are not well designed, a primer-dimer formation is possible. This technique has a very large diffusion and for example has been used in mapping gene mutations[5] and virus' DNA incorporation in human genoma[6].

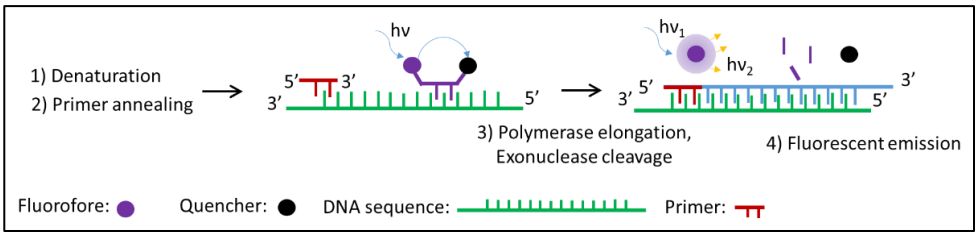


**Figure 1.3: mechanism of signal production by TaqMan Probe.**

Widely used probes are also molecular beacons hairpin probes. These kinds of probes are DNA hairpins of 25-40 nucleobase length where, at the two opposite ends of the sequence, a fluorophore and a quencher are linked. In the absence of target DNA, the fluorescent dye and quencher are in close proximity and the fluorescence is quenched. When the double strand of DNA is annealed, the hairpin opens and is hybridized with the target sequence and therefore the fluorophore emits fluorescence. The fluorescence is proportional to the quantity of amplicons produced during PCR cycle. In the amplification process, the molecular beacon is displaced. This technique offers a high specificity and low background fluorescence. In contrast, due to the intramolecular competitive binding, the signal levels are usually low. Probe-based fluorescence melting curve analysis is a methodology for investigating single point mutation (SPMs) with Hairpin Probes[7].

There are some modifications of molecular beacon probes that can act as PCR primers [8]. Scorpion Probes[9] are molecular beacons linked at 3' end to primers: firstly, the beacon is quenched and only the primer hybridize the target DNA sequence. During all the polymerization process, the fluorescence is quenched, only when the process is completed the hairpin opens because its loop sequence is complementary to the internal target sequence. Also in this case, the fluorescent signal is proportional to the total amount of amplified DNA. In order to avoid read-through during the extension of the opposite strand, this kind of probe must contain a PCR blocker (oligo(ethyleneglycol) linker) between primer and hairpin (Figure 1.4 A). Scorpion Probes can be used for detecting genetic mutations involved in cancer[10] or for pathogen's DNA[11]. Sunrise™ UniPrimer Probes instead do not contain a blocker unit. This probe act as primer and then the first polymerization occurs. In a second stage of amplification, Sunrise™ probe act as templating DNA and the enzyme does not stop when it finds the hairpin and a complementary sequence is added. In

this configuration, the fluorophore is detached from the quencher and the fluorescent signal is switched on (Figure 1.4 B).

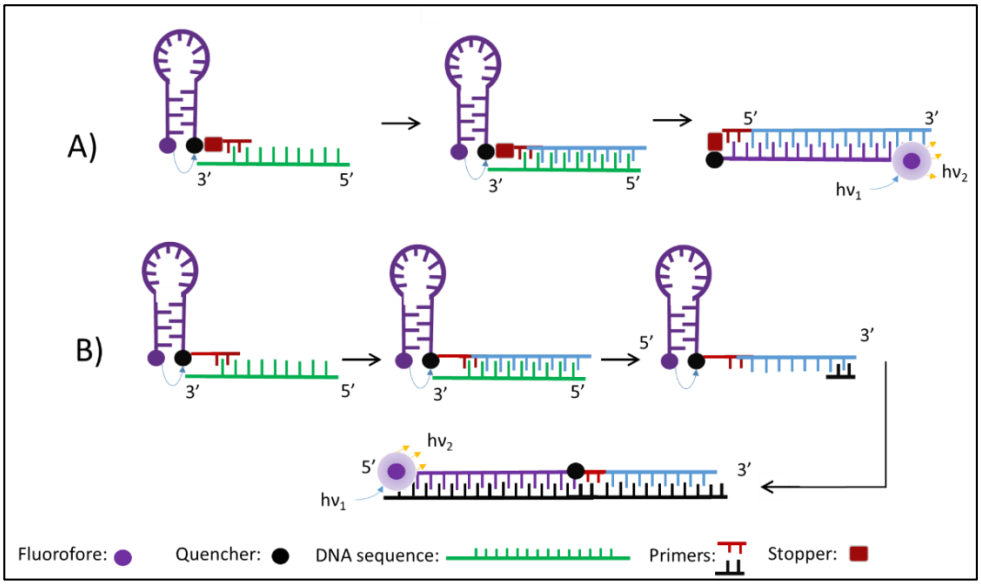


**Figure 1.4: mechanism of action of A) a Scorpion Probe B) a Sunrise Probe.**

Other types of PCR probes consist in two fluorescently-labelled oligonucleotides that bind consequent region of the target DNA. Exploiting FRET between the donor-dye of the first probe and the acceptor-dye of the second probe, it is possible to detect the quantity of amplified sequences. LUX™ (Light Upon Extension) Primers[12] are molecular beacon probes without a quencher: the initial fluorescence is quenched by an appropriate conformation of the 3' end of the hairpin probe. This type of probe was used principally for detections of virus[13] or protozoan[14] DNA.

The most modern methodology for performing a PCR analysis is droplet digital PCR (ddPCR). This method is based on a water-oil emulsion droplet system[15]. Droplets have the aim of separate template DNA molecules, in this way each droplet acts like a test tube, generating a massive sample partitioning. In each droplet DNA amplification is carried out. The normal PCR guarantee a single measure of the amplification, while ddPCR measure thousands of independent amplification events within a single sample. The amount of droplet with the target DNA that has to been amplified is proportional to the initial concentration of the sample, and this parameter can be statistically determined. This type of

PCR analysis avoids diluting steps and so pipetting errors. Moreover, it generates from one sample thousands of statistically relevant data and the robustness of the methodology is improved. Other benefits include the possibility to have a more precise absolute quantification of DNA, the reproducibility is improved and it reduce costs of consumable materials and equipment.
Finally, is fair to mention LAMP (loop mediated isothermal amplification), that is a low-cost alternative to PCR analysis. This technique is performed at constant temperature of 60-65°C using either two or three sets of primers and a polymerase with high strand displacement activity in addition to a replication activity. This technique is easy and can be used as cost-effective screening method, but it is also less versatile and so less developed. Nevertheless, amplicons produced by LAMP have been promising for applications in biomedicine, bioimaging, and biosensing[16].
In summary, in PCR analysis the amplification of the signal corresponds directly to an amplification of the DNA fragments. The detection method is in most cases based on fluorescence read-out.

## 1.1 COLORIMETRIC ANALYSIS

A colorimetric assay is based on the changing of color in presence of the target analyte. It can be performed in solution or on the surface of a chip. The most effective methods in this field are based on metal nanoparticles (MNPs), in particular gold nanoparticles, functionalized with a proper DNA[17] or DNA-mimic probe[18]. The binding event of the target fragment of nucleic acid is revealed by a shift in a visible range of color, usually from red to blue-purple. In a seminal work by Mirkin and co-workers, using a cross-linking approach, Au-Nanoparticles were functionalized by thiolated DNA probes, in high surface coverage: 200 probes on a 13 nm Au-NPs[19]. A target 30-mer DNA was bound to two different type of Au-NPs bearing two different thiolated DNA probes building a ‘bridge’ between NPs. Thus, their distance decreased and a shift from red to blue-purple color that can be detected by naked eye or by UV-VIS spectrometer[20] (Figure 1.5) was induced. Different types of anchoring system and size of Au-NPs were tested[21]. A similar approach was tested in combination with an enzyme activity in order to induce Au-NPs aggregation[22], for measuring melting temperatures (Tm), for sensing of triplex-binding agent (like benzo[e]pyridoindole (BePI) and coralyne (CORA)), which stabilizes triplex

formation and induce shift in Au-NPs' color[23]. In another work, the colorimetric assay was used for measuring pH by conformational change in i-motif DNA[24]. This conformational change has low kinetics and needs hours to be performed. It is possible to detect other kinds of molecules, like adenosine[25], by specific aptamers. A network of aptamers-modified Au-NPs is formed and the typical blue color turns on. Aptamers are usually modified in order to induce the formation of AU-NPs aggregation upon binding to their target molecule.

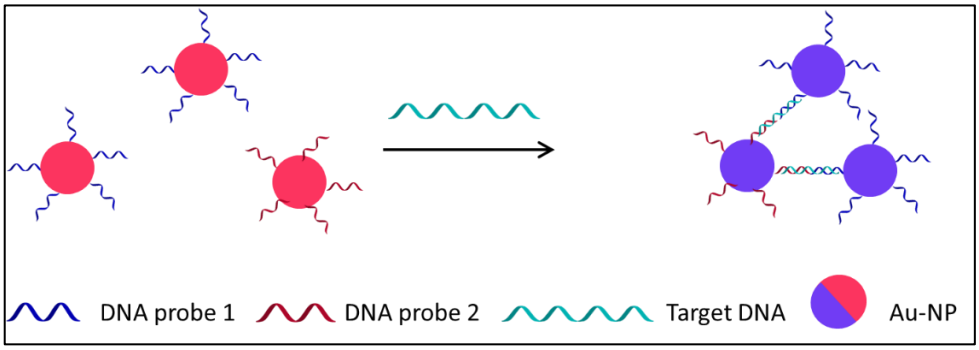


**Figure 1.5: scheme of DNA detection with thiol modified DNA probes on Au-NPs.**

It was discovered that functionalized Au-NPs with DNA strands are stabilized at high salt concentrations. This allows to detect DNA also without the cross-linking approach by change in the nanoparticle color.[26] This kind of colorimetric assay is simpler and quicker (few minutes) than the cross-linked type, because in this configuration the binding sites are more accessible. A negative characteristic is the quite high detection limit: 500 nM. This non-crosslinked methodology was also used for detect metal ions and molecules by using aptamers[27].

Further simplifying the colorimetric assay, it was discovered[28] that is possible to detect target DNA even without a covalent linking between Au-NPs and DNA probe. The affinity of nitrogen from nucleobases to gold surface is higher than the electrostatic repulsion between negatively charged DNA backbone and metal surface. Therefore, the ssDNA has enough conformational degree for wrap NPs. When the target sequence is added, the nitrogen of nucleobases starts to be involved in Watson-Crick interactions, so the electrostatic repulsion becomes the major force and the dsDNA is detached from NPs. Only in this case, by adding a proper amount of salts, it is possible to have aggregation of NPs and the change in color from red to blue (Figure 1.6). This assay is very

quick and it is capable to detect less than 100 femtomoles of target DNA. The same procedure can be used also in case of aptamer sensing[29].

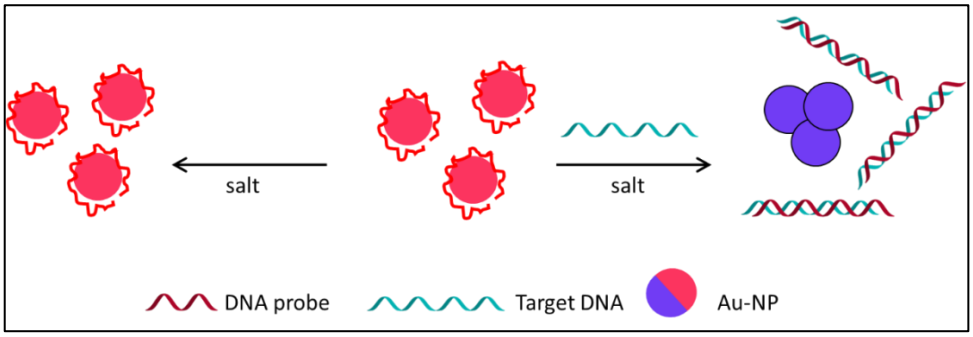


**Figure 1.6: DNA detection assay based on a non-covalently linked DNA probe on Au-NPs.**

DNA detection in homogeneous medium with linear light scattering was also tested, reaching a detection limit of 0.1 pM,[30] much higher than the colorimetric assay that use the same probes on gold NPs, with improved mismatch discrimination.

Other colorimetric assay can be performed on the surface of a sensor. For example Jenison et al[31] developed a sensor built on crystalline silicon surface (Figure 1.7). This silicon surface was modified with 47.5 nm of silicon nitride (from vapor deposition) and 13.5 nm of T-structure polydimethylsiloxane (spin coating) onto which poly-phenylalanine-lysine layer was passively adsorbed. The capture probe DNA was modified at 3'-end with a cross-linker molecule in order to have activate ester (N-hydroxysuccinimide) that can bind covalently to the amino groups on the surface. The optimal probe density was 25 fmol/mm$^2$, at which all capture probes were accessible for hybridization. After hybridization, a biotin-labelled reporter oligonucleotide was added and, subsequently, the tri-component complex was treated with an anti-biotin antibody conjugated with horseradish peroxidase. Finally, the substrate for the enzyme was added and the enzyme activity promoted the formation of a precipitate of several nm thickness. This precipitate altered the optical property of the surface and a shift in color was obtained. The chromatic shift was proportional to the thickness of precipitate and was visually detected in white light or by a CCD camera, with a 300 nm layer giving rise to the best shift. The detection limit was 10 fM, and the assay response was roughly linear with a dynamic range of two orders of magnitude.

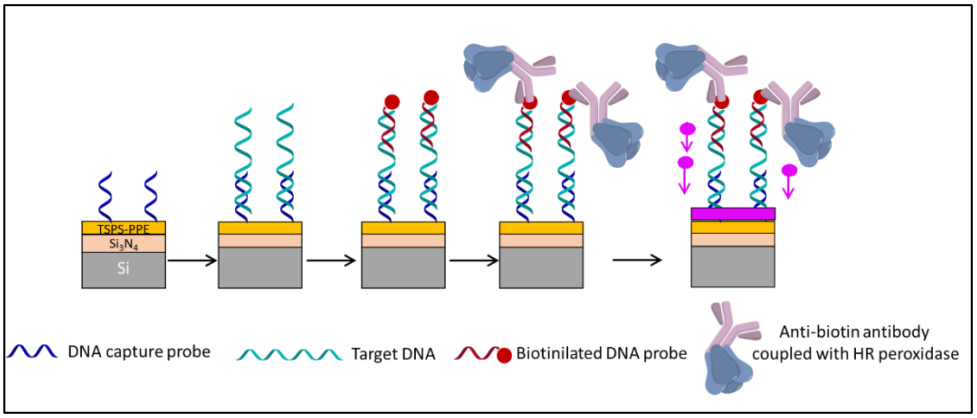


**Figure 1.7: schematic overview of the colorimetric approach on silicon surface.**

A similar design was used when a nucleotide mimic probe was linked to the surface[32]. After hybridization with target DNA, positively charged Au-NPs were added. These NPs got sticked on the negatively charged double helix and deposition of gold or silver was used for signal enhancement; the resulting change in color was detectable by using a commercialized optical grayscale flat-scanner or by naked eye.

## 1.2 FLUORESCENCE TECHNIQUES

Fluorescent methods are composed by a huge variety of techniques that exploit fluorescence as transduction system.
One widely used approach for DNA detection, also mentioned in paragraph 1.0, is the molecular beacon (MB) technology. Developed by Tyagi and Kramer in 1996[33], these probes usually have a fluorophore at 5' end and a quencher at 3' end. The probe is designed for having at its extremity from five to seven complementary nucleobases that form a hairpin. In this closed conformation, the light emitted by the fluorophore is totally quenched by the dark quencher. This quenching is due to a mechanism called FRET (Föster Resonance Energy Transfer) that describe the possibility that two light-sensitive molecules, at proper distance, transfer each other energy by dipole-dipole coupling (non-radiative mechanism). The addition of target DNA sequence generate a elongated conformation of the probe, enthalpy driven by the formation of more Watson-Crick interactions. Hence, the fluorophore and the quencher are too far

for FRET, so that fluorescence can be produced upon irradiation. The enthalpy required for opening the hairpin is a powerful tool to design appropriate probes able to discriminate point mutations in genome (PMs). The noise level of these types of analysis can increase in case of unspecific opening of the hairpin, not complete quenching or cleaving of fluorophore or quencher by enzymatic degradation of the probe. There are a lot of different molecular beacons developed using this hairpin configuration[34] (see Figure 1.8).

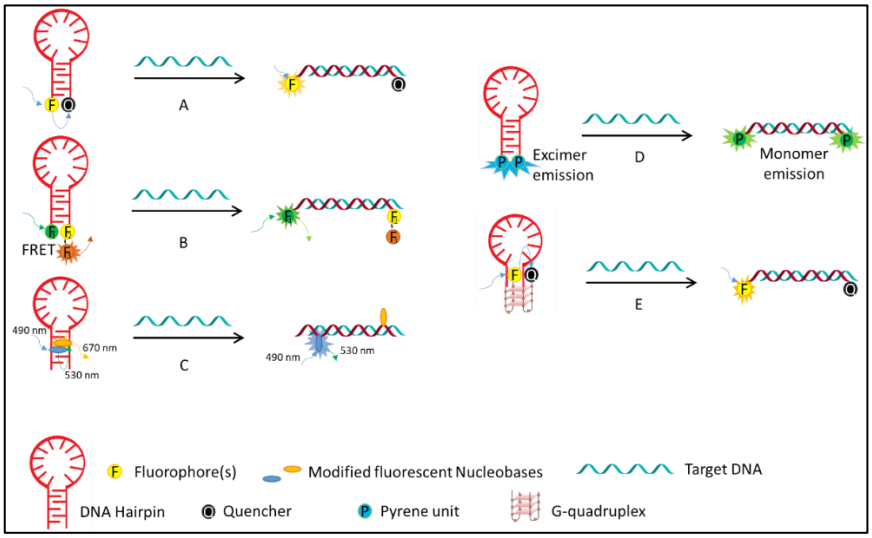


**Figure 1.8: schematic overview of molecular beacon approaches. A) original configuration with a fluorophore and a quencher. B) use of more than one fluorophore, for multiple FRET[35]. C) multiple FRET due to two types of fluorescent molecule used as artificial nucleobases[36]. D) pyrene units at 3' and 5' end that shift from excimer to monomer emission[37]. E) G-quadruplex structure with fluorophore and quencher at the end of the DNA strand[38].**

Dual or binary probes are also highly used: in this case a fluorescence donor and a fluorescence acceptor are at the opposite ends (5' and 3') of two single stranded oligonucleotides. When these oligonucleotides can bind to a target DNA sequence the two fluorophores come close enough for produce Foerster fluorescence energy transfer, producing an emission peak of the acceptor upon excitation at the donor maximum. Binary probes have the advantage that they can avoid false-positive signals, because the two independent probes have to be in close proximity and in the correct orientation. If the probes are in low concentration and the fluorophores have a very small or no overlap of adsorption spectra, the possibility of false positives is very low, so this system

have been used in complex environments.[39] It is also possible to monitor the ratio of bound/unbound probes using a two-channel detection fluorescence microscope[40]. Despite these advantages, the signal-noise ratio is generally very low and can be obscured by the inner fluorescence of cells. This disadvantage can be avoided using a time resolved fluorescence approach, in which the donor is a ruthenium complex[41] with a triplet spin state that cannot transfer energy to the singlet spin state of an organic acceptor: the transition is spin forbidden. This induce a long fluorescent lifetime compared to the short lifetime of the fluorescence of the cell; thus, using a proper gated time is possible to neglect the unwanted background fluorescence. This gated detection can be used also in the case of excimer of pyrenes[42] as fluorescent complex, which is longer than the fluorescent time of the cell. Another disadvantage is that the association with the target is less favorite respect to hairpin both thermodynamically and kinetically. In a thermodynamic picture, the loss of entropy is higher because three independent molecules have to interact to form a unique supramolecular complex. Kinetically, the ratio for having two hybridization process is higher with respect to standard molecular beacons.

Fluorescence in situ hybridization (FISH) is a technique that uses fluorescent DNA or DNA mimic probes for detecting specific regions of genome in cells. It can be used also for the detection of various species of RNA and so follow the pathway of gene expression. It requires a fluorescence microscope for the imaging of cells. Molecular beacons have also been used in this field; a very important example is the use of a double molecular beacon for the detection of K-Ras mRNA in living cells[43]. In this example the two molecular beacons are complementary to close regions of mRNA, one of the two, the “donor” MB, has the dye is at 5’ end, and the other, the “acceptor” MB, has its dye at 3’ end. Both MBs have at the other extremity a dark quencher. In this case, when the two MB opened, not only have recovered fluorescence, but also act as binary FRET probes. This architecture (Figure 1.9) diminish false positive and give a very high sequence selectivity.

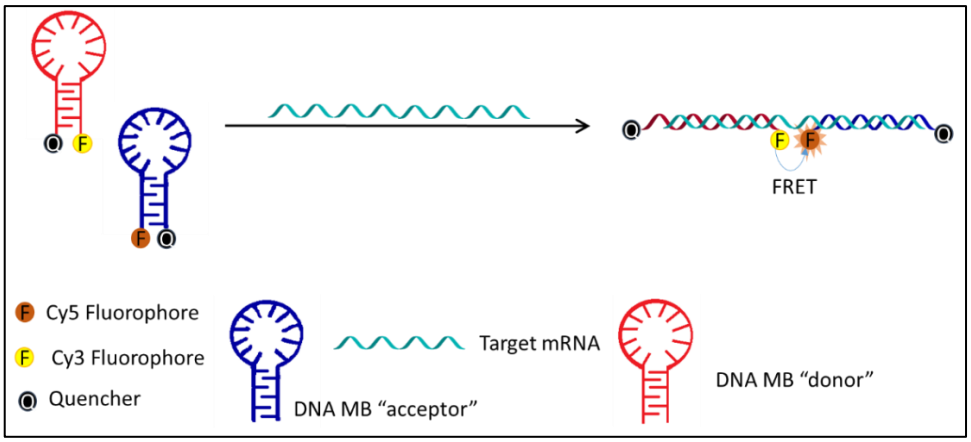


**Figure 1.9: schematic drawing of the mechanism of action of double molecular beacons for the detection of mRNA in living cells.**

Synthetic DNA analogous, like serinol nucleic acids (SNA) was employed for having non enzymatic-degradable probes for targeting mRNA[44]. A high flexibility of the serinol backbone stabilize interactions between nucleobases but can also give too much freedom degrees to the quencher, which not quench all the light emitted by the fluorophore. Another example of fluorescent probes for the measurement of RNA in cells is that of peptide nucleic acid (PNA) coupled with nano-graphene oxide (NGO) [45]. In this research, the PNA was conjugated to a fluorophore which can interact with graphene oxide (Figure 1.10). The NGO act as a very strong quencher and thus the probe is silent; once inside the cells, the binding of the PNA to its target produce a negatively charged complex which has no longer affinity for NGO, thus generating a switch-on of the probe fluorescence. This method has been used to pinpoint compounds able to modify the levels of miR-21 in screening tests.

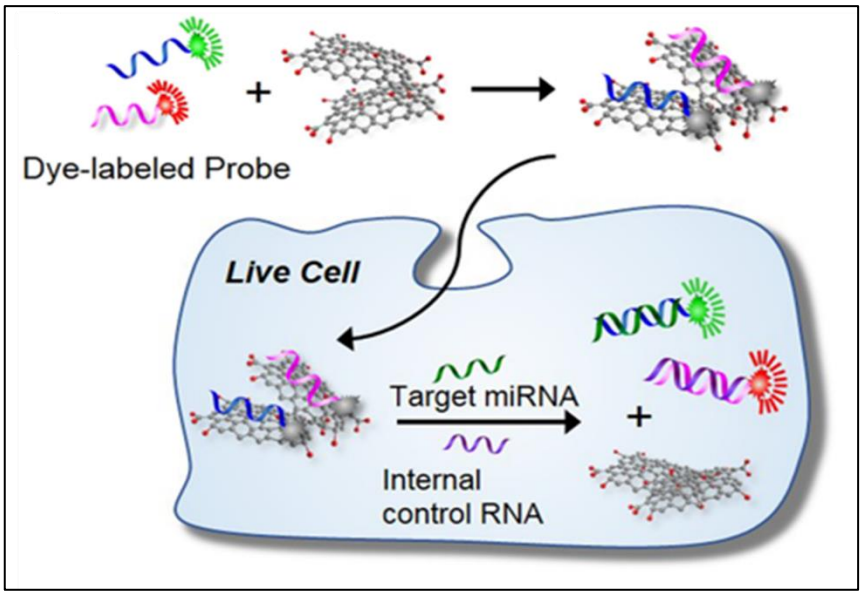


**Figure 1.10: mechanism of action of the PNA-NGO probes used for the detection of microRNA in living cells. Reprinted with permission from[46] SR Ryoo et al. Scientific Reports 2018, Copyright © 2018 Nature.**

Others kinds of fluorescent assays involve Quantum Dots (QDs). These are small semiconductors particles that have peculiar characteristics: their optical and electronic properties are correlated to their size and composition[47], so their spectroscopic properties (in particular the emission maximum) can be tuned [48]. The larger quantum dots (5-6 nm of diameter) emit at longer wavelengths, smaller QDs (2-3 nm of diameter) emits at shorter wavelengths, such as in the region of blue or green. The toxicity of QDs is an open issue[49]: some kinds of QDs are toxic for human health because metals can form very reactive free-radicals species. A special mention should be done for CdSe QDs: if they are exposed to UV light the release of free cadmium occur causing the death of cells[50]. In order to enhance the nanoparticle safety, carbon quantum dots have been developed[51,52].

A mixed approach QDs-molecular beacon was described by a paper by Kashanian and collaborators,[53] where 22-mer oligonucleotides characteristic of human papillomavirus were revealed using water soluble CdTe QDs functionalized with amino-modified 11-mer oligonucleotides. The assay was performed introducing in solution the sample and an 11-mer reporter probe labelled with Cyanine5 (Cy5): in this design, the target DNA hybridize with the

probe on the QDs and the reporter probe hybridize with the remaining 11 nucleotides of the target sequence. After hybridization, the Cy5 groups are at the proper distance from the QDs for FRET: irradiating at 390 nm (absorbance spectrum of QDs) the emitting light was observed at 687 nm (emission spectrum of Cy5). The linear range of this sensor system was found between 1.0 and 50.0 nM, with a limit of detection (LOD) of 0.2 nM.

Metal nano-clusters can also be used as sensing materials for fluorescence genosensors; for example a special molecular beacon approach have been developed by Li and coworkers[54], exploiting the ability of certain DNA sequences to act as templates for the production of silver nanoclusters (AgNCs) upon reduction of solutions containing $Ag^+$ with $NaBH_4$. A 28 nt sequence could produce red-emitting AgNCs, whereas the separation of this sequence into two segments gave rise to a green-emitting cluster only on one segment. However, if the second segment is brought in close proximity to the other sequence by a hairpin DNA segment (Figure 1.11) the emission turns red, due to the re-established cooperative effect of the two segments. So, after the hybridization with the target DNA sequence, when silver nanoclusters are formed, a green fluorescence signal is observed because the hairpin is displaced and the two connected DNAs fragment are not in proximity. Red fluorescence indicates a mismatched target sequence. This sensor system have a linear range of response between 1 and 500 nM concentration of target DNA, with a LOD of 0.5 nM.

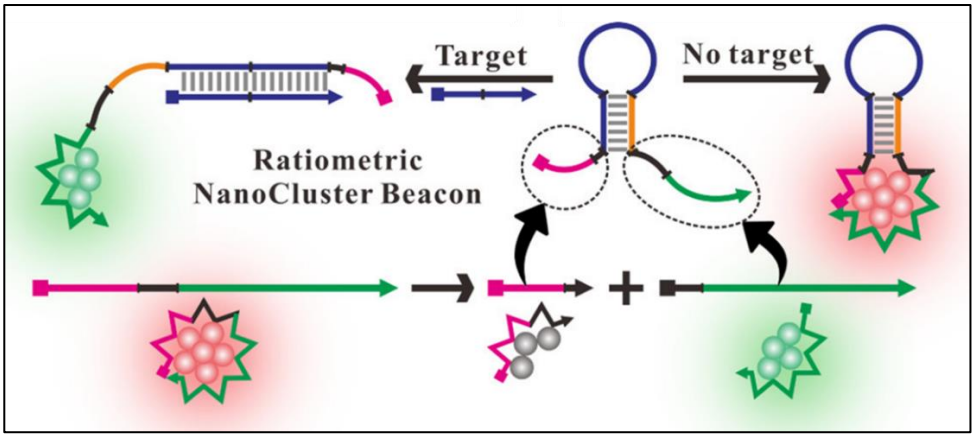


**Figure 1.11: schematics of the genosensor based on nanocluster-beacon. Reprinted with permission from L. Ge et al. Appl. Mater. Interfaces, 2017, Copyright © 2017 American Chemical Society.**

Although many of the above mentioned systems were shown to be performant using oligonucleotide targets, for ultrasensitive detection of real genomic DNA samples an amplification step is often required (usually through PCR): in this way a very little quantity of target DNA can generate a remarkable amount of signal. Rolling circle amplification (RCA) is also an excellent strategy for producing multiple copies of the original target DNA under isothermal conditions. In a recent work[61], exploiting the circularization of a polyA DNA segment templated by the target DNA (Figure 1.12), the RCA was triggered, thus generating multiple copies of the polyT complementary sequence. The polyT served as a template for the generation of fluorescent copper nanoparticles (CuNP), and multiple CuNPs were generated in a single reaction. Linear relationship between fluorescence intensity and logarithm of target DNA concentration was found in the range from 10 aM to 1 mM with the limit of detection of ca. 7.79 aM.

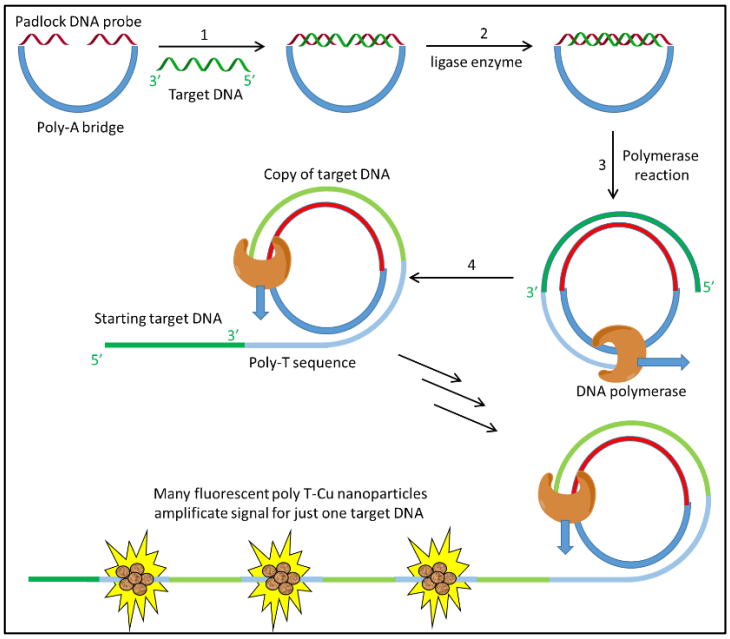


**Figure 1.12: scheme of DNA-triggered rolling circle amplification than allows the formation of multiple poly T-Cu NPs fluorescent clusters.**

Other nanomaterials can also be used as quenchers: for example[55] nano-ceria particles treated with HEPES (4-(2-hydroxyethyl)-1-piperazineethanesulfonic acid) gain a positively charge that attract a negatively charged DNA probe, fluorescently labelled. Therefore, not only the probe is electrostatically linked to the nanoceria surface, but also the adsorption process is quite fast due to the interactions between Ce and phosphate groups (1 minute claimed), and the interaction minimally suffer from variations of pH or ionic strength. When the probe is onto the surface of nano-ceria particles, the fluorescence is quenched. Only in presence of the target DNA sequence the fluorescent probe can be removed from nano-ceria and the fluorescence is turned on. The linear range of the response of this sensor is between 1.1 and 37 nM, with a LOD of 0.12 nM. A very similar strategy that involves different nanomaterial such as $WS_2$ nano-sheets and a PNA probe has been developed[56]. The fluorophore used was FAM (carboxyfluorescein) covalently linked to the PNA probe. Authors suggest that the nature of interaction between $WS_2$ and PNA are hydrophobic and Van der Waals (VdW) forces, so the neutral backbone of PNA plays a key role for the binding and it is not replaceable with DNA in this system. Watson and Crick interaction that occur when the target DNA is added can easily overtake hydrophobic and VdW interactions, thereby removing the fluorophore from the tungsten disulfide nano-sheet. The linear range of this sensor goes from 1 to 20 nM, with a LOD of 500 pM. A similar approach was reported using fluorescent PNA probes and nano-graphene oxide (n-GO) as a quencher.[43]

Another kind of nanomaterials used as quencher is that of metal-organic frameworks (MOFs), especially chromium based[57]. A comparison between negatively charged fluorescein-type fluorophore FAM and zwitterionic rhodamine-type fluorophore TAMRA was performed. DNA-FAM is more attracted to the positively charged surface of MOF, this attractive interaction became even higher when target DNA was added, producing a decrease of fluorescent signal. On the contrary, the DNA-TAMRA probe is detached from surface when target DNA is added, resulting is an increased fluorescence signal. Thus, tuning surface charge of MOFs would produce different effect on different type of probes, and this could give in future possibility of multi-analyte analysis.

Merging the quenching capability of varies allotropic-forms of carbon with the possibility to create safer carbon quantum dots new fluorescence sensors were developed. A simple but effective study of carboxylic-modified carbon QDs[58] use the same detection strategy reported above: a FAM-labelled DNA probe is quenched in absence of target sequence and starts to emit when it is added.

The study show different results based on the surface modification by citric or malic acid. In fact, the adsorption process of the DNA labelled probe is the result of a competition of electrostatic repulsive forces caused by negative charges and π-π stacking attractive forces between un-saturated carbon of QD and nucleobases of DNA. When these are involved in Watson Crick interaction with target DNA, the double helix formed has no longer the nucleobases exposed, and is therefore detached form the QD into the bulk solution and the fluorophore emits light. Malic acid functionalization gives more carboxylic units at the surface of QDs, resulting in a wider dynamic range (DR) and lower LOD: malic acid loaded QDs show DR 0.04÷40 nM, LOD 17.4 nM; citric acid DR 0.4÷40 nM, LOD 45.6 nM. Similar sensors[59] show even lower LOD (4 pM) and a 3 orders of magnitude linear range. The intrinsic fluorescence of graphene quantum dots (GQDs) can be used to produce a DNA sensor[60]. Reduced GQDs are obtained by reduction with $NaBH_4$ and are fluorescent. DNA probes were linked to the GQD surface by a condensation reaction, thus obtaining a fluorescent conjugate. The GQD-DNA conjugate was mixed with graphene oxide (GO), producing a strong association revealed by fluorescence quenching. Electrostatic π-π stacking not only between carbon species (GQDs and GO) but also involving nucleobases facilitate adsorption of the modified reduced GQDs. When target DNA was introduced, stacking interaction lose the contribution from nucleobases, and the DNA-GQD was released from GO, with recovery of fluorescence.

## 1.3 SURFACE PLASMON RESONANCE PLATFORMS

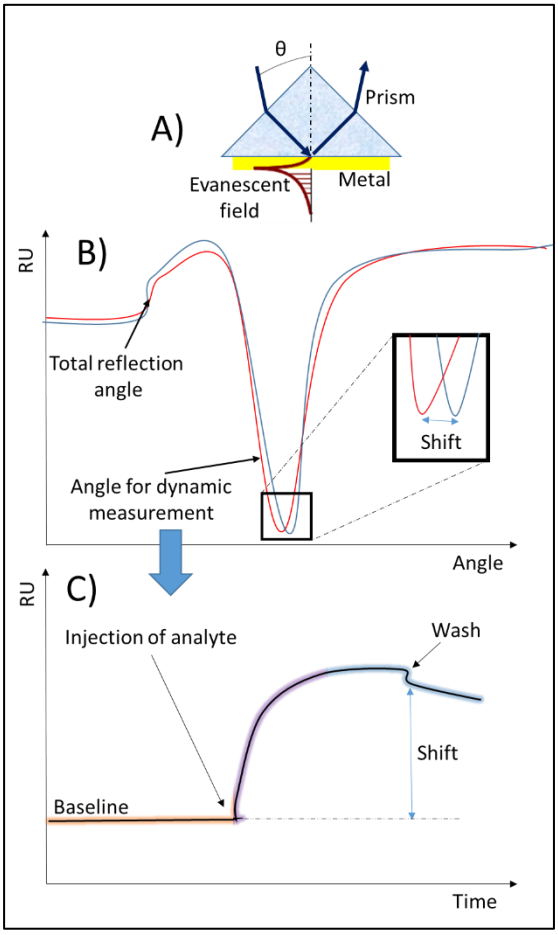


**Figure 1.13: A) SPR Kretschmann configuration; B) static mode analysis; C) Dynamic mode analysis.**

Surface Plasmon Resonance (SPR) represents the most used and developed optical sensor with a guided light, usually in Kretschmann configuration (Figure 1.13). Briefly, the incident light from a laser to a surface of a noble metal (mostly gold), at certain angle, can excite its valence electrons, forming an evanescent light-wave called plasmon. At the plasmon resonance angles there is a decrease of intensity of the light reflected. The guided wave pass through the thin metal, usually gold layer from 15 to 60 nm, and propagates in the medium for few nanometers. In this limited region, a variation of the refractive index cause a shift of the plasmon wavelength and angle. Molecules captured on the surface opposite to the incident light can vary the medium refractive index, due to the material captured. By having a proper sensing architecture it is possible to detect specific proteins, antigens or nucleic acids. Working with a flow cell, is possible to fix a proper angle at the minimum of reflected intensity (at a given wavelength) and register the variation of signal in the time domain: a dynamic measurement that is a very useful tool to determine physical parameters of the capture process (kinetic as well as association constants). An example of a typical sensogram obtained in this way is reported is reported in Figure 1.13 C.

DNA detected by SPR of real samples can be PCR-amplified or genomic in order to be enough massive for produce a reproducible signal, but in both cases the long double stranded DNA tracts are already paired through Watson-Crick interactions, and the association of the target with the sensor probe is weak or absent. To solve this problem, a lot of efforts were done in order to find the correct denaturation process for double helix DNA and analysis condition[62]. Most used denaturating agents are chemicals like urea or formamide, but also ionic strength and temperature are useful tools, though these can also affect probe-DNA interactions[63]. Especially in microbiologic studies where the extraction of the entire genome of microorganism is the best way to perform analysis, PCR was widely used[64]. Amplification schemes producing single-stranded copies of the target (e.g. unbalanced PCR) should be preferred. Furthermore, cheaper type of amplification was tested, in particular loop-mediated isothermal amplification (LAMP)[65]. In this study, a sensitivity of 10 copies of DNA per micro liter was achieved (17 aM c.a.).

Another detection strategy is to label the target with a fluorophore (which is done normally using a fluorescent PCR primer), and exploiting SPR enhanced fluorescence. In this setup, the fluorophore is excited by the plasmon wave that propagate trough the aqueous medium. Labelling sample is not the preferred way to conduct this type of analysis, but this technique is very useful in order to have a correct description of the system. Knoll's group tested different kinds of strategies for linking DNA probes onto the surface[66]. For functionalizing gold by forming a self-assembled monolayer (SAM), a hetero-bifunctional molecule is necessary, with one extremity with a thiol, in order to promote formation of stable Au-S bond (very similar to covalent bond). Two kinds of SAM were tested: the first one with a biotin SAM that was linked to a streptavidin and then through this to a biotinylated-DNA probe (see Figure 1.14). In the second approach, an amino-SAM was coupled with carboxylic acids functions of streptavidin and then the biotinylated probe was added. The well-studied biotin-streptavidin system is largely used in sensor and surface studies, due not only to the very low dissociation constant between these two molecules ($K_D \sim 10^{-14}$ mol/L), but also for the simplicity and high range of condition in which this system can be used. The first architecture was the most rigid and well-ordered, because streptavidin have only 4 sites for binding biotin: two in the lower side, two in the upper side of the protein. This geometry was found to be more sensitive, demonstrating that orientation of capture probes has an effect on hybridization effectiveness. LOD was determined as 20 nM, with a linear range between 10 and 150 nM.

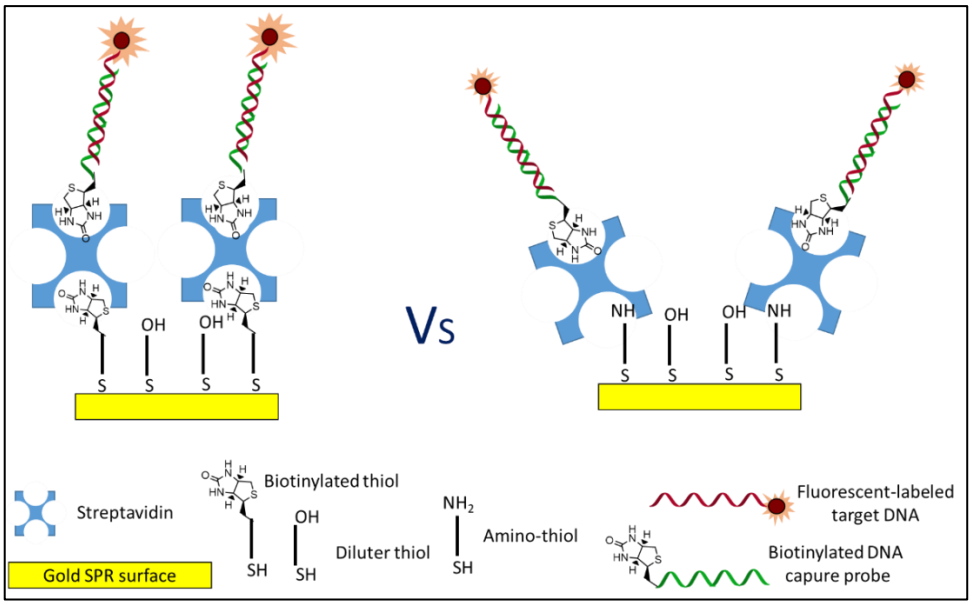


**Figure 1.14: strategies used for DNA detection with SPR-enhanced fluorescence detection. Left, most rigid and well-ordered architecture provides better sensing properties. Right, dissipative and less structured architecture.**

The functionalization of the gold surface was done with the layer-by-layer technique by Knoll and co-workers, using positively charged plasma-polymerized allylamine[67]. After a preliminary treatment of target DNA, the PNA:DNA hybrid was injected in the SPR flow cell. All DNA strands were shown to migrate to the surface, but not fluorescent ssPNA. The SPR-enhanced fluorescence was turned on only if PNA could form an hybrid with the full-match DNA.

SPR fluorescence was also used to gain information about the optimal probe concentration on the surface for sensing[68]: in fact, at high surface coverage electrostatic repulsion between DNA probes on the sensor and target DNA hampers the DNA capture on all the available sites; this effect is worse if DNA-probes were used instead of neutral of better positively-charged probes. This kind of study was then performed using temperature gradient surface plasmon resonance[69] and a correlation between stability of double stranded hybrid and probe density was established. Stability increases if probe-probe distance (i.e. probe density) and/or ionic strength (and hence the dielectric constant) increase. Under optimal conditions, the kinetics and thermodynamic properties

of hybridization (e.g. $k_{on}$, $k_{off}$, $K_A$ where $K_A = k_{on} / k_{off}$, $K_D = 1/K_A$) can be studied following Langmuir adsorption model[70]. For label-free detection of oligonucleotides, a sandwich-type strategy has been developed in SPR-enhanced fluorescence detection[71]. A 20-mer DNA capture probe (CP) was linked to the gold surface by a thiol-gold bond. After hybridization with a 40-mer target DNA, a fluorescent 20-mer reporter probe (RP) was added, resulting in the activation of the fluorescence by energy transfer from the plasmon resonance. A modification of this analysis is using a 60-mer target DNA with a patch sequence between the targets of CP and RP. After the adding of the fluorescent-RP, a complementary-patch sequence was added in order to create a more rigid structure and reach a proper distance to the gold surface, resulting in a 20% of increase of the fluorescent signal (Figure 1.15).

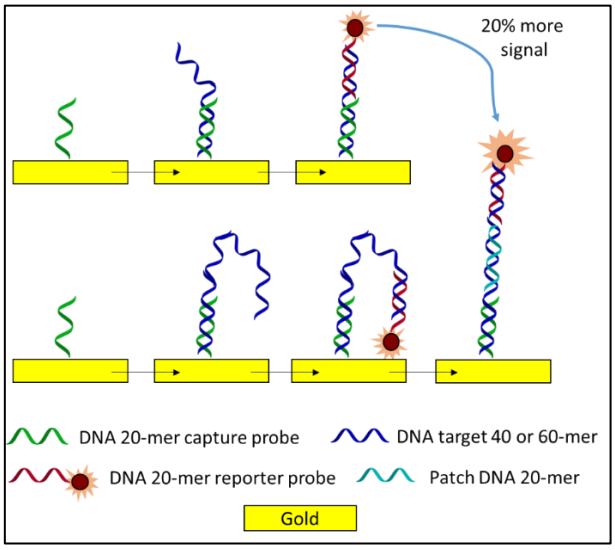


**Figure 1.15: sandwich-like strategy for SPR fluorescence.**

Another kind of SPR fluorescence assay was performed on nanoporous gold disk as source for plasmons[72]. A thiol and fluorescently labelled DNA hairpin can hybridize target DNA and can be linked to a nanoporous gold disk. Then the fluorescence can be turned on through the plasmon excitation. This assay has a LOD of 2.4 zeptomole of DNA oligonucleotide and an upper detection limit of 1 nM. QDs can be used as fluorophore for array sensors[73], and thus

they were also used for labelled-target DNA assay[74] using surface plasmon enhanced fluorescence.

The last method for increasing the signal in case of oligo-nucleotide detection is forming supramolecular aggregates with high-molecular weight molecules. Streptavidin enhanced SPR is the most used strategy. In a recent example,[75] a DNA capture probe was linked on the gold surface and hybridized with the target sequence; after this, a secondary reporter probe, constituted of biotinylated DNA sequence bound to streptavidin proteins (four DNA probes per protein) was added. The reporter probe was thus hybridized in a sandwich-type format, and the signal was found to be 5 fold increased compared to the bare target hybridization reaching a LOD of 1.7 fmol. Further developing the sandwich assay, a 'super sandwich' assembly was developed[76] using an hairpin DNA-capture probe on the SPR surface, which was opened when target DNA was added. Then an auxiliary probe, complementary to the end of the target sequence and a biotinylated probe complementary to another part of the auxiliary probe were added. This super-sandwich generated a signal amplification that could reach a LOD of 9 pM and a detection range between 10 pM and 1 µM. Beyond streptavidin as amplification tools nanoparticles, and especially gold-nanoparticles (Au-NPs) have successfully been used. Using PNA probes immobilized on a gold surface, Spoto and collaborators[77] developed a sandwich assay based on 12-mer DNA-modified Au-NPs for ultrasensitive detection of DNA. This system achieved detection of 1 fM target concentration with only 150 zeptomoles and still presenting single-nucleotide mismatch recognition.

Specific chemical reactions can also be used for signal enhancement; for example boronic acid can bind to cis-diol terminal groups of RNA (on carbon 3' and 2') that are not present in DNA. In this way, it is possible to detect micro RNA in an optic-fiber SPR sensor[78] placed in a flow cell as shown in Figure 1.16, in which arylboronic acids were linked to Au-NPs: this type of sandwich amplification led a LOD of 0.27 pM and a linear range between 1 pM and 10 µM.

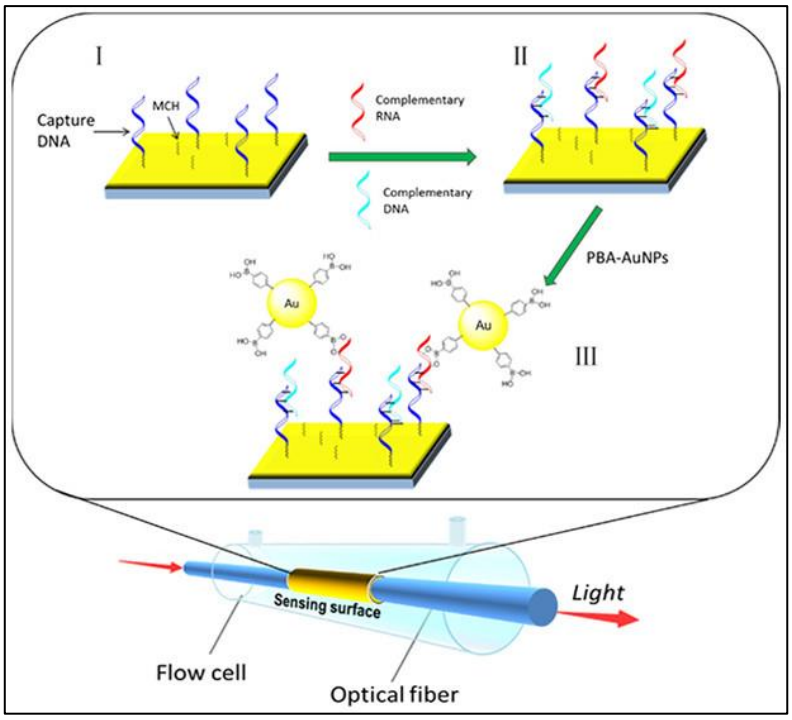


**Figure 1.16: scheme of detection of microRNA in optic-fiber SPR using boronate-modified AuNPs. Reprinted with permission from S. Quian et al. *ACS Sens.*, 2018 Copyright © 2018, American Chemical Society.**

## 1.4 OTHER NON-ELECTRONIC SENSORS

**QCM microbalances.**

Mass-sensitive sensors are Quartz Cristal Microbalance (QCM) that measure a mass variation per unit area by measuring the change in frequency of a quartz crystal resonator. Comparison between this type of sensor and SPR[79] showed that SPR is more suitable for kinetic study and quantitative analysis, meanwhile QCM is good for a qualitative analysis of viscoelastic properties of the film deposed onto the surface. QCM is sensitive to the solvation water bound to the target molecule and so, in DNA analysis, results can be comparable even if QCM is intrinsically 20 times less sensitive than SPR. In QCM analysis, as in SPR, oligonucleotide molecules are too small for being revealed at very low concentrations, so either a PCR amplification or signal amplification are necessary. As an example a screening of PCR product was performed with a

QCM sensor for detection of *Ehrlichia canis,* an obligate, intracellular bacterium that affects dogs[80]. The detection scheme used in this work was quite simple: the reference was placed in the same microbalance device by a SAM that avoided unspecific binding between DNA and gold. The sensing gold area was functionalized by a mercapto-CP. The addition of target DNA (PCR products) determined a significant decrease of the oscillating frequency only in the case of probe-modified QCM plate. Detection limit achieved was 22 copy of amplified gene per µL. Figure 1.17 show a typical sensogram obtained with this approach.

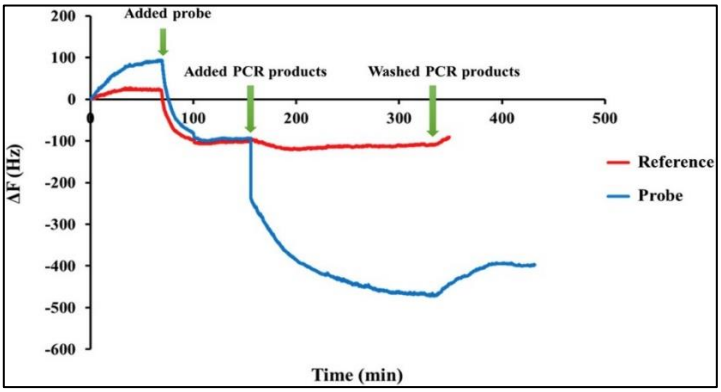


**Figure 1.17: sensograms of analysis of PCR-amplified target DNA by QCM: blue sample-sensing plates, red reference gold plate. Reprinted with permission from K. Bunroddith et al. *Analytica Chimica Acta*, 2018 Copyright © 2018, Elsevier.**

Sensing in QCM devices exploiting amplification with biotinylated DNA probes and streptavidin (SA) is a well-known procedure: a starting amplification used a capture DNA hairpin probe[81]. The hairpin-sequence have full complementarity to target DNA and a toehold sequence is present in order to favor a strand-displacement for the stem. The remaining part of the hairpin can be hybridized with a streptavidin-labeled DNA reporter probe. Without amplification of the SA-reporter probe, the QCM biosensor could only detect target above 10 nM, whereas using the reporter probe it was possible to reach a detection limit of 0.3 nM with a linear range of 0.5−20 nM. If the reporter probe has more than one biotinylated DNA bound to SA, a second SA-reporter probe complementary to the first can be used, and a further amplification can be obtained;[82] this strategy can be repeated by alternating the two type of reporter probes, thus forming a dendrimer. The LOD of this technique was 23 pM,

mainly thanks to subsequent signal amplifications, the linear range is between 0.05 and 15 nM. As in SPR, Au-NPs can be used for increasing the signal, to induce a larger decrease in the resonance frequency; a typical sandwich assay was performed with reporter DNA-modified Au-NPs[83]. In this case, the sensor exhibited a linear relationship between frequency change and the logarithm of target DNA concentration from 10 aM to 1 nM, with a LOD of 10 aM.

**Waveguides and optical fibers**

Other less commonly used method for detection of DNA involve guided light and optical fibers. Recently, a selective detection of point mutation (PM) in DNA was carried out using surface engineered microtoroids (optical ring resonators) modified with DNA probes[84]. Light passing through a tapered optical fiber, filtered by coupling with the microtoroid (wave guided mode, WGM) could be shifted of about 22 pm when the DNA capture probe, covalently linked on the microtoroid surface and immersed in a small droplet of aqueous solution (microaquarium), was hybridized with the complementary DNA target. The presence of one mismatch determined a reduced shift of only 5 pm. The LOD for full complementary sequence found was 2.32 nM. The device, the functionalization scheme, and the final output are described in Figure 1.18.

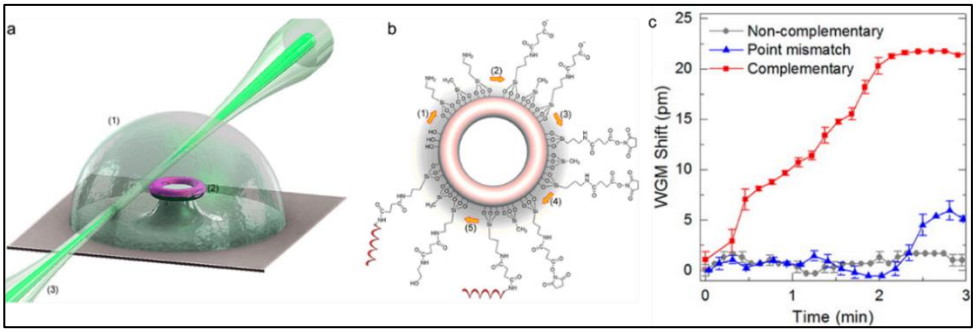


**Figure 1.18: a) biosensing platform consisting of a (1) microaquarium, (2) a probe conjugated microtoroid, and (3) a tapered fiber used to couple light to the microtoroid. b) chemical modification of the microtoroid surfaces: (1) APTES/TMMS, (2) Succinic anhydride, (3) EDC/NHS, (4) Covalent probe ss-DNA conjugation, and (5) ethanolamine capping. c) Wave Guided Mode shift (pm) of complementary (red), non-complementary (gray), and point mismatch (blue) strands versus time (min). Reprinted with permission from P. Toren et al. *Anal. Chem., 2015* Copyright © 201, American Chemical Society.**

A sensor for unamplified genomic DNA was developed using microstructured optical fiber (MOF) with Bragg-grating internally modified with PNA capture probes[85]. These fibers were used as an optofluidic device for the detection of DNA by measuring the shift in the wavelength of the reflected IR light. Enhancement of optical read-out was obtained using streptavidin coated Au-NPs interacting with the genomic DNA captured in the fiber channels in a sandwich-like assay. The minimal concentration of the unamplified target DNA detected was 0.3 ng/mL corresponding to an estimated 410 zM concentration. A scheme of the detection is shown in Figure 1.19.

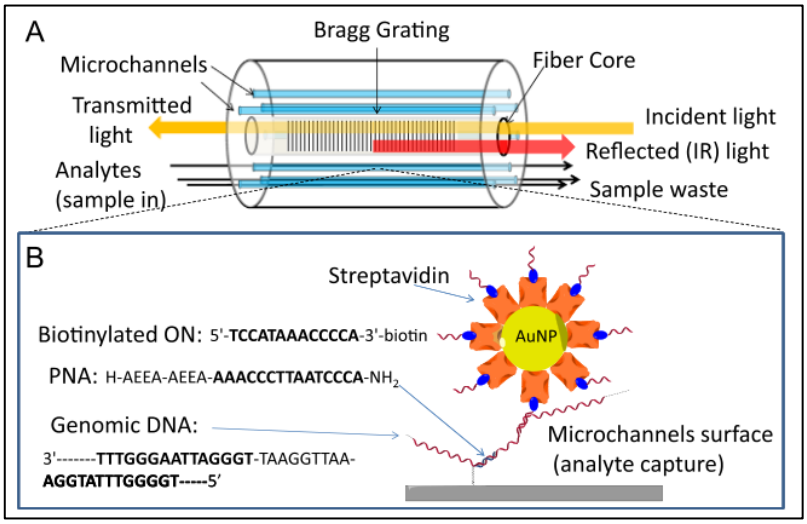


**Figure 1.19: biosensing with modified optical fiber. (A) Scheme of the optical setup. (B) Sequences of PNA, target DNA tract and oligonucleotide loaded on the gold nanoparticle. Reprinted with the permission of A. Bertucci et al. *Biosens Bioelectron*. 2015 Copyright © 2015 Elsevier.**

### Microcantilevers

Microcantilevers (MCs) are devices that can act as chemical sensor by detecting changes in cantilever bending (by laser reflection) or vibrational frequency. Microcantilevers moves up and down at a regular interval and molecules adsorbed on it cause vibrational frequency changes and deflection of MCs, caused by their different grade of charge or simply by their mass or volume. With a proper functionalization of their surface, these devices can act

as DNA-sensors. This technique is well studied in combination with PCR pre-amplification of the sample, in order to improve the sensitivity and specificity of detection. A gold coated microcantilever, with an embedded polysilicon wire as a piezo-resistive material, 250 µm long and 50 µm wide, was used as DNA-sensing platform[86]. The gold surface was modified by 3-mercaptopropionic acid (MPA) as SAM, an avidin layer was formed on it by formation of amide bonds, and 5′ biotinylated DNA-capture probe could thus be linked to this architecture. The hybridization between CP and target DNA creates nanomechanical bending and resistance change of piezoresistive material. This sensor was shown to have a LOD of 3.25 pg or 14 nM of target. In another setup[87], the sensing method relied on the quantification of the hydration-induced stress on microcantilever biosensors functionalized with oligonucleotide probes, before and after hybridization with specific targets. The limit of detection found was 10 fg/mL for 122-mer PCR amplified products. Other tests were performed with genomic DNA fragments, a more complex matrix respect to PCR amplicons with a huge amount of unspecific sequences; nevertheless, authors were able to detect 2 pg/mL target concentration and discriminating single mismatches.

**Electrochemiluminescence (ECL) sensors**

Electrochemiluminescence (ECL) sensors are borderline between fluorescent and electrochemical sensors: the read-out is optical but the signal is electronically-generated.

Different materials can be used as fluorescence emitter and electrochemical mediator. For example[88], carbon nitride nanosheets (CNNS) show cathodic electro-chemiluminescence emission in the presence of dissolved oxygen to produce an endogenous coreactant $H_2O_2$ on electrode surface. When a hemin-labelled DNA capture probe was adsorbed on CNNS surface, a decrease of formation of the coreactant and thus a quenching of the ECL emission was observed, due to in situ consumption of dissolved oxygen via hemin-mediated electrocatalytic reduction. When target DNA was added, the hemin-labelled capture probe was displaced from the surface and the ECL emission was recovered. The detection range was of 6-orders of magnitude wide, from 10 fM to 10 nM, with a LOD of 2.0 fM. The output-signal of the sensor diminished by introducing one or more mismatch in the target DNA sequence, showing good selectivity.

Others materials used in ECL are QDs. A layer by layer genosensor[89] was built as follows: CdSe/ZnS QDs were adsorbed on a glassy carbon electrode

(GCE), on these CdSe/ZnS QDs a long tailed hairpin-CP DNA was coupled. The tail of the hairpin was functionalized with an amino group, while the other extremity was thiol-modified, and was used to bind the DNA on luminol-functionalized Au-NPs. At this stage ECL emission was mainly due to QDs and the system was considered off. When target DNA was added, it disrupted the hairpin and the non-complementary system formed a G-quadruplex structure. G-quadruplex, in addition with hemin group, promoted hemin peroxidase mimicking DNAzyme activity that could enhance the ECL of luminol and quench the ECL of CdSe/ZnS simultaneously: the system in this state was in its on configuration. LOD found was 0.12 fM, with a linear range between 0.5 fM and 0.5 pM. QDs can be used also for multiple detection in arrays[90].

Very complicated amplification mechanism have been developed in ECL sensors, with the help of enzyme[91] or without[92]. The latter example is worth mentioning since it shows an interesting architecture including a sort of DNA nanomachine which use miRNA as 'fuel'; this generated a transduction signal based on electrochemiluminescence resonance energy transfer (ERET) between Alexa Flour 488 (AF 488), as the donor, and CdSe/ZnS quantum dots as the acceptor. The mechanism of this nanomachine is shown in Figure 1.20. Initially, a dual amplification strategy was employed to achieve the conversion of a small number of target fragment into a large amount of DNA reporters. This step include target recycling, as amplification mechanism: one target generates several DNA reporters (a $Pb^{2+}$ ion is necessary and, for another point of view, this sensor could be used as lead sensor). DNA reporters can interact with a DNA tweezer, initially kept in the "off" state. In this state tweezer have two arms labeled with QDs and AF488, respectively, too far for having energy transfer. In the presence of DNA reporters, that hybridize with tweezers, the distance between donor and acceptor decrease enough to generate ERET, which remarkably increased the ECL intensity of the QDs. The sensor could be regenerated using an oligonucleotide (S1), complementary to a tract of the reporter DNA. The linear range is from 0.1 fM to 10 pM with a detection limit of 0.03 fM. It is fair to say that the real application of these nanomachines is still in its early stage.

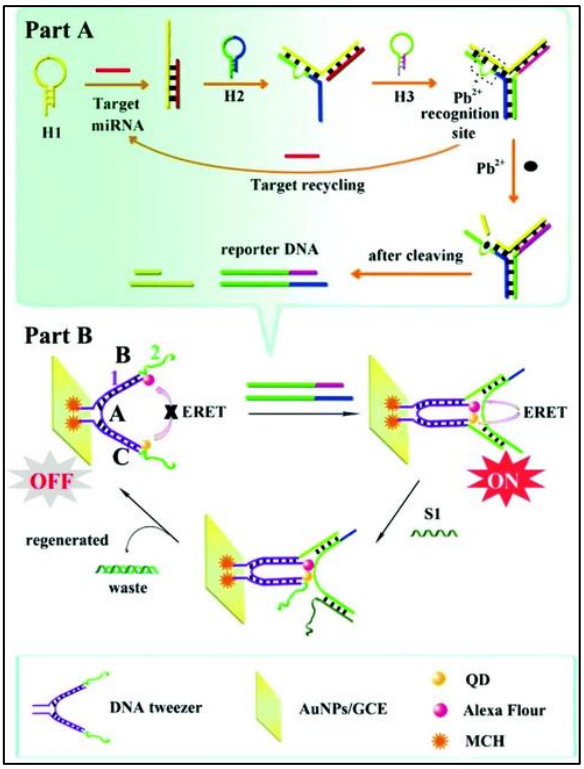


**Figure 1.20: mechanism of amplification in this ECL-nanomachines sensor. Reprinted with the permission of P. Zhang et al. *Nanoscale*. 2017 Copyright © 2017 Royal Chemistry Society.**

## 1.5 ELECTROCHEMICAL SENSORS

Electrochemical sensors are divided in various sub-categories: potentiometric, amperometric and resistive/impedance sensors. Field effect transistor will be treated in next paragraph.

Potentiometric sensors measure potential difference ($\Delta V$) provided by a spontaneous reaction. Usually besides the specific bio-receptor, there is a selective membrane for improving selectivity. This type of sensor are still not well developed for DNA sensing because there are intrinsic limitations in this kind of analysis. Amperometric sensors measure a current variation related to the applied voltage (V). A proper redox system captured or generated in proximity of the electrode is used to obtain a current signal, and the potential difference is chosen by the operator in order to avoid spontaneous reactions. The selectivity can be obtained using one electrode modified with a specific

receptor; this technique is not only quantitative (area of the amperometric peak) but also qualitative because oxidation or reduction reactions happen at a proper, specific voltage. In this kind of sensors, enzymatic amplification is quite common and convenient. For simplification here, impedance and resistive sensor will be treated as the same. If a condenser is present, it is correct to use the term impedance, which is a more general physical property.

Some potentiometric genosensors require tagged DNA as target[93,94]; this kind of detection is not easily performed, since it requires further manipulation for tagging, and probably will remain only for academic purposes. For example, a biotinylated target DNA, after binding with CP on magnetic nano-beads, was linked to streptavidin coated Au-NPs. These Au-NPs were later dispersed in buffer and used in an electrochemical stripping potentiometric detection. Another metal-mediated detection reported was based on potentiometric detection of DNA hybridization by a low-volume solid-contact silver ion-selective electrode ($Ag^+$-ISE)[95]. The target was partially hybridized with an oligonucleotide capture probe, bound to the gold surface of the sensor. In this case, the signal derived from the reduction of silver ions by p-aminophenol, produced by an enzymatic reaction of alkaline-phosphatase enzyme. This enzyme was tagged with a streptavidin which was captured on the surface when a second, biotinylated, reporter probe was hybridized with target DNA. A detection limit of 50 fM of target DNA (0.2 amol) was reported. A similar sensor[96] was developed using cadmium sulfide nanocrystal as label of the reporter probe in another sandwich-like assay. CdS nanocrystals were dissolved and detected with cadmium-selective microelectrodes. The reached LOD was 10 pM (2 fmol) of the target DNA; dynamic range was found to be 0.01−300 nM.

A good way to perform amperometric genosensing is tagging with a reporter molecule the DNA or DNA-mimic capture probe. This strategy was used by Metzler-Nolte and co-workers, [97] using two PNA probes with two differently modified ferrocenyl groups, that provided oxidation peak at different voltage. Ferrocene (Fc) was chosen as label for cyclic voltammetry (CV), due to its quasi-reversible redox processes of the $Fc^{0/+}$ redox couple. When the two PNA were immobilized on the gold surface of the electrode, the Fc moieties were free to move close to the surface, due to the flexibility of the PNA backbone, giving two different intense CV responses. These responses decreased when the target DNAs were added, since the PNA:DNA duplexes thus formed were much more rigid and did not allow the Fc moieties to interact with the surface, resulting in a strong decrease of the CV signals. Another similar detection

strategy involved the formation of a triplex structure between a methylene-blue-labelled DNA probe and target DNA[98]. In this case the rigid structure formed collapsed to the sensor surface, causing an increase in the amperometric signal. This approach can increase also affinity and selectivity of the recognition event, but is limited by the limited number of sequences which can form triple helices.

If not covalently bound to a capture or a reporter probe, an electron mediator can be used if its accessibility to the sensor surface is changed by the binding of the probe with target DNA. For example, using ferricyanide $[Fe(CN)_6]^{3-/4-}$ as redox-active molecule [99] and neutral PNA probes on a gold electrode surface, an amperometric signal was obtained due to the diffusion of ferricyanide to the surface. When target DNA was introduced, its hybridization with PNA probes generated an excess of negative charges on the surface, thus limiting diffusion, and decreasing the signal. Interestingly, authors have developed a method for avoiding false positives by enzymatically digesting the non-fully-complementary DNA. In a similar example, with opposite polarity, a sensor was developed where a positive electron mediator (a cobalt complex) was attracted by the negative charges of target DNA, which were not present when only PNA probes were on the gold electrode surface[100]. A linear relationship within the concentration range of 5.0 nM to 250 nM with a detection limit of 0.56 nM was achieved.

Amperometric DNA sensors were shown to operate also on PCR amplicons samples[101]. Streptavidin-modified magnetic microbeads were treated with a hairpin-capture probe biotinylated at both ends; the target DNA was hybridized with these CP-microbeads and then a biotinylated RP was added. The resulting biotinylated hybrids were coupled with a commercial streptavidin–peroxidase conjugate; the final modified magnetic microbeads were magnetically captured onto a screen-printed carbon electrode to perform amperometric detection, using hydrogen peroxide/benzoquinone ox-redox systems, as reported in Figure 1.21. A LOD of 0.72 pM was obtained for the synthetic target. Denatured PCR amplified samples showed a LOD of 20 pg of genomic DNA, and the linear range was from 20.0 pg to 2.0 ng of extracted DNA.

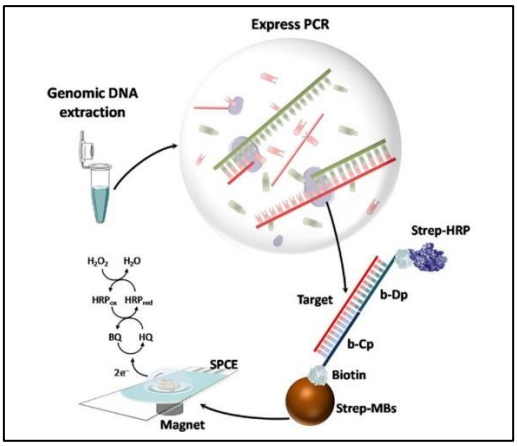


**Figure 1.21: detection scheme of amperometric sensor for PCR-amplified DNA. The amperometric detection is performed using the $H_2O_2$/HQ red-ox system. HRP is horseradish peroxidase, BQ is benzoquinone, HQ is hydroquinone. Reprinted with the permission of V. Ruiz-Valdepeñas Montiel et al. *Sensors and Actuators B: Chemical*. 2017 Copyright © 2017 Elsevier.**

A similar amperometric strategy was used in DNA tetrahedral nanostructures[102]: CP thiolated-DNA anchored onto the gold surface of the sensor through these DNA tetrahedral were hybridized with target DNA, followed by hybridization of a RP onto an adjacent sequence. The advantages of using rigid DNA tetrahedral are that capture probes are in well-controlled density and orientation, minimizing surface crowding resulting in an enhanced sensitivity. Different formats of the CP were tested; a) labelled with biotin, b) attached to Avidin-HRP modified nanoparticles, or c) with a second tetrahedral DNA nanostructure bearing multiple biotin-HRP units. The biotin-tagged three-dimensional DNA tetrahedral nanostructures were employed for efficient signal amplification as shown in Figure 1.22. This approach, with both geometrical and enzymatic amplification showed the best performances, with a LOD of 1 fM; moreover, the amperometric signal increased monotonically with the logarithm of the target DNA concentration from 1 fM to 10 nM; the proper linear range found was from 1 fM to 100 pM.

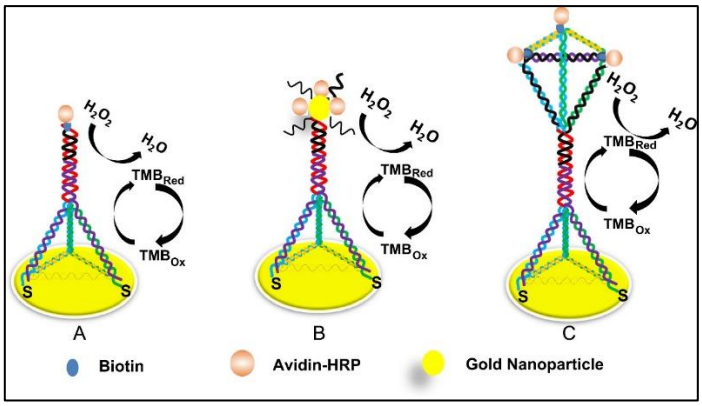


**Figure 1.22: A) detection scheme with tetrahedral structure only for Cps, B) detection with Au-NPs coated with avidin-Horse Radish Peroxidase, C) tetrahedral geometry both for CPs and RPs provide signal amplification. Reprinted with the permission of D. Zeng et al. Biosens. and Bioelectr. 2017 Copyright © 2017 Elsevier.**

Amperometric genosensor have been developed also using microfluidic system,[103] similarly using a sandwich assay and HRP enzyme-amplification of the signal ; the LOD reached in this work was 6 pM.

If more than one enzyme is used for amplification of the signal, the performance of sensing system can be further increased, as shown by Wan et al[104] using elongation of an hairpin capture probe which, after DNA capture, can undergo a reaction from terminal deoxynucleotidyl transferase, leading to incorporation of biotinylated 2'-deoxyadenosine 5'-triphosphate (biotin–dATP) at 3' end. Subsequent binding of avidin-HRP and enzymatic reaction with amperometric detection led to a calculated LOD of 43 pM, and the signal was logarithmically related to the target concentration in the range from 100 pM to 100 nM.

An example of impedance sensor is a label-free electrochemical DNA sensor, based on pyrrolidinyl peptide nucleic acid (acpcPNA)-immobilized on a paper-based analytical device (PAD)[105] (see Figure 1.23). AcpcPNA was covalently immobilized onto partially oxidized cellulose paper for an easy regeneration of the sensor by simple PAD replacement. The DNA sensor initial target was a synthetic 15-mer oligonucleotide. Measurement were conducted by measuring the change in the charge transfer resistance, obtained from electrochemical impedance spectroscopy (EIS). The charge transfer resistance of $[Fe(CN)_6]^{3-/4-}$ before and after hybridization with the target DNA could be clearly distinguished, due to the switch from neutral probes to negative charged

probe:target complex. Linearity of the calibration curve was in the range of 2–200 nM and the LOD found was 1.24 nM. The device was successfully applied to detect PCR-amplified DNA samples. A similar sensor, build on a more conventional substrate, reached a limit of detection of 0.15 nM and a linear range from 1 to 200 nM[106].

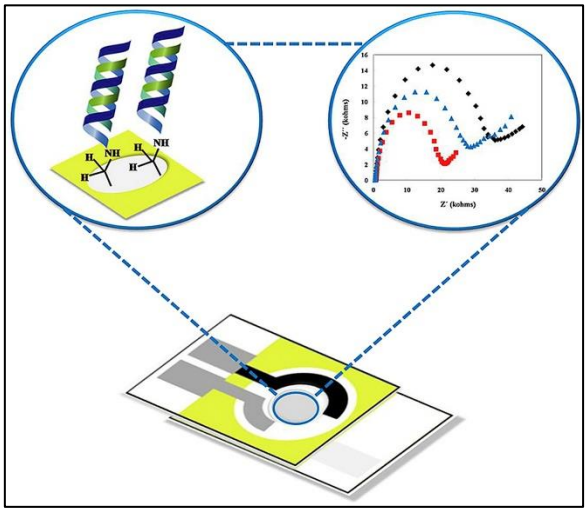

**Figure 1.23: impedance sensor based on pyrrolidinyl peptide nucleic acid. Reprinted with the permission of P. Teengam et al. Analytica Chimica Acta 2018 Copyright © 2018 Elsevier.**

Another electrode surface used for impedance sensing of DNA is constituted by microfabricated thin alumina nanopore membranes[107]. A challenge for authors was in this case developing a methodology for reproducible nanoscale-manufacturing of the electrode: each membrane was 100 μm × 100 μm large and 2 μm thick, with pore diameter of 120 nm; one single chip (1 $cm^2$) contained an array of 69 membranes. During the immobilization of capture probe DNA to (3-glycidoxypropyl) trimethoxysilane functionalized surface, the nanopore resistance dropped significantly but after hybridization with complementary DNA, it was increased. Thus, there was no need of addition of redox reporters. LOD found is 12.5 nM, and the linearity found was from this value to 500 nM.

A capacitance sensor was developed in order to have a rapid (2.5 min sample reaction) and label free analysis of PCR amplified sequences[108]. The number of negative charges carried by target DNA generated a difference in terms of

capacitance. The detection limit was less than 1 pM for the single-stranded amplified oligonucleotide and 4 pM for the double-stranded target.

## 1.6 FIELD EFFECT TRANSISTOR SENSORS

The field-effect transistor (FET) is a device that regulates current or voltage flow and acts as a switch or gate for electronic signals. The conductivity between the drain and source terminals is controlled by an electric field in the device, which is generated by the voltage difference between the body and the gate of the device. A FET bio-sensor is a field-effect transistor in which the gate potential is regulated by changes in the surface potential induced by the binding of molecules. When charged molecules, such as DNA, bind to the FET gate or onto the semi-conductive material layer, they change the charge distribution, resulting in a change in conductance of the FET channel. Schematic representation of FET geometries are shown in Figure 1.24.

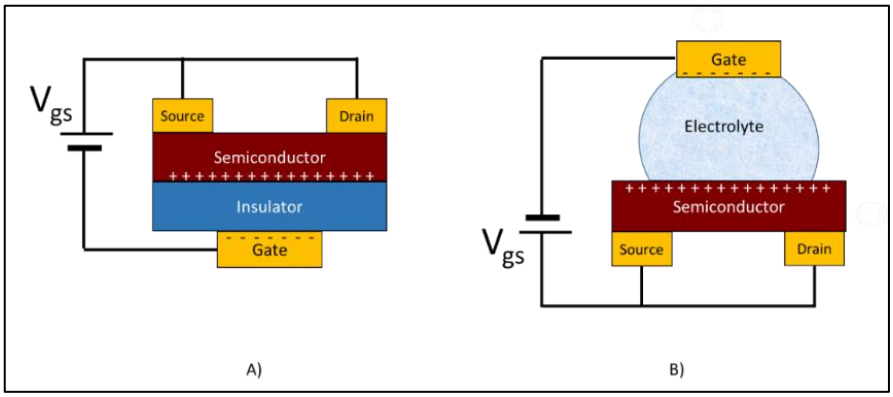


**Figure 1.24: general scheme of A) an organic field-effect transistor (O-FET) b) electrolyte-gated organic field-effect transistor (EGO-FET).**

Bio-receptors, that in the case of genosensors are DNA capture probes, can be placed on the semiconductor layer or directly attached to the gate electrode. For example, an electrical double layer (EDL) gated high electron mobility transistor (HEMT) was used as DNA sensor[109]. The sensing area was on the gate electrode (which is separated from the transistor channel). Before the immobilization process, the drain current of the device was measured in 1X PBS solution to set the device baseline. A capture probe DNA was linked to the

gold gate electrode by a thiol moiety, to capture target DNA from physiological salt environment. DNA detection was performed in flow regime by measuring the current between source and gate electrodes; this increased in a nonlinear way upon increase of the target DNA concentration up to 100 fM. LOD of this sensor was 1 fM. The specificity of the DNA sensor was demonstrated by choosing the hybridization temperature.

Another type of FET are extended gate field-effect transistors (EGFETs), in which the metal oxide semiconductor have two functions: passivation layer for protect electronic circuits below and sensor's surface, without other modifications, except the sensing molecule. These factors not only diminish sensor complexity, but also enhances the sensor reliability and facilitates massive production for commercialization. An example of application is an aptamer bio-sensing of growing factor protein involved in several cancer cases[110]. Rolling circle amplification, mentioned above (Figure 1.2.5) was used for amplify the signal.

The floating-gate FET is a field-effect transistor, whose gate is electrically isolated. The current can pass through this electrode in several ways, among these, tunneling effect. These sensors are capable to work in very difficult conditions in term of temperature or pressure, and for what concern bio sensing, it can diminish unwanted currents. A genosensor of this type was developed by Park and co-worker[111], exploiting pentacene as semi conductive material, a gold floating gate and thiolated DNA probes.

In recent works, a widely used semiconductor material is graphene or other allotropic forms of carbon like nanotubes. Graphene has attracted much attention in bio sensing applications for its unique properties: its one-atom layer structure with every atom exposed to the environment makes the electronic properties of graphene very sensitive to charged analytes. A graphene based field effect transistor with DNA-tweezers has been developed[112]. Very good sensitivity in single mismatch detection was achieved by observing changes in Dirac point shift and resistance change. The Dirac point in graphene define the potential at which electrons and wholes can move with the same probability. This is the cusp point of the graph $I_{ds}$ versus $V_{gs}$ and for graphene is symmetrical and around 0 Volt. Dirac point measurements are performed at the end of hybridization and are static measurement of the current between source and drain electrodes ($I_{ds}$) versus the applied voltage between source and gate electrodes ($V_{gs}$). These changes are due to a different conformation of DNA probes after hybridization with target DNA. The molecular cartoon and explanation is in Figure 1.25. The use of DNA-tweezers probe with high-quality

graphene FET significantly improves analytical characteristics of single point mutations detection by enhancing the sensitivity. The electrical output can be recorded and transmitted to personal electronics.

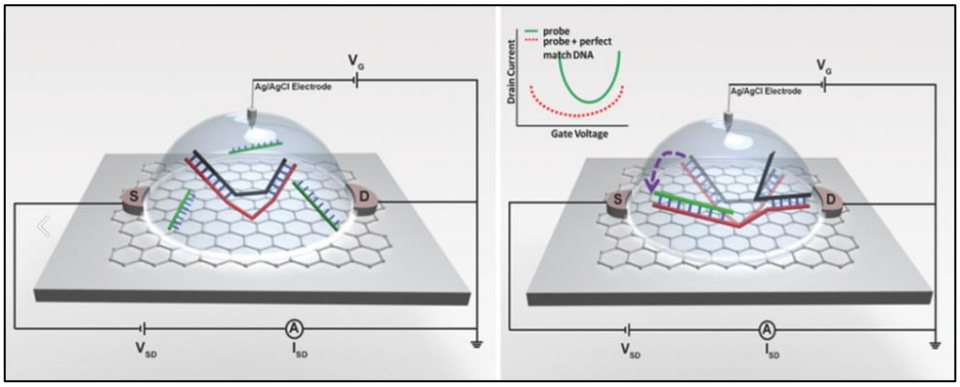


**Figure 1.25: left, initial situation where capture probe is hybridized with another DNA fragment that form a tensioned tweezer. Right, the full match DNA operate a strand displacement reaction and the system reaches a less tensioned status in which more negative charges are close to the graphene surface. Reprinted with the permission of M. T. Hwang et al. Advanced Materials. 2018 Copyright © 2018 John Wiley and Sons.**

Chemical vapor deposition (CVD) has been demonstrated to be the most successful method for fabricating large area graphene. After the synthesis, graphene have to been transferred onto the insulant material and this procedure can produce little defects that severely degrade the sensing performance of graphene. Xu et al[113] directly fabricated graphene on sapphire substrate by high temperature treatment. Interestingly, in this case DNA capture probes were not covalently bound to the surface of graphene, in order not to damage its electronic properties, but were conjugated to pyrene which could bind to graphene trough π-π stacking interactions. This novel semiconductor device was tested as DNA sensor exploiting the effect of additional charges captured on the graphene surface when target DNA was hybridized. This kind of sensor was used in batch measurements and variations were registered in the $I_{ds}$ vs $V_{gs}$ graphs. It is not clear if this non-covalent interaction is enough strong for sensing in a high flow rate regime without detachment of capture probes. The sensors showed a DNA detection limit of 100 fM and a linear range from 100 fM to 1 nM. The same strategy, but with a synthetic PNA capture probe, reached a similar value of LOD[114]. Also a preliminary work with carbon nanotubes[115] followed the same strategy and

showed a LOD of 1 pM with a linear range of from 1 pM to 10 nM. $I_{ds}$ - $V_{gs}$ curves were used also in this case, which were found to change as a function of the quantity of target DNA.

Graphene field-effect transistors (GFETs) were also tested in combination with amplification of the electrochemical signal [116]. The proposed mechanism has two steps: target recycling reaction and hybridization chain reaction (see Figure 1.26). The CVD graphene was functionalized by 1-pyrenebutyric acid N-hydroxysuccinimide ester (PBASE) that reacted with amino functionalized DNA hairpin capture probe. The hairpin opened when target DNA was added. Target recycling was obtained with another hairpin probe (helper probe 1) that performed a toehold-mediated strand displacement reaction; in this way target DNA could bind to more than one capture probe and could generate more than one signaling complex. The second step consisted in an hybridization chain reaction and is performed by other two hairpin probes (helper 2 and 3) that bound to the ending parts of the helper probe 1. Dirac-point voltages were evaluated before and after treatment with target DNA and helper probes. LOD for 21-mer target was ~5 fM, and after 15 hours of analysis was further decreased to 100 aM.

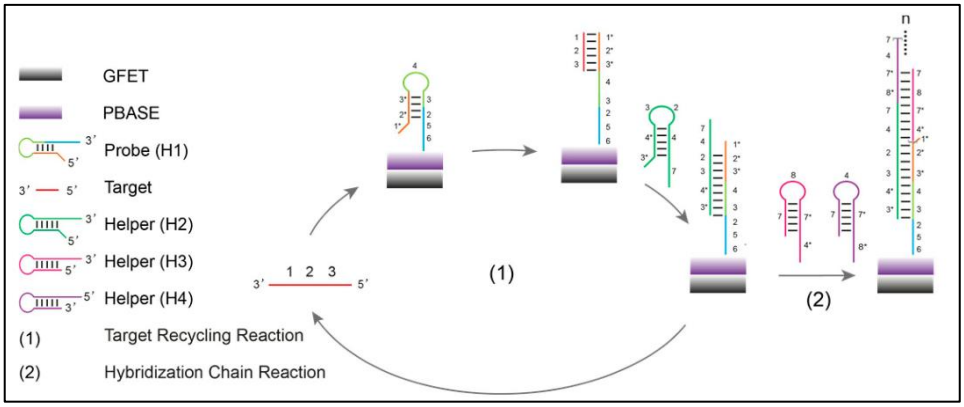


**Figure 1.26: double amplification mechanism proposed; target recycling reaction (1) and hybridization chain reaction (2). Reprinted with the permission of Z. Gao et al. Nano Lett. 2018 Copyright © 2018 American Chemical Society.**

A summary of all the mentioned genosensing examples cited in this chapter is given in Table 1.1.

**Table 1.1: summary table of type of sensors and their performances.**

| Type of sensor (key-words) | First author - year | Limit of detection | Dynamic range |
|---|---|---|---|
| colorimetric- AuNPs | Han - 2006 | 500 nM | |
| colorimetric- AuNPs | Sato - 2003 | < 100 fmol | |
| light scattering- AuNPs | Du - 2006 | 0.1 pM | |
| colorimetric- silicon + amplification | Jenison - 2001 | 10 fM | |
| fluorescence - QDs | Shamsipur - 2017 | 0.2 nM | 1 - 50 nM |
| fluorescence - nanocluster beacon | Ge - 2017 | 0.5 nM | 1 - 500 nM |
| fluorescence - nanoceria | Bülbül - 2018 | 0.12 nM | 1.1 - 37 nM |
| fluorescence - $WS_2$ nanosheet | Wang - 2015 | 500 pM | 1 - 20 nM |
| fluorescence - carbon QDs | Loo - 2016 | 17.4 nM | 0.04 - 40 nM |
| fluorescence - carbon QDs | Yew - 2017 | 4.0 pM | |
| fluorescence - CuNPs + amplification | Park - 2018 | 7.79 aM | 10 aM - 1 mM |
| SPR - LAMP mediated | Nawattanapaiboon - 2015 | 17 aM | |
| SPR - QCM - streptavidin coating | Xiaodi - 2004 | 20 nM | 10 - 150 nM |
| SPR - fluorescence - nanoporous gold | Santos - 2015 | 2.4 zmol | |
| SPR - streptavidin coating | Zhang - 2013 | 1.7 fmol | |
| SPR - supersandwich | Ding - 2015 | 9.0 pM | 10.0 pM - 1 µM |
| SPR- AuNPs enhanced | D'Agata - 2008 | 1 fM / 150 zmol | |
| SPR - optic fiber - AuNPs | Qian - 2018 | 0.27 pM | 1.0 pM - 10 µM |
| QCM | Wang - 2012 | 0.3 nM | 0.5 - 20 nM |
| QCM - dendrimer approach | Zhao - 2015 | 23 pM | 0.05 - 15 nM |
| QCM - AuNps enhanced | Rasheed - 2016 | 10.0 aM | 10 aM -1 nM |
| waveguides - microtoroid | Toren - 2015 | 2.32 nM | |
| optical fiber - AuNPs enhanced | Bertucci - 2015 | 410 zM / 0.3 ng $mL^{-1}$ | |
| microcantilever | Khemthongcharoen - 2015 | 14 nM / 3.25 pg | |
| microcantilever | Dominguez - 2015 | 10 fg $mL^{-1}$ | |
| el.chemiluminescence - carbon nitride | Feng -2015 | 2 fM | 10 fM - 10 nM |
| el.chemiluminescence - AuNPs | Wang - 2018 | 0.12 fM | 0.5 fM - 0.5 pM |
| el.chemiluminescence - nanomachine | Zhang - 2017 | 0.03 fM | 0.1 fM - 10 pM |
| potentiometric -enzyme ampl. | Wu - 2009 | 50 fM / 0.2 amol | |
| potentiometric | Numnuam - 2007 | 10 pM / 2 fmol | 0.01 - 300 nM |
| electrochemical - metal complex | Liu - 2010 | 0.56 nM | 5 - 250 nM |
| amperometric - magnetic beads | Montiel - 2017 | 0.72 pM / 20 pg | 20 pg - 2 ng |
| amperometric - enzyme ampl. | Zeng - 2015 | 1 fM | 1 fM - 100 pM |
| amperometric - NPs | Ölcer - 2015 | 6.0 pM | |
| amperometric - enzyme ampl. | Wan - 2014 | 43 pM | 100 pM - 100 nM |
| impedentiometric | Teengam - 2018 | 1.24 nM | 2 - 200 nM |
| impedentiometric | Ribovski - 2017 | 0.15 nM | 1 nM - 200 nM |
| impedentiometric | Wu - 2015 | 12.5 nM | 12.5 - 500 mM |
| capacitive | Liu - 2015 | < 1 pM | |
| FET | Chen - 2018 | 1 fM | |
| FET - sapphire graphene | Xu - 2018 | 100 fM | 100 fM - 1 nM |
| FET - carbon nanotubes | Tran - 2017 | 1.0 pM | 1 pM - 10 nM |
| FET - graphene + aplification | Gao - 2018 | 100 aM | |

## 1.7 LIQUID BIOPSY FOR EARLY CANCER DIAGNOSIS

One of the major challenge in DNA detection is find in complex matrix, like blood, little amount of DNA that come from cell apoptosis. Being able to detect such kind of circulating DNA make possible a very early stage detection of pathologies, like cancer, and so increase the rate of success in treatment meanwhile cost for health can diminish[117]. Not only tumor DNA, but also overexpression of micro RNAs can be used as indicator of pathologies[118].
All the above mentioned technologies for genosensing can be applied to give fast and reliable quantitative results for this type of applications, and recent examples point in this direction. In particular, the possibility to avoid difficult biopsy by a simple blood collection is less disturbing for patients, avoid contaminations and reduce time between collection and results[119].
A new blood test, named CancerSEEK (Figure 1.27), can identify eight common cancers: ovary, liver, esophagus, pancreas, stomach, colorectal, lung, and breast cancer[120]. The new liquid biopsy measures circulating tumor DNA (ctDNA) from 16 genes and 8 protein biomarkers. The first component of CancerSEEK determines mutations in ctDNA purified from plasma. A preliminary amplification by multiplex–polymerase chain reaction is needed, using a 61-amplicon panel designed to amplify 66 to 80 base-pair segments of the DNA in regions of interest from 16 genes. The amplified products were uniquely labeled with a DNA barcode and were matched to reference sequences. To determine the tissue of origin in patients with a positive CancerSEEK test, an algorithm can be used that takes into account the type of ctDNA, the level of any of the 8 protein biomarkers as well as the 31 other proteins determined by the panels in the immunoassay, and the sex of the patient. For this analysis, esophageal and gastric cancer patients can be grouped together, because endoscopy is the suggested follow-up in both cases. Without using any other information, CancerSEEK test was able to localize the origin to two anatomic locations in a median of 83% of patients and to a single organ in a median of 63%. On problem of the test is that cancer-related proteins reflect tissue damage and can appear in people with inflammatory diseases such as arthritis. Due to these inflammatory processes, false positive ratio is about 1%. The researchers also estimate that the cost of this single test will be less than $500, anyway too much for a screening of a biggest part of population. More efforts have to be done in order to achieve a sensitive, robust and cost-effective test for early cancer diagnosis, but CancerSEEK is a first promising step.

Recently, European Union have funded, by program Horizon 2020, the developing of an ultrasensitive early cancer diagnosis SPR sensor (ULTRAPLACAD). This novel sensor will be able to detect colorectal cancer markers in blood such as protein and circulating DNA and micro RNA. This detection strategy is oriented in several checks for avoid false positive and discriminate various type of genetic mutation that have caused cancer: in this way, it will be possible to determine the best therapeutic strategy for each patient. Chapter 4 of this thesis is dedicated to activities within this project.

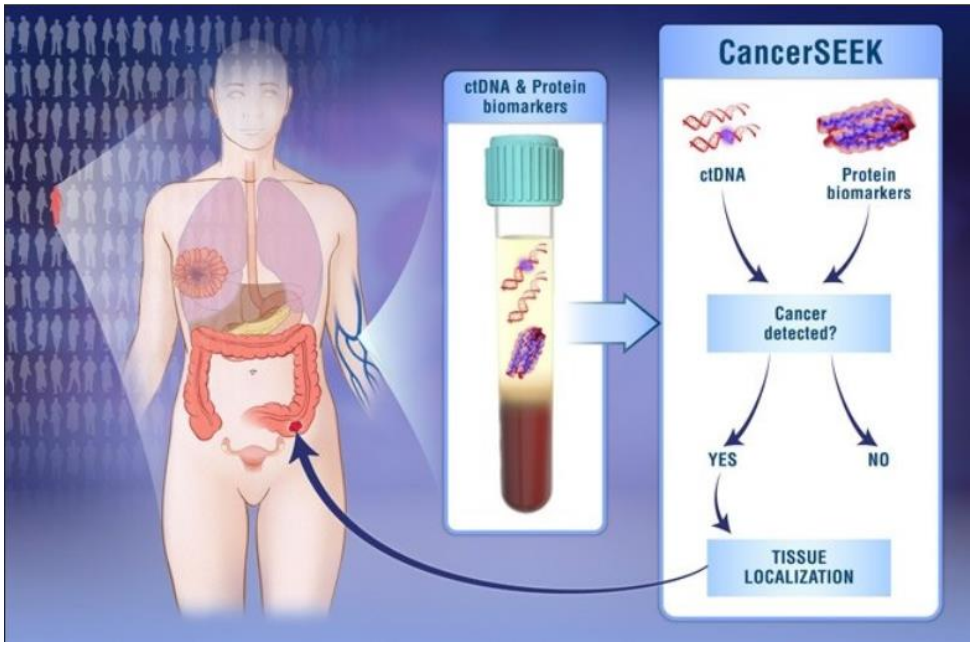


**Figure 1.27: illustrative explanation of early cancer diagnosis achieved by CancerSEEK. Reprinted with permission of J. D. Cohen et al. Science 2018. Copyright © 2018 Science.**

## Bibliography:


1. Higuchi R, Dollinger G, Walsh PS, Griffith R. Simultaneous amplification and detection of specific DNA sequences. *Biotechnology (N Y)*. 1992;10(4):413-417.
2. Pfaffl M. Quantification strategies in real-time PCR Michael W . Pfaffl. *A-Z Quant PCR*. 2004:87-112.
3. Schmittgen TD, Zakrajsek BA, Mills AG, Gorn V, Singer MJ, Reed MW. Quantitative reverse transcription-polymerase chain reaction to study mRNA decay: Comparison of endpoint and real-time methods. *Anal Biochem*. 2000;285(2):194-204.
4. Breveglieri G, Travan A, D'Aversa E, et al. Postnatal and non-invasive prenatal detection of β-thalassemia mutations based on Taqman genotyping assays. *PLoS One*. 2017;12(2):1-16.
5. Wei Z-H, Guo W-H, Wu J, Suo W-H, Fu G-H. A nonsense mutation in the Xeroderma pigmentosum complementation group F (XPF) gene is associated with gastric carcinogenesis. *Gene*. 2014;537(2):238-244.
6. Gravel A, Sinnett D, Flamand L. Frequency of Chromosomally-Integrated Human Herpesvirus 6 in Children with Acute Lymphoblastic Leukemia. Banfield BW, ed. *PLoS One*. 2013;8(12):e84322.
7. Huang Q, Liu Z, Liao Y, Chen X, Zhang Y, Li Q. Multiplex Fluorescence Melting Curve Analysis for Mutation Detection with Dual-Labeled, Self-Quenched Probes. Mokrousov I, ed. *PLoS One*. 2011;6(4):e19206.
8. Wong ML, Medrano JF. Real Time for mRNA quantitation. 2005;39(1):1-11.
9. Whitcombe D, Theaker J, Guy SP, Brown T, Little S. Detection of PCR products using self-probing amplicons and fluorescence. *Nat Biotechnol*. 1999;17(8):804-807.
10. Zhang Z, Xiao H, Xie F, et al. High-incidence of PTEN mutations in Chinese patients with primary small cell carcinoma of the esophagus. *BMC Cancer*. 2014;14(1):19.
11. Naserpour Farivar T, Johari P, Najafipour R, et al. The Relationship Between Gastric Cancer and Helicobacter Pylori in Formaldehyde Fixed Paraffin Embedded Gastric Tissues of Gastric Cancer Patients-Scorpion Real-Time PCR Assay Findings. *Pathol Oncol Res*. 2014;20(1):113-117.
12. Nazarenko I, Lowe B, Darfler M, Ikonomi P, Schuster D, Rashtchian A. Multiplex quantitative PCR using self-quenched primers labeled with a single fluorophore. *Nucleic Acids Res*. 2002;30(9):37e-37.
13. Vilcek S, Vlasakova M, Jackova A. LUX real-time PCR assay for the detection of porcine circovirus type 2. *J Virol Methods*. 2010;165(2):216-221.
14. Lucchi NW, Narayanan J, Karell MA, et al. Molecular Diagnosis of Malaria by Photo-Induced Electron Transfer Fluorogenic Primers: PET-PCR. Schallig HDFH, ed. *PLoS One*. 2013;8(2):e56677.
15. Hindson BJ, Ness KD, Masquelier DA, et al. High-Throughput Droplet

Digital PCR System for Absolute Quantitation of DNA Copy Number. *Anal Chem*. 2011;83(22):8604-8610.
16. Zhao Y, Chen F, Li Q, Wang L, Fan C. Isothermal Amplification of Nucleic Acids. *Chem Rev*. 2015;115(22):12491-12545.
17. Spengler J, Ruíz-Rodríguez J, Yraola F, et al. A novel protecting/activating strategy for β-hydroxy acids and its use in convergent peptide synthesis. *J Org Chem*. 2008;73(6):2311-2314.
18. Su X, Kanjanawarut R. Control of metal nanoparticles aggregation and dispersion by PNA and PNA-DNA complexes, and its application for colorimetric DNA detection. *ACS Nano*. 2009;3(9):2751-2759.
19. Linette M. Demers, Chad A. Mirkin, Robert C. Mucic, et al. A Fluorescence-Based Method for Determining the Surface Coverage and Hybridization Efficiency of Thiol-Capped Oligonucleotides Bound to Gold Thin Films and Nanoparticles. 2000; 72(22), 5535-5541.
20. Elghanian R, Storhoff JJ, Mucic RC, Letsinger RL, Mirkin CA. Selective colorimetric detection of polynucleotides based on the distance-dependent optical properties of gold nanoparticles. *Science*. 1997;277(5329):1078-1081.
21. Nourisaeid E, Mousavi A, Arpanaei A. Colorimetric DNA detection of transgenic plants using gold nanoparticles functionalized with L-shaped DNA probes. *Phys E Low-dimensional Syst Nanostructures*. 2016;75:188-195.
22. Amini B, Kamali M, Salouti M, Yaghmaei P. Spectrophotometric, colorimetric and visually detection of Pseudomonas aeruginosa ETA gene based gold nanoparticles DNA probe and endonuclease enzyme. *Spectrochim Acta Part A Mol Biomol Spectrosc*. 2018;199:421-429.
23. Han MS, Lytton-Jean AKR, Mirkin CA. A Gold Nanoparticle Based Approach for Screening Triplex DNA Binders. *J Am Chem Soc*. 2006;128(15):4954-4955.
24. Wenxing Wang, Huajie Liu, Dongsheng Liu, Yun Xu, Yang Yang and, Dejian Zhou. Use of the Interparticle i-Motif for the Controlled Assembly of Gold Nanoparticles. *Langmuir* 2007; 23(24), 11956-11959.
25. Li F, Zhang J, Cao X, et al. Adenosine detection by using gold nanoparticles and designed aptamer sequences. *Analyst*. 2009;134(7):1355.
26. Kae Sato, Kazuo Hosokawa and, Maeda* M. Rapid Aggregation of Gold Nanoparticles Induced by Non-Cross-Linking DNA Hybridization. *Journal of the American Chemical Society*, 2003;*125*(27), 8102-8103.
27. Zhao W, Chiuman W, Brook MA, Li Y. Simple and Rapid Colorimetric Biosensors Based on DNA Aptamer and Noncrosslinking Gold Nanoparticle Aggregation. *ChemBioChem*. 2007;8(7):727-731.
28. Li H, Rothberg L. Colorimetric detection of DNA sequences based on electrostatic interactions with unmodified gold nanoparticles. *Proc Natl Acad Sci U S A*. 2004;101(39):14036-14039.
29. Wang L, Liu X, Hu X, Song S, Fan C. Unmodified gold nanoparticles as a colorimetric probe for potassium DNA aptamers. *Chem Commun*. 2006;(36):3780-3782.

30. Du B-A, Li Z-P, Liu C-H. One-Step Homogeneous Detection of DNA Hybridization with Gold Nanoparticle Probes by Using a Linear Light-Scattering Technique. *Angew Chemie Int Ed*. 2006;45(47):8022-8025.
31. Jenison R, Yang S, Haeberli A, Polisky B. Interference-based detection of nucleic acid targets on optically coated silicon. *Nat Biotechnol*. 2001;19(1):62-65.
32. Kim SK, Cho H, Jeong J, Kwon JN, Jung Y, Chung BH. Label-free and naked eye detection of PNA/DNA hybridization using enhancement of gold nanoparticles. *Chem Commun*. 2010;46(19):3315-3317.
33. Tyagi S, Kramer FR. Molecular Beacons: Probes that Fluoresce upon Hybridization. *Nat Biotechnol*. 1996;14(3):303-308.
34. Guo J, Ju J, Turro NJ. Fluorescent hybridization probes for nucleic acid detection. *Anal Bioanal Chem*. 2012;402(10):3115-3125.
35. Li X, Li Z, Mart AA, et al. Combinatorial fluorescence energy transfer molecular beacons for probing nucleic acid sequences. *Photochem Photobiol Sci*. 2006;5(10):896.
36. Holzhauser C, Wagenknecht H-A. In-Stem-Labeled Molecular Beacons for Distinct Fluorescent Color Readout. *Angew Chemie Int Ed*. 2011;50(32):7268-7272.
37. Kazuhisa Fujimoto, Hisao Shimizu and, Masahiko Inouye. Unambiguous Detection of Target DNAs by Excimer−Monomer Switching Molecular Beacons. *The Journal of organic chemistry*, 2004;*69*(10), 3271-3275.
38. A. Bourdoncle, A. Estévez Torres, C. Gosse, et al. Quadruplex-Based Molecular Beacons as Tunable DNA Probes. *Journal of the American Chemical Society*, 2006;*128*(34), 11094-11105.
39. Sei-Iida Y, Koshimoto H, Kondo S, Tsuji A. Real-time monitoring of in vitro transcriptional RNA synthesis using fluorescence resonance energy transfer. *Nucleic Acids Res*. 2000;28(12):59e-59.
40. Tsuji A, Koshimoto H, Sato Y, et al. Direct Observation of Specific Messenger RNA in a Single Living Cell under a Fluorescence Microscope. *Biophys J*. 2000;78(6):3260-3274.
41. Angel A. Martí, Cindy A. Puckett, Joanne Dyer, et al. Inorganic−Organic Hybrid Luminescent Binary Probe for DNA Detection Based on Spin-Forbidden Resonance Energy Transfer. *Journal of the American Chemical Society*, 2007;*129*(28), 8680-8681.
42. Marti AA, Li X, Jockusch S, et al. Pyrene binary probes for unambiguous detection of mRNA using time-resolved fluorescence spectroscopy. *Nucleic Acids Res*. 2006;34(10):3161-3168.
43. Santangelo PJ, Nix B, Tsourkas A, Bao G. Dual FRET molecular beacons for mRNA detection in living cells. *Nucleic Acids Res*. 2004;32(6):e57-e57.
44. Murayama K, Kamiya Y, Kashida H, Asanuma H. Ultrasensitive molecular beacon designed with totally serinol nucleic acid (SNA) for monitoring mRNA in cells. *ChemBioChem*. 2015;16(9):1298-1301.
45. Bertucci A, Lülf H, Septiadi D, Manicardi A, Corradini R, De Cola L. Intracellular Delivery of Peptide Nucleic Acid and Organic Molecules Using Zeolite-L Nanocrystals. *Adv Healthc Mater*. 2014;3(11):1812-1817.

46. Ryoo S-R, Yim Y, Kim Y-K, et al. High-throughput chemical screening to discover new modulators of microRNA expression in living cells by using graphene-based biosensor. *Sci Rep*. 2018;8(1):11413.
47. Rossetti R, Nakahara S, Brus LE. Quantum size effects in the redox potentials, resonance Raman spectra, and electronic spectra of CdS crystallites in aqueous solution. *J Chem Phys*. 1983;79(2):1086-1088.
48. Murray CB, Kagan CR, Bawendi MG. Synthesis and Characterization of Monodisperse Nanocrystals and Close-Packed Nanocrystal Assemblies. *Annu Rev Mater Sci*. 2000;30(1):545-610.
49. Tsoi KM, Dai Q, Alman BA, Chan WCW. Are Quantum Dots Toxic? Exploring the Discrepancy Between Cell Culture and Animal Studies. *Acc Chem Res*. 2013;46(3):662-671.
50. Austin M. Derfus, Warren C. W. Chan and, Bhatia SN. Probing the Cytotoxicity of Semiconductor Quantum Dots. *Nano letters*, 2003;*4*(1), 11-18.
51. Li H, He X, Kang Z, et al. Water-Soluble Fluorescent Carbon Quantum Dots and Photocatalyst Design. *Angew Chemie Int Ed*. 2010;49(26):4430-4434.
52. Li L, Yan X. Colloidal Graphene Quantum Dots. *J Phys Chem Lett*. 2010;1(17):2572-2576.
53. Shamsipur M, Nasirian V, Mansouri K, Barati A, Veisi-Raygani A, Kashanian S. A highly sensitive quantum dots-DNA nanobiosensor based on fluorescence resonance energy transfer for rapid detection of nanomolar amounts of human papillomavirus 18. *J Pharm Biomed Anal*. 2017;136:140-147.
54. Ge L, Sun X, Hong Q, Li F. Ratiometric NanoCluster Beacon: A Label-Free and Sensitive Fluorescent DNA Detection Platform. *ACS Appl Mater Interfaces*. 2017;9(15):13102-13110.
55. Bülbül G, Hayat A, Mustafa F, Andreescu S. DNA assay based on Nanoceria as Fluorescence Quenchers (NanoCeracQ DNA assay). *Sci Rep*. 2018;8(1):2426.
56. Wang S, Zhang Y, Ning Y, Zhang G-J. A $WS_2$ nanosheet-based platform for fluorescent DNA detection via PNA–DNA hybridization. *Analyst*. 2015;140(2):434-439.
57. Wang H-S, Liu H-L, Wang K, et al. Insight into the Unique Fluorescence Quenching Property of Metal-Organic Frameworks upon DNA Binding. *Anal Chem*. 2017;89(21):11366-11371.
58. Loo AH, Sofer Z, Bouša D, Ulbrich P, Bonanni A, Pumera M. Carboxylic Carbon Quantum Dots as a Fluorescent Sensing Platform for DNA Detection. *ACS Appl Mater Interfaces*. 2016;8(3):1951-1957.
59. Yew YT, Loo AH, Sofer Z, Klímová K, Pumera M. Coke-derived graphene quantum dots as fluorescence nanoquencher in DNA detection. *Appl Mater Today*. 2017;7:138-143.
60. Qian ZS, Shan XY, Chai LJ, Ma JJ, Chen JR, Feng H. A universal fluorescence sensing strategy based on biocompatible graphene quantum dots and graphene oxide for the detection of DNA. *Nanoscale*. 2014;6(11):5671-5674.

61. Park KW, Lee CY, Batule BS, Park KS, Park HG. Ultrasensitive DNA detection based on target-triggered rolling circle amplification and fluorescent poly(thymine)-templated copper nanoparticles. *RSC Adv*. 2018;8(4):1958-1962.
62. Wang R, Tombelli S, Minunni M, Spiriti MM, Mascini M. Immobilisation of DNA probes for the development of SPR-based sensing. *Biosens Bioelectron*. 2004;20(5):967-974.
63. Zezza F, Pascale M, Mulè G, Visconti A. Detection of Fusarium culmorum in wheat by a surface plasmon resonance-based DNA sensor. *J Microbiol Methods*. 2006;66(3):529-537.
64. Prabhakar N, Arora K, Arya SK, et al. Nucleic acid sensor for M. tuberculosis detection based on surface plasmon resonance. *Analyst*. 2008;133(11):1587-1592.
65. Nawattanapaiboon K, Kiatpathomchai W, Santanirand P, et al. SPR-DNA array for detection of methicillin-resistant Staphylococcus aureus (MRSA) in combination with loop-mediated isothermal amplification. *Biosens Bioelectron*. 2015;74:335-340.
66. Xiaodi Su, Ying-Ju Wu, Rudolf Robelek and, Wolfgang Knoll. Surface Plasmon Resonance Spectroscopy and Quartz Crystal Microbalance Study of Streptavidin Film Structure Effects on Biotinylated DNA Assembly and Target DNA Hybridization. *Langmuir*, 2004;*21*(1), 348-353.
67. Chu LQ, Förch R, Knoll W. Surface-plasmon-enhanced fluorescence spectroscopy for DNA detection using fluorescently labeled PNA as “DNA indicator.” *Angew Chemie - Int Ed*. 2007;46(26):4944-4947.
68. Xu F, Pellino AM, Knoll W. Electrostatic repulsion and steric hindrance effects of surface probe density on deoxyribonucleic acid (DNA)/peptide nucleic acid (PNA) hybridization. *Thin Solid Films*. 2008;516(23):8634-8639.
69. Macedo LJA, Miller EN, Opdahl A. Effect of Probe–Probe Distance on the Stability of DNA Hybrids on Surfaces. *Anal Chem*. 2017;89(3):1757-1763.
70. Tawa K, Yao D, Knoll W. Matching base-pair number dependence of the kinetics of DNA–DNA hybridization studied by surface plasmon fluorescence spectroscopy. *Biosens Bioelectron*. 2005;21(2):322-329.
71. Su Q, Nöll G. A sandwich-like strategy for the label-free detection of oligonucleotides by surface plasmon fluorescence spectroscopy (SPFS). *Analyst*. 2016;141(20):5784-5791.
72. Santos GM, Zhao F, Zeng J, Li M, Shih W-C. Label-free, zeptomole cancer biomarker detection by surface-enhanced fluorescence on nanoporous gold disk plasmonic nanoparticles. *J Biophotonics*. 2015;8(10):855-863.
73. Yi-Ping Ho, Matthew C. Kung, Samuel Yang and, Tza-Huei Wang. Multiplexed Hybridization Detection with Multicolor Colocalization of Quantum Dot Nanoprobes. *Nano Letters*, 2005;*5*(9), 1693-1697.
74. Rudolf Robelek, Lifang Niu, Evelyne L. Schmid and, Wolfgang Knoll. Multiplexed Hybridization Detection of Quantum Dot-Conjugated DNA Sequences Using Surface Plasmon Enhanced Fluorescence Microscopy and Spectrometry. *Analytical chemistry*, 2004; *76*(20), 6160-6165.
75. Zhang D, Yan Y, Cheng W, et al. Streptavidin-enhanced surface plasmon

resonance biosensor for highly sensitive and specific detection of microRNA. *Microchim Acta*. 2013;180(5-6):397-403.
76. Ding X, Yan Y, Li S, et al. Surface plasmon resonance biosensor for highly sensitive detection of microRNA based on DNA super-sandwich assemblies and streptavidin signal amplification. *Anal Chim Acta*. 2015;874:59-65.
77. D'Agata R, Corradini R, Grasso G, Marchelli R, Spoto G. Ultrasensitive Detection of DNA by PNA and Nanoparticle-Enhanced Surface Plasmon Resonance Imaging. *ChemBioChem*. 2008;9(13):2067-2070.
78. Qian S, Lin M, Ji W, et al. Boronic Acid Functionalized Au Nanoparticles for Selective MicroRNA Signal Amplification in Fiber-Optic Surface Plasmon Resonance Sensing System. *ACS Sensors*. 2018;3(5):929-935.
79. Su X, Wu Y-J, Knoll W. Comparison of surface plasmon resonance spectroscopy and quartz crystal microbalance techniques for studying DNA assembly and hybridization. *Biosens Bioelectron*. 2005;21(5):719-726.
80. Bunroddith K, Viseshakul N, Chansiri K, Lieberzeit P. QCM-based rapid detection of PCR amplification products of Ehrlichia canis. *Anal Chim Acta*. 2018;1001:106-111.
81. Wang D, Tang W, Wu X, et al. Highly selective detection of single-nucleotide polymorphisms using a quartz crystal microbalance biosensor based on the toehold-mediated strand displacement reaction. *Anal Chem*. 2012;84:7008-7014.
82. Zhao Y, Wang H, Tang W, Hu S, Li N, Liu F. An in situ assembly of a DNA–streptavidin dendrimer nanostructure: a new amplified quartz crystal microbalance platform for nucleic acid sensing. *Chem Commun*. 2015;51(53):10660-10663.
83. Abdul Rasheed P, Sandhyarani N. Quartz crystal microbalance genosensor for sequence specific detection of attomolar DNA targets. *Anal Chim Acta*. 2016;905:134-139.
84. Toren P, Ozgur E, Bayindir M. Real-Time and Selective Detection of Single Nucleotide DNA Mutations Using Surface Engineered Microtoroids. *Anal Chem*. 2015;87(21):10920-10926.
85. Bertucci A, Manicardi A, Candiani A, et al. Detection of unamplified genomic DNA by a PNA-based microstructured optical fiber (MOF) Bragg-grating optofluidic system. *Biosens Bioelectron*. 2015;63:248-254.
86. Khemthongcharoen N, Wonglumsom W, Suppat A, Jaruwongrungsee K, Tuantranont A, Promptmas C. Piezoresistive microcantilever-based DNA sensor for sensitive detection of pathogenic Vibrio cholerae O1 in food sample. *Biosens Bioelectron*. 2015;63:347-353.
87. Domínguez CM, Kosaka PM, Sotillo A, Mingorance J, Tamayo J, Calleja M. Label-Free DNA-Based Detection of *Mycobacterium tuberculosis* and Rifampicin Resistance through Hydration Induced Stress in Microcantilevers. *Anal Chem*. 2015;87(3):1494-1498.
88. Feng Y, Wang Q, Lei J, Ju H. Electrochemiluminescent DNA sensing using carbon nitride nanosheets as emitter for loading of hemin labeled single-stranded DNA. *Biosens Bioelectron*. 2015;73:7-12.
89. Wang Y, Shan D, Wu G, et al. A novel "dual-potential" ratiometric

electrochemiluminescence DNA sensor based on enhancing and quenching effect by G-quadruplex / hemin and Au-Luminol bifunctional nanoparticles. *Biosens Bioelectron*. 2018;106:64-70.
90. Liu L, Wang X, Ma Q, et al. Multiplex electrochemiluminescence DNA sensor for determination of hepatitis B virus and hepatitis C virus based on multicolor quantum dots and Au nanoparticles. *Anal Chim Acta*. 2016;916:92-101.
91. Yang L, Tao Y, Yue G, et al. Highly Selective and Sensitive Electrochemiluminescence Biosensor for p53 DNA Sequence Based on Nicking Endonuclease Assisted Target Recycling and Hyperbranched Rolling Circle Amplification. *Anal Chem*. 2016;88(10):5097-5103.
92. Zhang P, Li Z, Wang H, Zhuo Y, Yuan R, Chai Y. DNA nanomachine-based regenerated sensing platform: a novel electrochemiluminescence resonance energy transfer strategy for ultra-high sensitive detection of microRNA from cancer cells. *Nanoscale*. 2017;9(6):2310-2316.
93. Joseph Wang, Danke Xu, Abdel-Nasser Kawde and, Polsky R. Metal Nanoparticle-Based Electrochemical Stripping Potentiometric Detection of DNA Hybridization. *Analytical chemistry*, 2001;*73*(22), 5576-5581.
94. Nakano K, Kimura T, Kitamura Y, Ihara T, Ishimatsu R, Imato T. Potentiometric DNA sensing platform using redox-active DNA probe pair for sandwich-type dual hybridization at indicator electrode surface. *J Electroanal Chem*. 2014;720-721:71-75.
95. Wu J, Chumbimuni-Torres KY, Galik M, Thammakhet C, Haake DA, Wang J. Potentiometric Detection of DNA Hybridization using Enzyme-Induced Metallization and a Silver Ion Selective Electrode. *Anal Chem*. 2009;81(24):10007-10012.
96. Apon Numnuam, Karin Y. Chumbimuni-Torres, Yun Xiang, et al. Potentiometric Detection of DNA Hybridization. *Analytical chemistry*, 2007;*81*(24), 10007-10012.
97. Hüsken N, Gębala M, Schuhmann W, Metzler-Nolte N. A single-electrode, dual-potential ferrocene-PNA biosensor for the detection of DNA. *ChemBioChem*. 2010;11(12):1754-1761.
98. Idili A, Amodio A, Vidonis M, Feinberg-Somerson J, Castronovo M, Ricci F. Folding-Upon-Binding and Signal-On Electrochemical DNA Sensor with High Affinity and Specificity. *Anal Chem*. 2014;86(18):9013-9019.
99. Shin S, Won BY, Jung C, et al. Electrochemical detection of DNA mutations on a PNA-modified electrode utilizing a single-stranded DNA specific endonuclease. *Chem Commun*. 2011;47(23):6611-6613.
100. Liu X, Qu X, Fan H, Ai S, Han R. Electrochemical detection of DNA hybridization using a water-soluble branched polyethyleneimine-cobalt(III)-phenanthroline indicator and PNA probe on Au electrodes. *Electrochim Acta*. 2010;55(22):6491-6495.
101. Montiel VR-V, Torrente-Rodríguez RM, Rivera GG de, et al. Amperometric determination of hazelnut traces by means of Express PCR coupled to magnetic beads assembled on disposable DNA sensing scaffolds. *Sensors Actuators B Chem*. 2017;245:895-902.

102. Zeng D, Zhang H, Zhu D, et al. A novel ultrasensitive electrochemical DNA sensor based on double tetrahedral nanostructures. *Biosens Bioelectron*. 2015;71:434-438.
103. Ölcer Z, Esen E, Ersoy A, et al. Microfluidics and nanoparticles based amperometric biosensor for the detection of cyanobacteria (Planktothrix agardhii NIVA-CYA 116) DNA. *Biosens Bioelectron*. 2015;70:426-432.
104. Wan Y, wang P, Su Y, et al. Ultrasensitive electrochemical DNA sensor based on the target induced structural switching and surface-initiated enzymatic polymerization. *Biosens Bioelectron*. 2014;55:231-236.
105. Teengam P, Siangproh W, Tuantranont A, Vilaivan T, Chailapakul O, Henry CS. Electrochemical impedance-based DNA sensor using pyrrolidinyl peptide nucleic acids for tuberculosis detection. *Anal Chim Acta*. July 2018.
106. Ribovski L, Zucolotto V, Janegitz BC. A label-free electrochemical DNA sensor to identify breast cancer susceptibility. *Microchem J*. 2017;133:37-42..
107. Wu S, Ye W, Yang M, et al. Impedance sensing of DNA immobilization and hybridization by microfabricated alumina nanopore membranes. *Sensors Actuators B Chem*. 2015;216:105-112.
108. Liu Y, Hedström M, Chen D, Fan X, Mattiasson B. A capacitive DNA sensor-based test for simple and sensitive analysis of antibiotic resistance in field setting. *Biosens Bioelectron*. 2015;64:255-259.
109. Chen Y-W, Tai T-Y, Hsu C-P, et al. Direct detection of DNA using electrical double layer gated high electron mobility transistor in high ionic strength solution with high sensitivity and specificity. *Sensors Actuators B Chem*. 2018;271:110-117.
110. Lin M-Y, Hsu W-Y, Yang Y-S, Huang J-W, Chung Y-L, Chen H. Immobilized rolling circle amplification on extended-gate field-effect transistors with integrated readout circuits for early detection of platelet-derived growth factor. *Anal Bioanal Chem*. 2016;408(17):4785-4797.
111. Park M-H, Han D, Chand R, Lee D-H, Kim Y-S. Mechanism of Label-Free DNA Detection Using the Floating Electrode on Pentacene Thin Film Transistor. *J Phys Chem C*. 2016;120(9):4854-4859.
112. Hwang MT, Wang Z, Ping J, et al. DNA Nanotweezers and Graphene Transistor Enable Label-Free Genotyping. *Adv Mater*. July 2018:1802440.
113. Xu S, Jiang S, Zhang C, et al. Ultrasensitive label-free detection of DNA hybridization by sapphire-based graphene field-effect transistor biosensor. *Appl Surf Sci*. 2018;427:1114-1119.
114. Cai B, Wang S, Huang L, Ning Y, Zhang Z, Zhang GJ. Ultrasensitive label-free detection of PNA-DNA hybridization by reduced graphene oxide field-effect transistor biosensor. *ACS Nano*. 2014;8(3):2632-2638.
115. Tran TL, Nguyen TT, Huyen Tran TT, Chu VT, Thinh Tran Q, Tuan Mai A. Detection of influenza A virus using carbon nanotubes field effect transistor based DNA sensor. *Phys E Low-dimensional Syst Nanostructures*. 2017;93:83-86.
116. Gao Z, Xia H, Zauberman J, et al. Detection of Sub-fM DNA with Target Recycling and Self-Assembly Amplification on Graphene Field-Effect

Biosensors. *Nano Lett*. 2018;18(6):3509-3515.
117. Heitzer E, Ulz P, Geigl JB. Circulating tumor DNA as a liquid biopsy for cancer. *Clin Chem*. 2015;61(1):112-123.
118. Toiyama Y, Okugawa Y, Fleshman J, Richard Boland C, Goel A. MicroRNAs as potential liquid biopsy biomarkers in colorectal cancer: A systematic review. *Biochim Biophys Acta - Rev Cancer*. May 2018.
119. Crowley E, Di Nicolantonio F, Loupakis F, Bardelli A. Liquid biopsy: monitoring cancer-genetics in the blood. *Nat Rev Clin Oncol*. 2013;10(8):472-484.
120. Cohen JD, Li L, Wang Y, et al. Detection and localization of surgically resectable cancers with a multi-analyte blood test. *Science*. 2018;359(6378):926-930.

# 2- DNA ANALOGS AND PEPTIDE NUCLEIC ACIDS: SYNTHETIC ASPECTS

Abstract:

In this chapter a brief introduction to DNA synthesis will be followed by explanation of synthesis and application of several synthetic DNAs focusing on Peptide Nucleic Acids (PNA). Generally, synthetic probes offer more possibility of tuning with reporter or active molecules and guarantee better performance in application, both therapeuctics and diagnostic.

## 2.1 DNA/RNA SYNTHESIS

A scheme of deoxyribose involved in nucleoside formation, nucleobases structure and atom numbers is shown in Figure 2.1.

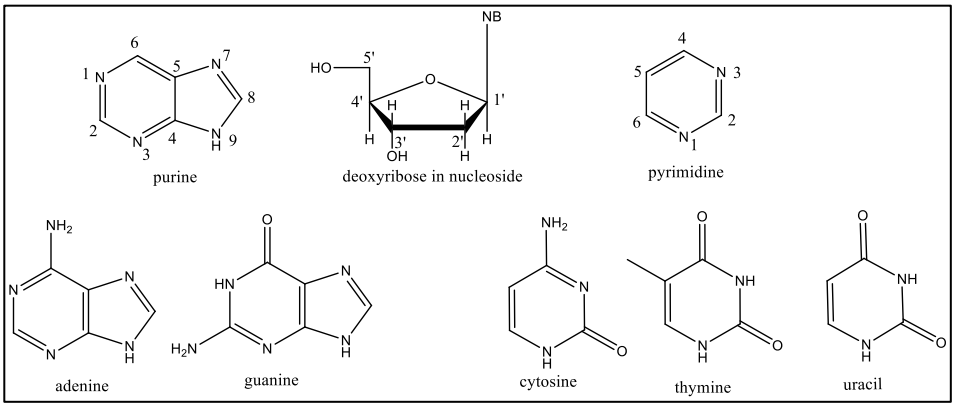


**Figure 2.2.1: Up: atoms number of purines bases, pyrimidines bases and deoxyribose. Bottom: the five nucleobases present in DNA and, far right, uracil that is present in RNA instead of thymine.**

DNA chemical synthesis is a mild and controlled procedure because the bond between nucleobases and sugar moiety can be broken, nucleobases are prone to alkylation, oxidation or reduction, and phosphodiester bonds can be hydrolyzed. The hydroxyl group in position 2' promotes this hydrolysis, which is the reason why RNA is less stable than DNA. The natural synthesis of DNA

involves 5’ triphosphate nucleotides, and the chain growth is from 5’ to 3’ end. In chemical non-enzymatic synthesis the preferred direction is 3’ to 5’, because in 5’ position there is a primary alcohol that is more nucleophilic that the secondary alcohol present at 3’ position. In solution synthesis, 3’ position is protected by an acetic or benzoic ester. These groups are basic-sensitive, so 5’ end have to been protected with an orthogonal protective group (PG) such as 4,4'-dimethoxytrityl (DMT). In solid phase synthesis (SPS), 3’ of the first nucleotide is anchored to the resin. Semi-permanent PGs are used to protect heterocyclic nitrogen of nucleobases. Different coupling methodologies have been developed: phosphotriester, H-phosphonate and phosphoramidite. The latter is the most widely used, because P(III) is more reactive than P(V), so it will be the one treated in detail in its version for solid phase synthesis (SPS). A scheme of DNA solid phase synthesis is reported in Figure 2.2.

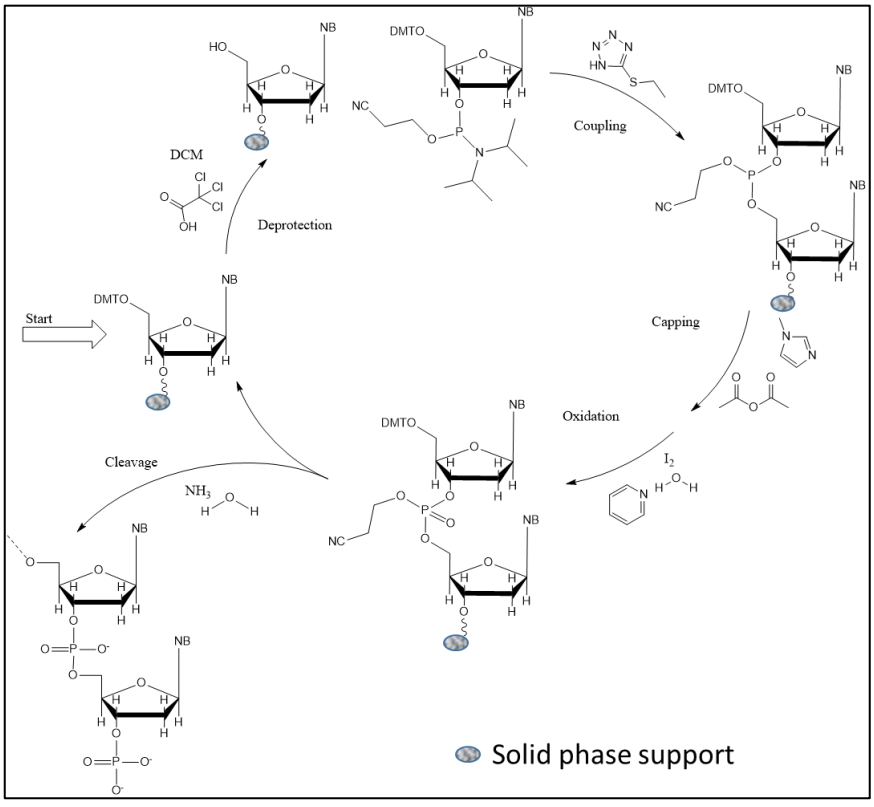


**Figure 2.2: Scheme of DNA synthesis on sold phase. For details, see text.**

The phosphoramidite monomer is prepared in one of the three sequent way: 1) the most used method[1] involves reaction of a protected nucleoside with a single free OH group with phosphorodiamidite under a mild acid catalysis. Some bisamidites were reported as thermally unstable compounds, but 2-cyanoethyl *N,N,N′,N′*-tetraisopropylphosphorodiamidite, the amidite used to prepare commercial nucleoside phosphoramidites, is relatively stable[2] and also give selectivity to the coupling reaction. 2) The second method[3] involve phosphorochloridite that reacts with the protected nucleoside in the presence of a sterically hindered organic base, usually *N*-ethyl-*N,N*-diisopropylamine (Hunig's base or DIPEA). 3) In the third method[4], the protected nucleoside is treated with chloro *N,N,N′,N′*-tetraisopropyl phosphorodiamidite in presence of DIPEA to form a protected nucleoside diamidite. The latter is let react with 2-cyanoethanol in the presence of a weak acid.

Resins for SPS could be of various nature: controlled-pore glass beads[5], polystyrene-grafted poly(tetrafluoroethylene)[6], catechol-based support[7]. The first step of the synthesis is deprotection of DMT, the PG of 5'-OH. DMT is acid sensitive: 5'-OH can be protonated and subsequently eliminate the tertiary carbocation. Deprotection is normally achieved by treatment with 3% dicholoroacetic acid or 2% of trichloroacetic acid in toluene or dichloromethane (DCM). The eliminated DTM cation is orange and, by a spectrophotometer, it is possible to determine the yield of deprotection. A solution too concentrated of acid or a too long time of deprotection leads to depurination and hence, lowers the yield of the final oligonucleotide.

The second step involves coupling with the deprotected monomer on the resin and a new phosphoramidite monomer, usually dissolved in acetonitrile (ACN); the reaction is promoted by activation of the phosphoramidite with an acidic azole catalyst[8] (1H-tetrazole, 5-ethylthio-1H-tetrazole[9], 2-benzylthiotetrazole[10], 4,5-dicyanoimidazole[11], or several others). Usually, for a little scale of synthesis, a high excess of phosphoramidites is necessary. A phosphite triester is formed in this reaction step. The coupling of 2'-deoxynucleoside phosphoramidites is very rapid and requires, on small scale, only 20 s for its completion. For RNA synthesis, the same scheme is followed, with the exception that the OH in position 2' have to been protected, with t-butyldimethylsilyl (TBDMS)[12] or with tri-iso-propylsilyloxymethyl (TOM)[13], both removable by treatment with fluoride ion[14]. This protection generate sterically hindrance and so the coupling times rise to 15 minutes for a complete reaction[15]. The reaction has to be performed in anhydrous environment. After the coupling, a capping step is performed for blocking eventually unreacted

nucleotides on the solid phase (0.1 to 1%). This prevent the formation of oligonucleotides with an internal base deletion, not separable by the wanted oligomer. The eventually unreacted free OH in position 5' is capped by treating with a mixture of acetic anhydride and 1-methylimidazole, rarely 4-dimethylaminopyridine (DMAP) is used as catalyst. Moreover, phosphoramidites activated with 1H-tetrazole can react, in little percentage, with the oxygen in position 6 of guanosine[16]. After the final stage of oxidation, this unwanted product can promote depurination, possibly by migration of phosphoramidites on N-7. Capping reagents can remove the O-6 modifications avoiding that the apurinic sites formed can be cleaved during the final deprotection of the oligonucleotide under the basic conditions, reducing the yield.

The tricoordinated phosphite triester linkage is not the target molecule and also shows limited stability if kept in this form for remaining steps of the synthesis. This group has to be oxidized into a tetracoordinated phosphate triester, usually by treatment with iodine and water, in the presence of a weak base, for example pyridine. Other oxidation procedures involves tert-Butyl hydroperoxide[17] in anhydrous conditions or, showing more efficiently, (1S)-(+)-(10-camphorsulfonyl)-oxaziridine (CSO)[18].

The final step of the synthesis is usually the deprotection of DMT. If the desired purification method is reversed phase HPLC DMT group should be removed after purification by treatment with 80% aqueous acetic acid for 15–30 min at room temperature. After the end of the synthesis, DNA has to be cleaved from the solid support, cyanoethyl groups have to been removed and heterocyclic nitrogen from nucleobases have to been deprotected. All these reactions can be performed in basic environment, orthogonal to DMT deprotection. Different kinds of bases and solvents can be employed, but the solid support-bound oligonucleotides should be treated with solutions of bases in an organic solvent, such as 50% triethylamine in acetonitrile[19], or 10% diethylamine in acetonitrile[20]. These treatment should be controlled because the cleavage of 2-cyanoethyl phosphate protection forms acrylonitrile as a side product, which can induce alkylation of nucleic bases. To eliminate unwanted truncation products, the oligonucleotides can be purified via polyacrylamide gel electrophoresis or anion-exchange HPLC followed by desalting. The desalting procedure is performed using ethanol precipitation, size exclusion chromatography, or reverse-phase HPLC. Characterization is usually performed with electron spray mass spectrometry (ES-MS) or matrix-assisted laser desorption/ionization time-of-flight mass spectrometry (MALDI-TOF).

## 2.2 OLIGONUCLEOTIDES MIMICS

An antisense therapy is a treatment against genetic disorder derived by infections or mutation of the genome involved in illnesses like cancer, diabetes or amyotrophic lateral sclerosis[21]. The treatment consists in blocking the mRNA that transmit the genetic information for building proteins. For achieving this blocking effect, oligo-DNA and oligo-RNA drugs are not optimal, because they are prone to nuclease degradation. In this scenario first DNA mimics were developed; some DNA variants were designed to be resistant to nuclease and at the same time capable to recruit RNase-H[22] (a type of nuclease that catalyzes the degradation of RNA in DNA:RNA duplexes). It was discovered that by substituting an oxygen atom of the phosphate group with a sulfur, thus forming a phosphorothioate, the resistance to nuclease was improved[23]. Nowadays, phosphorothioates are largely used as drugs for antisense therapy (for example Fomivirsen that is an antisense antiviral drug, used in the treatment of cytomegalovirus retinitis infections) and a lot of them are involved in clinical trials. The replacement of one non-bridging oxygen with sulfur creates a new center of chirality at phosphorus[24]. For a simple dinucleotide, a diastereomeric pair is formed that could be $R_p$ or $S_p$. They shows different chemical properties, including that $S_p$ diastereomers are more stable to enzymatic degradation than their all $R_p$ analogs[25]. Usually, diastereomeric oligonucleotides phosphorothioate are used, due to the synthetic difficulties to control the phosphorous stereochemistry. Another strategy is a careful positioning of the modified-monomers or adding more modifications in conjunction with the phosphorothioate bonds[26]. Synthesis of phosphorothioate oligonucleotides is very similar to that of natural oligonucleotides: the difference is that the oxidation step is replaced by sulfur transfer reaction (sulfurization) and that the capping step is performed after the sulfurization. There are three commonly used sulfurization reagents. 3-(Dimethylaminomethylidene)amino-3H-1,2,4-dithiazole-3-thione (DDTT)[27] provides rapid kinetics of sulfurization and high stability in solution. 3H-1,2-benzodithiol-3-one 1,1-dioxide (Beaucage reagent)[28] displays a better solubility in acetonitrile and short reaction times but show limited stability in solution. *N,N,N′N′*-Tetraethylthiuram disulfide (TETD) is well soluble in acetonitrile but the reaction time is ten time slower that other reagents. Disadvantages of first generation oligonucleotide mimics are low binding affinities, possibility of non-specific interactions and cellular toxicity in high doses that cause immune stimulation.

Other types of synthetic oligonucleotide mimics, shown in Figure 2.2.0, are 2'-O-methyl RNA, 2'-O-methoxyethyl RNA, N3'-P5'-phosphoroamidate, tricyclo-DNA, glycerol nucleic acid (GNA), threose nucleic acid (TNA), pyranosyl-RNA, cyclohexene nucleic acids (CeNA), locked nucleic acids (LNA) and morpholino phosphoroamidates (PMO). These are only some of the total, large number of synthetic mimics of DNA. All the structures shown in Figure 2.3 have similar phosphorous-based synthesis.

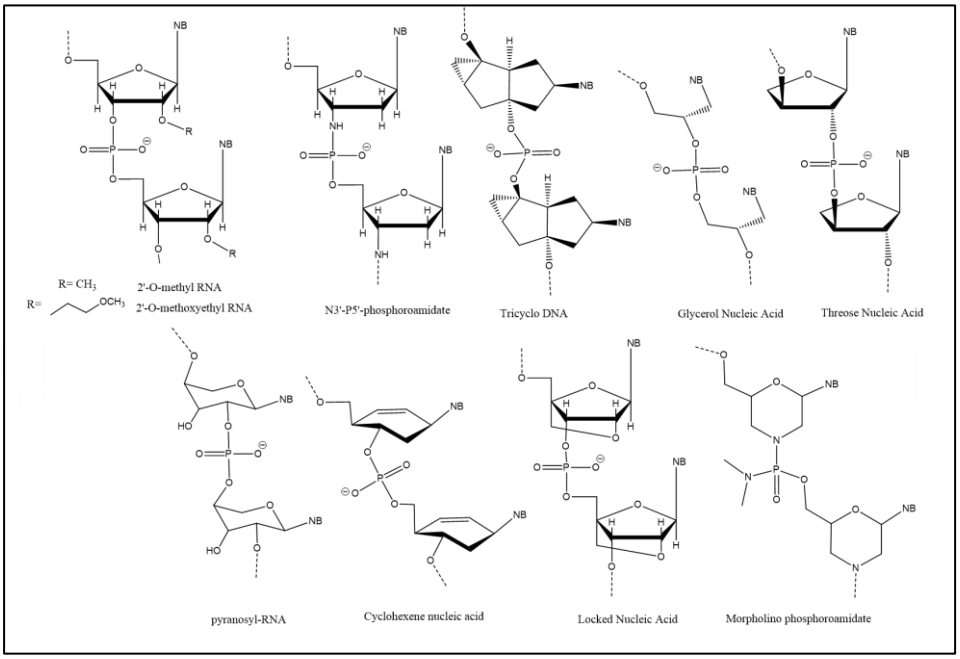


**Figure 2.3: types of synthetic oligonucleotide mimics. All of them have phosphorous backbone, only Morpholino have not negative charges in the backbone.**

2′ OMe RNA have been used for different applications, for example, they were functionalized with fluorophore moiety in order to visualize RNA in living cells[29]. Their hybridization rate is faster than that of DNA probes and in general, they are well suited for RNA detection in living cells. They have been studied both kinetically (rate of hybridization) and thermodynamically (measuring the melting temperatures, Tm)[30]. 2′-O-methyl oligoribonucleotide probes greatly enhanced Tm when bound to RNA, in fact it was shown that they can efficiently bind to double-stranded regions of structured RNA molecules. These probes were tested also for interactions with double-stranded DNA, exploiting Hoogsteen

interactions[31]. They have been used as scaffolds for molecular beacons (MB)[32], in which they shown fast kinetics, and an improved stability compared to natural nucleic acids. On the other hand, they had a slightly reduced specificity compared with other types of probes. In order to overcome this difficulty scientist have evaluated the intracellular stability of MBs composed of 2′ OMe monomers with various phosphorothioate (PS) modifications, and found that false-positive signals could be reduced when the MBs have a fully PS-modified loop domain and a phosphodiester stem[33]. In recent applications, 2′ OMe RNA have been used for aptamer sensing[34]. 2'-O-methoxyethyl (MOE) RNA was used for in-vivo treatment of spinal muscular atrophy;[35] in this study the 2'OMOE structure resulted as the best-performing type of antisense oligonucleotide, with a duration after the treatment in central nervous system of mice of six months. At higher concentration 2'-O-methoxyethyl RNA chimeras were found toxic in macaques monkeys[36], but preliminary test on human healthy volunteers indicates no toxicity for a proper dose of antisense drug. Other test[37] found that these RNA mimics accumulate in the kidney and metabolites are cleared in urine, no significant difference were found on healthy state of patients treated with such drug compared to placebo test. Modification in 2' with other group, such as 2′-O-methyldithiomethyl[38] was used for gene silencing. Moreover, a modified RNA as previously mentioned can be converted into unmodified RNA under reducing conditions in cells: Reducing-Environment-Dependent Uncatalyzed Chemical Transforming RNA (REDUCT RNA).

N3'-P5'-phosphoroamidate chimeras are formed following a different pathway than traditional SPS of DNA[39]: a H-phosphonate group is added at 5' oxygen of deoxyribose of the growing chain and then a 5'-DMT-3'-aminonucleoside is added. Another strategy provides use of standard phosphoramidite moiety, attached to 5'-oxygen; the reaction with 5'-DMT-3'-aminonucleoside is an amine-exchange reaction[40]. This method generates yields for each cycle of 92–95% range, and overall yields t 3–6 times higher than the previously reported. Melting temperature experiments show that these compounds form very stable duplexes with single-stranded DNA, RNA, and with themselves. The duplex thermal stability was enhanced by about 2.5 °C per modified linkage compared with natural phosphodiesters bonds. Even in physiological conditions, where natural phosphodiesters fail, N3'-P5' phosphoroamidates form stable triplexes with double-stranded DNA. Studies of duplex formation in solution show that the duplex conformation is an A-type helix that is different from DNA canonical B-type helix[41]. The sugar ring-conformation changes from predominantly C2′-

endo to C3′-endo when a phosphoroamidate group replaces the 3′-phosphoester (see Figure 2.4).

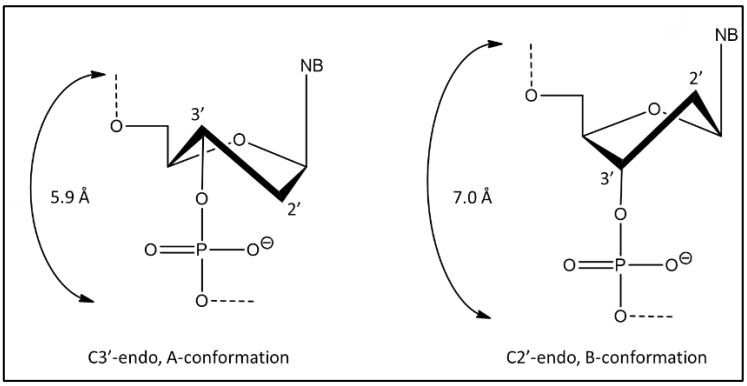


**Figure 2.4: A and B conformations of double helix correspond respectively to C3'-endo and C2'-endo conformation of deoxyribose moiety.**

For what concern the use of N3'-P5'-phosphoroamidate as drugs, it was demonstrated that they are more potent antisense agents in vivo than phosphorothioate derivatives[42]. Myeloid leukemia cells were injected in immunodeficiency mice and a treatment with equal doses of either phosphoramidate or phosphorothioate was performed. Experimental evidences showed that both oligonucleotides were efficiently taken up by leukemic cells in vivo. Survival of the phosphoramidate-treated mice was significantly longer than that of the phosphorothioate-treated mice even if both types showed the same tissue distribution. Lipid-modified N3′-P5′ thio-phosphoramidate oligonucleotide have been tested as inhibitors of telomerase activity for cancer therapy. The action of modified-antisense drug is major compared to non-conjugated thio-phosphoramidate sequence[43].

The DNA analogue tricyclo-DNA[44], differs structurally from DNA by an additional ethylene bridge between the centers C3‘ and C5‘ of the nucleosides, to which a cyclopropane unit is fused for further enhancement of structural rigidity. It can be synthesized from the corresponding phosphoramidites by conventional solid-phase cyanoethyl phosphoramidite chemistry. 5‘-end phosphorylated tricyclo-DNA sequences are chemically stable in aqueous environment, with neutral pH in a wide range of temperatures and have shown resistance to phosphodiesterase enzymatic hydrolysis. The tricyclo-DNA duplexes show higher Tm than the corresponding bicyclo-DNA duplexes,

confirming the fact that the first have a “preorganized” structure that thermodynamically favor hybridization[45]. According to data from circular dichroism (CD), duplex with tricyclo-DNA are preferably in A-conformation. Triple-helix stability depends on the sequence composition and can be higher when compared to that of natural DNA. Although the synthesis of the tricyclo-DNA oligomers follow a well-established strategy, the synthesis of the monomer is quite difficult and requires many steps, so new pathway are currently searched[46]. Their activity as antisense agent was tested[47]. Systematically incorporated tricyclo-DNA units at various positions in a small interfering RNA duplex (siRNA) was tested for silencing gene activity. It was found that the best position for the modified nucleotide unit is in the center of the sequence[48]. In addition, this modified structure was tested for the correction of muscular dystrophy in mouse models with success[49].

Glycerol nuclei acids (GNA) have been discover in 2005 by Zhang et al[50]. A chiral carbon is present in this synthetic oligonucleotide, so either R or S configuration can be used. Its synthesis is carried out starting by commercial glycidol[51]: an initial protection of OH-group with DMT is followed by the opening of the epoxide ring by a nucleophilic nitrogen of a nucleobase. This generates a secondary alcohol that can be used in the preparation of phosphoramidite monomer for SPS as shown in Figure 2.5. GNA forms duplex structure with corresponding DNA with antiparallel strands following a canonical Watson−Crick base pairing scheme. The duplex secondary structure is right-handed helical ribbon wrapped around the helix axis, resulting in a large hollow core, distinct from nucleic acids A- and B-form. GNAs have been used as templates for enzymatic replication of DNA[52] or for structural DNA origami[53].

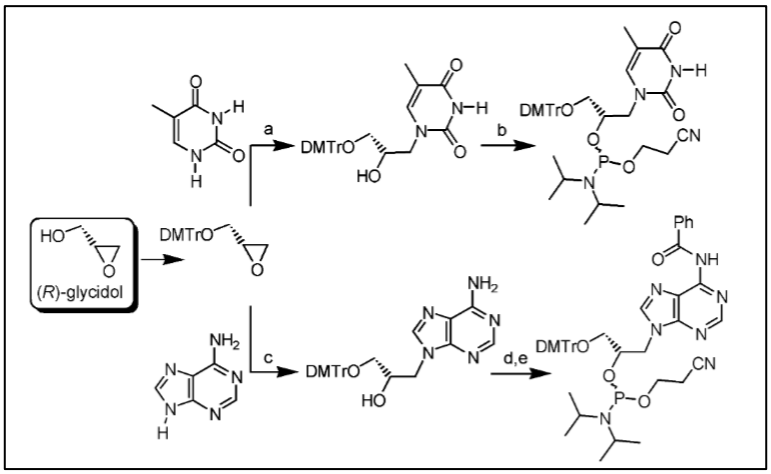


**Figure 2.5: Synthesis of glycol nucleotides for the automated solid-phase oligonucleotide synthesis. Reproduced with permission from L. Zhang et al. J. AM. CHEM. SOC., 2005 Copyright © 2005 American Chemical Society.**

TNAs (α-threofuranosyl nucleic acids) are derived from a tetrose monosaccharide, so it is structurally the simplest of all potentially natural oligonucleotide-type nucleic acid[54]. TNA monomers can be obtained in 10 synthetic steps from L-ascorbic acid, for an overall yield between 16 and 23%, depending of the nucleobase desired[55]. This nucleic acid is resistant to enzymes that promote DNA and RNA degradation, but can be used in DNA amplification because capable of transcription and retro-transcription[56]. TNAs have been used as antisense agents; remarkably, they can penetrate in cells without a transfecting agent and show no toxicity[57]. TNAs were also studied for DNA nanotechnology application such as G-quadruplex[58]: they can form stable quadruplexes like DNA in presence of $K^+$ or $Na^+$.

Pyranosyl-RNA (p-RNA) is an oligonucleotide variant in which the ribose units are in the pyranose form[59]. Monomers are linked together repetitively by phosphodiester groups between the hydroxyl groups at positions C2′ and C4′. In this oligonucleotide, base pairing is not only stronger than in DNA and RNA, but also more selective: this oligonucleotide does not form triplexes with Hoogsteen interactions. This pairing selectivity is explained with a large inclination between backbone axis and base-pair axes in p-RNA duplexes, and the higher rigidity of the p-RNA backbone compared with RNA and DNA. Despite this rigidity, p-RNA can form hairpin with a minimum of three nucleotides in the loop[60]. These synthetic oligonucleotides have been studied

by NMR spectroscopy and molecular dynamic calculations[61]; their behavior in ligation reactions was successfully tested[62].
Cyclohexenyl nucleic acid (CeNA) is a nucleic acid mimic, where the deoxyribose sugar has been replaced by cyclohexenyl moieties. CeNAs can be obtained by the classical phosphoramidite chemisty starting from protected cyclohexenyl nucleoside building blocks. In the cyclohexene unit, the conformation can change from C3' endo (N-type) to C2' endo (S-type); these changes have been detected monitoring J-coupling in 1D NMR and in NOESY spectra[63] when the CeNA unit is involved in a double helix with DNA. The two conformations are shown in Figure 2.6.

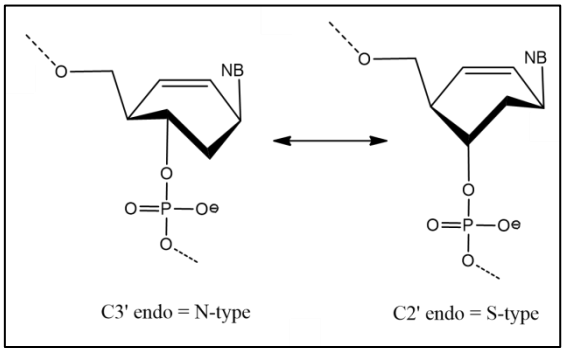


**Figure 2.6: When complementary DNA is added CeNA monomer or oligomer change conformation from N to S-type.**

This represents the first example of a synthetic nucleoside that adopts different conformations when incorporated in different double-stranded DNA sequences[64]. Different kinds of DNA polymerases from different evolutionary families were examined for their ability to incorporate CeNA in a growing chain of oligonucleotides. The best result was obtained when seven consecutive cyclohexenyl nucleotides were incorporated. Enzymes were also capable to synthetize DNA from CeNA oligomer, making this type of synthetic oligonucleotide a tool for polymerase methods[65]. CeNA have been tested as mediator for RNase-H cleavage[66] and they have been evaluated as antisense agent with other kinds of synthetic oligonucleotides[67].
A very important class of synthetic oligonucleotides are LNA (Locked Nucleic Acids). They consist in 2′-O,4′-C-methylene bicyclonucleoside monomers, and are efficiently synthesized following phosphoramidite chemistry. They form very stable complexes with DNA and RNA, with increased melting temperature from

3 up to 8°C per modified nucleotide in the chain[68]. Selectivity is also improved using fully modified LNA sequences. Differently from CeNA, these monomers are locked (as suggested by their name) in an N-type conformation that provide formation of A-type double helices. This rigid structure acts like a templanting agent, and the loss in entropy is minimal when the double helix is formed. LNA monomer is synthesized starting from 4'-C-hydroxymethyl nucleosides, whose synthesis is reported in many papers,[69,70,71] and is depicted in Figure 2.7.

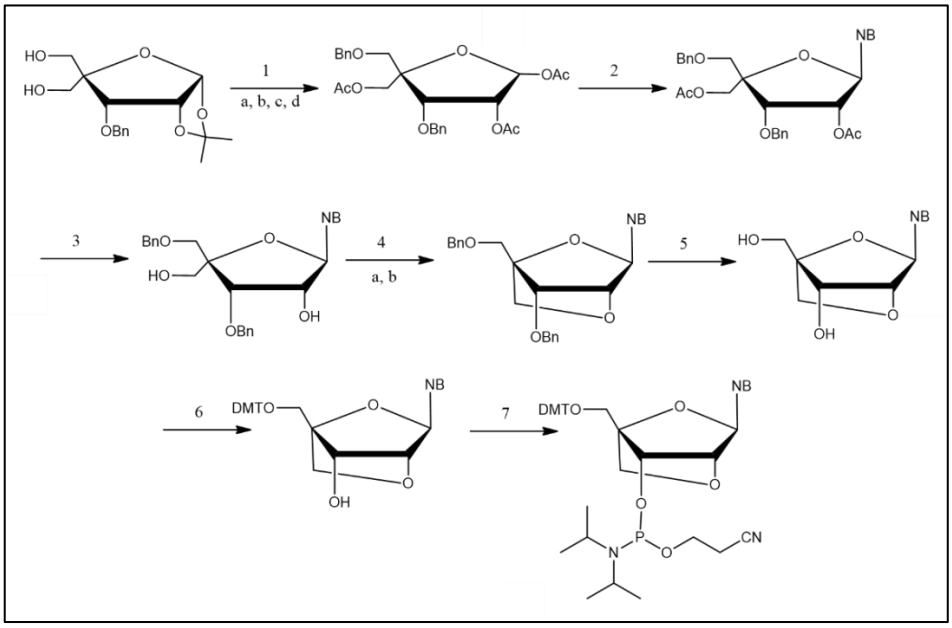


**Figure 2.7: Synthesis scheme of LNA phosphoramidite monomer. 1a) NaH, BnBr, DMF; b) acetic anhydride, pyridine; c) 80% AcOH; d) acetic anhydride, pyridine; 2) nucleobase, N,O-bis(trimethylsilyl)acetamide, TMS-triflate, ACN; 3) $NaOCH_3$ , MeOH; 4a) p-toluenesulphonyl chloride, pyridine; b) NaH, DMF; 5) $Pd(OH)_2/C$, EtOH, $H_2$; 6) DMTCl, pyridine; 7) DIPEA, 2-eyanoethyl N,N-diisoproylphosphoramidochloridite, DCM. Adapted from Koshkin et al. Tetrahedron Letter 1998.**

LNAs have been used as antisense agent, for example in cancer treatment. In fact, malign cancer cells, derived from bladder cancer, can translate across the organism because family of miRNA 130 is over-expressed and there is a bad regulation of important proteins[72]. The tested LNA was complementary to the seed region of miRNA 130 family (a little trait of RNA common to all miRNA from the same family). Results suggest that these LNA can suppress bladder cancer-cell proliferation, migration and invasion. Another example is the

blocking of mRNA associated to lung cancer genesis[73]. LNA was tested in vivo (mice) showing significant therapeutic benefit. It is also possible to use short, all LNA-oligonucleotides, from 8 to 10 monomer-long, in order to bind CUG repeat RNA and prevent the formation of toxic transcripts containing expanded CUG repeats[74]. Selectivity of LNA was tested and results showed that non-target sequence containing CUG triplet were not affected by LNA.

In order to enhance their properties not only as antisense agents but also for other kind of therapeutic or diagnostic purposes, LNA can be chemically modified. One possible modification is to replace the oxygen on C2' with a nitrogen. 2′-amino-LNA allow the addition of tags to the nitrogen, both during or after the automatic synthesis. Attachment of fluorescent groups to the 2′-amino group results in very high fluorescent quantum yields of the duplexes and remarkable sensitivity of the fluorescence signal to target binding. A classical fluorophore is pyrene, which in presence of two probes complementary to following sequence of a gene can switch from monomer to excimer fluorescence emission[75]. It is also possible to use these modified LNA to link peptides or proteins for therapeutic applications[76] or for diagnostic purposes,[77] by exploiting "click" reactions, for example the azido-alkyne cycloaddition. The Huisgen cycloaddition have been employed for linking two nucleosides, both LNA or mixed DNA-LNA. This procedure is called Isobe triazole linkage[78] (see Figure 2.8) and gives oligonucleotide with high binding affinity when incorporated at the 3′ or 5′ termini, but low binding affinity at internal positions. Antisense oligonucleotides containing this modification were tested and were showed to be highly active and resistant to nuclease activity[79]. LNA can also be a part of a longer oligonucleotide: for example their insertion in a loop of a DNA molecular beacon for detection of LAMP-amplified DNA (loop mediated isothermal amplification), gives to the system more selectivity and enhances the strength of the double helix formed[80]. Modified versions of LNAs using different nucleobase moiety were also described[81]: for instance, a fluorophore molecule was added on C5 of a thymine and characterized in terms of thermal denaturation, enzymatic stability, and fluorescence properties[82]. Results show that C5-functionalized LNA could be promising class of building blocks for RNA-targeting applications and nucleic acid diagnostics.

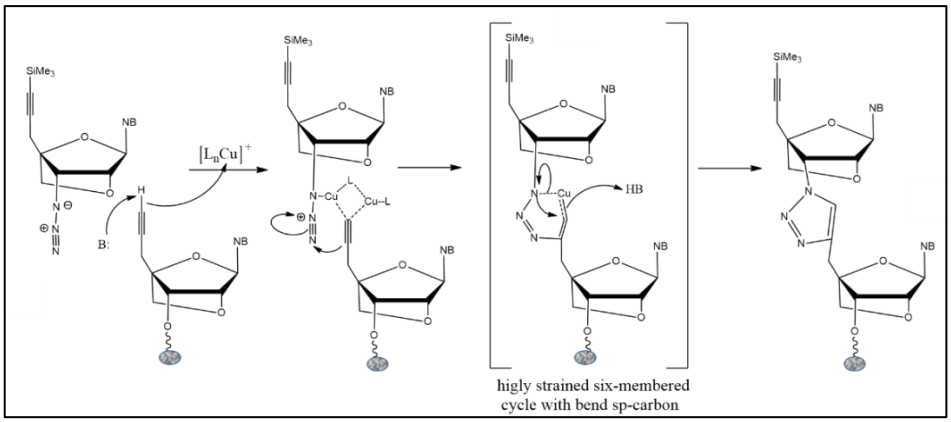


**Figure 2.8: Proposed mechanism for Cu-mediated cycloaddition in nucleotide synthesis.**

LNA oligonucleotides can cause hepatotoxicity, and this risk is currently not fully understood. In vitro screening has not yet clarified the relationship between sequence of LNA probe and hepatotoxicity[83]. Test on mice have shown the presence of two trinucleotide motifs (TCC and TGC) that were present only in hepatotoxic sequences. Motif containing sequences were more likely to bind to hepatocellular proteins in vitro and increased enzymatic stress pathway activity in vivo. A sequence of LNA that do not show toxicity is an anti-miRNA 221 LNA for antisense therapy (miRNA 221 in involved in several tumors)[84]. Experiments in vivo were conducted inoculating 25 mg/kg on mice and monkeys, studying pharmacokinetics. After a single dose, LNA was found in tissue from 2 up to 7 days after, with no toxic effect observed. At higher dosage, no toxicity was found for this LNA and HPLC-MS/MS showed that LNA-oligonucleotides have short half-life in plasma (that means minimally urine excretion) and it is rapidly uptaken by tissues.

Last but not least, DNA mimics with a phosphorous-based backbone are phosphoramidate morpholino oligomers (PMOs). These oligonucleotides have been obtained by replacement of the ribose unit with a morpholine one and the negatively charged phosphate group with a neutral phosphorodiamidate group. The monomer is obtained from treatment of natural ribonucleosides (with protected nucleobases) by an oxidation with periodate followed by a reductive amination with ammonia and sodium cyanoborohydride. The synthesis of oligomers follows the opposite direction with respect to synthetic oligonucleotides in order to exploit the nucleophilicity of the nitrogen of morpholine which is higher than that of the 5'-hydroxy group. This nitrogen is

protected with a trityl group and the hydroxyl group activated with phosphoroamidate linking agent. The monomer synthesis is described graphically in Figure 2.9. The synthesis of the oligonucleotide is performed by repeating deprotection and coupling steps, similar to phosphoramidate strategy but without oxidation step.

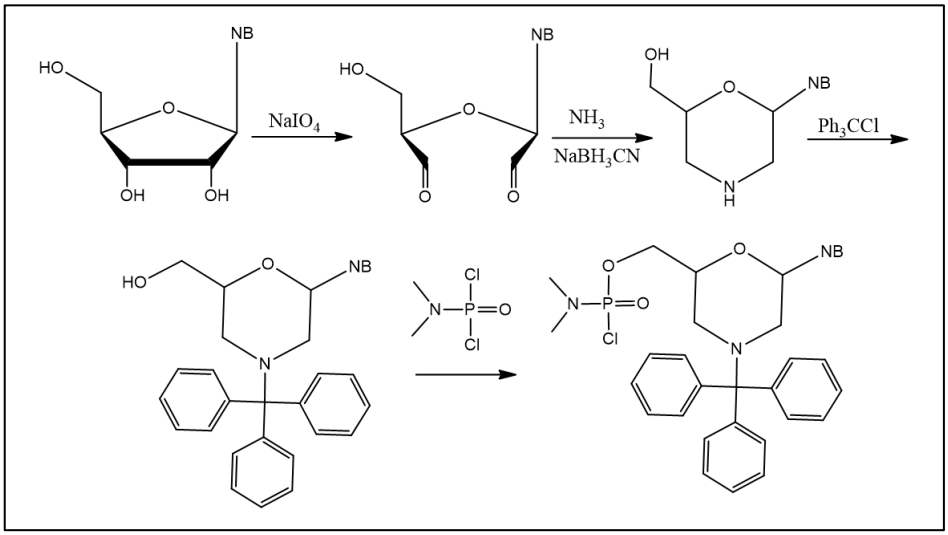


**Figure 2.9: Synthesis of phosphoramidite morpholino monomer.**

PMO shows high affinity for target DNA, promoted by Watson and Crick interaction between nucleobases but also enhanced by the lack of negative charges in the backbone. For their properties, PMO have been used in antisense therapy for tratment of tumor growth[85], spinal muscular atrophy[86], protozoa infection[87] and so on. These synthetic oligonucleotides have been also used in studies of individual gene function in cellular processes by blocking specific trait of genome[88]. For a suppression of a protein involved in cancer progression some modified PMOs for antisense therapy were tested[89]. Another approach provides the use of morpholino nucleic acid uridine phosphoramidite (instead of phosphorous diamidite) as antisense agent. [90].

Morpholinos have been used for several sensing platforms. A fluorescent sensor has been developed on silicon chip[91]. PMO was firstly immobilized to the surface of silicon by using 3-Aminopropyltriethoxysilane (APTES) as the silane coupling agent and 1,4-Phenylenediisothiocyanate (PDITC) as the cross linker. After the functionalization with an amino-terminal PMO the target DNA

was added. A fluorescence label was introduced (rhodamine B), and $Zr^{4+}$ ions, in order to form a strong binding with DNA by phosphate-zirconium-carboxylate (from rhodamine) coordination reaction. This sensor presented a good linear relationship between the fluorescence intensity and logarithm of target DNA concentrations in the range from 1 pM to 1 nM with a LOD of 4.52 pM. PMO are also widely used in conductimetric sensors, exploiting the neutral character of their backbone. One of these has been developed exploiting surface charge-induced change in conductance through a nanoporous alumina membrane[92]. The sensor's surface was modified with neutral silanes as spacers, and neutral PMO as probe. When the highly negative target DNA was captured, a strong variation in conductance could be observed. The same principle was used for the ultrasensitive detection of DNA on silicon nano-wire[93], on an opportunely functionalized gold surface[94], and miRNA in functionalized-nano-channel[95]. A limit of detection of 1 fM in PBS and 10 fM in serum sample was achieved. Ultrasensitive detection with PMO probes was also obtained by amplification of the signal by an enzymatic reaction using a sandwich approach[96]. This biosensor showed a good linear relationship between the fluorescence intensity and logarithm of single-stranded DNA concentrations in the range from 0.1 pM to 0.1 nM, with a low detection limit of 9.32 fM. The possibility to discriminate single mismatch and to analyze serum samples were tested with success.

## 2.2 PEPTIDE NUCLEIC ACIDS

In 1991 Nielsen and collaborators[97] developed a model where the deoxyribose and the phosphate backbone of DNA were substituted with achiral polyamide backbone. Then, they synthesized oligomers consisting of thymine-linked 2-aminoethylglycyl units and tested their properties. Scientist discovered that the binding efficiency with the new DNA mimic and DNA was extraordinary strong: so strong that the synthetic oligonucleotide was able to perform a strand displacement reaction in a double stranded DNA target. In that case, a PNA:DNA:PNA triplex structure was formed. It was later on discovered that also PNA: DNA duplexes formed by mixed sequences are more stable (and so have high Tm) than DNA: DNA. This is due principally to the lack of negative charges in the PNA backbone, which, avoid repulsive electrostatic interactions with the negatively charged backbones. The new molecule was named peptide nucleic acid (PNA) and in the last 27 years, it has become a widely used tool for therapeutic and diagnostic purposes. A picture of the hybridization between PNA and DNA is showed in Figure 2.10.

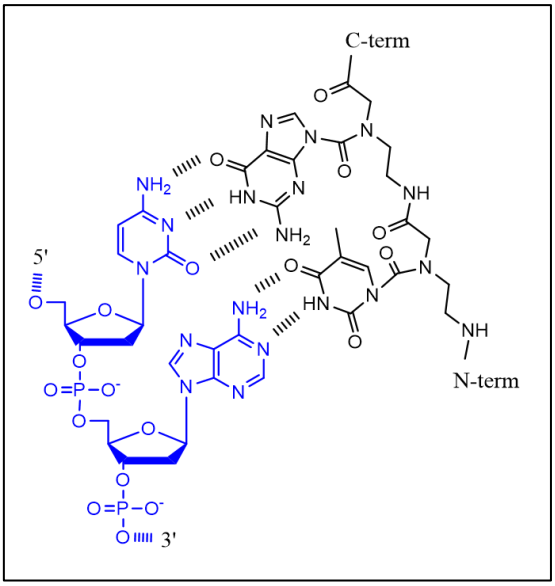


**Figure 2.10: Watson-Crick interaction between DNA (blue) and PNA (black). The duplex is more stable if the N-term of PNA is complementary to 3'-end of DNA, in an antiparallel configuration.**

The strength of the PNA: RNA duplex is higher than PNA:DNA, because, in the first case, the helical structure formed is more similar to the A-form which is preferred by RNA under physiological conditions. The most favorable orientation in a PNA:DNA duplex is antiparallel: N-term facing the 3′-end of DNA or RNA or N-term of another PNA. Moreover, PNA can form very stable triplexes with DNA exploiting both Watson-Crick and Hoogsteen interactions[98]. These hydrogen bonds are possible when PNA is constituted by pyrimidine bases and DNA has purine bases (Figure 2.11).

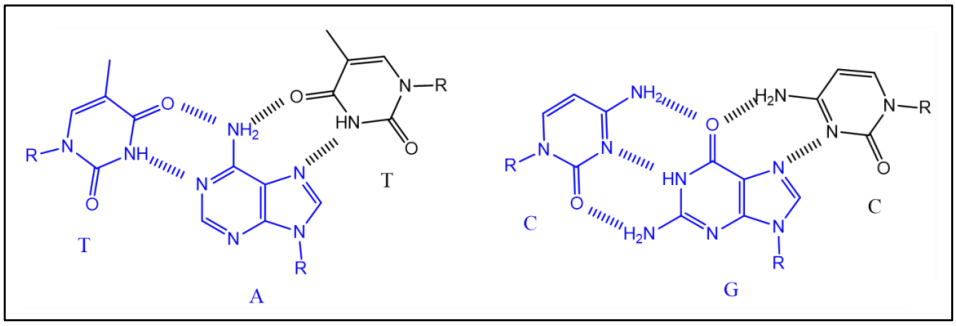


**Figure 2.11: Scheme of Watson and Crick interactions in a duplex PNA:DNA (blue color) and the formation of a triplex structure via Hoogsteen interactions with PNA (black).**

PNAs can be synthesized using solid phase synthesis (SPS), on an appropriate resin pre-loaded with the first monomer or by an amino acid. Side reactions are avoided by protecting with a semi-permanent protective group (PG) heterocyclic nitrogen of nucleobases and with a temporary protective group the primary amino function. Semi-permanent protective groups cleavage has to occur in orthogonal conditions respect the temporary PGs. This temporary protective group can be acid (Boc) or basic sensitive (Fmoc), and in the first step SPS it has to be removed. Next monomer is linked to the growing chain by formation of amide bond, after a brief activation of the carboxylic acid of the monomer exploited by activators. The active esters formed in the activation step are sensitive to water, so it is mandatory to perform the reaction is anhydrous solvent, usually DMF (*N,N*-dimethylformamide) or *N*-methylpyrrolidone(NMP). The yield of this reaction is very high, but not always quantitative. In order to avoid truncated sequences, a capping step is highly recommended to stop the wrong growing chain using acetylation of the unreacted primary amine. After the end of the synthesis and final deprotection of N-term, the oligomer is cleaved from the resin used as solid phase support.

The conditions of the cleavage are dictated by the type of resin, but usually are useful even for semi-permanent PGs deprotection. The crude reaction mixture is usually treated with diethyl ether to precipitate the PNA and separate it from organic reagents, followed by purification, normally by reverse-phase HPLC, and characterized by a mass spectrometry analysis (MALDI or ESI). Quantification is possible with an UV-vis spectrophotometer, knowing the extinction molar coefficients of nucleobases at 260nm (maximum of absorbance). A scheme of the synthesis is reported in Figure 2.12.

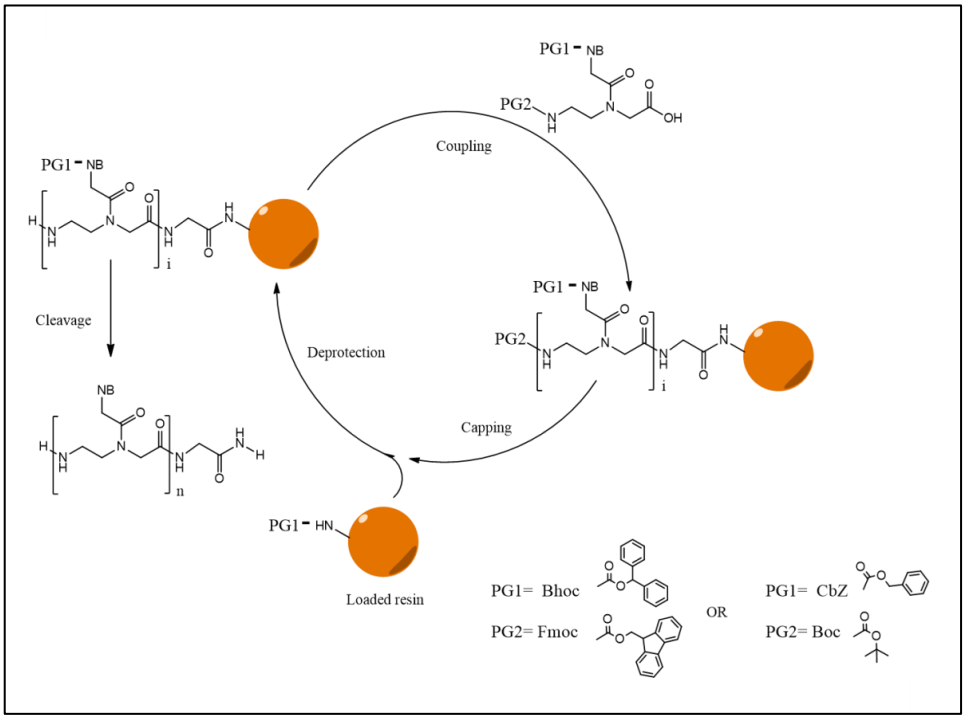


**Figure 2.12: Solid phase synthesis scheme of PNA. The two most common strategy involves semi-permanent PG1 and temporary PG2 showed.**

Using Fmoc-protecting group, it is possible to determine the loading of the resin and the yields of the synthetic steps using UV-absorbance measurements on the deprotection solution. The mechanism of Fmoc deprotection and an adsorption spectrum of resulting dibenzofulvene (absorbance versus wavelength) is showed in Figure 2.13. The Fmoc deprotection reaction in SPS is performed in a solution of 20% piperidine in DMF.

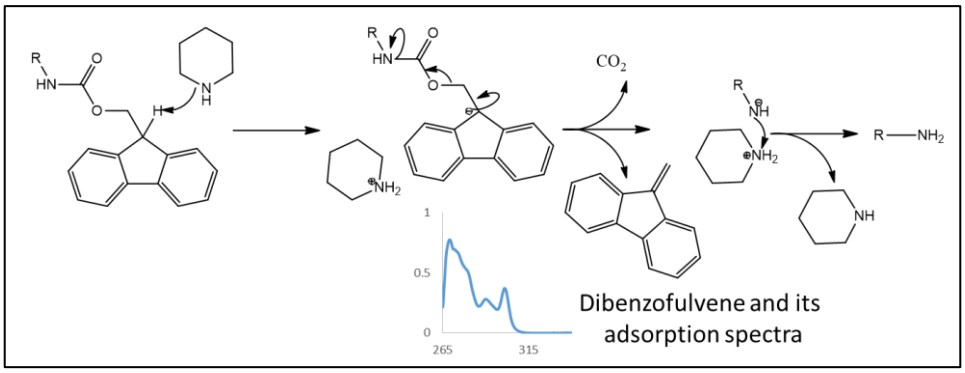


**Figure 2.13: Mechanism of Fmoc deprotection, the generated dibenzofulvene is used for evaluating resin loading or yield of deprotection/previous coupling by measuring its absorbance spectrum (absorbance in function of wavelength).**

The other principal synthesis strategy involves an acid-sensitive temporary protective group: Boc. The deprotection mixture in this case is TFA/m-cresol 95/5, where TFA is trifluoroacetic acid. This very strong acid make automatic synthesis difficult in Boc-strategy and synthesizers have shorter lifetime and have to undergo frequent maintenance.
A side-product of deprotection is tert-butyl cation, which can re-arrange to give isobutylene and a proton or can be attacked by lone pairs, for avoid this possibility m-cresol, a scavenger, is added in the mixture. The mechanism of deprotection is depicted in Figure 2.14.

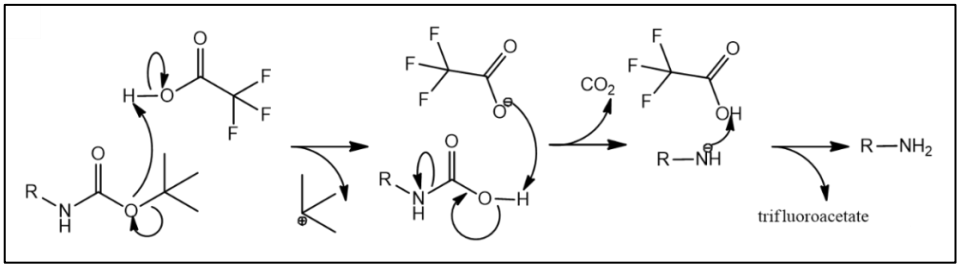


**Figure 2.14: Boc deprotection mechanism**

Another protective group that have been used for PNA synthesis is trityl group and its derivatives Mmt (methoxytrityl) and Mtt (methyltrityl)[99]. Mmt have been successfully used for synthesize PNA-DNA chimeras[100], used in duplex and triplex helices. Otherwise, it has been used as semi-permanent, acid sensitive

protective groups for nucleobases nitrogen, while Fmoc group have been used as temporary base sensitive protective group for the main chain[101]. Mtt group was exploited as Fmoc-orthogonal group in creation of libraries for protein ligand detection[102].

An easily fleeting protective group such as Trt and derivatives is useful for synthesize PNA with acid-sensitive groups such as sugar[103]. Most commonly, avoiding strong cleavage conditions in Boc synthesis is enough for preserve sensitive groups such as cyanine[104], azide[105] or alkyne.

One of the major issues in peptide chemistry is the proper choice of coupling agents. The coupling reaction is the formation of the amide bond between a deprotected N-terminal growing chain and a carboxylic moiety of the next monomer. An excess of monomer, activator and non-nucleophilic base are added to the growing chain of PNA. The mechanism of HBTU activation is depicted in Figure 2.15, while some activators and additives for coupling reactions[107] are shown in Table 2.1.

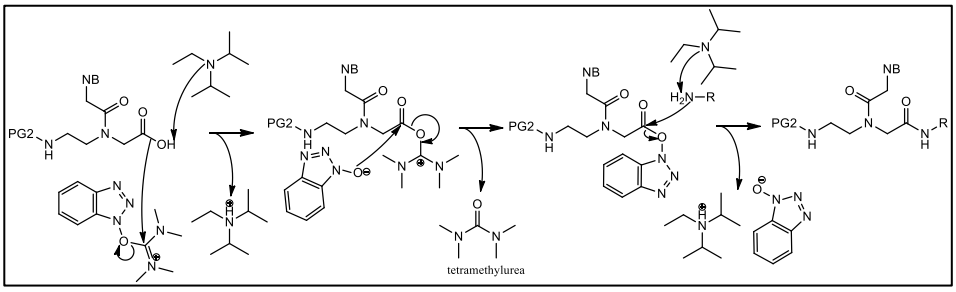


**Figure 2.15: Reaction mechanism of HBTU-assisted coupling of a PNA monomer on a growing chain.**

**Table 2.1: Brief summary of some of most used coupling activators. In organic chemistry several type of coupling reactions, involving different participating and non-participating groups have been studied, and research for novel and better activators is still active.**

| Name | Formula | Properties |
|---|---|---|
| DIC<br>(N,N′-Diisopropylcarbodiimide) | 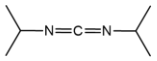 | Mostly in combination with additives in order to reduce epimerization, only if the amino acid derivatives is provided as salts require one equivalent of a tertiary base. |
| EDC · HCl<br>(N-(3-Dimethylaminopropyl)-N′-ethylcarbodiimide · HCl) | 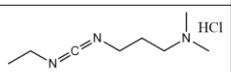 | Designed for couplings in aqueous solution, even if stability under these conditions is limited. |
| DhBtOH, HOOBt, HODhbt<br>(Hydroxy-3,4-dihydro-4-oxo-1,2,3-benzotriazine) | 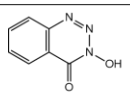 | More reactive than HOBt (1-Hydroxy-benzotriazole) esters. Limitation: explosive character, especially in water-free form. |
| NHS, HoSu<br>(N-Hydroxysuccinimide) | 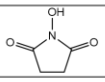 | Well-known additive in carbodiimide-mediated reactions. Completely shelf-stable. |
| PyBOP ®<br>(Benzotriazol-1-yloxy-tripyrrolidino-phosphonium hexafluorophosphate) | 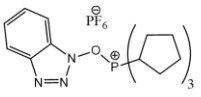 | Non-toxic version of BOP (Benzotriazol-1-yloxy-tris(dimethylamino)-phosphonium hexafluorophosphate).<br>Excellent coupling behavior, no guanylation-activity to amino functions. |
| HBTU<br>(2-(1H-Benzotriazol-1-yl)-N,N,N′,N′-Tetramethylaminium-hexafluoro-phosphate) | 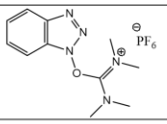 | Most popular coupling reagents. Their application is widespread in solid-phase reactions as well as in solution. |
| COMU<br>(1-[1-(Cyano-2-ethoxy-2-oxoethylidene-aminooxy)-dimethylamino-morpholino]-uronium hexafluorophosphate) | 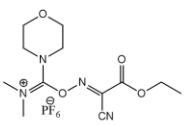 | The incorporation of Oxyma as part of the molecule results in safer handling in combination with better solubility and a reduced allergenic potential than. COMU is especially suited for microwave-accelerated SPS. |

In a typical protocol, after coupling, capping procedure is performed by acetic anhydride solution. Finally, PNA is cleaved from the resin while deprotection of semi-permanent protective groups occur.

A smart alternative protective group/coupling strategy was developed by Lee and coworker[106]: a benzothiazole-2-sulfonyl (Bts) group is used as an amine-protecting group as well as an acid-activating group. The coupling reaction with these monomers require more time than a standard one (120 min) but it does not require neither activators nor anhydrous conditions, so it could be very useful in scale-up of the synthesis. A scheme of monomer synthesis and reaction conditions is showed in Figure 2.16.

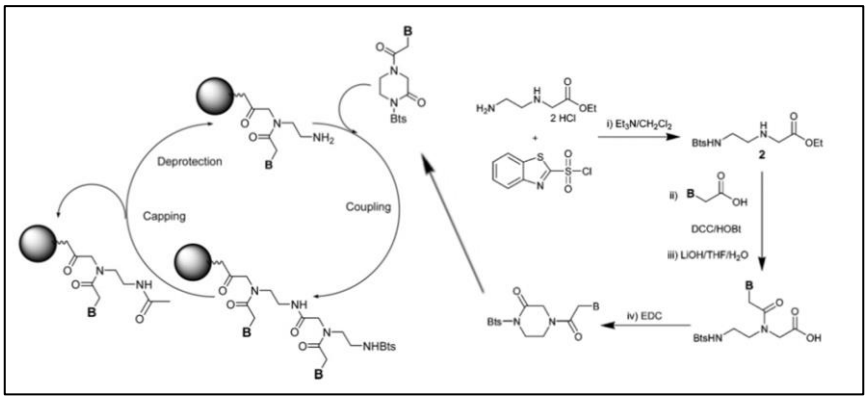


**Figure 2.16: Synthesis of the monomer (right) and synthesis of the PNA (left). Used solutions: coupling 0.3 M PNA monomer (20 equiv) and 0.2 M DIPEA solution in DMF (120 min, 40 °C); capping (1) 5% $Ac_2O$ and 6% lutidine solution in DMF (3 min, rt) , (2) 10% piperidine in DMF (3 min, rt); deprotection 0.8 M 4-ethoxybenzenethiol and 0.4 M DIPEA in DMF (10 min, 40 °C). Adapted from H. Lee et al. Organic Letters 2007 Copyright © 2007 American Chemical Society.**

Most of the PNA syntheses are performed on polymeric resins developed for peptide synthesis; however in the literature there are examples of PNA synthesized on other solid supports such as glass or porous silicon. In the latter case[108], a silicon surface was silanized with APTES ((3-aminopropyl)triethoxysilane) in order to produce a monolayer with amino groups, and this support was used for coupling with commercial Fmoc-monomer, Bhoc-protected nucleobases. It was studied that the loading of the surface (expressed in thickness increasing) is major in case of in situ synthesis instead of physical absorption or conjugation (disulfide bond with thiolated PNA was used as conjugation strategy). Synthesized PNA were tested as therapeutic tools in vitro analysis, hydrolytic degradation of the porous silicon matrix is the primary mechanism of PNA release.

PNA were also synthesized directly on glass surface[109], exploiting a light-sensitive temporary protective group like o-Nitroveratryloxycarbonyl (NVOC), anisoyl protected cytosine and adenine, isobutyryl protected guanine. As silanization agent GPTS ((3-Glycidyloxypropyl)trimethoxysilane) was used, the epoxide group was opened with a diamine and a peptide spacer was introduced. Synthesis was performed under a virtual mask that create an array of probes. After the synthesis, a final NVOC deprotection and acid removal of nucleobases protective group gave the desired PNA that was able to discriminate full match and mis match DNA sequences.

## 2.3 MODIFIED PNAs

PNA are very effective DNA mimics, but as such, they present some drawbacks: the low cellular absorption, little solubility in water and, sometimes, not excellent specificity. Fortunately, due to their chemical stability, PNAs can be easily modified both in the backbone or/and at the nucleobase level for enhancing their performances in many fields. Schematic representations of differently backbone-modified PNAs are shown in Figure 2.17.

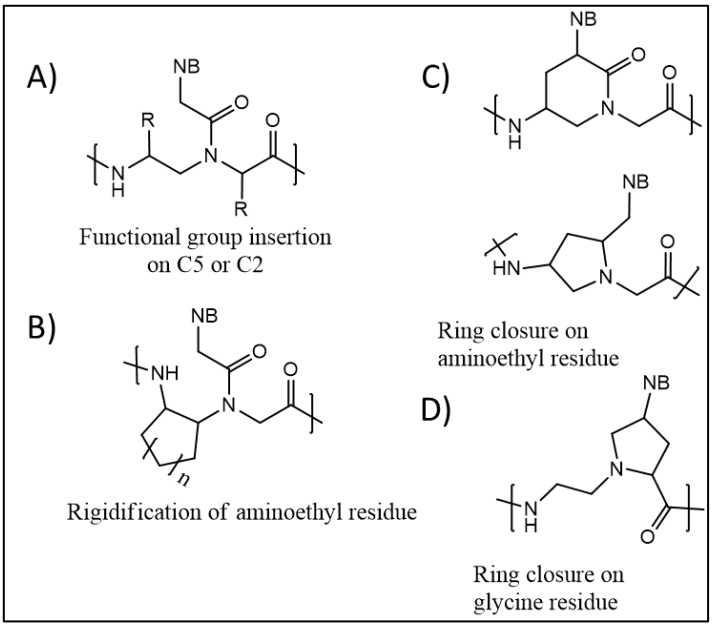


**Figure 2.17: A) Control of helix handedness by chiral groups insertion on the backbone. B) Preorganization through conformational constraints. C, D) Preorganization through rigid structure.**

The backbone of open-chain PNAs has been modified on C2 (α) and C5 (γ), and less frequently on C4 (β). The first two can be obtained by reductive amination of an amino acid (aa), which will form C2 modification, and an aminoaldehyde derived from an amino acid, which allows to introduce the C5 modification.

Alternatively, it is possible to exploit a Mitsunobu reaction starting from amino acids and amino alcohols[110]. C4 modification can be obtained by this route, using chiral diamines as synthons[111]. The modification of the backbone with

substituents in position C2, C4 and C5 introduces a chiral center; in these cases stereochemistry play a very important role in determining affinity for DNA or RNA. In fact, non- modified PNA can form PNA:PNA duplexes with both left- or right-handed helices, while a chiral center on the backbone induces a preference for one of the two helicities. Using circular dichroism measurements on PNA:PNA duplexes and on their complexes with cyanine dyes, it was possible to establish the stereochemistry-helicity correlations. For instance, if the substituting group is a methyl, the right-handed helix is formed if a C2-substituted monomer with S configuration (derived from L-aa) is inserted, while C5-substituted have the same helicity if it has R configuration (derived from D-aa); finally C4-substituted monomer have preference for right-handedness if in S-configuration (see Figure 2.18). The preference for right-handed helicity enhances the PNA:DNA stability, since it can adopt the conformation needed for the duplex formation with less energy cost, with less steric hindrance. The substituent can be used for adding functional groups to the PNA, and if a positively charged (Lys or Arg) side chain is added, attractive interactions with negatively charged DNA[112] can increase the duplex stability, thus enhancing the DNA affinity of the PNA.

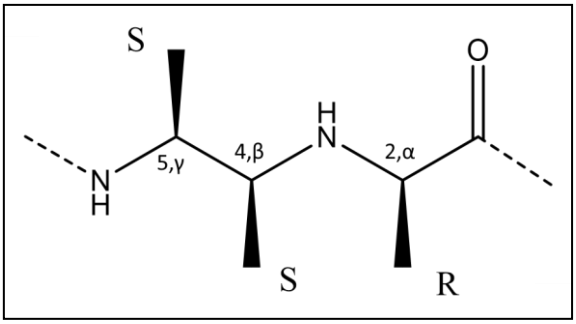


**Figure 2.18: Position and stereochemistry of a modified-monomer.**

The substituents in the side chain of modified monomers can be used also for tethering to the PNA backbone other molecules with a functional role. For example, conjugation with a cationic cell penetrating peptide or a fatty acid, improves the cellular uptake of PNA[113]. The effect increases with increasing length of the fatty acid or the cationic peptide, but in parallel also the cellular toxicity is increased.

C5-modified cationic PNA bearing an aminopropyl group was used for stabilizing DNA:PNA duplex and enhance their cell penetrating behavior[114]. Moreover, the positive charges can be incorporated directly in the backbone, exploiting guanidinuim group from arginine, producing at the same time increased cellular uptake and strength of hybrid double helix[115].

Another kind of backbone modification for PNA is the so-called aminoethylprolyl-PNA (aep-PNA). They have been studied as i-motif stabilizing agents in vivo conditions[116]. A cytosine pentamer of aep-PNA was reported, and its biophysical studies for the formation of hybrid DNA:aep-PNA i-motif structure with a DNA cytosine pentamer under acidic pH have been performed. This kind of architecture could be used in DNA origami as pH-dependent switchable nanomachines.

A simple strategy to access modified PNAs from iterative Ugi couplings has been reported,[117] allowing to incorporate multiple modifications in the backbone. This protocol allows modular modifications at the α, β or γ position of the PNA backbone from simple starting materials. The Ugi reaction can be used for the synthesis in the standard direction, from C to N terminus, but also in the opposite direction, from N to C terminus. Exploiting this multi-component reaction, now it is possible to synthesize directly in SPS PNA with modified backbones, as shown in Figure 2.19. The drawback of this method is the necessity to produce and store reactive isonitriles.

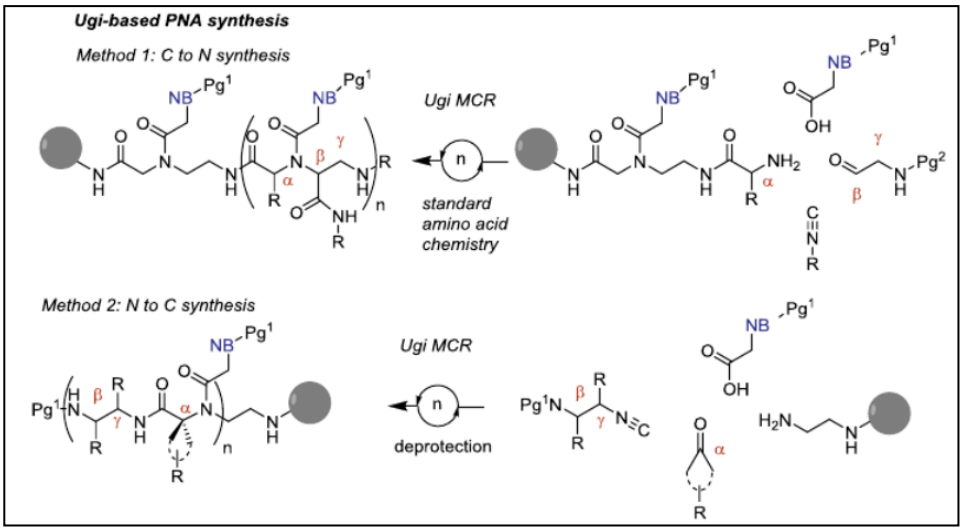


**Figure 2.19: Scheme of the two synthetic pathway for modified-PNA. Different components of the backbone are transformed in different synthones, switching from one to the other synthesis way. Two methods were compared: from C to N synthesis and vice-versa. Reprinted with permission of J. Saarbach et al. Bioorganic & Medicinal Chemistry 2017 Copyright © 2017 Elsevier.**

Many nucleobases modification have been reported in the literature regarding PNA[118] and other kind of synthetic DNAs[119], with the aim of improving binding affinity or to introduce specific functional groups or reporter moieties. Several studies have been done; in particular, improving binding affinity could be achieved by providing additional stacking or hydrogen bonding interactions. This is the case of a G-clamp nucleobase (Figure 2.20 A, B, C): it creates additional Hoogsteen hydrogen bonds and also increase stacking capability[120]. The resulting modified-PNA shows increased affinity but also selectivity for the target DNA[121]. A modified-nucleobases can not only create new hydrogen bonds, but also generate a fluorescence change when it interacts with DNA, for detection of hybridization; this is the case of a phenylpyrrolocytosine-modified PNA (Figure 2.20 D)[122]. Scientist have developed a PNA hybridization probe for imaging of RNA in cell using a fluorescent nucleobase analogue, obtained by attaching the Lucifer chromophore (1,8-naphthalimide) at the 5-position of uracil (Figure 2.20 H)[123]. The fluorescence observed is highly responsive to its neighboring base environment and the PNA base reports the presence of a poly-adenine group in an RNA with reasonable enhancement in fluorescence. Modified nucleobases have been also used for a fluorescence sensor in a

graphene oxide platform for the detection of human telomeric repeats[124]. For sequence-selective recognition of complex RNAs in live cells, 2-aminopyridine modified PNAs (Figure 2.20 I) and their conjugates with lysine and arginine tripeptides were tested[125]. Such modified PNA was able to recognize and specifically form triple helices with RNA hairpins at physiological pH and salt concentration. Modified PNA–peptide conjugates were not cytotoxic and were efficiently delivered in the cytosol: even PNAs without peptide conjugation were taken up by cells, providing a first example of heterocyclic base modification that enhances the cellular uptake of PNA. In some applications, the precise target sequence information is not available, and in such cases, a universal nucleobase is desirable. Ambiguous nucleobase analogues, like 3-nitropyrrole and 5-nitroindole (Figure 2.20 F, G)[126] or thiazole orange (Figure 2.20 E)[127] have been tested; the last one is interesting since its fluorescent properties varies upon PNA:DNA duplex formation, being forced to intercalate between the nucleobases. These unspecific bases have been inserted in one modified-monomer and showed a very little variation in terms of Tm, paired to all four natural nucleobases.

PNA can also be modified in order to act as ligands for metal ions; a PNA for complexation of $Cu^{2+}$ was synthesized with some L-lysine side chain on C5 carbons and by replacing one nucleobase with 2,2′:6′,2″-terpyridine (Tpy)[128]. The C5 modification induce right helicity, but it was observed that, in a $PNA_2Cu$ complex, the helicity was changed to left-handed helix: thus the preferred handedness of a ligand-modified PNA could be switched as a consequence of metal coordination to the ligand. This finding could be used as a tool in the design of functional nucleic-acid based nanostructures and nanomachines.

Substitution of bipyridine for a nucleobase leads to modified PNA able to coordinate a $Ni^{2+}$ ion and form a duplex with a conserved helicity[129,130]. Duplexes that contain two adjacent bipyridine pairs are more stable compared to the others, and additional metal ions lower the duplex stability, an important contributor to the destabilization due to the electrostatic repulsions. This type of PNA can be used for future sensing of metal ions or sequestration of such ions in the environment.

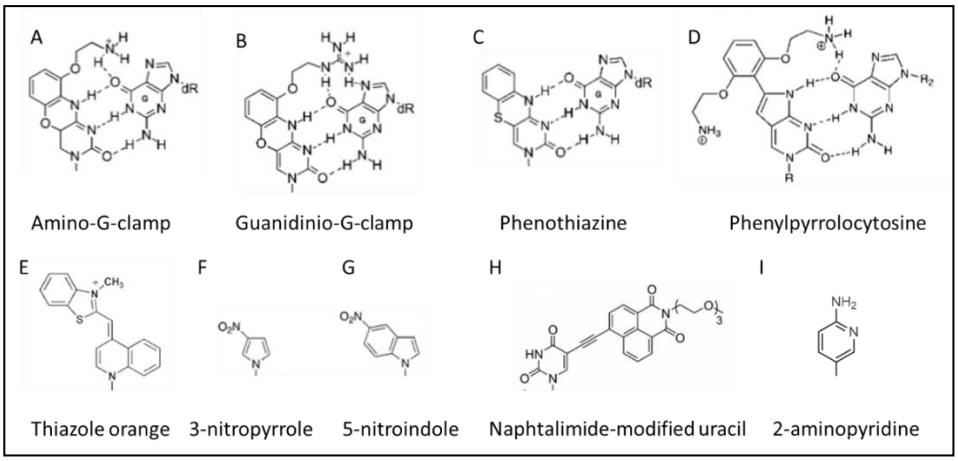


**Figure 2.20: Examples of modified nucleobases, all trounced at methylene carboxylic bridge. A, B, C, D are shown with their interactions with guanine.**

Another interesting approach is the combination of modification of the backbone with modification at the nucleobase level, in this way a polyfunctional PNA is obtained which has greatly improved performances[131]. The combination of C5-modifed backbone and G-clamp nucleobase motioned above allowed to perform a strand-displacement reaction on a double stranded DNA, which was insensitive to little variations from physiological conditions[132]. Selective isolation of dsDNA fragment or affinity capture of supercoiled plasmid DNA from a DNA mixture are application fields of such type of modified-PNA[133].

In anti-gene strategy, the high affinity and specificity of PNA can be exploited in combination with reactive groups for obtaining a semi-permanent linking with double strand DNA in nuclei. In this way, the gene blocked cannot be transcribed, achieving the same effect as antisense therapy but with a different mechanism leading to permanent damage. A tailor-made furan-modification was tested for covalent targeting of single stranded (ss) DNA through a crosslinking strategy[134]. Different configurations have been synthesized, and preliminary results are promising. The furan-modified nucleobase was also employed in a polyfunctional PNA by insertion on a C5 modified backbone[135]. These modifications have been done in order to add positive charged groups for enhancing attractive interactions with DNA and for having a better cellular uptake (see Figure 2.21).

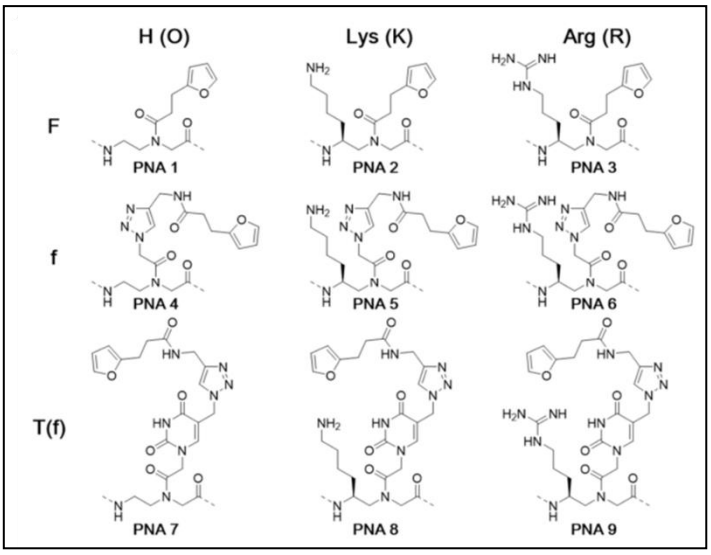


**Figure 2.21: Combinations of modification on the C5 carbon on the backbone and nucleobase level. For what concerns backbone modification three possibility were tested: hydrogen or no modification, lysine and arginine. Three are also the modifications for the nucleobase: "F" in which 2-furylpropionic acid was linked to the PNA backbone, thus substituting the nucleobase; " f " using a strategy similar to "F" but with the furan moiety introduced after the PNA cleavage from the resin, by exploiting a copper catalyzed 1,3-dipolar cycloaddition (CuAAC); "T(f)" if the click reaction is performed on an azido-modified thymine. Adapted from Manicardi et al. Molecules 2017 Copyright © 2017 MDPI.**

In summary: after more than 27 years from their discovery, PNAs have been successfully employed in therapeutic, diagnostic and theranostic purposes, not only in their basic form but, mostly, exploiting modifications in the backbone or/and at the nucleobases. Reaching higher complexity in PNA structure for achieving more complex functions while maintaining or increasing simplicity of synthesis is a further step and a challenging task for future applications.

Bibliography:


1. Nielsen J, Taagaard M, Dahl O, Marugg JE, van Boom JH. Polymer-supported synthesis of deoxyoligonucleotides using in-situ prepared deoxynucleoside 2-cyanoethyl phosphoramidites. *Recl des Trav Chim des Pays-Bas*. 2010;105(1):33-34.
2. Beaucage SL. Oligodeoxyribonucleotides Synthesis: Phosphoramidite Approach. In: *Protocols for Oligonucleotides and Analogs*. New Jersey: Humana Press; 1993:33-62.
3. Sinha ND, Biernat J, Köster H. β-Cyanoethyl N,N-dialkylamino/N-morpholinomonochloro phosphoamidites, new phosphitylating agents facilitating ease of deprotection and work-up of synthesized oligonucleotides. *Tetrahedron Lett*. 1983;24(52):5843-5846.
4. Marugg JE, Burik A, Tromp M, van der Marel GA, van Boom JH. A new and versatile approach to the preparation of valuable deoxynucleoside 3′-phosphite intermediates. *Tetrahedron Lett*. 1986;27(20):2271-2274.
5. Damha MJ, Giannaris PA, Zabarylo S V. An improved procedure for derivatization of controlled-pore glass beads for solid-phase oligonucleotide synthesis. *Nucleic Acids Res*. 1990;18(13):3813-3821.
6. Birch-Hirschfeld E, Gührs K-H, Földes-Papp Z, Seliger H. Oligonucleotide Synthesis on Polystyrene-Grafted Poly(tetrafluoroethylene) Support. *Helv Chim Acta*. 1996;79(1):137-150.
7. Keith M. Anderson, Laurent Jaquinod, Michael A. Jensen, Nam Ngo and, Ronald W. Davis. A Novel Catechol-Based Universal Support for Oligonucleotide Synthesis. *The Journal of organic chemistry*, 2007;*72*(26), 9875-9880.
8. Wei X. Coupling activators for the oligonucleotide synthesis via phosphoramidite approach. *Tetrahedron*. 2013;69(18):3615-3637.
9. Sproat B, Colonna F, Mullah B, et al. An Efficient Method for the Isolation and Purification of Oligoribonucleotides. *Nucleosides and Nucleotides*. 1995;14(1-2):255-273.
10. Welz R, Müller S. 5-(Benzylmercapto)-1H-tetrazole as activator for 2′-O-TBDMS phosphoramidite building blocks in RNA synthesis. *Tetrahedron Lett*. 2002;43(5):795-797.
11. Vargeese C, Carter J, Yegge J, et al. Efficient activation of nucleoside phosphoramidites with 4,5- dicyanoimidazole during oligonucleotide synthesis. *Nucleic Acids Res*. 1998;26(4):1046-1050.
12. Ogilvie KK, Theriault N, Sadana KL. Synthesis of oligoribonucleotides. *J Am Chem Soc*. 1977;99(23):7741-7743.
13. Pitsch S, Weiss PA, Jenny L, Stutz A, Wu X. Reliable Chemical Synthesis of Oligoribonucleotides (RNA) with 2′-O-[(Triisopropylsilyl)oxy]methyl(2′-O-tom)-Protected Phosphoramidites. *Helv Chim Acta*. 2001;84(12):3773-3795.
14. Westmanu E, Stromberg R. Removal of f-butyldimethylsilyl protection in RNA-synthesis. Triethylamine trihydrofluoride (TEA, 3HF) is a more reliable alternative to tetrabutylammonium fluoride (TBAF). *Nucleic Acids Res*.

1994;22(12):2430-2431.
15. Wu T, Ogilvie KK, Perreault JP, Cedergren RJ. Convenient procedure for the preparation of specific mixed DNA-RNA polymers. *J Am Chem Soc*. 1989;111(22):8531-8533.
16. Pon RT, Usman N, Damha MJ, Ogilvie KK. Prevention of guanine modification and chain cleavage during the solid phase synthesis of oligonucleotides using phosphoramidite derivatives. *Nucleic Acids Res*. 1986;14(16):6453-6470.
17. Alul RH, Singman CN, Zhang G, Letsinger RL. Oxalyl-CPG: a labile support for synthesis of sensitive oligonucleotide derivatives. *Nucleic Acids Res*. 1991;19(7):1527-1532.
18. Prakash TP, Johnston JF, Graham MJ, Condon TP, Manoharan M. 2'-O-[2-[(N,N-dimethylamino)oxy]ethyl]-modified oligonucleotides inhibit expression of mRNA in vitro and in vivo. *Nucleic Acids Res*. 2004;32(2):828-833.
19. Daniel C. Capaldi, Hans Gaus, Achim H. Krotz, et al. Synthesis of High-Quality Antisense Drugs. Addition of Acrylonitrile to Phosphorothioate Oligonucleotides: Adduct Characterization and Avoidance. *Organic process research & development*, 2003;*7*(6), 832-838.
20. Boal JH, Wilk A, Harindranath N, Max EE, Kempe T, Beaucage SL. Cleavage of oligodeoxyribonucleotides from controlled-pore glass supports and their rapid deprotection by gaseous amines. *Nucleic Acids Res*. 1996;24(15):3115-3117.
21. Crooke ST, Lebleu B. *Antisense Research and Applications*. CRC; *Antisense research and applications*. CRC Press.1993.
22. Kurreck J. Antisense technologies. Improvement through novel chemical modifications. *Eur J Biochem*. 2003;270(8):1628-1644.
23. Vosberg HP, Eckstein F. Effect of deoxynucleoside phosphorothioates incorporated in DNA on cleavage by restriction enzymes. *J Biol Chem*. 1982;257(11):6595-6599.
24. Frey PA, Sammons RD. Bond order and charge localization in nucleoside phosphorothioates. *Science*. 1985;228(4699):541-545.
25. Lebedev A V., Wickstrom E. The chirality problem in P-substituted oligonucleotides. *Perspect Drug Discov Des*. 1996;4(1):17-40.
26. Le BT, Chen S, Abramov M, Herdewijn P, Veedu RN. Evaluation of anhydrohexitol nucleic acid, cyclohexenyl nucleic acid and d -altritol nucleic acid-modified 2′-O-methyl RNA mixmer antisense oligonucleotides for exon skipping in vitro. *Chem Commun*. 2016;52(92):13467-13470.
27. Guzaev AP. Reactivity of 3H-1,2,4-dithiazole-3-thiones and 3H-1,2-dithiole-3-thiones as sulfurizing agents for oligonucleotide synthesis. *Tetrahedron Lett*. 2011;52(3):434-437.
28. Iyer RP, Egan W, Regan JB, Beaucage SL. 3H-1,2-Benzodithiole-3-one 1,1-dioxide as an improved sulfurizing reagent in the solid-phase synthesis of oligodeoxyribonucleoside phosphorothioates. *Journal American Chemical Soc*. 1990;112(3):1253-1254.
29. Molenaar C, Marras SA, Slats JCM, et al. Linear 2' O-Methyl RNA probes for the visualization of RNA in living cells. *Nucleic Acids Res*.

2001;29(17):89e-89.
30. Majlessi M, Nelson NC, Becker MM. Advantages of 2'-O-methyl oligoribonucleotide probes for detecting RNA targets. *Nucleic Acids Res*. 1998;26(9):2224-2229.
31. Shimizu M, Konishi A, Shimada Y, Inoue H, Ohtsuka E. Oligo(2′- *O* -methyl)ribonucleotides Effective probes for duplex DNA. *FEBS Lett*. 1992;302(2):155-158.
32. Tsourkas A, Behlke MA, Bao G. Hybridization of 2'-O-methyl and 2'-deoxy molecular beacons to RNA and DNA targets. *Nucleic Acids Res*. 2002;30(23):5168-5174.
33. Zhao D, Yang Y, Qu N, et al. Single-molecule detection and tracking of RNA transcripts in living cells using phosphorothioate-optimized 2′-O-methyl RNA molecular beacons. *Biomaterials*. 2016;100:172-183.
34. Maio GE, Enweronye O, Zumrut HE, Batool S, Van NA, Mallikaratchy PR. Systematic Optimization and Modification of a DNA Aptamer with 2'-O-Methyl RNA Analogues. *ChemistrySelect*. 2017;2(7):2335-2340.
35. Rigo F, Chun SJ, Norris DA, et al. Pharmacology of a central nervous system delivered 2'-O-methoxyethyl-modified survival of motor neuron splicing oligonucleotide in mice and nonhuman primates. *J Pharmacol Exp Ther*. 2014;350(1):46-55.
36. Crooke ST, Baker BF, Kwoh TJ, et al. Integrated Safety Assessment of 2′-O-Methoxyethyl Chimeric Antisense Oligonucleotides in NonHuman Primates and Healthy Human Volunteers. *Mol Ther*. 2016;24(10):1771-1782.
37. Crooke ST, Baker BF, Pham NC, et al. The Effects of 2′- *O* -Methoxyethyl Oligonucleotides on Renal Function in Humans. *Nucleic Acid Ther*. 2018;28(1):10-22.
38. Ochi Y, Imai M, Nakagawa O, Hayashi J, Wada S, Urata H. Gene silencing by 2′-O-methyldithiomethyl-modified siRNA, a prodrug-type siRNA responsive to reducing environment. *Bioorg Med Chem Lett*. 2016;26(3):845-848.
39. Gryaznov SM, Lloyd DH, Chen JK, et al. Oligonucleotide N3'-->P5' phosphoramidates. *Proc Natl Acad Sci U S A*. 1995;92(13):5798-5802.
40. McCurdy SN, Nelson JS, Hirschbein BL, Fearon KL. An improved method for the synthesis of N3′→P5′ phosphoramidate oligonucleotides. *Tetrahedron Lett*. 1997;38(2):207-210.
41. Ding D, Gryaznov SM, Lloyd DH, et al. An oligodeoxyribonucleotide N3'--> P5' phosphoramidate duplex forms an A-type helix in solution. *Nucleic Acids Res*. 1996;24(2):354-360.
42. Skorski T, Perrotti D, Nieborowska-Skorska M, Gryaznov S, Calabretta B. Antileukemia effect of c-myc N3'-->P5' phosphoramidate antisense oligonucleotides in vivo. *Proc Natl Acad Sci U S A*. 1997;94(8):3966-3971.
43. Herbert B-S, Gellert GC, Hochreiter A, et al. Lipid modification of GRN163, an N3′ → P5′ thio-phosphoramidate oligonucleotide, enhances the potency of telomerase inhibition. *Oncogene*. 2005;24(33):5262-5268.
44. Steffens, R., & Leumann, C. J. Synthesis and thermodynamic and

biophysical properties of tricyclo-DNA. *Journal of the American Chemical Society*, 1999;*121*(14), 3249-3255.
45. Renneberg, D., & Leumann, C. J. Watson− Crick base-pairing properties of tricyclo-DNA. *Journal of the American Chemical Society*, 2002;*124*(21), 5993-6002.
46. Vonlanthen D, Leumann CJ. Hydroxycyclopentanone Derivativesfrom d -Mannose via Ring Closing Metathesis:An Improved Synthesis of a Key Intermediate of Tricyclo-DNA. *Synthesis (Stuttg)*. 2003;2003(07):1087-1090.
47. Renneberg D, Bouliong E, Reber U, Schümperli D, Leumann CJ. Antisense properties of tricyclo-DNA. *Nucleic Acids Res*. 2002;30(13):2751-2757.
48. Ittig D, Luisier S, Weiler J, Schumperli D, Leumann C. Improving gene silencing of siRNAs via tricyclo-DNA modification. *Artif DNA PNA XNA*. 2010;1(1):9-16.
49. Goyenvalle A, Griffith G, Babbs A, et al. Functional correction in mouse models of muscular dystrophy using exon-skipping tricyclo-DNA oligomers. *Nat Med*. 2015;21(3):270-275.
50. Lilu Zhang, Adam Peritz and, Meggers* E. A Simple Glycol Nucleic Acid. *Journal of the American Chemical Society*, 2005;*127*(12), 4174-4175.
51. Schlegel MK, Essen L-O, Meggers E. Duplex Structure of a Minimal Nucleic Acid. *J Am Chem Soc*. 2008;130(26):8158-8159.
52. Tsai C-H, Chen J, Szostak JW. Enzymatic synthesis of DNA on glycerol nucleic acid templates without stable duplex formation between product and template. *Proc Natl Acad Sci U S A*. 2007;104(37):14598-14603.
53. Zhang RS, McCullum EO, Chaput JC. Synthesis of Two Mirror Image 4-Helix Junctions Derived from Glycerol Nucleic Acid. *J Am Chem Soc*. 2008;130(18):5846-5847.
54. Beier M, Reck F, Wagner T, Krishnamurthy R, Eschenmoser A, Eschenmoser A. Chemical etiology of nucleic acid structure: comparing pentopyranosyl-(2'-->4') oligonucleotides with RNA. *Science*. 1999;283(5402):699-703.
55. Sau SP, Fahmi NE, Liao J-Y, Bala S, Chaput JC. A Scalable Synthesis of α-l -Threose Nucleic Acid Monomers. *J Org Chem*. 2016;81(6):2302-2307.
56. Yu H, Zhang S, Dunn MR, Chaput JC. An Efficient and Faithful in Vitro Replication System for Threose Nucleic Acid. *J Am Chem Soc*. 2013;135(9):3583-3591.
57. Liu LS, Leung HM, Tam DY, Lo TW, Wong SW, Lo PK. α- l -Threose Nucleic Acids as Biocompatible Antisense Oligonucleotides for Suppressing Gene Expression in Living Cells. *ACS Appl Mater Interfaces*. 2018;10(11):9736-9743.
58. Liao J, Anosova I, Bala S, Van Horn WD, Chaput JC. A parallel stranded G-quadruplex composed of threose nucleic acid (TNA). *Biopolymers*. 2017;107(3):e22999.
59. Pitsch S, Krishnamurthy R, Bolli M, et al. Pyranosyl-RNA ('p-RNA'): Base-pairing selectivity and potential to replicate. Preliminary communication. *Helv Chim Acta*. 1995;78(7):1621-1635.

60. Micura R, Bolli M, Windhab N, Eschenmoser A. Pyranosyl-RNA Also Forms Hairpin Structures. *Angew Chemie Int Ed English*. 1997;36(8):870-873..
61. Schlönvogt I, Pitsch S, Lesueur C, Eschenmoser A, Jaun B, Wolf RM. Pyranosyl-RNA ('p-RNA'): NMR and Molecular-Dynamics Study of the Duplex Formed by Self-pairing of Ribopyranosyl-(C-G-A-A-T-T-C-G). *Helv Chim Acta*. 1996;79(8):2316-2345.
62. Bolli M, Micura R, Pitsch S, Eschenmoser A. Pyranosyl-RNA: Further Observations on Replication. *Helv Chim Acta*. 1997;80(6):1901-1951.
63. Jing Wang, Birgit Verbeure, Ingrid Luyten, et al. Cyclohexene Nucleic Acids (CeNA): Serum Stable Oligonucleotides that Activate RNase H and Increase Duplex Stability with Complementary RNA. *Journal of the American Chemical Society*, 2000;*122*(36), 8595-8602.
64. Nauwelaerts K, Lescrinier E, Sclep G, Herdewijn P. Cyclohexenyl nucleic acids: conformationally flexible oligonucleotides. *Nucleic Acids Res*. 2005;33(8):2452-2463.
65. Kempeneers V, Renders M, Froeyen M, Herdewijn P. Investigation of the DNA-dependent cyclohexenyl nucleic acid polymerization and the cyclohexenyl nucleic acid-dependent DNA polymerization. *Nucleic Acids Res*. 2005;33(12):3828-3836.
66. Verbeure B, Lescrinier E, Wang J, Herdewijn P. RNase H mediated cleavage of RNA by cyclohexene nucleic acid (CeNA). *Nucleic Acids Res*. 2001;29(24):4941-4947.
67. Le BT, Chen S, Abramov M, Herdewijn P, Veedu RN. Evaluation of anhydrohexitol nucleic acid, cyclohexenyl nucleic acid and d -altritol nucleic acid-modified 2′-O-methyl RNA mixmer antisense oligonucleotides for exon skipping in vitro. *Chem Commun*. 2016;52(92):13467-13470.
68. Koshkin AA, Singh SK, Nielsen P, et al. LNA (Locked Nucleic Acids): Synthesis of the adenine, cytosine, guanine, 5-methylcytosine, thymine and uracil bicyclonucleoside monomers, oligomerisation, and unprecedented nucleic acid recognition. *Tetrahedron*. 1998;54(14):3607-3630.
69. Youssefyeh RD, Verheyden JPH, Moffatt JG. 4'-Substituted nucleosides. 4. Synthesis of some 4'-hydroxymethyl nucleosides. *J Org Chem*. 1979;44(8):1301-1309.
70. Jones GH, Taniguchi M, Tegg D, Moffatt JG. 4'-Substituted nucleosides. 5. Hydroxymethylation of nucleoside 5'-aldehydes. *J Org Chem*. 1979;44(8):1309-1317.
71. Thrane H, Fensholdt J, Regner M, Wengel J. Novel linear and branched oligodeoxynucleotide analogues containing 4′-c-(hydroxymethyl)thymidine. *Tetrahedron*. 1995;51(37):10389-10402.
72. Egawa H, Jingushi K, Ueda Y, et al. Abstract A20: Innovative drug discovery for bladder cancer by miR-130 family seed-targeting locked nucleic acid. *Cancer Res*. 2016;76(6 Supplement):A20-A20.
73. Delgado E, Okabe H, Preziosi M, et al. Complete response of Ctnnb1-mutated tumours to β-catenin suppression by locked nucleic acid antisense in a mouse hepatocarcinogenesis model. *J Hepatol*. 2015;62(2):380-387.
74. Wojtkowiak-Szlachcic A, Taylor K, Stepniak-Konieczna E, et al. Short

antisense-locked nucleic acids (all-LNAs) correct alternative splicing abnormalities in myotonic dystrophy. *Nucleic Acids Res*. 2015;43(6):3318-3331.
75. Umemoto T, Hrdlicka PJ, Babu BR, Wengel J. Sensitive SNP Dual-Probe Assays Based on Pyrene-Functionalized 2′-Amino-LNA: Lessons To Be Learned. *ChemBioChem*. 2007;8(18):2240-2248.
76. Astakhova IK, Hansen LH, Vester B, Wengel J. Peptide–LNA oligonucleotide conjugates. *Org Biomol Chem*. 2013;11(25):4240.
77. Jørgensen AS, Gupta P, Wengel J, Astakhova IK. “Clickable” LNA/DNA probes for fluorescence sensing of nucleic acids and autoimmune antibodies. *Chem Commun*. 2013;49(91):10751.
78. Isobe H, Fujino T, Yamazaki N, Guillot-Nieckowski M, Nakamura E. Triazole-Linked Analogue of Deoxyribonucleic Acid ( $^{TL}$ DNA): Design, Synthesis, and Double-Strand Formation with Natural DNA. *Org Lett*. 2008;10(17):3729-3732.
79. Sharma VK, Singh SK, Krishnamurthy PM, et al. Synthesis and biological properties of triazole-linked locked nucleic acid. *Chem Commun*. 2017;53(63):8906-8909.
80. Bakthavathsalam P, Longatte G, Jensen SO, Manefield M, Gooding JJ. Locked nucleic acid molecular beacon for multiplex detection of loop mediated isothermal amplification. *Sensors Actuators B Chem*. 2018;268:255-263.
81. Østergaard ME, Kumar P, Baral B, et al. C5-functionalized DNA, LNA, and α- L -LNA: Positional control of polarity-sensitive fluorophores leads to improved SNP-Typing. *Chem - A Eur J*. 2011;17(11):3157-3165.
82. Kumar P, Østergaard ME, Baral B, et al. Synthesis and Biophysical Properties of C5-Functionalized LNA (Locked Nucleic Acid). *J Org Chem*. 2014;79(11):5047-5061.
83. Burdick AD, Sciabola S, Mantena SR, et al. Sequence motifs associated with hepatotoxicity of locked nucleic acid—modified antisense oligonucleotides. *Nucleic Acids Res*. 2014;42(8):4882-4891.
84. Gallo Cantafio ME, Gulla A, Amodio N, et al. Pharmacokinetics and Biodistribution of Locked Nucleic Acid (LNA)-Mir-221 Inhibitor: A New Promising Anti-Myeloma Agent. *Blood*. 2015;126(23):3025.
85. Jiang S. Abstract 715: Vivo-Morpholino antisense oligomers decrease tumor growth in mice by altering mVEGF mRNA splicing to knock down mVEGF expression. *Cancer Res*. 2014;74(19 Supplement):715-715.
86. Osman EY, Washington CW, Kaifer KA, et al. Optimization of Morpholino Antisense Oligonucleotides Targeting the Intronic Repressor Element1 in Spinal Muscular Atrophy. *Mol Ther*. 2016;24(9):1592-1601.
87. Hashimoto M, Nara T, Mita T, Mikoshiba K. Morpholino antisense oligo inhibits trans-splicing of pre-inositol 1,4,5-trisphosphate receptor mRNA of Trypanosoma cruzi and suppresses parasite growth and infectivity. *Parasitol Int*. 2016;65(3):175-179.
88. Nakagawa S, FitzHarris G. Quantitative Microinjection of Morpholino Antisense Oligonucleotides into Mouse Oocytes to Examine Gene Function

in Meiosis-I. In: Humana Press, New York, NY; 2016:217-230.
89. Hayakawa M, Kaizawa H, Moritomo H, et al. Synthesis and biological evaluation of 4-morpholino-2-phenylquinazolines and related derivatives as novel PI3 kinase p110α inhibitors. *Bioorg Med Chem*. 2006;14(20):6847-6858.
90. Chen S, Le B, Rahimizadeh K, et al. Synthesis of a Morpholino Nucleic Acid (MNA)-Uridine Phosphoramidite, and Exon Skipping Using MNA/2′-O-Methyl Mixmer Antisense Oligonucleotide. *Molecules*. 2016;21(11):1582.
91. Hu W, Hu Q, Li L, Kong J, Zhang X. Detection of sequence-specific DNA with a morpholino-functionalized silicon chip. *Anal Methods*. 2015;7(6):2406-2412.
92. Wang X, Smirnov S. Label-Free DNA Sensor Based on Surface Charge Modulated Ionic Conductance. *ACS Nano*. 2009;3(4):1004-1010.
93. Zhang G-J, Luo ZHH, Huang MJ, Tay GKI, Lim E-JA. Morpholino-functionalized silicon nanowire biosensor for sequence-specific label-free detection of DNA. *Biosens Bioelectron*. 2010;25(11):2447-2453.
94. Tercero N, Wang K, Gong P, Levicky R. Morpholino Monolayers : Preparation and Label-free DNA Analysis by Surface Hybridization Morpholino Monolayers : Preparation and Label-free DNA Analysis by Surface Hybridization. *Portf Mag Fine Arts*. 2009;(Dcc):1-8.
95. Liao T, Li X, Tong Q, et al. Ultrasensitive Detection of MicroRNAs with Morpholino-Functionalized Nanochannel Biosensor. *Anal Chem*. 2017;89(10):5511-5518.
96. Hu W, Ning Y, Li L, Kong J, Zhang X. Highly sensitive detection of sequence-specific DNA with morpholino-functionalized magnetic microspheres. *Anal Methods*. 2015;7(16):6712-6717.
97. Nielsen PE, Egholm M, Berg RH, Buchardt O. Sequence-selective recognition of DNA by strand displacement with a thymine-substituted polyamide. *Science*. 1991;254(5037):1497-1500.
98. Betts L, Josey JA, Veal JM, Jordan SR. A nucleic acid triple helix formed by a peptide nucleic acid-DNA complex. *Science*. 1995;270(5243):1838-1841.
99. Ferrer E, Shevchenko A, Eritja R. Synthesis and Hybridization Properties of DNA–PNA Chimeras Carrying 5-Bromouracil and 5-Methylcytosine. *Bioorg Med Chem*. 2000;8(2):291-297.
100. Uhlmann E, Peyman A, Breipohl G, Will DW. PNA: Synthetic Polyamide Nucleic Acids with Unusual Binding Properties. *Angew Chemie Int Ed*. 1998;37(20):2796-2823.
101. Breipohl G, Knolle J, Langner D, O'Malley G, Uhlmann E. Synthesis of polyamide nucleic acids (PNAs) using a novel Fmoc/Mmt protecting-group combination. *Bioorg Med Chem Lett*. 1996;6(6):665-670.
102. Chouikhi D, Ciobanu M, Zambaldo C, Duplan V, Barluenga S, Winssinger N. Expanding the Scope of PNA-Encoded Synthesis (PES): Mtt-Protected PNA Fully Orthogonal to Fmoc Chemistry and a Broad Array of Robust Diversity-Generating Reactions. *Chem - A Eur J*. 2012;18(40):12698-12704.
103. Ciobanu M, Huang K-T, Daguer J-P, et al. Selection of a synthetic glycan oligomer from a library of DNA-templated fragments against DC-SIGN and

inhibition of HIV gp120 binding to dendritic cells. *Chem Commun*. 2011;47(33):9321.
104. Bethge L, Jarikote DV. New cyanine dyes as base surrogates in PNA: Forced intercalation probes (FIT-probes) for homogeneous SNP detection. *Bioorg Med Chem*. 2008;16(1):114-125.
105. Manicardi A, Bertucci A, Rozzi A, Corradini R. A Bifunctional Monomer for On-Resin Synthesis of Polyfunctional PNAs and Tailored Induced-Fit Switching Probes. *Org Lett*. 2016;18(21):5452-5455.
106. Hyunil Lee *, Jae Hoon Jeon, Jong Chan Lim, Hoon Choi, Yeohong Yoon and, Kim* SK. Peptide Nucleic Acid Synthesis by Novel Amide Formation. 2007.
107. Bachem. Coupling Reagents. *Tetrahedron*. 1996;(Dcc):5603-5606.
108. Beavers KR, Mares JW, Swartz CM, Zhao Y, Weiss SM, Duvall CL. In situ synthesis of peptide nucleic acids in porous silicon for drug delivery and biosensing. *Bioconjug Chem*. 2014;25(7):1192-1197.
109. Liu ZC, Shin DS, Shokouhimehr M, et al. Light-directed synthesis of peptide nucleic acids (PNAs) chips. *Biosens Bioelectron*. 2007;22(12):2891-2897.
110. Synthesis of achiral and chiral peptide nucleic acid (PNA) monomers using Mitsunobu reaction. *Tetrahedron*. 2001;57(37):7909-7917.
111. β-PNA: Peptide nucleic acid (PNA) with a chiral center at the β-position of the PNA backbone. *Bioorg Med Chem Lett*. 2011;21(24):7317-7320.
112. Corradini R, Sforza S, Tedeschi T, Totsingan F, Manicardi A, Marchelli R. Peptide Nucleic Acids with a Structurally Biased Backbone. Updated Review and Emerging Challenges. *Current topics in medicinal chemistry*, 2011;*11*(12), 1535-1554.
113. Koppelhus U, Shiraishi T, Zachar V, Pankratova S, Nielsen PE. Improved Cellular Activity of Antisense Peptide Nucleic Acids by Conjugation to a Cationic Peptide-Lipid (CatLip) Domain. *Bioconjug Chem*. 2008;19(8):1526-1534.
114. kumar P, Jain DR. Cγ-Aminopropylene peptide nucleic acid (amp-PNA): chiral cationic PNAs with superior PNA:DNA/RNA duplex stability and cellular uptake. *Tetrahedron*. 2015;71(21):3378-3384.
115. Manicardi A, Fabbri E, Tedeschi T, et al. Cellular Uptakes, Biostabilities and Anti-miR-210 Activities of Chiral Arginine-PNAs in Leukaemic K562 Cells. *ChemBioChem*. 2012;13(9):1327-1337.
116. Gade CR, Sharma NK. Hybrid DNA i-motif: Aminoethylprolyl-PNA (pC5) enhance the stability of DNA (dC5) i-motif structure. *Bioorg Med Chem Lett*. 2017;27(24):5424-5428.
117. Saarbach J, Masi D, Zambaldo C, Winssinger N. Facile access to modified and functionalized PNAs through Ugi-based solid phase oligomerization. *Bioorg Med Chem*. 2017;25(19):5171-5177.
118. Hudson RHE, Viirre RD, Liu YH, Wojciechowski F, Dambenieks AK. Chemistry for the synthesis of nucleobase-modified peptide nucleic acid. *Pure Appl Chem*. 2004;76(7-8):1591-1598.
119. Malyshev DA, Romesberg FE. The Expanded Genetic Alphabet. *Angew Chemie Int Ed*. 2015;54(41):11930-11944.

120. Flanagan WM, Wolf JJ, Olson P, et al. A cytosine analog that confers enhanced potency to antisense oligonucleotides. *Proc Natl Acad Sci U S A*. 1999;96(7):3513-3518.
121. Cristina Ausín, José-Antonio Ortega, Jordi Robles, Anna Grandas and, Pedroso* E. Synthesis of Amino- and Guanidino-G-Clamp PNA Monomers. 2002.
122. Wojciechowski F, Hudson RHE. Fluorescence and Hybridization Properties of Peptide Nucleic Acid Containing a Substituted Phenylpyrrolocytosine Designed to Engage Guanine with an Additional H-Bond. *J Am Chem Soc*. 2008;130(38):12574-12575.
123. Sabale PM, Ambi UB, Srivatsan SG. A Lucifer-Based Environment-Sensitive Fluorescent PNA Probe for Imaging Poly(A) RNAs. *ChemBioChem*. 2018;19(8):826-835.
124. Sabale PM, George JT, Srivatsan SG. A base-modified PNA–graphene oxide platform as a turn-on fluorescence sensor for the detection of human telomeric repeats. *Nanoscale*. 2014;6(18):10460..
125. Hnedzko D, McGee DW, Karamitas YA, Rozners E. Sequence-selective recognition of double-stranded RNA and enhanced cellular uptake of cationic nucleobase and backbone-modified peptide nucleic acids. *RNA*. 2017;23(1):58-69.
126. Hemavathi Challa, Melanie L. Styers and, Woski* SA. Nitroazole Universal Bases in Peptide Nucleic Acids. *Organic letters*, 1999;*1*(10), 1639-1641.
127. Köhler O, Seitz O. Thiazole orange as fluorescent universal base in peptide nucleic acids. *Chem Commun*. 2003;0(23):2938-2939.
128. Bezer S, Rapireddy S, Skorik YA, Ly DH, Achim C. Coordination-Driven Inversion of Handedness in Ligand-Modified PNA. *Inorg Chem*. 2011;50(23):11929-11937.
129. Raphael M. Franzini, Richard M. Watson, Goutam K. Patra, et al. Metal Binding to Bipyridine-Modified PNA. Inorganic chemistry, 2006;45(24), 9798-9811.
130. Delia-Laura Popescu, Terry J. Parolin and, Achim C. Metal Incorporation in Modified PNA Duplexes. *Journal of the American Chemical Society*, 2003;*125*(21), 6354-6355.
131. Manicardi A, Rozzi A, Korom S, Corradini R. Building on the peptide nucleic acid (PNA) scaffold: a biomolecular engineering approach. *Supramol Chem*. 2017;29(11):784-795.
132. Chenna V, Rapireddy S, Sahu B, Ausin C, Pedroso E, Ly DH. A Simple Cytosine to G-Clamp Nucleobase Substitution Enables Chiral γ-PNAs to Invade Mixed-Sequence Double-Helical B-form DNA. *ChemBioChem*. 2008;9(15):2388-2391.
133. Kuhn H, Sahu B, Rapireddy S, Ly D, Frank-Kamenetskii MD. Sequence specificity at targeting double-stranded DNA with a gamma-PNA oligomer modified with guanidinium G-clamp nucleobases. *Artif DNA PNA XNA*. 2010;1(1):45-53.
134. Manicardi A, Gyssels E, Corradini R, Madder A. Furan-PNA: a mildly inducible irreversible interstrand crosslinking system targeting single and

double stranded DNA. *Chem Commun*. 2016;52(42):6930-6933.
135. Elskens J, Manicardi A, Costi V, et al. Synthesis and Improved Cross-Linking Properties of C5-Modified Furan Bearing PNAs. *Molecules*. 2017;22(11):2010.

# 3- POLY-FUNCTIONAL PNAS: THE EXAMPLE OF A PYRENE-BASED SWITCHING PROBE


## Abstract:

In this chapter, synthesis, characterization and performances of a doubly-modified PNA suitable for DNA recognition will be discussed. The use of a PNA monomer with modifications both in the backbone and at the nucleobase level, allowed the addition of independent reporter groups. This could be used for the synthesis of polyfunctional PNA structures by exploiting a three orthogonal protective groups strategy with on-resin stepwise introduction of functional groups. With this approach, pyreneacetic acid was linked to the side chain of a lysine in position C5 of the backbone and on a modified uracil base (Figure 3.1). In the doubly-modified PNA, when is in single strand state, pyrenes moieties are involved in stacking interactions, resulting in excimer fluorescence emission. When fully complementary target DNA or RNA was added, a switch in the fluorescence spectra from excimer to monomer emission was observed. The fluorescence switch-off was shown to be sequence selective, thus allowing to reveal the target sequence. This is an example of a rationally-design probe undergoing an 'induced-fit' movement upon pairing interaction. Preliminary data on this system were reported in a previous PhD work, and in the present thesis they were applied to a wider scope and completed.

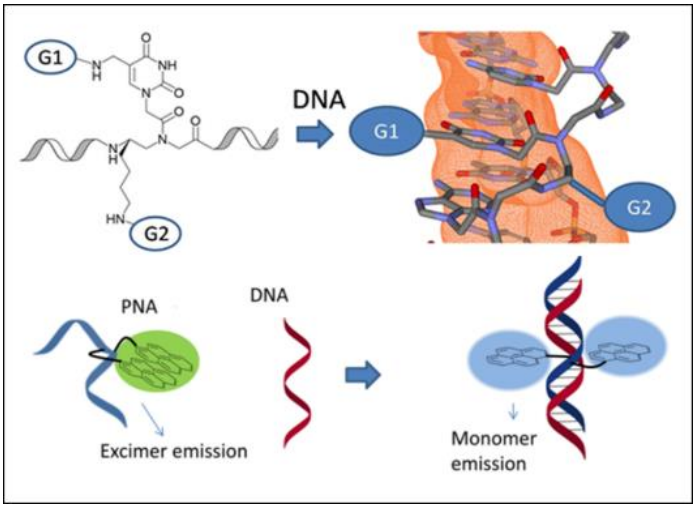


**Figure 3.1: UP: left, the modified monomer with group linked to the modified uracil and side chain of lysine. UP: right, the reporter groups stacking interactions are prevented when target DNA is added and the monomer fluorescent emission is switched on. Bottom: the mechanism though which the excimer emission is switched into monomer emission. Reprinted with permission from A. Manicardi et al. *Organic letters,* 2016 Copyright © 2016, ACS.**

## 3.0 INTRODUCTION

A difficult goal in modern gene-detection is to obtain a signal from the DNA recognition event without the need of labelling; this can be accomplished by label-free instrumental techniques or by using self-reporting colorimetric or fluorimetric probes. PNAs are powerful tools for achieving this goal, and many efforts have been performed in the fluorescent-sensors field. Despite most molecular beacons need a quencher, a very useful strategy is exploiting a switching in fluorescence spectra like in pyrene monomer/excimer emission that does not require a quencher. In DNA probes, pyrene units are usually linked at the end of the nucleotide sequence or bound on modified nucleobase. As an example, Sonogashira coupling have successfully been used to couple pyrene units to nucleobases[1]. Only in few cases the pyrene groups have been introduced in the oligonucleotide backbone, most notably, in the so-called invader LNA probes developed by Sau et al[2] (Figure 3.2) for detection of

double stranded DNA. As described in chapter 2, PNA can easily be modified the both at the backbone and on the nucleobase. As example, acpc-PNA backbone has been modified with pyrene units not only at the N-terminal but also in the middle[3]. In our research group, the pyrene unit was previously inserted as nucleobase substituent, exploiting 5-(aminomethyl) uracil as modified precursor. A PNA modified with this nucleobase was shown to present excimer emission in the presence of target DNA, due to the formation of a triplex structure; the modified PNA behaved hence as a switching probe, and was found to be have e high discrimination ability for detection of full-match vs singly mismatched DNA targets[4].

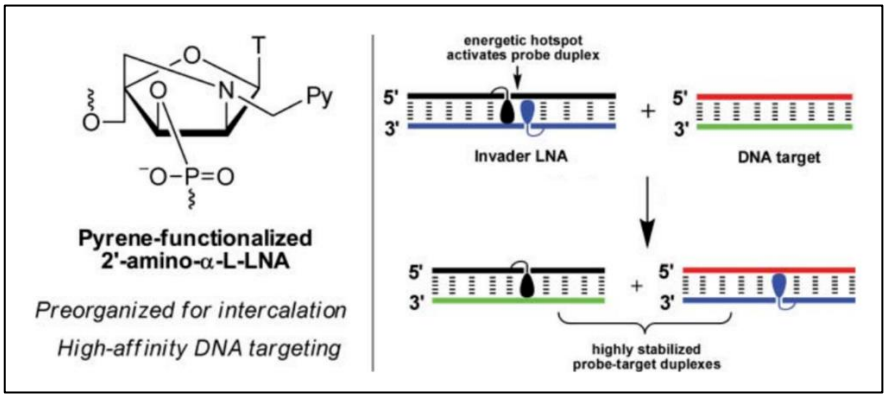


**Figure 3.2: left, modified-LNA monomer with pyrene moiety. Right, action mechanism of the LNA invader: the unstable LNA duplex shows excimer fluorescence, after the double invasion the fluorescence is switched to the characteristic monomer peaks. Reproduced with permission from S.P Sau et al. *Org. Biomol. Chem.* 2010 Copyright © Royal Chemistry Society 2010.**

The main approach for the synthesis of poly-functional PNAs is preparing the monomer with the wanted groups and then insert it into the growing chain of PNA. In this way, it is possible to exploit automatic synthesizers but is not the best choice for producing libraries of compounds. For achieving this goal, a modified-monomer with “hidden” reactive sites is necessary, and these sites have to been activated by orthogonal reactions or deprotection during solid phase synthesis (SPS). Introducing functionalities in SPS is advantageous because the monomer could remain a relatively simple molecule, capable to react better than a hindered one and possibly more soluble. Therefore, a very important choice concern orthogonal protective groups that can be used and their compatibility with the other parts of the synthesis.

## 3.1 RESULTS AND DISCUSSION

Since the possibility to introduce functional groups at different positions in the sequence and on different sites (backbone or nucleobase) on PNAs have a great potential in several applications, especially in sensing technologies, we planned to develop a method for building polyfunctional modified PNA directly on solid phase synthesis using different orthogonal protective groups. PNAs obtained in this way might then be useful for detection of single mismatched, short sequence of DNA and RNA.

For this purposes, we chose as synthons C5-modified PNA backbone derived from L-lysine and 5-azidomethyl uracil. The side chain of lysine, placed on the C5, provides one amine function for tethering functional moieties and reporter groups. Modification at this position has a stabilizing effect on PNA:DNA duplex, and L-stereochemistry was chosen based on our previous works on preferential right-handedness of these derivatives. The modified uracil previously developed with an azide moiety (5-azidomethyluracil) can provide another amino function on the nucleobase[5]. By performing a Staudinger reduction, it is possible to reduce the azide to amine (see Figure 3.2). Staudinger Reaction is a very mild azide reduction compared to hydrogenation, and is suitable for solid phase synthesis (SPS). The azide function can also be used for 1,3-dipolar cycloadditions in Huisgen's conditions. One disadvantage of the azide group is that during cleavage from the sold-phase support it is degraded using harsh acidic conditions, as in Boc-synthesis, making mass spectra not well interpretable, whereas it can stand standard Fmoc-synthesis cleavage. It can be however used in Boc-based strategy if used as masked amino group to be transformed during SPS.

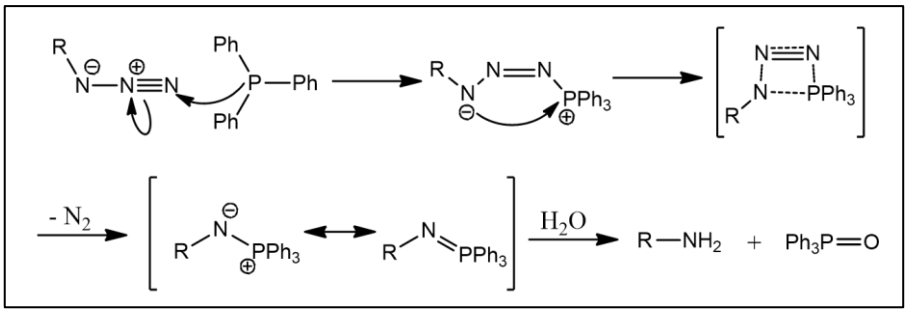

**Figure 3.2: mechanism of Staudinger reduction of azide. Triphenylphosphine ($PPh_3$) reacts with the azide to generate a phosphazide, which loses molecular nitrogen to form an iminophosphorane. Aqueous work up leads to the amine and phosphine oxide.**

The Staudinger reduction is orthogonal to Boc and Fmoc deprotection, the two most used strategy for peptide synthesis. A doubly-modified PNA monomer was designed with Boc as main protective group and Fmoc-protected lysine side chain at C5 (Figure 3.3). The monomer was synthesized starting with the commercially available Boc-L-Lys(Fmoc)-OH monomer.

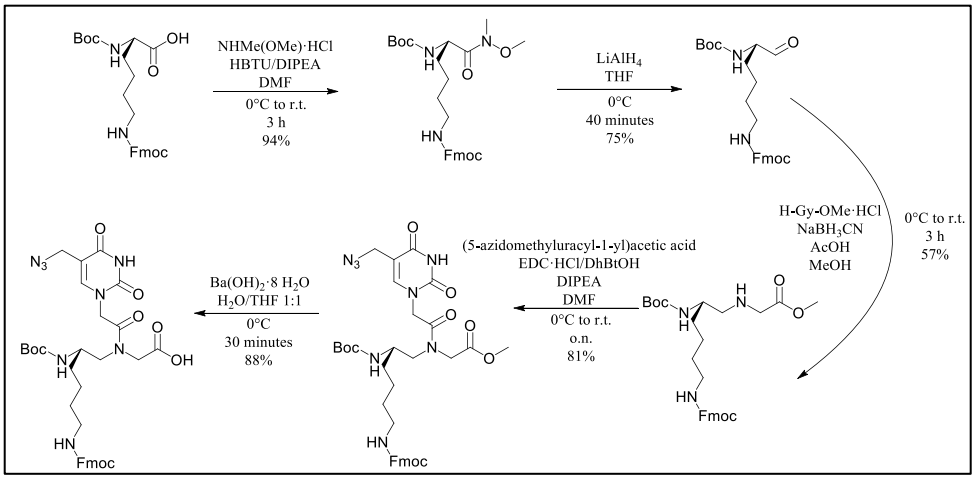


**Figure 3.3: Five step scheme for building the tri-protected monomer.**

The starting, commercial amino acid Boc-Lys(Fmoc), was reduced to amino aldehyde through the formation of the Weinreb amide intermediate. This is formed by coupling with *N,O*-dimethylhydroxylamine hydrochloride, in dry DMF. HBTU (*N,N,N′,N′*-Tetramethyl-O-(1H-benzotriazol-1-yl)uronium hexa

fluorophosphate) was used as activator and DIPEA as non-nucleophilic base. The product was obtained in high yields and did not need further purifications. The second step was the reduction of the Weinreb amide using lithium aluminum hydride ($LiAlH_4$). In this reaction oxygens chelate the lithium ion and the hydride can attack the carboxylic carbon, as shown in Figure 3.4. The work-up is performed by adding acid water, thus producing the target aldehyde. The reaction was carried out in dry THF, because little trace of water can promote the formation of basic lithium hydroxide that is capable to deprotect the Fmoc group on the side chain of the lysine. Moreover, the Fmoc-deprotection is slower than the reduction of the Weinreb amide so the reaction was kept at 0°C, under kinetic control.

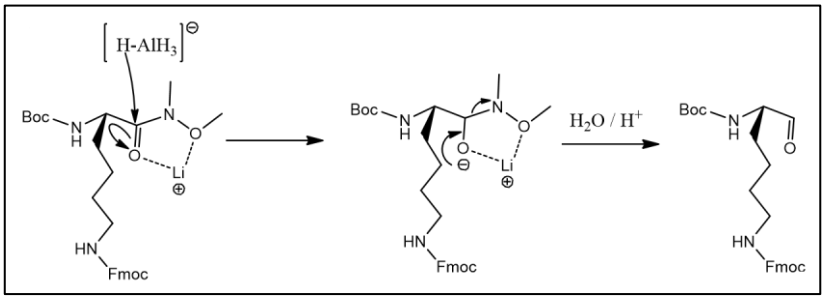


**Figure 3.4: reduction mechanism of Weinreb amide. It is possible to obtain ketones instead of aldehydes by substituting the reducing agent with an organolithium compound.**

The next step of the synthesis is the most difficult: a reductive amination between Boc-Lys(Fmoc)-H and glycine methyl ester. The initial step is the attack of the amine to the carbonyl group to form a hemiaminal species, which subsequently loses one molecule of water by alkylimino-de-oxo-bisubstitution, to form the imine. The loss of water is reversible, so an anhydrous solvent is recommended, in our case methanol. If the chosen solvent has high boiling temperature, the equilibrium of the reaction can be shifted towards the product by removing water. Sometimes, it is also possible to isolate the imine and perform the reduction in a second time, but both these conditions were not applicable in this case. We have thus performed a direct reductive amination with the adding of a reducing agent such as sodium cyanoborohydride ($NaBH_3CN$) and acetic acid. The latter reactant is added because it promotes both the formation of the iminium ion more suitable for the reduction by sodium cyanoborohydride.

In alternative, sodium triacetoxyborohydride $NaBH(OCOCH_3)_3$ can be used, especially if water amount is significant. Tests performed with this reactant give lower yields. One disadvantage of $NaBH_3CN$ is that it can form HCN in acid environment, so careful choice of the quenching and work-up conditions is recommended in order to avoid hazards.
Next step was the coupling with the backbone and a modified thymine: 2-(5-azidomethyluracil-1-yl) acetic acid. This coupling involves a secondary amine, so strong activators are necessary, like EDC· HCl and DhBtOH (see chapter 2.2). DIPEA was used as tertiary non-nucleophilic organic base and the reaction was performed in dry DMF. The reaction was left overnight and the obtained PNA modified-monomer was deprotected at its carboxylic terminal group with a basic hydrolysis. The O-methyl monomer was dissolved in THF without stabilizing agent (such as BHT dibutylhydroxytoluene) and an equivalent volume of acqueous solution of $Ba(OH)_2$ was added. Barium hydroxide was chosen because its reaction with methyl ester can be done without deprotection of the Fmoc group. Performing the reaction at 0°C helped to control this unwanted side reaction. After obtaining the desired monomer as carboxylate, THF is evaporated and HCL 37% was added dropwise to the solution, causing precipitation of the product in its carboxylic acid form. It is worth to remember that an elevate amount of acid is capable of Boc deprotection, so this procedure has to be performed carefully. The modified monomer was inserted in a growing chain of PNA synthesized on an MBHA resin, following Boc protocol, after six monomer: MBHA-Gly-TCGATG-T*, called PNA 1.
Not only the possibility of performing these modifications directly on SPS fully orthogonal were tested, but also the order of reaction for having better results. We found that, on MBHA resin, this order is arbitrary. Before completing the sequence, tests of orthogonal reactivity were performed by selective deprotection and acetylation of the free amine in the following three cases:

- PNA 2: reduction of the azide (trimethylphosphine 0.33M in THF / $H_2O$ 1:1 mixture, 10 minutes, 2 cycles; Figure 3.5, A)
- PNA 3: deprotection of the N-terminal Boc protected (5% m-cresol in TFA, 4 minutes, 2 cycles; Figure 3.5, B)
- PNA 4: deprotection of the amine of the lysine side chain Fmoc protected (20% piperidine in DMF, 8 minutes, 2 cycles; Figure 3.5, C)

As shown in Figure 3.6, PNAs cleaved with the azide group still present show a series of degradations products, with characteristic pattern of mass ions. Most important, in all cases there is no more starting material or unwanted side product caused by unselective deprotections. Due to these results, the synthesis was performed until the end of the desired sequence.

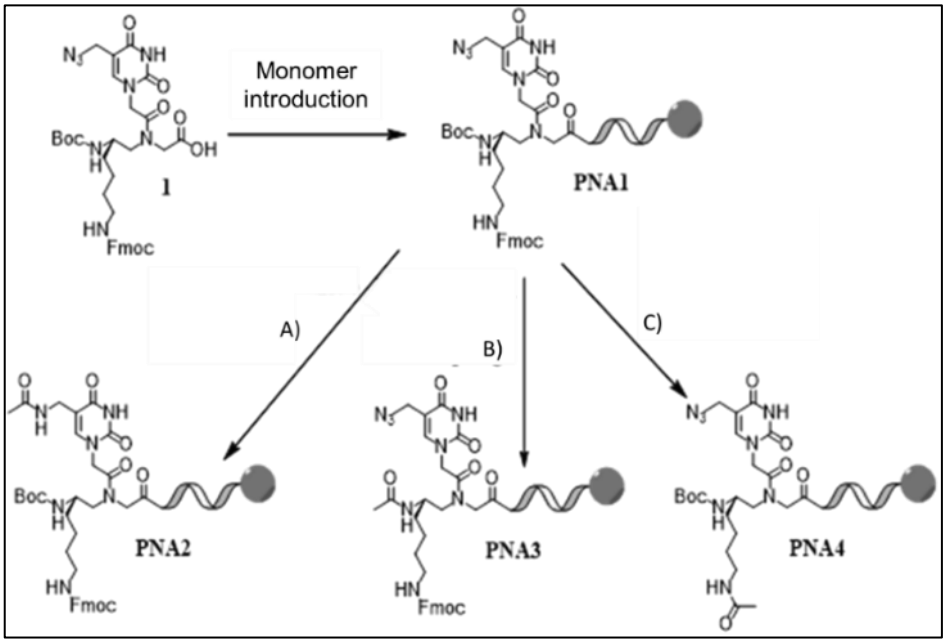


**Figure 3.5: acetylation after A) azide reduction B) Boc deprotection of main chain C) Fmoc deprotection of lysine side chain.**

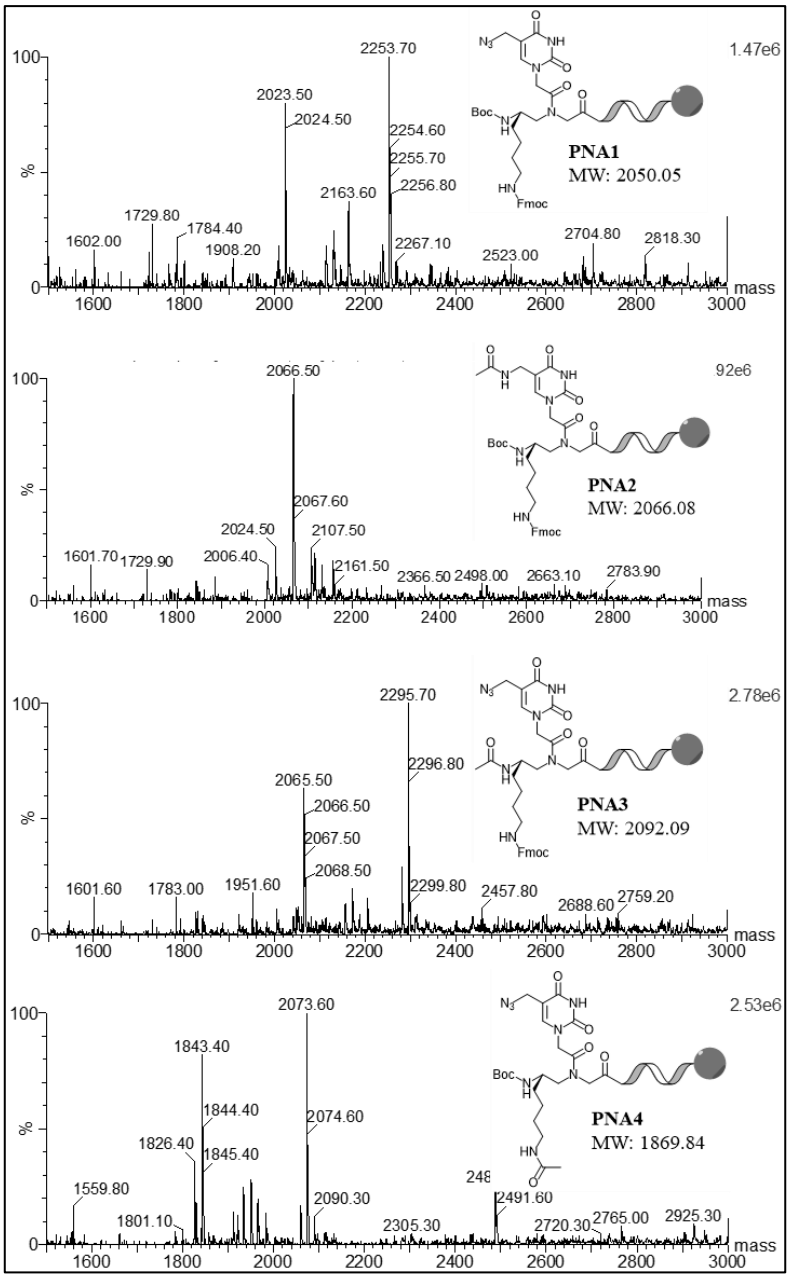


**Figure 3.6: mathematical deconvolution of the multicharged signals of ESI-MS spectra for PNA 1 to PNA 4 after cleavage from the resin. In PNAs where the azide is still present, characteristic peak at about MW+3 and MW-27 (molecular nitrogen) are present.**

A PNA library was also synthesizes following this strategy; the list is present in Figure 3.7. Experimental details of these syntheses are reported in a paper published by our research group[6], and only one of them bearing two pyrene units on the same monomer (SEQ 6) is subject of the present thesis.

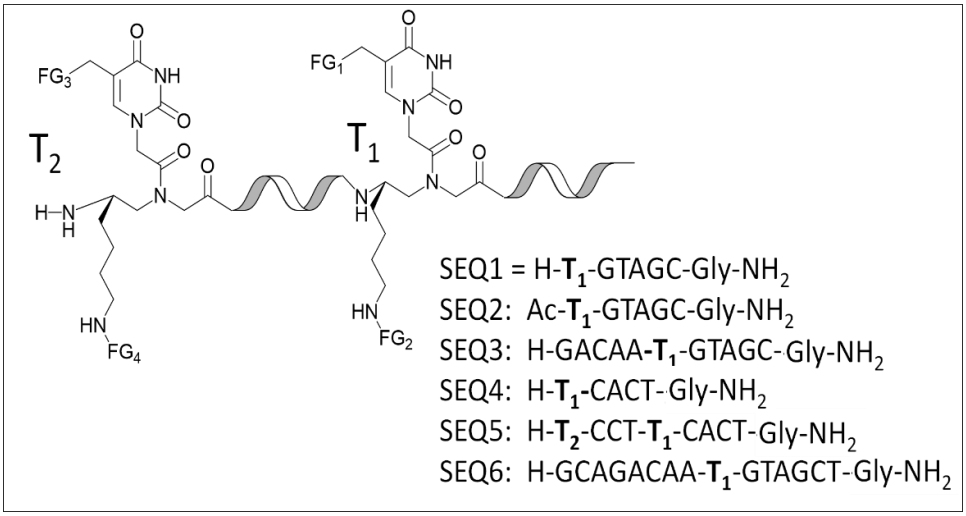


**Figure 3.7: different kinds of functional groups (FG) used: Ac = acetylation; Fl = fluorescein / 5(6)fluoresceincarbonyl; AEEA= spacer / 2-(2-aminoethoxy)ethoxyacetyl; Rh= rhodamine /Rhodamine B; Py= pyrene /1-pyrenylacetyl.**

For the synthesis of the doubly- modified PNA, sequence 6 was chosen, which is complementary to miR-221, a micro RNA that is involved in several cancer diseases. After insertion of the modified PNA monomer, the sequence was completed with standard monomers, then the reactions reported in Figure 3.8 were performed, with first reduction of the azide to amino group, then removal of the Fmoc group, and finally coupling of both amino groups with an excess of pyreneacetic acid in the presence of activators.

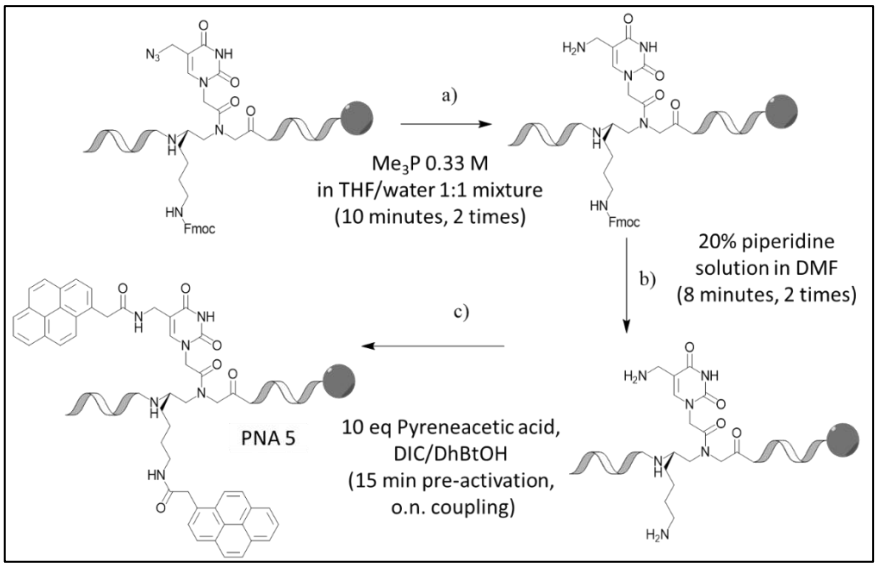


**Figure 3.8: Deprotection of amine functionalities on the nucleobase and on the side chain of the backbone. These reactions are fully orthogonal.**

A non-modified sequence, PNA 6, was also synthesized for comparison.
The doubly modified PNA was previously described in a PhD thesis and preliminary tests showed that the single-stranded probe presented a pyrene excimer fluorescence emission, which was lost upon interaction with the complementary DNA. However, a full characterization of the binding processes and of the selectivity was not performed.
In order to clarify the properties of this probe, melting temperatures (Tm) measurements were performed with a spectropolarimeter exploiting both CD and HT spectra (High Tension, applied at photomultiplier, correlated to UV-Vis spectrum). The mismatched base in MM DNA is in correspondence of the pyrene-tweezer unit of PNA 5. The sequence of these PNA and oligonucleotides target are:

- PNA 5: H-GCA GAC AAT* GTA GCT-Gly-$NH_2$
- PNA 6: H-GCA GAC AAT GTA GCT-Gly-$NH_2$
- DNA FM (full match): 5'-AGC TAC ATT GTC TGC-3'
- DNA MM (mis match): 5'-AGC TAC **G**TT GTC TGC-3'
- DNA RDM (random): 5'-GGT GAA TGA GTA AC-3'
- RNA FM (full match): 5'-AGC UAC AUU GUC UGC-3'

One problem on previous data (A. Bertucci, PhD thesis) was that the random sequence showed a melting transition at relatively high temperatures, which was attributed to self-melting. In order to complete the data and to clarify this aspect, measurements were done using circular dichroism in addition to UV-curves.

Melting temperatures were measured by monitoring not only CD spectra but also HT channel of the CD instrument at 260 nm, which is proportional to the absorbance. This allowed to have both UV and CD melting curves on the same samples. The temperature was varied from 18 °C to 90 °C with a heating rate of 1 °C/min and recording every 0.1 °C. Conditions: strand concentration = 1 µM in pH 7.0 PBS buffer (100 mM NaCl, 10 mM $NaH_2PO_4$) at 2% acetonitrile concentration.

Figure 3.9 shows graphs obtained after treatment of data from CD with software MatLab, Tm were calculated from the first derivative of the heating curves. Pervious measurement at UV-Vis spectrophotometer showed hysteresis between the melting and cooling curves, indicating slow complexation processes. Below the melting curves, a summary table illustrates the measured Tm.

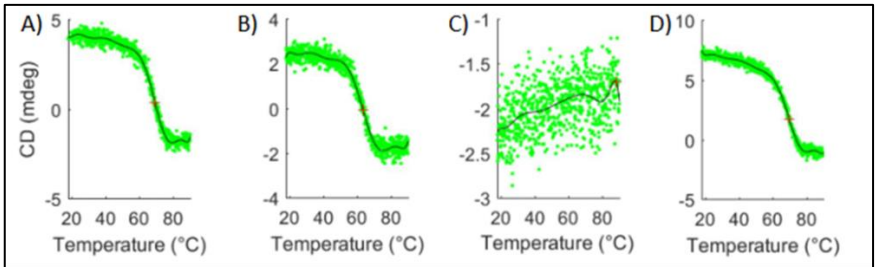


| | PNA 5 | | PNA 6 (unmodified) | |
|---|---|---|---|---|
| | Tm HT [°C] | Tm CD [°C] | Tm HT [°C] | Tm CD [°C] |
| DNA FM | 69.8 | 69.3 (A) | 71.9 | 72.7 |
| DNA MM | 67.2 | 63.4 (B) | 64.8 | 63.9 |
| DNA RDM | 62.9* | <18 (C) | n.d. | n.d. |
| RNA FM | 69.6 | 70.6 (D) | 74.4 | n.d. |

**Figure 3.9: Up, CD spectrum measured at 260nm of 1µM in PBS (2% acetonitrile) of PNA 5 duplex with A) DNA FM, B) DNA MM, C) DNA RDM, D) RNA FM. Bottom: table of melting temperatures. *Transition only visible in the HT curve of the CD spectropolarimeter, not corresponding to a duplex melting.**

As expected, modified PNA 5 have good affinity with target DNA and RNA, slightly lower than the unmodified PNA 6. PNA 5 is also capable to distinguish FM and MM DNA, with low discrimination ability, according to Tm. Pyrenes group seems to destabilize mainly the FM sequence, while the MM stability is less affected for their presence, resulting in a diminishing of selectivity. RDM DNA does not form stable duplex with PNA 5.

Changes in fluorescence of pyrene-modified PNA were also evaluated at 25°C. The pyrene excimer band was exhibited by PNA 5 in solution (broad band at 464 nm), suggesting that the two pyrene units are able to interact in aqueous environment. Stacking interactions and hydrophobic effect guide the formation of the excimer. Fluorescence measurement showed that the excimer peak diminish quickly when FM DNA is added meanwhile monomer peaks increase (for calculations only the peak at 381 nm was considered).

The fluorescence response of this PNA were the analyzed in detail considering: a) process rate (including data after one day); b) selectivity (including 5MM and RNA); c) salt effects.

Initial measurements were conducted for comparing two different concentration of probe and target DNA: 1 μM and 5 μM (Figure 3.10). As expected, higher concentration led to more pronounced switching in fluorescence emission. However, these data also showed that the system undergoes two different process: a first, relatively quick, process is accompanied by the decreasing of excimer fluorescent emission, a second, slow, process involve the rising of the monomers emission peaks. The first one can be explained as change in conformation of the PNA when target DNA is added: Watson and Crick interactions induced helicity and excimer is desegregated (π-π stacking and hydrophobic interactions are weak compared to hydrogen bonds between nucleobases). Nevertheless, pyrene units can have stacking interaction with nucleobases and therefore the monomer peaks are slowly increased instead a simultaneous conversion.

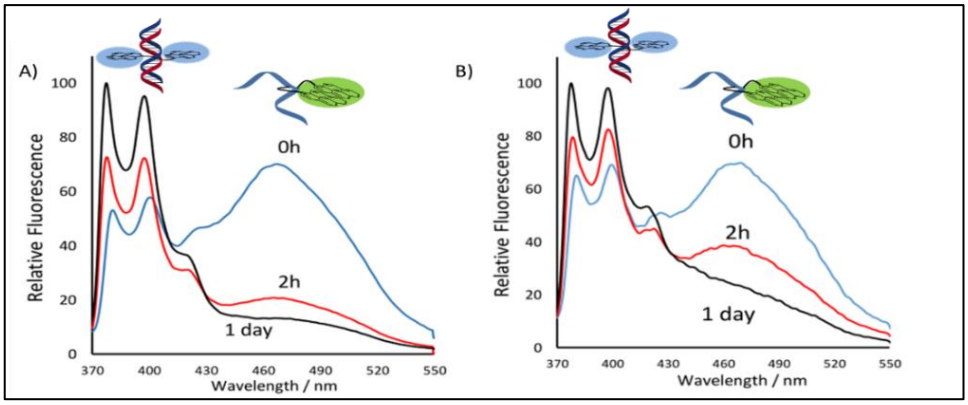


**Figure 3.10: Kinetic effects in the PNA 5:DNA complexation. Normalized (to maximum intensity) fluorescence emission spectra of a A) 5 μM, B) 1 μM aqueous solution of PNA 5, T = 25° C in PBS buffer with 0.7% acetonitrile. Spectra are recorded for PNA 5 initially alone, and at 120 min and 1 day after addition of full match DNA (DNA-FM).**

Since the duplex formation could be directly correlated to excimer emission decrease, the same experiment was carried out for a comparison between full-match and single-mismatch DNA sequences. In the latter case, the decrease of the broad excimer peak is less pronounced respect to the full match (Figure 3.11). This difference is better visible in Figure 3.12, where the ratio between excimer fluorescence and monomer fluorescence is plotted as a function of time.

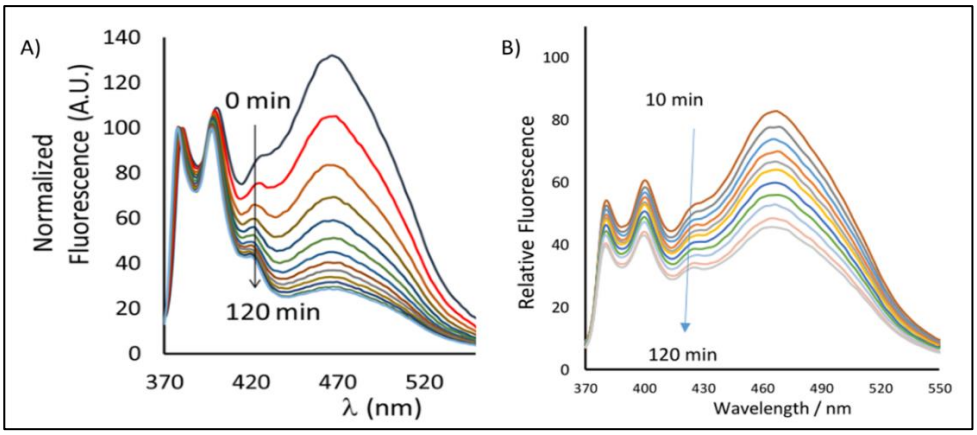


**Figure 3.11: Normalized fluorescence emission spectra of a 5 μM solution of PNA 5 hybridizing with A) the target DNA sequence, B) mismatch sequence (T = 25 °C, at different incubation times: top to bottom 0/10−120 min, time gaps of 10 min).**

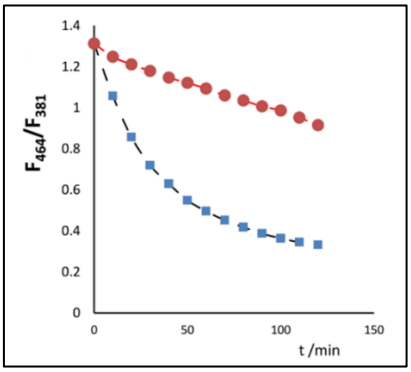


**Figure 3.12: Excimer/monomer fluorescence intensity ratio vs time, red profile = DNA-MM, blue profile = DNA- FM. The mismatched base in DNA-MM was in correspondence of the pyrene-modified unit of PNA 5. A slight fall of the excimer band was observed with slower kinetics and is however less pronounced than the one obtained for the full-match target.**

Other selectivity tests were conducted with random DNA and full match RNA. Histograms of response for vary type of target after annealing at 90°C to eliminate the kinetic effect are shown in Figure 3.1.12, this system is capable to recognize presence of full match DNA and RNA, while selectivity of WT versus mismatched DNA target was not very high, in spite of the great difference observed in the complexation kinetics. These data confirm Tm observations: the presence of pyrene seems to destabilize more the FM sequence compared

to the MM DNA. This not excellent thermodynamic selectivity is balanced by the kinetic information that are observable in Figure 3.13, which show that the kinetic discrimination is more effective. Hence, if measurements are made without annealing after a reasonable time delay, clear differences are seen in the fluorescence intensity between the full-match and the mismatch sequences.

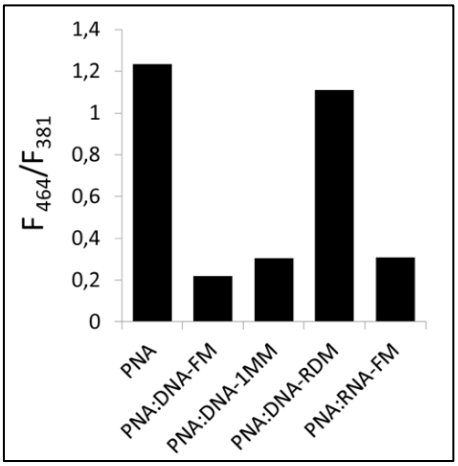


**Figure 3.13: Excimer/monomer emission intensity ratio for PNA 5 (1 µM) at 50 °C (after annealing at 90 °C) in the presence of full match (FM), single mismatch (MM), and random (RDM) DNA sequences, and full match RNA. Measurements were in PBS with 0.7% acetonitrile at pH 7.0.**

The ionic strength influence was evaluated by comparison of kinetic behavior in different salts concentration. As shown in figure 3.14, the disruption of pyrene excimer is faster in low salts concentration. This can be explained, because it is known that hydrophobic effect, that drive excimer formation, is weaker if the ionic strength of the aqueous is lower. In ionic strength is minimal, negative charges on DNA are less shielded by counterions and the DNA chain would be less likely be engaged in self-pairing and secondary structures, thus increasing the PNA complexation rates.

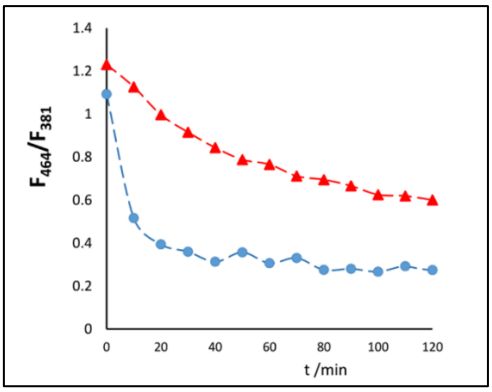


**Figure 3.14: Effect of ionic strength on the hybridization kinetics for PNA 14 (1 μM) with DNA-FM: red line: phosphate saline buffer (0.1 M NaCl) pH = 7.0, blue line: phosphate buffer with no NaCl.**

In order to establish if the observed fluorescence changes were due to a pyrene movement or to more complex conformational changes, CD spectra were acquired of PNA 5 itself (showing very weak CD signals), full match DNA, and on the complexes PNA 5:FM DNA and PNA 6:FM DNA (Figure 3.15). It is well known that unmodified PNA:DNA system show characteristic helicity after hybridization: since the CD signals of the duplex formed by the pyrene modified PNA 5 are similar to that of unmodified PNA 6, we could infer that the same kind of helical conformation is present in both duplexes, i.e. that the duplex structure for PNA5 is not significantly distorted by the presence of the pyrene units. Thus, in Figure 3.15, we can see the conformational change that occur to PNA 5 after hybridization; by adopting the typical PNA:DNA conformation the pyrene units are forced apart, and therefore the excimer fluorescence peak decrease. Other experiments at CD shows that at room temperature single mismatch DNA form the typical helical complex with PNA 6, confirming the poor thermodynamic discrimination of this probe, while random DNA does not form stable complex at room temperature with PNA 5.

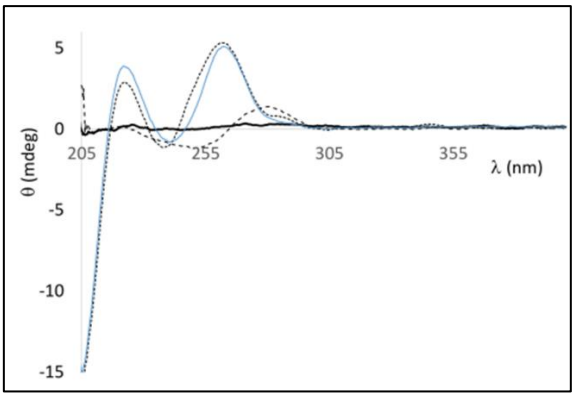


**Figure 3.15: Circular dichroism spectra at 25°C of single stranded PNA 5 (solid thick line, flat), fully complementary ssDNA-FM (dashed line), PNA 5: DNA-FM (dotted black line) and unmodified PNA6: DNA-FM (blue solid line), in PBS buffer, pH = 7.0 (2% acetonitrile); c = 1 μM of each strand. The conformation assumed by PNA 5: DNA duplex is similar to that of unmodified PNA 6; thus, the modified monomer conformation is expected to be rearranged to adapt to this structure.**

Static models of PNA 5 and PNA 5:DNA duplex could be built using classical parameters for the ssPNA and PNA:DNA duplex in Figure 3.16. These models are accurate in atom and bond size but the energy was not minimized and their aim is purely illustrative. In the proposed model, the single stranded PNA portion containing the two pyrene units was built using one of the minimum energy conformations of a MD simulation previously reported[7] showing the possibility of the pyrene pairing suggested by the excimer band. The second model was built using a script developed in our laboratory for PNA:DNA duplex construction with appropriate conformational parameters (M. D. Verona, PhD thesis). Different arrangements of the pyrene units are possible in this case, but pairing between them is only possible by disruption of the duplex conformation. Thus, the fluorescent peak quickly decrease after hybridization with target DNA because the formation of the helix disrupt excimer through the pyrenes forcing one in the major groove and the other in the minor groove of the duplex. After this stage, the pyrene units can undergo interaction with the duplex nucleobases, but this process is both difficult to interpret and appropriate models are not available, as they would require long MD calculation times or metadynamic approaches.

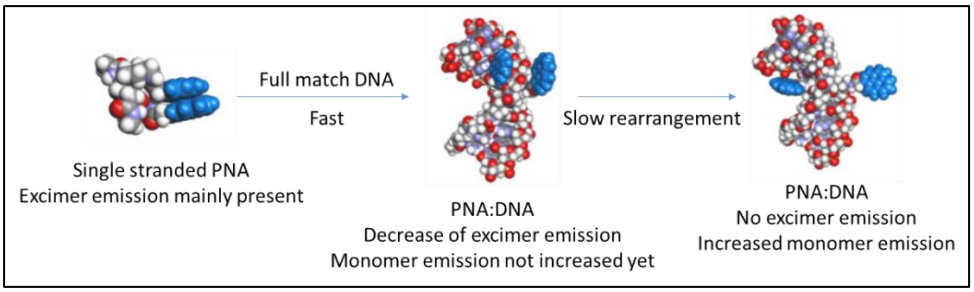


**Figure 3.16: Single stranded PNA 5 that hybridize with target DNA and form firstly a folded, then an extended geometry of the side arms. These geometries were built in order to have staggered geometry for each C-C bond; the side arms are geometry optimized, and structures are not energy minimized. Argus-Lab software was used for geometry optimization.**

## Conclusions

The developed synthetic strategy in solid phase synthesis with the modified monomer has been proved to give the possibility to obtain polyfunctional PNAs. These PNAs can be built inserting different moieties by fully orthogonal protective groups. As shown in the example presented here with two pyrene moieties on the same monomer, these modified PNA are not only able to bear reporter groups at specific positions within the PNA chain, but they can undergo programmed movements upon interaction with the DNA counterpart, giving rise to an 'induced-fit' movement. The possibility of designing PNAs with programmable switching properties enables to rationally design new switching probes not only for DNA analysis, but also as components of supramolecular systems.

## 3.2 EXPERIMENTAL PROCEDURE

**General**

The reagents were purchased from Sigma-Aldrich, Fluka, Merck, Carlo Erba, TCI Europe, ASM and used without further purification. DMF was dried over 4 Å molecular sieves and purged with nitrogen to avoid the presence of dimethylamine. THF was dried by distillation over sodium and stored over 3 Å molecular sieves. TLCs were run on Merck 5554 silica 60 aluminum sheets. Column chromatography was performed as flash chromatography on Merck 9385 silica 60 (0.040- 0.063 mm). NMR spectra (shown from Figure 3.3.1- to Figure 3.3.6) were registered on a Brucker Avance 400. δ values are expressed in ppm relatively either to CDCl 3 (7.29 ppm for proton and 76.9 ppm for carbon) or DMSO-d 6 (2.50 ppm for proton and 39.5 ppm for carbon). The following abbreviations are used to explain the multiplicities: s=singlet, d=doublet, t=triplet, q=quartet, m=multiplet, and br=broad. Fluorescence spectroscopy was performed on a LS-55 Perkin Elmer Fluorescence Spectrometer connected to a Lauda ecoline RE104 temperature controller. Circular dichroism spectra were recorded with a Jasco J715 spectropolarimeter and a PTC 348 temperature controller unit. UPLC-ESI-MS was carried out by using a Waters Acquity Ultra Performance LC with Waters Acquity SQ Detector and with ESI interface, and equipped with a Waters Acquity UPLC BEH 300 (50x2.1 mm, 1.7 µm, C18) (UPLC1, 0.90 minutes in H 2 O 0.2% FA, then linear gradient to 50% MeCN 0.2% FA in 5.70 minutes at a flow rate of 0.25 mL/min; UPLC2, 0.90 minutes in H 2 O 0.2% FA, then linear gradient to 100% MeCN 0.2% FA in 5.70 minutes at a flow rate of 0.25 mL/min). PNA oligomers were purified with RP-HPLC using a Phenomenex Jupiler C18 (5 µm, 300 Å, 250x10 mm) (HPLC1, linear gradient from H 2 O 0.1% TFA to 50% MeCN 0.1 % TFA in 30 minutes at a flow rate of 4.0 ml/min). HPLC-DAD-HR-MS were performed on a Dionex Ultimate 3000 with Thermo LTQ ORBITRAP XL detector equipped with a AERIS peptide (3.6 µm, XB-C18, 150x2.1 mm) (HPLC2, 5 minutes isocratic at 95% H 2 O 0.2% FA 5% MeCN 0.2% FA, then linear gradient to 50% MeCN 0.2% FA in 30 miuntes).

**Monomer synthesis**

See scheme in figure 3.3.

**N-methoxy-N-methyl-Nα-Boc-Nω-Fmoc-S-Lysinamide (s1)** was synthesized using a variant of a previously reported procedure 2 in a round-bottom flask, Boc-L-Lys(Fmoc)-OH (3.78 g, 8.07 mmol) was solubilized in DMF (38 ml) and cooled to 0°C with an ice bath. HBTU (3.37 g, 8.88 mmol) and DIPEA (4.2 ml, 24.11 mmol) were subsequently added to the solution, which was stirred for 15 minutes at 0°C and further 15 minutes at RT. Then, *N,O*-dimethylhydroxylamine hydrochloride (1.58 g, 16.20 mmol) was added. After 3 hours the solvent was evaporated under reduced pressure and the resulting oil was taken up with EtOAc (200 ml), transferred in a separatory funnel and washed with saturated $KHSO_4$ (2 x 400 ml), saturated $NaHCO_3$ (2 x 400 ml) and brine (2 x 200 ml). The organic layer was dried over $Na_2SO_4$ and the solvent removed under reduced pressure to yield **s1** (4.25 g, 94%) as a white foamy solid. Characterizations are compatible with those previously reported[8] and are listed for comparison. Corresponding original NMR spectra are reported below.
TLC (EtOAc) Rf = 0.51;

$^1$H NMR ($CDCl_3$, 400 MHz) δ 1.40-1.48 (11H, m) **H5 H13 H14 H15**, 1.50-1.62 (3H, m) **H6 H4'**, 1.65-1.75 (1H, m) **H4''**, 3.21 (5H, br s**) H7 H35**, 3.77 (3H, s) **H37**, 4.22 (1H, t, J= 6.7 Hz) **H20**, 4.39 (2H, d, J= 6.8 Hz) **H19**, 4.69 (1H, s) **H2**, 5.04 (1H, s) **H8**, 5.30 (1H, d, J= 8 Hz) **H1**, 7.32 (2H, t, J= 6.8 Hz) **H27 H30**, 7.40 (2H, t, J= 7.4 Hz) **H26 H31**, 7.60 (2H, d, J= 7.2 Hz**) H28 H29**, 7.77 (2H, d, J= 7.4 Hz) **H25 H32**.(Figure A1, Appendix)

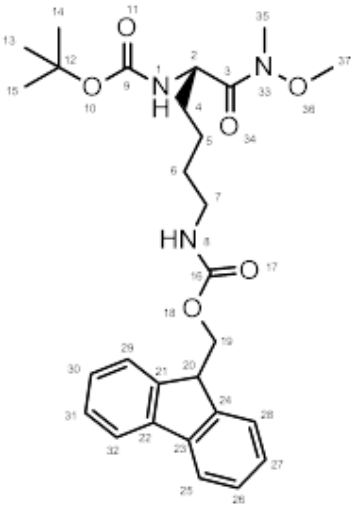

$^{13}$C NMR ($CDCl_3$, 100 MHz) δ 22.5 **C5**, 28.4 **C13 C14 C15**, 29.3 **C6**, 32.1 **C35**, 32.6 **C4**, 40.8 **C7**, 47.3 **C20**, 50.1 **C2**, 61.6 **C37**, 66.5 **C19**, 79.6 **C12**, 119.9 **C25 C32**, 125.1 **C28 C29**, 127.0 **C27 C30**, 127.7 **C26 C31**, 141.3 **C22 C23**, 144.0 **C24 C21**, 155.7 **C9**, 156.5 **C16**, 173.1 **C3**. (Figure A1 Appendix)

MS (ESI, MeOH) m/z calcd for $[C_{28}H_{37}N_3O_6]$ 511.28824, found: 534 $[M+Na]^+$ , 550 $[M+K]^+$ ;

HRMS (ESI, MeOH) found 534.2569 for $[M+Na]^+$.

**Nα-Boc-Nω-Fmoc-S-Lysinal (s2)** was synthesized using a variant of a previously reported procedure[8]; in a round-bottom flask **s1** (2.52 g, 4.93 mmol) was solubilized in THF (100 ml) and cooled down to 0° C with an ice bath. Under vigorous stirring, a 1M solution of $LiAlH_4$ in THF (6 mL, 5.91 mmol) was added dropwise over 10 minutes and the reaction was periodically checked to control the disappearing of the starting material. After 40 minutes the reaction was quenched by adding saturated $KHSO_4$ (65 ml), the organic layer was then removed under reduced pressure and the aqueous phase was extracted with EtOAc (200 ml). The organic phase was washed with saturated $KHSO_4$ (2 x 200 ml), saturated $NaHCO_3$ (2 x 200 ml) and brine (200 ml). The organic phase was dried over $Na_2SO_4$ and the solvent removed under reduced pressure to yield **s2** (1.68 g, 75%) as a white foamy solid. Characterizations are compatible with those previously reported[8] and are listed for comparison. Corresponding original NMR spectra are reported below.
TLC (EtOAc) Rf = 0.60;

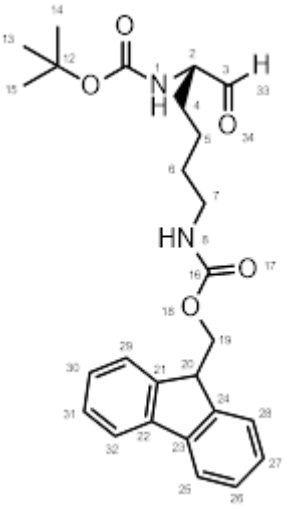

$^1$H NMR ($CDCl_3$ , 400 MHz) δ 1.35-1.50 (11H, m) **H5 H13 H14 H15**, 1.50-1.65 (3H, m) **H4' H6**, 1.82-1.97 (1H, m) **H4''**, 3.22 (2H, q, J= 6.1 Hz) **H7**, 4.15-4.30 (2H, m) **H2 H20**, 4.43 (2H, d, J= 6.4 Hz) **H19**, 4.93 (1H, br s) **H8**, 5.23 (1H, d, J= 6.6 Hz) **H1**, 7.34 (2H, t, J= 7.4 Hz) **H27 H30**, 7.42 (2H, t, J= 7.4 Hz) **H26 H31**, 7.61 (2H, d, J= 7.4 Hz) **H28 H29**, 7.78 (2H, d, J= 7.5 Hz) **H25 H32**, 9.59 (1H, s) **H33**. (Figure A2 Appendix)

$^{13}$C NMR ($CDCl_3$, 100 MHz) δ 22.2 **C5**, 28.3 **C13 C14 C15**, 28.7 **C4**, 29.6 **C6**, 40.4 **C7**, 47.3 **C20**, 59.6 **C2**, 66.6 **C19**, 80.2 **C12**, 119.9 **C25 C32**, 125.0 **C28 C29**, 127.1 **C27 C30**, 127.7 **C26 C31**, 141.3 **C22 C23**, 144.0 **C21 C24**, 155.7 **C9**, 156.6 **C16**, 200.0 **C3**. (Figure A2 Appendix)

MS (ESI, MeOH) m/z calcd for $[C_{26}H_{32}N_2O_5]$: 452.23112, found: 507 $[M+Na+CH_3OH]^+$ , 523 $[M+K+CH_3OH]^+$ ;

HRMS (ESI, MeOH) found: 475.24554 for $[M+Na]^+$ .

**Nα-Boc-Ψ-(Nω-Fmoc-S-Lysin)glycine methyl ester (s3)**: in a round-bottom flask **s2** (1.60 g, 3.53 mmol) and glycine methyl ester hydrochloride (1.33 g, 10.60 mmol) were solubilized in MeOH (40 ml) and cooled to 0° C with an ice bath. After 20 minutes $NaBH_3CN$ (266 mg, 4.24 mmol) and acetic acid (0.24 mL, 4.24 mmol) were added and the reaction mixture was allowed to react for further 3 hours before evaporating the solvent under reduced pressure. The resulting solid was dissolved in EtOAc (250 ml), transferred in a separatory funnel and washed with saturated $NaHCO_3$ (2 x 150 ml) and brine (150 ml). The organic layer was dried over $Na_2SO_4$ , the solvent removed under reduced pressure, and the residue was purified by flash chromatography (from AcOEt/hexane 7:3 to AcOEt) to afford s3 (1.05 g, 57%) as a yellowish foamy solid.
TLC (EtOAc) Rf = 0.28;

$^1$H NMR ($CDCl_3$ , 400 MHz) δ 1.35-1.60 (15H, m) **H4 H5 H6 H13 H14 H15**, 1.89 (1H, br s) **H33**, 2.56-2.73 (2H, m) **H3**, 3.21 (2H, q, J= 5.8 Hz) **H7**, 3.39 (1H, d, J= 17.5 Hz) **H34'**, 3.37 (1H, d, J= 17.3 Hz) **H34''**, 3.60-3.68 (1H, m) **H2**, 3.72 (3H, s) **H38**, 4.22 (1H, t, J= 6.5 Hz) **H20**, 4.40 (2H, d, J= 6.2 Hz) **H19**, 4.81 (1H, s) **H1**, 5.04 (1H, s) **H8**, 7.32 (2H, t, J= 7.4 Hz) **H27 H30**, 7.41 (2H, t, J= 7.3 Hz) **H26 H31**, 7.61 (2H, d, J= 7.2 Hz) **H28 H29**, 7.77 (2H, d, J= 7.4 Hz) **H25 H32**. (Figure A3 Appendix)

$^{13}$C NMR ($CDCl_3$ , 100 MHz) δ 23.0 **C5**, 28.4 **C13 C14 C15**, 29.6 **C6**, 32.8 **C4**, 40.7 **C7**, 47.3 **C20**, 50.1 **C34**, 50.7 **C38**, 51.8 **C3**, 53.0 **C2**, 66.5 **C19**, 79.2 **C12**, 119.2 **C25 C32**, 125.1 **C28 C29**, 127.0 **C27 C30**, 127.7 **C26 C31**, 141.3 **C22 C23**, 144.0 **C21 C24**, 156.0 **C9**, 156.5 **C16**, 173.0 **C35**. (Figure A3 Appendix)

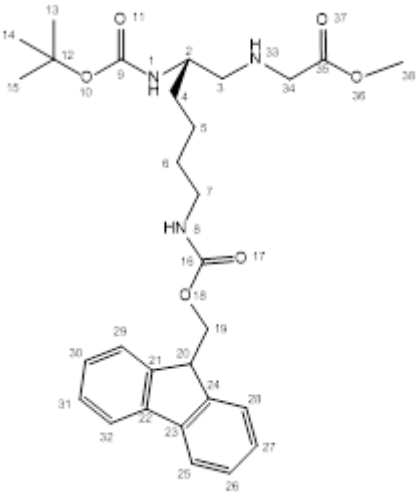

MS (ESI, MeOH) m/z calcd for $[C_{29}H_{39}N_3O_6]$: 525.28389, found 526 $[M+H]^+$, 548 $[M+Na]^+$ .

HR-MS (LTQ-Orbitrap, MeOH) m/z calcd for $[C_{29}H_{39}N_3O_6]$: 525.23389, found 526.29053 $[C_{29}H_{40}N_3O_6]^+$ .

**Boc-PNA (5L-Lys(Fmoc))-T(N3)-OMe (s4)**: in a round-bottom flask 2-(5-azidomethyluracil-1-yl) acetic acid (398 mg, 1.77 mmol), EDC·HCl (338 mg, 1.77 mmol), DhBtOH (288 mg, 1.77 mmol) and DIPEA (308 µL, 1.77 mmol) were solubilized in dry DMF (5 ml) and cooled down to 0°C with an ice bath. Then **s3** was added to the mixture, which was stirred for 30 minutes, then warmed to RT and allowed to react overnight. The solvent was then evaporated under reduced pressure. The resulting solid was dissolved in EtOAc (250 ml), transferred in a separatory funnel and washed with saturated $KHSO_4$ (2 x 250 ml), saturated $NaHCO_3$ (2 x 250 ml) and brine (250 mL). The organic phase was dried over $Na_2SO_4$ , the solvent removed under reduced pressure and the residue was purified by flash chromatography (gradient elution from EtOAc/hexane 9:1 to EtOAc), to yield s4 (874 mg, 81%) as a yellowish foamy solid.
TLC (EtOAc) Rf = 0.30;

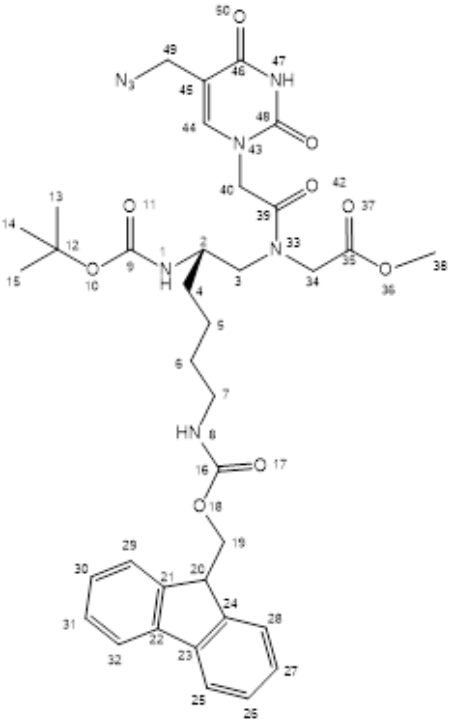

$^{1}H$ NMR ($CDCl_3$ , 400 MHz, major rotamer) δ 1.35-1. 63 (15H, m,) **H4 H5 H6 H13 H14 H15**, 3.15-3.25 (2H, m) **H7**, 3.32-3.41 (1H, m) **H2**, 3.45-3.53 (2H, m) **H3**, 3.74 (3H, s) **H38**, 3.98-4.09 (2H, m) **H34**, 4.14 (1H, t, J= 7.0 Hz) **H20**, 4.20-4.32 (2H, m) **H19**, 4.40-4.89 (4H, m) **H40 H49**, 4.73 (1H, d, J= 8.3 Hz) **H8**, 5.02 (1H, br s) **H1**, 7.27 (1H, s) **H44**, 7.33 (2H, t, J= 7.2 Hz) **H27 H30**, 7.42 (2H, t, J= 7.5 Hz) **H26 H31**, 7.61 (2H, d, J= 7.5 Hz) **H28 H29**, 7.78 (2H, d, J= 7.6 Hz) **H25 H32**, 9.12 (1H, s) **H47**. (Figure A4 Appendix)

$^{13}C$ NMR ($CDCl_3$ , 100 MHz, major rotamer) δ 22.8 **C5**, 28.3 **C13 C14 C15**, 29.4 **C6**, 31.4 **C4**, 40.2 **C7**, 47.1 **C49**, 47.3 **C40**, 47.7 **C20**, 49.3 **C2**, 52.4 **C3**, 53.0 **C38**, 66.6 **C19**, 80.0 **C12**, 109.4 **C45**, 120.0 **C25 C32**, 125.0 **C28 C29**, 127.1 **C27 C30**, 127.7 **C26 C31**, 141.3 **C22 C23**, 143.6 **C44**, 144.0 **C21 C24**, 150.7 **C48**, 156.0 **C9**, 156.7 **C16**, 162.8 **C46**, 167.2 **C39**, 169.5 **C35**. (Figure A4 Appendix)

MS (ESI, MeOH) m/z calcd for [$C_{36}H_{44}N_8O_9$]: 732,32313, found 755 $[M+Na]^+$ , 771 $[M+K]^+$.
HR-MS (LTQ-Orbitrap, MeOH) m/z calcd for [$C_{36}H_{44}N_8O_9$]: 732.32313, found 755.31282 $[C_{36}H_{44}N_8O_9Na]^+$

**Boc-PNA (5L-Lys(Fmoc))-T(N3)-OH (1)**: a solution of $Ba(OH)_2 \cdot 8\ H_2O$ (412 mg, 1.30 mmol) in water (45 ml) was added to a solution of **s4** (863 mg, 1.18 mmol) in THF (45 ml) at 0°C. The reaction was periodically controlled with TLC until disappearing of the starting material. After 30 minutes the reaction was quenched with 1M HCl (2.7 ml), the solvent was removed under reduced pressure and the pH was adjusted to 2.5. The solution was then cooled to 4°C for 2 hours and the product 1 (874 mg, 88%) was then collected by Büchner filtration.
TLC (EtOAc/MeOH 9:1) Rf = 0.35;

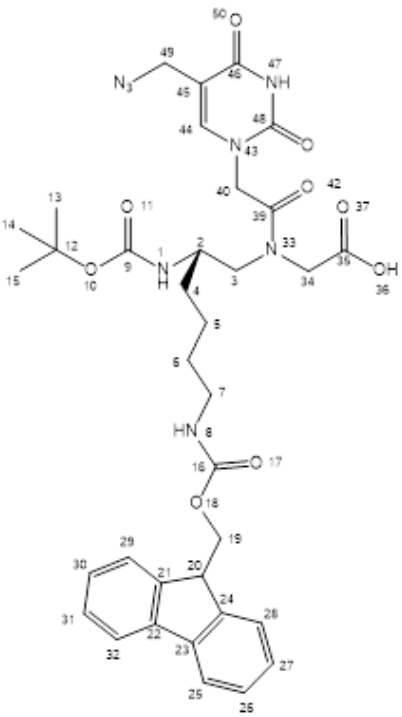

$^1$H NMR (DMSO-d 6 , 400 MHz, major rotamer) δ 1.10-1.55 (15H, m) **H4 H5 H6 H13 H14 H15**, 2.90-3.02 (2H, m) **H7**, 3.2-3.6*, 3.90 (4H, d, J= 17.0 Hz**) H3 H34**, 4.01 (1H, d, J= 17.0 Hz) **H2**, 4.07 (2H, s) **H49**, 4.21 (1H, t, J= 6.5 Hz) **H20**, 4.29 (2H, d, J= 6.6 Hz) **H19**, 4.52-4.83 (2H, m) **H40**, 6.80 (1H, d, J= 8.8 Hz) **H1**, 7.23-7.30 (1H, m) **H8** , 7.34 (2H, t, J= 7.4 Hz) **H27 H30**, 7.42 (2H, t, J= 7.4 Hz) **H26 H31**, 7.59 (1H, s) **H44**, 7.69 (2H, d, J= 7.3 Hz) **H28 H29**, 7.89 (2H, d, J= 7.6 Hz) **H25 H32**, 11.58 (1H, br s) **H47**.(Figure A5 Appendix)

$^{13}$C NMR (DMSO-d 6 , 100 MHz, major rotamer) δ 23.3 **C5**, 28.6 **C13 C14 C15**, 29.7 **C6**, 31.6 **C4**, 39.2- 40.8** **C7**, 47.1 **C49**, 47.2 **C20**, 48.5 **C40**, 49.3 **C2**, 50.5 **C34**, 51.9 **C3**, 66.6 **C19**, 78.4 **C12**, 107.7 **C45**, 120.6 **C25 C32**, 125.6 **C28 C29**, 127.9 **C37 C30**, 128.1 **C26 C31**, 141.2 **C22 C23**, 144.4 **C21 C24**, 145.9

**C44**, 151.1 **C48**, 156.1 **C9**, 156.5 **C16**, 163.9 **C46**, 168.0 **C39**, 170.9 **C35.** (Figure A5 Appendix)

COSY Spectra (Figure A6 Appendix)

MS (ESI, MeOH) m/z calcd for [$C_{35}H_{42}N_8O_9$]: 718,30747, found 741 $[M+Na]^+$ , 757 $[M+K]^+$ .

HR-MS (LTQ-Orbitrap, MeOH) m/z calcd for [$C_{35}H_{42}N_8O_9$]: 718.30747, found 741.29731 [$C_{35}H_{42}N_8O_9Na]^+$

* Integral not defined due to signal overlap with water peak. ** Signal overlap with DMSO.

**PNA synthesis**

The following solutions were used for the solid-phase synthesis of PNA

| Solutions for Boc synthesis | | Proportion |
|---|---|---|
| Capping resin | $Ac_2O$/py/dry DMF | 1:2:2 |
| Deprotection | TFA/m-cresol | 95:5 |
| Capping | $Ac_2O$/py/dry DMF | 1:25:25 |
| Piperidine wash | Piperidine/DMF | 1:9 |
| Cleavage | TFA/TFMSA/m-cresol/thioanisole | 6:2:1:1 |

Boc protocol was composed of the following steps: a) deprotection 2x4min ; b) DCM Wash; c) DMF Wash; d) Kaiser test (1 min, should be positive); e) coupling 1x30 min (activation 2 min, activation solution: 5 eq of monomer and activator, 10 eq of DIPEA in dry DMF); f) DMF wash; Kaiser test (1min, should be negative); g) capping 2x1min; h) DMF wash; i) piperidine wash 2x2 min; l) DMF wash; m) DCM wash.

The ninhydrin test was performed using the following solutions:

| Kaiser Test | |
|---|---|
| K1 | 1g of ninidrin in 10 mL absolute ethanol |
| K2 | 8g phenol in 2 mL of absolute ethanol |
| K3 | 0.2 mL acqueous solution 0.001M of KCN diluited at 10 mL with pyridine |

**The following protocol was used: put 2-3 drops of each solution in a tube where some part of the resin was previously added with a capillary. Put the tube in an oil bath at 100°C for 1 minute. The test is positive if the resin became blue.**

The synthesis of the modified PNA probes was performed in 5 µmol scale, with standard manual Boc-based solid phase synthesis with HBTU/DIPEA as coupling mixture, using the preformed monomer (when needed) in addition to commercially available Boc-PNA(Bhoc)-OH monomers. MBHA resin was first loaded with Fmoc-Gly-OH as first monomer (0.2 mmol/g). Once the whole sequence was synthesized, modifications on the lysine side chain were carried out removing Fmoc protective group with 20% piperidine solution in DFM (8 minutes, 2 times) and subsequently coupling the desired molecule using standard HBTU/DIPEA strategy. Modification of the nucleobase side was obtained by preliminary reduction of the azide group using an established solid phase Staudinger reaction with 0.33 M trimethylphosphine in THF/water 1:1 mixture (10 minutes, 2 times), followed by condensation with desired carboxylic acid using 10 equivalents and DIC/DhBtOH as activating mixture (15 minutes pre-activation and overnight coupling). Cleavage was performed using standard solution, collecting the filtered liquid and precipitate PNA by adding at least 10 volumes of diethyl ether. The purity and identity of the PNAs were evaluated by cleavage of a part of the resin and analysis by UPLC-ESI/MS, then PNA 5 and 6 were completely deprotected, cleaved entirely from the resin, and purified.

Quantification by UV-Vis spectroscopy (ε 260 T 8600 $M^{-1}cm^{-1}$, C 6600 $M^{-1}cm^{-1}$, A 13700 $M^{-1}cm^{-1}$, G11700 $M^{-1}cm^{-1}$, pyrene 6338 $M^{-1}cm^{-1}$) of the PNA dilution dissolved in 1 mL of water.

PNA 5: yield 13.9%. HPLC-DAD-HR-MS characterization: 4736.04156 [M]: m/z found 1580.30523 $[M+3H]^{3+}$, 1185.48085 $[M+4H]^{4+}$, 949.58621 $[M+5H]^{5+}$, 790.65637 $[M+6H]^{6+}$, 677.84913 $[M+7H]^{7+}$. (Figure A7 Appendix)

PNA 6: yield 4.2%. Rt : 2.91; UPLC-ESI-MS characterization: m/z calcd 4168.0 [M]: 1390.3 $[M+3H]^{3+}$, 1043.1 $[M+4H]^{4+}$, 834.6 $[M+5H]^{5+}$, 695.9 $[M+6H]^{6+}$, 596.5 $[M+7H]^{7+}$, 522.1 $[M+8H]^{8+}$. (Figure A8 Appendix)

Circular dichroism spectra were obtained using annealed solutions at 1 μM strand concentration in pH 7.0 PBS buffer (100 mM NaCl, 10 mM $NaH_2PO_4$) at 2% acetonitrile concentration, scanning the 200÷500 nm range at 50 nm/min. Spectra are obtained as sum of 5 different scans, background corrected and recorded at 25 °C and 50 °C. Thermal denaturation profiles were measured by monitoring both the ORD and HT signal at 260nm from 18 °C to 90 °C with a heating rate of 1 °C/min. Melting temperatures were calculated from the first derivative of the $10^{th}$ order polynomial that best fitted the experimental data (using Matlab script).
Fluorescence emission spectra were recorded at $\lambda_{ex}$ = 343 nm (slit ex = 5 nm, slit em = 10 nm) for working volumes of 200 μL, using quartz cuvettes (0.3 x 1 cm path lengths). Aqueous solutions of PNA 5 were obtained by diluting the PNA and DNA stock solutions in PBS (87.6 mM NaCl, 8.76 mM phosphate, pH = 7) to final concentrations either 1 or 5 μM (containing 0.7% acetonitrile). An equimolar ratio 1:1 PNA 5: DNA (FM, MM, RDM) or RNA (FM) was always employed. Fluorescence intensity was normalized, either at maximum intensity or to fluorescence intensity at 381 nm (monomer emission).

Bibliography:


1. Seo YJ, Hwang GT, Kim BH. Quencher-free molecular beacon systems with two pyrene units in the stem region. *Tetrahedron Lett*. 2006;47(24):4037-4039.
2. Sau SP, Kumar TS, Hrdlicka PJ. Invader LNA: Efficient targeting of short double stranded DNA. *Org Biomol Chem*. 2010;8(9):2028.
3. Boonlua C, Ditmangklo B, Reenabthue N, et al. Pyrene-labeled pyrrolidinyl peptide nucleic acid as a hybridization-responsive DNA probe: comparison between internal and terminal labeling. *RSC Adv*. 2014;4(17):8817-8827.
4. Manicardi A, Guidi L, Ghidini A, Corradini R. Pyrene-modified PNAs: Stacking interactions and selective excimer emission in PNA2DNA triplexes. *Beilstein J Org Chem*. 2014;10:1495-1503.
5. Manicardi A, Accetta A, Tedeschi T, Sforza S, Marchelli R, Corradini R. PNA bearing 5-azidomethyluracil. *Artif DNA PNA XNA*. 2012;3(2):53-62.
6. Manicardi A, Bertucci A, Rozzi A, Corradini R. A Bifunctional Monomer for On-Resin Synthesis of Polyfunctional PNAs and Tailored Induced-Fit Switching Probes. *Org Lett*. 2016;18(21):5452-5455.
7. Verona MD, Verdolino V, Palazzesi F, Corradini R. Focus on PNA Flexibility and RNA Binding using Molecular Dynamics and Metadynamics. *Sci Rep*. 2017;7(1):42799.
8. Englund EA, Appella DH. Synthesis of γ-Substituted Peptide Nucleic Acids: A New Place to Attach Fluorophores without Affecting DNA Binding. *Org Lett*. 2005;7(16):3465–3467.


.

# 4-PNA PROBES FOR EARLY DETECTION OF CANCER


## Abstract:

In this chapter is described the work done to produce PNA probes for SPRi (Surface Plasmon Resonance imaging) detection, to be used in new instrumentation capable of reading microfluidic, nanostructured, disposable chips, for detection of colorectal cancer, also in the frame of a large collaborative EU project (ULTRAPLACAD). The PNA probes were designed in order to target both microRNA (miR) and DNA containing point mutation of the KRAS and NRAS genes. In particular, for DNA analysis the thermal stability of PNA:DNA full-match and singly mismatched sequences was measured. C2-modified PNAs were synthesized in order to improve the sequence selectivity. For this purpose, a novel strategy based on minimally protected chiral monomers has been developed.


## 4.0 INTRODUCTION

In many applications sensing technologies are beneficial, and they are especially expected to produce a quantum leap in the case of early detection of pathologies, in particular cancer. Early detection of cancer is one of the strategic issue in healthcare, since if the patients are treated in early stages, the survival rate would increase and costs would diminish. Genosensing is very important in this field since cancers are associated with DNA specific alterations and dysregulation of other nucleic acid components (mRNA and microRNA).

Depending on the specific gene expression, different treatment can be applied, making DNA detection a powerful tool for patient follow-up. Ultrasensitive techniques can allow to detect circulating cancer-related nucleic acids by a simple blood analysis (liquid biopsy)[1,2,3]. With this aims, scientist of different countries and backgrounds, placed in different states of European Union (Figure 4.1), joined their effort in order to realize a novel sensing platform in the ULTRAPLACAD project (Grant Agreement no.: 633937, http://ultraplacad.eu/). This project was aimed to develop plasmonic-based instrument and components for efficient detection of cancer markers. Two types of marker were chosen: tumor autoantibodies (a-TAAs), which can bind to specific

diagnostic peptides, and circulating DNAs and miRNAs, derived from apoptosis or necrosis of cancer cells that will be captured by PNA probes immobilized on the sensor's surface. NESPRI (Nanoparticle Enhanced Surface Plasmon Resonance Imaging) and PEFSI (Plasmon Enhanced Fluorescent Surface Imaging) were used in combination for the detection of the above mentioned biomarkers. Concerning nucleic acids detection, the main goal of the project has been to achieve PCR-free detection, which is possible because of the ultra-sensitivity of the NESPRI technique. Monitoring three different markers can help in avoiding false positive results and give a large picture of the status of the patient.

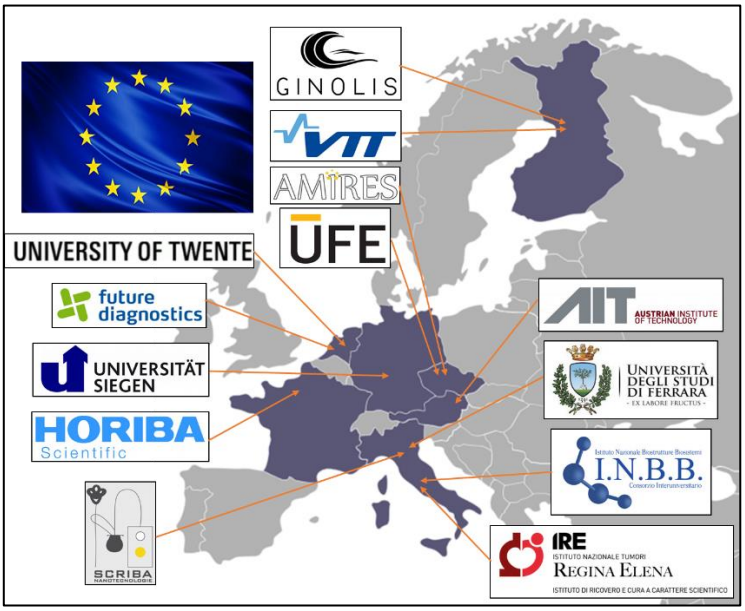


**Figure 4.1: map of Europe with location of consortium members. University of Parma is a part of INBB (National Institute for Biosystems and Biostructures).**

The chosen DNA traits are from genes NRAS exon 2 and KRAS exon 2 and 3. These genes code for G-proteins that can be activated by EGFR (Epidermal Growth Factor Receptor). These proteins are present on the surface of cells and can bind guanosine triphosphate (GTP). If the RAS protein binds a GTP molecule, it is activated and a cascade of reactions promote cell replication. After that, GTP is transformed in GDP (guanosine diphosphate) and the protein becomes inactive. Some point mutation can cause the presence of a wrong

amino acid in the primary structure of the protein RAS which induces a misfolding, in which the protein is always active, and the continuous signaling induces a cascade of effects that ultimately can induce the cell to replicate uncontrollably. Colorectal cancer can be treated by a therapy with monoclonal antibody against protein EGFR (cetuximab and panitumumab[4]), blocking its downstream effects, and in particular RAS activation, but in case a point mutation is present in the RAS gene the corresponding signal pathway can remain active and the treatment is not effective. About 50% of colorectal cancer cases show a mutation of RAS genes (Figure 4.2). Other kinds of antibody have VEGF (Vascular Endothelial Growth Factor) as target. This is a growth factor for little blood vessels; cancer cells produce this protein because they need a lot of oxygen and nutritive substances present in blood for replication. Limiting VEGF therefore can help in limiting cancer cells proliferation. Moreover, cancer cells can use blood vessels as way for migrate in different body districts and produce metastasis. At the moment, two antibodies have been developed for targeting VEGF: bevacizumab and aflibercept. Usually these antibodies are given to the patients in combination with classical chemotherapy. Currently, RAS gene evaluation is performed by biopsy of cancer tissue or metastasis and results are ready after 7-10 days. Ultrasensitive PNA-based SPRi sensor can significantly decrease this time and at the same time give rise to very specific signals.

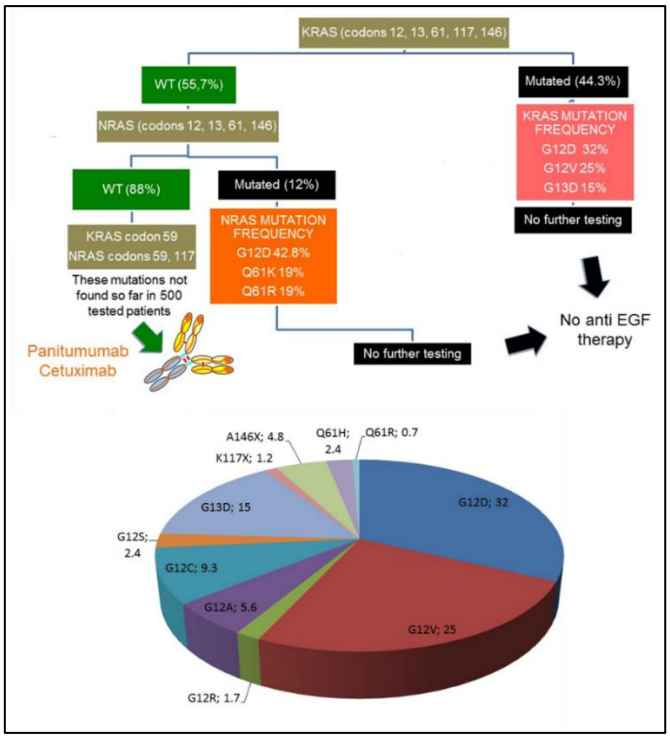


**Figure 4.2: Flow chart of RAS mutations screening and cake diagram representing percentages of type of point mutation in about 50% of colorectal cancer caused by modification at RAS protein.**

PNA probes complementary to these point mutations should take into account that a long PNA sequence gives better stability, but discrimination between single base mismatch is not optimal; so the sequence of PNA should be designed long enough to be stable but short enough to be selective.

Very important markers for colorectal cancer are also micro RNAs (miR). These are small, endogen, non-coding RNAs (usually around 19-23 monomers) that are active in gene regulation (see Chapter 1). Their pathway of synthesis involves an initial transcription into precursors (1-3 k bases), called primary miRs. These pri-miRNAs are enzymatically cut into fragments of 70-100-nt long stem-loop structures called precursor miR (pre-miRNA). In this stage, they can migrate from nucleus to cytoplasm, where a second enzymatic process create mature miR. Mature miRNAs can regulate gene expression, in particular, they hybridize with target messenger RNA (mRNA) and induce gene silencing, by being incorporated into RISC (RNA Induced Silencing Complex, a

complex of RNA molecules and proteins); the RISC acts on target mRNA principally by enzymatic degradation or by simple repression. In this process a crucial role is played by the so called 'seed region' of the mature miRNA that is a conserved heptameric sequence, situated at positions 2-7 from the miRNA 5´-end region. A full match between miRNA seed region and its target mRNA is required for gene silencing. Very high affinity probes are necessary for miR detection by liquid biopsy of blood, due to the low abundance of circulating miRs.

There are miRs particularly clinically relevant in colorectal cancer: for example miR-221, miR-222 and miR-141. The first two inhibit the formation of mast/stem cell growth factor receptor (SCFR) that prevents cell migration and proliferation in endothelial tissues;[5] furthermore, they have been shown to inhibit the $P27^{KIP1}$ protein, which is a key regulator of cell cycle and a tumor suppressor gene. In colorectal cancer, these miRNAs are overexpressed, so SCFR factor in not enough expressed and cancer cells are allowed to migrate and form metastasis. For what concern miR-141, it is not present in abundance in cancer tissue, hypothesis suggest that miR-141 could be elevated only in metastases and not in the primary tumor and that the circulating miR-141 could be a reflect of differential inflammatory response[6]. Dysregulation of miR-141 is depending on the type of cancers[7], but in colorectal cancer it is overexpressed and blocks production of ZEB2 protein that is a transcriptional corepressor. Due to the nature of ZEB2 protein, it is difficult to explain its role in colorectal cancer development.

## 4.1 RESULTS AND DISCUSSION

**Design of PNA probes for KRAS and NRAS DNA mutations**

PNA probe sequences for the selected all-RAS mutations have been designed by the procedure described below. The mutation was located in the gene sequence, and this point mutation was centered in a hypothetical 30-mer probe. Possible interferents were found by blasting the sequence (http://blast.ncbi.nlm.nih.gov/Blast.cgi). Then, a shorter sequence of 15-18 nucleobases that shows the minimum number of interferents was converted into PNA sequence. Only anti-parallel orientation of the PNA:DNA (N-term of PNA facing the 3'-end of DNA) was considered as target, due to the higher stabilities obtained with this arrangement . Stability of generated probes were calculated by an available online tool by Applied Biosystem (http://www6.

appliedbiosystems.com/cgi-bin/calculator/ab_configured/oligodesigner/designer.cgi) that calculate Tm and possible self-pairing for PNAs. Thus, the sequences reported in Table 4.3 were selected, with putative melting temperature around 70°C. The selection was done by also considering that interferences should not be present and the point mutation should be in the middle of the probe, for best sequence selectivity.

**Table 4.3: list of PNA sequences complementary to wild types and mutations of KRAS and NRAS genes selected. Bolded letters are used to highlight the position of the RAS mutation. Tm refers to the calculated melting temperature of PNA:DNA dimers.**

| Target (Gene, Exon) | Mutation | PNA sequence | Theoretical Tm (@ 1µM) |
|---|---|---|---|
| KRAS exon 2 | WT | CTACGCCACCAGCT | 72 |
| | G12A | CTACGCCA**G**CAGCT | 73 |
| | G12D | CTACGCCA**T**CAGCT | 68 |
| | G12C | CTACGCCAC**A**AGCT | 71 |
| | G12V | CTACGCCAA**A**CAGCT | 71 |
| | G13D | CTACG**T**CACCAGCT | 68 |
| | G12R | CTACGCCAC**G**AGCT | 73 |
| | G12S | CTACGCCAC**T**AGCT | 67 |
| NRAS exon 2 | WT | CCAACCACCACCAG | 72 |
| | G12D | CCAACCA**T**CACCAG | 70 |
| NRAS exon 3 | WT | TACTCTTCTTGTCCAGCT | 69 |
| | Q61K | TACTCTTCTT**T**TCCAGCT | 65 |
| | Q61H1 | TACTCTTC**G**TGTCCAGCT | 73 |
| | Q61H2 | TACTCTTC**A**TGTCCAGCT | 70 |
| | Q61L | TACTCTTCT**A**GTCCAGCT | 69 |
| | Q61R | TACTCTTCT**C**GTCCAGCT | 71 |

**Synthesis of PNA probes for RAS mutations with different terminal groups**

In order to study the best performing linking modes for the SPRi sensor surface, several immobilization strategies have been tested, related to different linking molecules (Scheme 4.4). PNA probes for detecting RAS mutation were linked to the surface at N-terminal. PNAs that had to be linked to self-assembled monolayer (SAM) modified Au surface, exposing NHS (N-hydroxy succinimide) ester groups were designed in order to have two 'O' spacers ([2-(2-(Fmoc-amino)ethoxy)ethoxy]acetic acid) at their N-terminal. A second type of functionalization selected was with an azide group: after 'O' spacers, azido acetic acid was added in order to allow attachment to the SAM by a Cu-mediated Huisgen cycloaddition. A third type of PNA produced was modified with a protected thiol, in order to exploit the well-established thiol-maleimide (Michael-type) reaction.

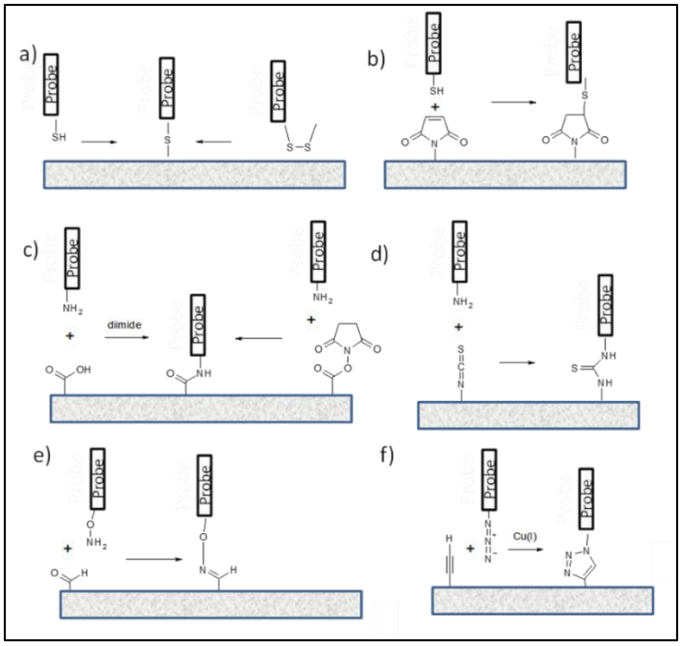


**Scheme 4.4: a) thiolated or di-sulfur probe that directly binds to Au surface. b) Thiolated probe that perform a Michael reaction with an immobilized maleimide. c) Amide bond formation between amino probe and carboxylic or NHS-modified sensor's surface. d) Amino probe that form a thiourea bound with an immobilized iso-thiocinate. e) Linking of probe via oxima formation. f) Huisgen cycloaddition between an azido probe and immobilized alkyne.**

The list of all PNA for detection of KRAS and NRAS mutations synthesized in the project is displayed in Table 4.1.5, of which a large part was synthesized in the present work. Most of them were synthesized using an automatic synthesizer for the PNA part, and the final linker and eventually spacers were added manually. A special attention was dedicated to KRAS Ex2 WT and G12D, since these were chosen as a test case due to the clinical relevance of the G12D mutation. These have been synthesized with different terminal groups: amine, azide and protected thiol. Most of the other PNAs were synthesized only with a N-terminal amino group because this was the one used in the SPRi protocols within the ULTRAPLACAD project. Prof. Jurriaan Huskens of University of Twente tested thiol and azide PNAs on different surfaces, with the aim of establishing possible alternatives of the composition of the sensing surface and different linking chemistries.

**Performances of the RAS PNA probes.**

Before the addition of linking molecule, a little amount of each PNA sequence, corresponding to the WT and mutated form of KRAS and NRAS considered, was cleaved from the resin, purified and used for measurement of the experimental Tm. A comparison between Tm of mutated PNA probes respect full match sequence (mutated DNA) and mismatch sequence (WT DNA) was performed, and the results are shown in Table 4.1.0. Each PNA probe targeting a specific mutation was tested against its (mutated) target and the corresponding wild type (KRAS exon 2, KRAS Exon 3 and NRAS exon 3). The PNA probes showing low differences in the melting temperature of target sequence vs WT are marked in red. The probes giving low Tm differences are likely to give false positive results, because there is a high percentage of WT circulating DNA compared to mutated sequences, and the binding of this can be interpreted as due to the presence of the mutated form. The selectivity shown by the wild-type PNA probes with respect to the mutated DNA of the same region was also evaluated and the results shown in Table 4.2.

**Table 4.1: Selectivity of PNA probes of mutated sequences: possibility of false positive. The color depends on the difference between melting temperatures: green > 15°C, 15°C > yellow > 10°C, red < 10°C.**

| | PNA of mutated sequence | | |
|---|---|---|---|
| K-RAS Ex 2 | G12A | 72.1 | 7.8 |
| | wild type DNA | 64.3 | |
| | G12D | 80.6 | 13.8 |
| | wild type DNA | 66.7 | |
| | G12C | 76.4 | 14.5 |
| | wild type DNA | 61.9 | |
| | G12V | 75.2 | 7.6 |
| | wild type DNA | 67.6 | |
| | G13D | 72.2 | 8.1 |
| | wild type DNA | 64.1 | |
| | G12R | 83.0 | 15.3 |
| | wild type DNA | 67.6 | |
| | G12S | 75.6 | 10.2 |
| | wild type DNA | 65.4 | |

| | PNA of mutated sequence | | |
|---|---|---|---|
| N-RAS Ex | G12D | 70.7 | 9.7 |
| | wild type DNA | 61.0 | |

| | PNA of mutated sequence | | |
|---|---|---|---|
| N-RAS Ex 3 | Q61K | 66.3 | 6.9 |
| | wild type DNA | 59.4 | |
| | Q61H1 | 74.1 | 11.2 |
| | wild type DNA | 62.9 | |
| | Q61H2 | 72.6 | 11.4 |
| | wild type DNA | 61.2 | |
| | Q61L | 74.7 | 12.7 |
| | wild type DNA | 62.0 | |
| | Q61R | 75.8 | 8.9 |
| | wild type DNA | 66.9 | |

**Table 4.2: Selectivity of WT PNA: possibility of false negative. The color depends on the difference between melting temperatures: green > 14°C, 14°C > yellow > 10°C, red < 10°C.**

| | PNA of Wild Type | | |
|---|---|---|---|
| K-RAS Ex 2 | WT | 75.8 | |
| | G12A | 65.2 | 10.6 |
| | G12D | 61.6 | 14.2 |
| | G12C | 64.6 | 11.2 |
| | G12V | 61.6 | 14.2 |
| | G13D | 62.6 | 13.2 |
| | G12R | 61.4 | 14.4 |
| | G12S | 61.4 | 14.4 |

| | PNA of Wild Type | | |
|---|---|---|---|
| N-RAS Ex | WT | 73.0 | |
| | G12D | 57.7 | 15.3 |

| | PNA of Wild Type | | |
|---|---|---|---|
| N-RAS Ex 3 | WT | 68.3 | |
| | Q61K | 60.6 | 7.7 |
| | Q61H1 | 58.3 | 10.0 |
| | Q61H2 | 64.9 | 3.4 |
| | Q61L | 63.3 | 5.0 |
| | Q61R | 64.8 | 3.5 |

High difference of this will reflect in the possibility to detect that a mismatch is present. Since the sensor array will contain both WT and mut PNA probes, the possible outcome of the analysis is dependent on the responsiveness of the probe to both types of DNA, as depicted in Figure 4.5.

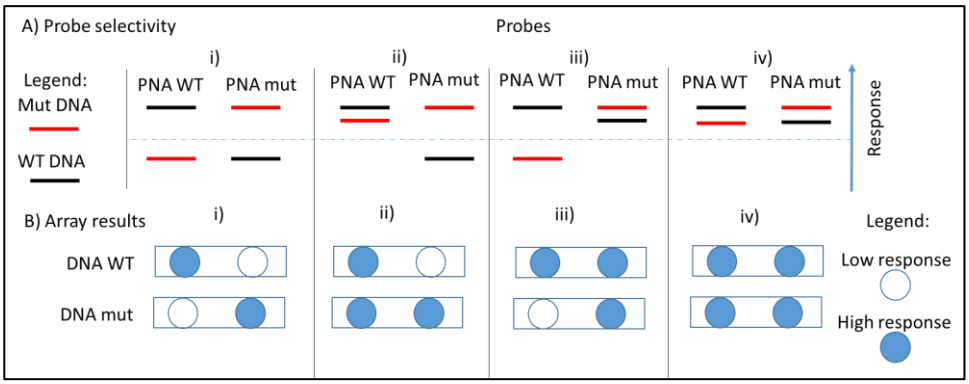


**Figure 4.5: Outcome of the array analysis based on selectivity of WT and mutated Probes in the response. In a real case, a difference in intensity rather than an all-or-none response is expected.**

The ideal case i) is when both probes are selective for the corresponding targets; worst case is that of non selective probes iv) which makes the detection of mutation impossible. In case ii) it is still possible to detect the specific mutation, though false positive are more likely to occur; in case iii) the response of WT probe indicates the presence of a mutation, but the specific mutation fails to be detected significantly different from the WT (false negative). According to this scheme, only two cases are likely to fall within case iv), i.e. Q61K and Q61R of NRAS exon 3, whereas for the two major KRAS mutations, G12D of exon 2, fall into a case between i) and iii), whereas G12V has a Tm selectivity pointing towards the case iii). As summary, Table 4.3 gives a hint of what type of behavior we can expect from probes in the final SPR array sensor. These data have been collected by measurement is solution and behavior on the surface could be different.

**Table 4.3: Expected behavior of PNA probes in the final SPR instrument, based on evaluation of Tm. Two cases i) and two cases iv) can be figured out. Probes for detection of KRAS mutations are prone to case iii), while probes for detection of NRAS shows opposite selectivity case ii).**

| KRas mutation | Type of array analysis |
|---|---|
| G12A | iii |
| G12D | iii |
| G12C | i |
| G12V | iii |
| G13D | iii |
| G12R | i |
| G12S | iii |

| NRas mutation | Type of array analysis |
|---|---|
| G12D | iii |
| Q61K | iv |
| Q61H1 | ii |
| Q61H2 | ii |
| Q61L | ii |
| Q61R | iv |

However, it should be pointed out that differences in selectivity in the sensor response maybe strongly affected by surface effects and are therefore likely to be different from solution data obtained by Tm measurements.

A general trend in the Tm results is that the discrimination obtained for the mutated probes is generally lower than those obtained with the WT probe. This means that it would be easier to detect WT in the presence of mutated DNA than to detect mutated DNA in the presence of WT. These results were in accordance with preliminary studies of immobilized probes onto SPR surface performed by group of Prof. Giuseppe Spoto (University of Catania) and Prof. Maria Minunni (University of Florence).

A summary of all PNA for detection of single point mutation is present in Table 4.4.

**Table 4.4: list of PNA probes for genome mutations used in the ULTRAPLACAD project. PNAs with AR as internal code were synthesized in the present work.**

| Entry | Sequence | Target | Internal Code/batch |
|---|---|---|---|
| 1 | H-OO-CTA-CGC-CAC-CAG-CT-Gly-NH2 | K-RAS exon 2 WT | AR4-9-WT |
| 2 | N3-O-O-CTA-CGC-CACCAGCT-Gly-NH2 | K-RAS exon 2 WT | AR4-10-WT |
| 3 | SPDP-CTACGCCACCAGCT-Gly-NH2 | K-RAS exon 2 WT | AR4-11-WT |
| 4 | H-O-O-CTA-CGC-CAC-CAG-CT-Lys(biotin)-NH2 | K-RAS exon 2 WT | sk-02-37-07 |
| 5 | H-O-O-CTA-CGC-CAT-CAG-CT-Gly-NH2 | K-RAS exon 2 G12D | AR4-9-G12D |
| 6 | N3-O-O-CTA-CGC-CAT-CAG-CT-Gly-NH2 | K-RAS exon 2 G12D | AR4-10-G12D |
| 7 | SPDP-CTA-CGC-CAT-CAG-CT-Gly-NH2 | K-RAS exon 2 G12D | AR4-11-G12D |
| 8 | H-O-O-CTA-CGC-CAT-CAG-CT-Lys(biotin)-NH2 | K-RAS exon 2 G12D | sk-02-37-09 |
| 9 | H-O-O-CTA-CGC-CAC-TAG-CT-Gly-NH2 | K-RAS exon 2 G12S | DS2-5 D3 |
| 10 | H-O-O-CTA-CGC-CAG-CAG-CT-Gly-NH2 | K-RAS exon 2 G12A | DS2-3- C4(1) |
| 11 | H-O-O-O-CTA-CGC-CAG-CAG-CT-Gly-NH2 | K-RAS exon 2 G12A | DS2-3- C4(3) |
| 12 | H-O-O-CTA-CGC-CAC-AAG-CT-Gly-NH2 | K-RAS exon 2 G12C | DS2-2 C5 (1) |
| 13 | H-O-O-O-CTA-CGC-CAC-AAG-CT-Gly-NH2 | K-RAS exon 2 G12C | DS2-2 C5 (2) |
| 14 | H-O-O-CTA-CGC-CAA-CAG-CT-Gly-NH2 | K-RAS exon 2 G12V | sk-01-137-a |
| 15 | H-O-O-CTA-CGC-CAC-GAG-CT-Gly-NH2 | K-RAS exon 2 G12R | DS2-6-D2 |
| 16 | H-O-O-CTA-CGT-CAC-CAG-CT-Gly-NH2 | K-RAS exon 2 G13D | sk-01-137-b |
| 17 | H-O-O-CCA-ACC-ACC-ACC-AG-Gly-NH2 | N-RAS exon 2 WT | sk-01-137-c |
| 18 | H-O-O-CCA-ACC-ATC-ACC-AG-Gly-NH2 | N-RAS exon 2 G12D | sk-01-137-d |
| 19 | H-O-O-TAC-TCT-TCT-TGT-CCA-GCT-Gly-NH2 | N-RAS exon 3 WT | sk-01-137-e |
| 20 | H-O-O-TAC-TCT-TCT-AGT-CCA-GCT-Gly-NH2 | N-RAS exon 3 Q61L | DS2-7 C2 |
| 21 | H-O-O-TAC-TCT-TCG-TGT-CCA-GCT-Gly-NH2 | N-RAS exon 3 Q61H1 | DS2-8 B6 |
| 22 | H-O-O-TAC-TCT-TCA-TGT-CCA-GCT-Gly-NH2 | N-RAS exon 3 Q61H2 | DS2-9 C1 |
| 23 | H-O-O-TAC-TCT-TCT-TTT-CCA-GCT-Gly-NH2 | N-RAS exon 3 Q61K | sk-01-137-f |
| 24 | H-O-O-TAC-TCT-TCT-CGT-CCA-GCT-Gly-NH2 | N-RAS exon 3 Q61R | sk-01-137-g |
| 25 | SPDP-GCA-GCG-CGT-TGG-CAC-Gly-NH2 | PNA control for deposition test | sk-01-91 |
| 26 | N3-GCA-GCG-CGT-TGG-CAC-Gly-NH2 | PNA control for deposition test | sk-01-10-B |
| 27 | N3-O-O-GCA-GCG-CGT-TGG-CAC-Gly-NH2 | PNA control for deposition test | sk-01-10-C |

In a first series of experiments, performed by Minunni and co-workers, using thiolated PNA for direct functionalization of gold chips and BiaCore SPR instrumentation, detection of DNA was performed using PNA probes targeting WT and G12D of KRAS, exon 2 (results not shown). In this case, a comparison of PNA with DNA probes was made, showing higher sequence-selectivity of the PNAs. The WT probe turned out to be more selective than the corresponding mutated one.
In the experiments carried out by the Spoto's group the procedure for SPRi detection using the synthesized probes is composed of the following steps: a) probe immobilization; b) DNA capture; c) binding of DNA-modified gold nanoparticles to the captured DNA. A scheme of this detection strategy is depicted in Figure 4.6.

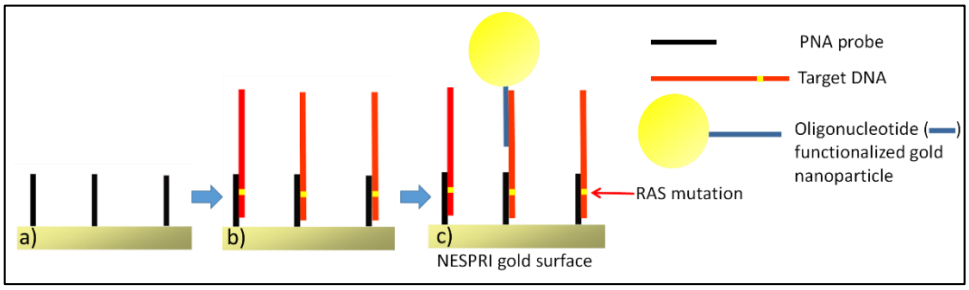


**Figure 4.6: NESPRI detection configuration adopted for RAS DNA detection.**

As is visible by sensograms of Figure 4.1.2, PNA WT probe exhibit better selectivity than PNA G12D probe. These results are remarkable, because target DNA was detected, after treatments, in real blood samples. All the PNA produced with amino terminal groups were tested using this assay, and discrimination of the principal mutations from wild type was clearly demonstrated using genomic DNA and discrimination of the G12D mutation from wild type was performed in serum (results not shown).
The selectivity, however, was not optimal in the SPR experiments for all PNA probes: for example, PNA probes for G12C, G12S and G12R KRAS mutation gave a signal derived from full match genomic DNA very similar to what obtained with wild type genomic DNA (false positive). The results showed a sensitivity (true positive/(true positive+false negative)=100%, which can be seen as the capacity of the sensory system to detect positive test. Specificity of the system was defined as = (true negative/true negative+false positive) =82%. This parameter explains the behavior of probes in recognizing a negative test

from healthy patients or ill patients which tumor was not caused by a point mutation of genome.
As an example, the data of the sensograms obtained for genomic DNA wild-type and DNA containing the mutation G12 of the KRAS gene (exon 2) with WT and G12D PNA probes are reported in Figure 4.7

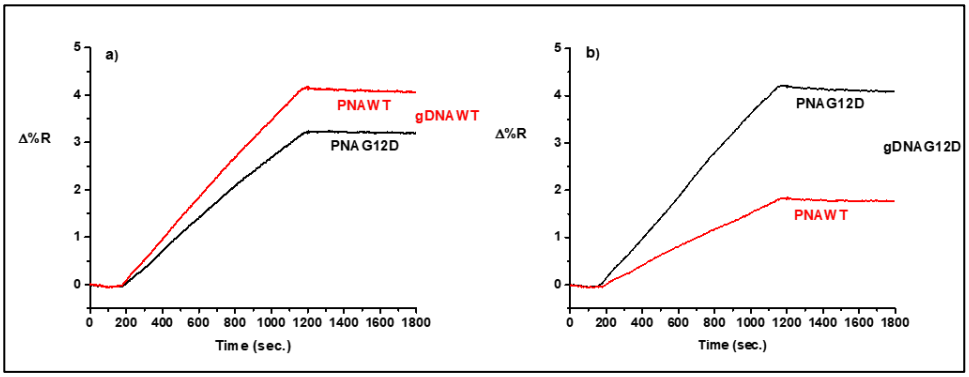


**Figure 4.7: Time-dependent SPRI curves obtained after the adsorption of modified AuNPs on (a) WT and (b) G12D genomic DNA (gDNA) hybridized with a previously immobilized PNA-WT (red curve) and PNA-G12D (black curve) probes. gDNA concentration was 5 pg µL-1.**

The group of Prof. Jurriaan Huskens of University of Twente tested also other immobilization strategies using the thiol and azide PNAs produced in this present work on different surfaces. In a first series of experiments, PNA KRAS of WT and G12D were immobilized on the sensor's surface modified with a polyethyleneglycol-type self-assembled monolayer (SAM) bearing a thiol group on one end and a OH (diluter) or activated COOH group (active sites) on the other end. The amine-coupling reaction involved the N-terminal group of a double 2-(2-aminoethoxy)ethoxyacetyl spacer (OO-spacer) introduced at 5'-position of PNA probes and N-hydroxysuccinimidyl (NHS) ester ends of the bifunctional SAM. Spacers on PNA were introduced in order to have an increased nucleophilicity and for minimizing the surface effects caused by the steric hindrance of immobilized systems. The thiol-maleimide reaction was used with the thiolated PNA in combination with a modified poly-lysine containing maleimide residues, allowing to obtain a surface with a precisely defined probe density ("Control of Probe DNA Density at Biosensor Surfaces using Poly-L-Lysine with Appended Reactive Groups", Movilli J. et al, Bioconjugate Chem., 2018, 29, 4110−4118).

**Design of PNA probes for microRNA**

PNA probes were designed for the above mentioned miR-221, miR-222 and miR-141. The length of the probes was chosen in order to produce high affinity without generating partial binding to other miR or mRNA. Possible mRNA interferents were evaluated during the design by using an oligonucleotide Blast search. The list of anti-miR PNA selected is reported in Table 4.5. Different length and different geometries were considered.

**Table 4.5: PNA sequences evaluated for microRNAs 221, 222 and 141.**

| Sequence name | Sequence | Tm (calc) | Free nt on 3'-end of target |
|---|---|---|---|
| miR221-1 | AAACCCAGCAGACAATGT | 81°C | 2 |
| miR221-2 | CCAGCAGACAATGTAGCT | 79°C | 6 |
| miR221-3 | GACAAT*GTAGC | n.a. | 12 |
| miR221-4 | CCAGCAGACAAT*GTAGCT | n.a. | 6 |
| miR222-1 | CAGTAGCCAGATGTAGCT | 78°C | 3 |
| miR222-2 | GTAGCCAGATGTAGCT | 74°C | 5 |
| miR141-1 | CTTTACCAGACAGTGTTA | 72°C | 4 |
| miR141-2 | CCATCTTTACCAGACAGT | 73°C | 1 |

Three different geometries were considered for the orientation of the probes on the surface of the sensor, as shown in Figure 4.8. These configurations are related to the linking part of the PNA probes, which can be placed at the N or C terminal of PNA. N-terminal attachment was accomplished by a simple addition of an amine terminated spacer to the PNA during solid-phase synthesis. PNAs with a linking group at C-term were produced using a Fmoc(Dde)-protected lysine as first monomer before PNA synthesis, and acetylation of the amino group of the last monomer. Selective removal of the side chain group allows to introduce spacers at this site during solid-phase synthesis. The third case was more complex and involved a modified monomer with a 5-L-lysine in the backbone. This was obtained by incorporation of a Fmoc(Boc) protected C5-modified monomer derived from L-Lysine, and also in this case acetylation of the N-terminal amino group. The side chain was deprotected during cleavage, providing an amino functionality for linking. This moiety could also be

opportunely modified after PNA synthesis, as linking component if used in combination of an appropriate solid support.

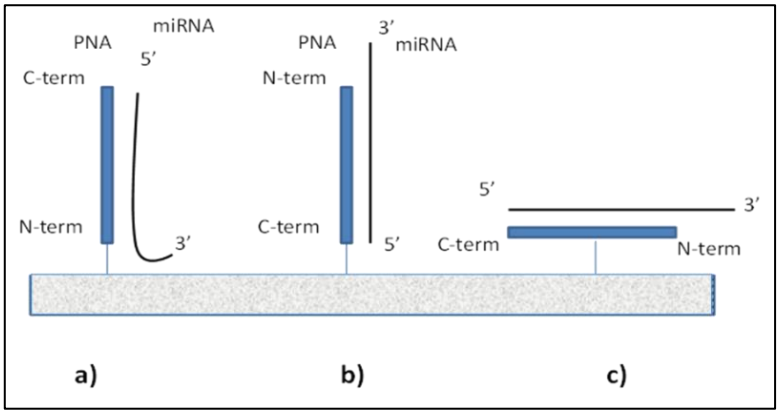


**Figure 4.8: Schematic representation of PNA probes with different geometries; a) N-term linking, b) C-term linking, c) 'T-shaped' linking.**

These different geometries have to been selected because the region of interest of mature miR contain the seed region, the most important part of miR for recognizing target mRNA, and it is close to the 5'end of the miR. Therefore, for sensing on surface, a steric problem due to the interaction of the dangling 3' tail with the surface may be significant. Moreover, the sensing scheme proposed for SPRi imaging by Prof. Spoto's group involves a capture of the miR on the surface, followed by an elongation step obtained by enzymatic modification of the 3' end of the miRNA target by adding a polyadenine chain (Figure 4.9); the assay is then completed by capture of Poly-T modified nanoparticles by this polyA tail. The length of the dangling 3'-end could be critical for priming the polyadenylation reaction. For this reason, a different number of non-targeted, and hence free after binding, nucleobases at 3' end of miR was considered in the design.

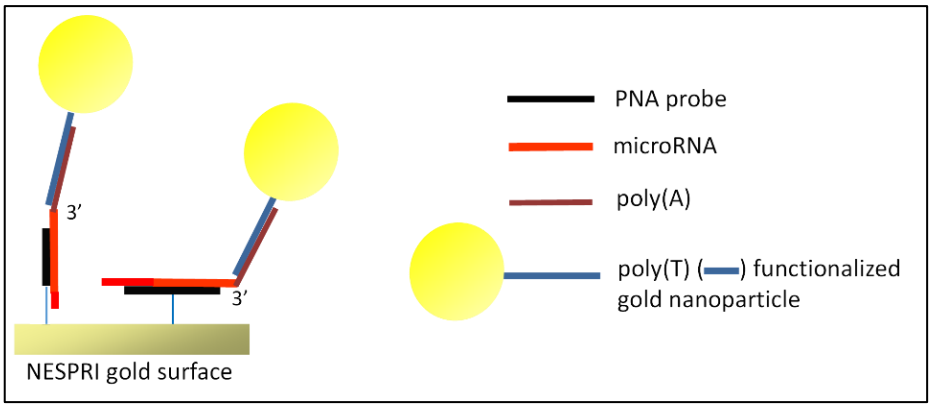


**Figure 4.9: Scheme of NESPRI detection with sandwich approach that will be used for miRNAs after enzymatic formation of a poly-adenine tail.**

### Synthesis of PNA probes for miR detection with different geometries

PNA probes anti miR were also synthesized; a list of the probes produced within the ULTRALACAD project is reported in Table 4.6. Probes with N-terminal amino group were synthesized following the standard Fmoc protocol, C-term linking probes were synthesized by loading the resin with Fmoc-Lys(Dde)-OH protected amino acid. After standard Fmoc-synthesis of the monomer sequence, the N-terminus was acetylated. Then, deprotection of the side chain of lysine was performed using imidazole/hydroxylamine method, spacers were added at this new amino function. The first coupling on the lysine side chain was particularly difficult, probably because of limited accessibility of the reactive site, and thus it was repeated twice with double equivalents. For the T-shaped probes, manual Boc-synthesis was used and a thymine monomer T* with Boc-protecting group on main amino group and Fmoc-protected lysine side chain was employed (produced similarly to product 1 of chapter 3). After completion of the PNA synthesis, the terminal Boc group was cleaved and the terminal amino group was acetylated. Fmoc-group of the T* monomer was removed and the synthesis of the side arm was completed with two subsequent O-spacer (Fmoc-2-(2-aminoethoxy) ethoxyacetic acid). The Fmoc-group was then removed and the PNA was cleaved from the resin with a free amine in a central region of the oligomer.

**Table 4.6: list of PNA probes anti miR. PNAs with AR and DS as internal code were synthesized in the present work. Red characters are used for mismatch nucleobases.**

| Entry | Sequence | Target | Internal Code/batch |
|---|---|---|---|
| 1 | H-O-O-AAA-CCC-AGC-AGA-CAA-TGT-Lys(Ac)-$NH_2$ | miR-221-1 N-term | sk-02-37-01c |
| 2 | H-O-O-AATCCCACCAGAGAAAGT-Gly-$NH_2$ | miR 221-1 4 mismatches | AR4-69 |
| 3 | Ac-AAA-CCC-AGC-AGA-CAA-TGT-Lys(O-O-$NH_2$)-$NH_2$ | miR-221-1 C-term | sk-02-37-12b |
| 4 | Ac-AACCCCATCAGAGAAAGT-Lys(OO-H)$NH_2$ | miR 221-1 C-term 4 mismatches | AR5-004 |
| 5 | Ac-AAT-CCC-ACC-AGT*(O-O-NH2)-GAA-AGT-Gly-$NH_2$ | miR-221-1 T-shaped 4 mismatches | sk-01-129 |
| 6 | H-OO-CCAGCAGACAATGTAGCT-Gly-$NH_2$ | miR 221-2 N-term | AR4-40 |
| 7 | $N_3$-OO-CCAGCAGACAATGTAGCT-GlyN$H_2$ | miR 221-2 azide | AR4-41 |
| 8 | SPDP-CCAGCAGACAATGTAGCT-Gly-$NH_2$ | miR 221-2 thiol | AR4-42 |
| 9 | Ac-CCAGCAGACAATGTAGCT-Lys(OO-H)-$NH_2$ | miR 221-2 C-term) | DS1-26 |
| 10 | H-GACAAT*GTAGC-$NH_2$ | miR-221-3 T-shaped (11mer) | CC1-01 |
| 11 | Ac-CCAGCAGACAAT*(OO-H) GTAGCT-Gly-$NH_2$ | miR 221-4 T shaped | AR4-43 |
| 12 | H-GCA-GAC-AAT-GTA-GCT-Gly- NH2 | miR221 for doubly-modified PNA | DS2-1 |
| 13 | H-O-O-CAG-TAG-CCA-GAT-GTA-GCT-Lys(Ac)-$NH_2$ | miR-222-1 N-term | sk-02-37-02c |
| 14 | Ac-CAG-TAG-CCA-GAT-GTA-GCT-Lys(O-O-$NH_2$)-$NH_2$ | miR-222-1 C-term | sk-02-37-13b |
| 15 | Ac-CAG-TAG-CCA-GAT*(O-O-$NH_2$)-GTA-GCT-Gly-$NH_2$ | miR-222-1 T-shaped | sk-02-37-11e |
| 16 | H-O-O-GTAGCCAGATGTAGCT-Gly-$NH_2$ | miR 222-2 | AR4-67 |
| 17 | Ac-GTA-GCC-AGA-TGT-AGC-T-Lys(O-O-$NH_2$)-$NH_2$ | miR-222-2 C-term | sk-02-37-05d |
| 18 | Ac-GTA-GCC-AGA-T*(O-O-H )GT-AGC-T-Gly-$NH_2$ | miR-222-2 T-shaped | DS2-17 (1) |
| 19 | H-O-O-CTT TAC CAG ACA GTG TTA-GlyN$H_2$ | miR-141-1 | FF1-01 |
| 20 | Ac-CTT-TAC-CAG-ACA-GTG-TTA-Lys(O-O-$NH_2$)-$NH_2$ | miR-141-1 C-term | sk-02-37-04d |
| 21 | Ac-CTT-TAC-CAG-ACA-GT*(O-O-H)G-TTA-Gly-$NH_2$ | miR-141-1 T-shaped | sk-01-142 |
| 22 | H-O-O-CCA-TCT-TTA-CCA-GAC-AGT-Gly-$NH_2$ | miR 141-2 N-term | AR4-68 |
| 23 | H-O-O-CCA-TCT-TTA-CCA-GAC-AGT-Lys(Ac)-NH2 | miR-141-2 N-term | sk-02-37-03c |
| 24 | Ac-CCA-TCT-TTA-CCA-GAC-AGT-Lys(O-O-NH2)-NH2 | miR-141-2 C-term | sk-02-37-14b |
| 25 | Ac-CGC-TGT*(O-O-H)-CAC-AC-Gly-NH2 | miR-210 (control probe) | DS2-10 |

Preliminary results obtained by Prof. Giuseppe Spoto, University of Catania, in detection of miR with amplification by polyadenylation and nanoparticles enhancement, showed that the T-shaped probes were the best performing in the detection of all corresponding target miRs. In fact, the using PNA AR4-40 (Table 4.6, entry 6) for miR221 detection at 10 fM concentration gave an

average signal/blank value of 1.95, whereas the corresponding value for the T-shaped PNA AR4-42 (Table 4.6, entry 8) was 2.19. The corresponding values obtained or miR222 (entries 16 and 18 of table 4.6) were 1.95 and 2.52, and those for miR141 (entries 19 and 21 in table 4.6) were 2.27 and 2.92 respectively. Results obtained with C-terminal linker were similar to the N-terminal one. It is therefore likely that T-shaped probes allow best condition for both hybridization of the target sequence and for the elongation reaction. Detection of all target miRs was possible at a concentration as low as 1fM, with a signal increasing as the concentration of miR increased, as shown in Figure 4.10 for miR221.

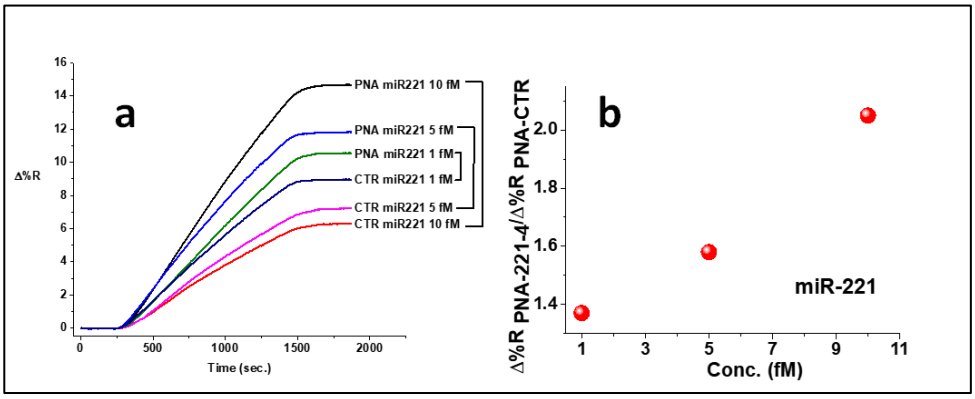


**Figure 4.10: (a) ∆%R over time obtained after the nanoparticle enhanced SPRI detection of 1 fM, 5 fM and 10 fM solutions of miR-221. (b) %R PNA-miR221/%R PNA-CTR ratio dependence on concentration of miR 221. PNA miR221-4 T-linker and PNA CTR miR221-4 T-linker probes were used for the specific and control interaction.**

These results showed that the PNA probes produced can actually be used for the detection of this type of tumor biomarkers, and thus add important details in the profiling of patients and early detection of cancer using liquid biopsy.

### Modified 'Chiral box' PNA probes-A new synthetic route

From the data obtained on the sensing strategies targeting the single point mutations (KRAS and NRAS targets mentioned above) emerges that for point mutation discrimination, standard PNA probes are performing better than DNA probes. Their performances should be further improved for optimal sensor performance, especially in view of detecting small percentages of mutated DNA in the presence of a large quantity of wild-type DNA.

To achieve this goal, the synthesis of 2D-chiral box PNA was considered[8]. Chiral box PNAs were previously designed for obtaining a better discrimination in presence of single point mutation of the genome. They present three consecutive modified monomers, with the mismatched base of the target facing the central PNA base in the box. It was shown that, if the point mutation is in the central position, the destabilization of the DNA:PNA duplex is maximal. The backbone modification consist in a chiral side chain of amino acid, on carbon 2, although a chiral box containing C5 modified monomers was also tested, this turned out to have lower sequence selectivity[9]. The chiral box generates a steric hindrance that destabilize the conformation that the PNA assumes in the duplex, partially compensated by the electrostatic interactions when the side chains are positively charged as in the case of lysine and arginine. However, the duplex formed with singly-mismatched DNA is even more destabilized, since the highly constrained structure cannot easily rearrange to adapt to the mismatched duplex. Modification with D-amino acid derived side chain in position 2 or L-amino acid side chain in position 5 leads PNAs to preferably adopt a right-handed conformation, so these stereochemistries should be chosen for probe design. Chiral box PNAs have been used for several application[10], like SPR, microarray[11] and capillary electrophoresis[12].
A special procedure was necessary in the case of C2-modified chiral PNAs, since during the activation of a C2-modified PNA monomer, the presence of two withdrawing carbonyl groups close to the chiral center of the activated ester promotes epimerization (see Figure 4.11). Although for the coupling of N-acylated amino acids and peptide segments a possible mechanism for epimerization is also the formation of oxazolone, previous studies showed no evidence of this intermediate, thus suggesting a direct proton abstraction mechanism[13].

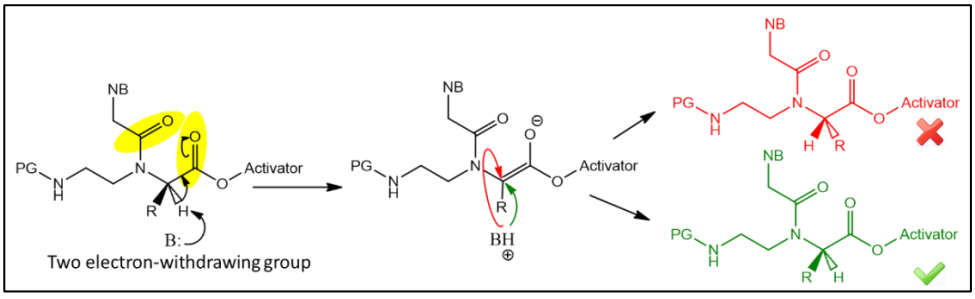


**Figure 4.11: epimerization of 2D-modified monomer in standard synthesis.**

As stated in the Chapter 2, C2-modified PNAs should thus be synthesized using a 'submonomeric approach', i.e. by using the doubly-protected backbone, with orthogonal groups on the N3 and N6 amino nitrogens. The N3 amino group is deprotected after incorporation of the PNA backbone into the growing chain, and the carboxymethylnucleobase is then introduced by a series of subsequent coupling with a large excess of reagent. A scheme of this synthesis exploiting Boc-strategy is reported in Figure 4.12.[14]

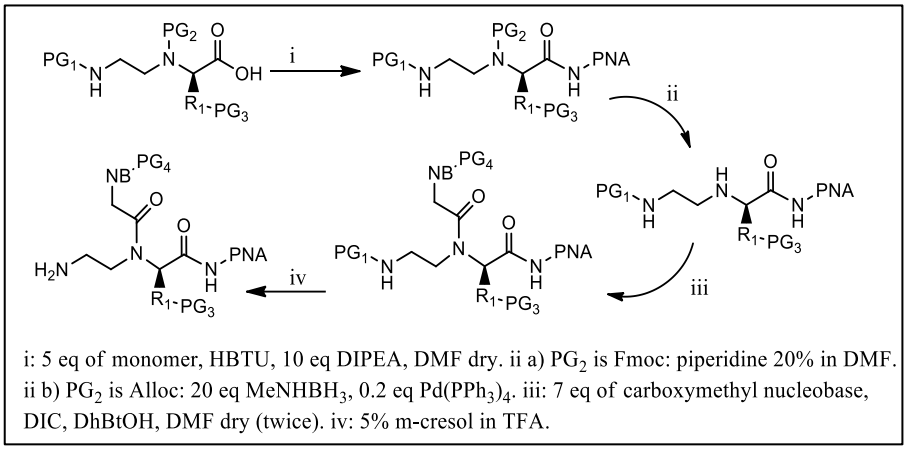


i: 5 eq of monomer, HBTU, 10 eq DIPEA, DMF dry. ii a) $PG_2$ is Fmoc: piperidine 20% in DMF. ii b) $PG_2$ is Alloc: 20 eq $MeNHBH_3$, 0.2 eq $Pd(PPh_3)_4$. iii: 7 eq of carboxymethyl nucleobase, DIC, DhBtOH, DMF dry (twice). iv: 5% m-cresol in TFA.

**Figure 4.12: Submonomer synthesis in Boc-strategy with Fmoc-protection of secondary amine[14]**

The inconvenience of this method is especially evident when using lysine as side chain, since in this case three orthogonal protecting groups are needed, which have to be removed at different stages, and this creates severe limitation on the choice of these protecting groups, and risk of inadverted deprotection. In the case of Boc-PNA synthesis, the combination of Boc (main, for N6), Fmoc (for N3) and 2-Cl-CBz (for side chain) led to good results, but is not compatible with most of modern automatic synthesizers which are designed for Fmoc chemistry. A previous work has shown that the combination of Fmoc (for N6), allyoxycarbonyl (Alloc, for N3) and Boc (for side chain) could be performed. However, reagents for the removal of Alloc are not well suited for the solid-phase reactions and this procedure is not easily integrated in automatic solid-phase synthesis protocols.

Furthermore, the reason for protecting N3 amino group is not evident *per se*, and is rather a precautionary method than a real need. In fact, since the introduction of the carboxymethylnucleobase turned out to be very slow, the

reaction of the PNA backbone on itself should be even slower, due to the highly hindered nature of both the carboxylic and the secondary amino groups. If this is true, we reasoned that both protection and deprotection of the N3 amino group could be avoided. In a previous work[15], the synthesis of the protected submonomer was studied, and it was concluded that that protection of the secondary amine with the free carboxylic function can diminish yields (Figure 4.13); thus a temporary protection of the carboxylic function as allyl ester or with silyl groups was necessary. However, if the protection of the secondary amine is not necessary, then protection of the carboxylic group and removal of the protecting group can also be avoided, thus simplifying the entire process. A further advantage is that the unprotected amino group is not activating toward racemization of the C2 carbon, thus lowering the racemization risk. Following this new route, it is also possible to start directly from amino acid with an extremely simplified procedure.

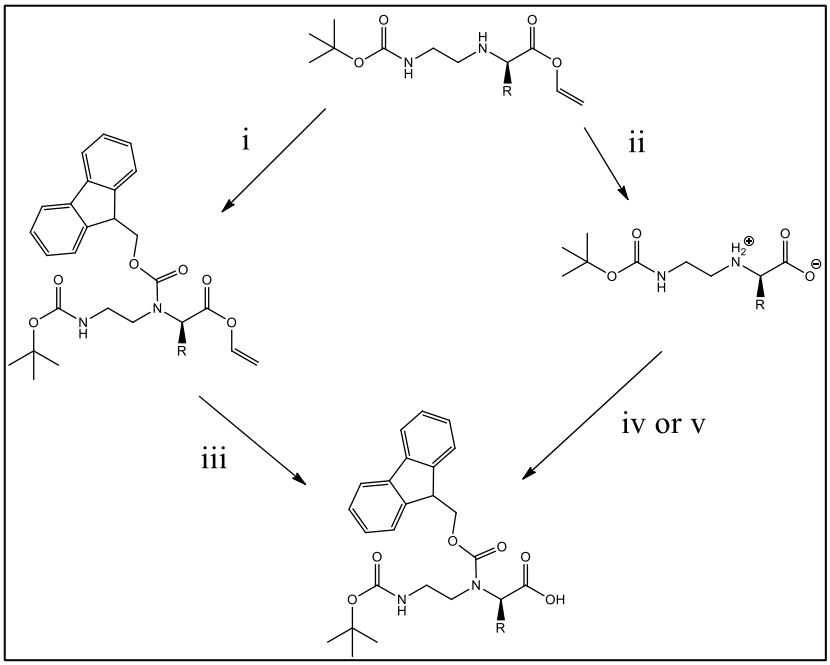


**Figure 4.13: i) Fmoc-Cl, DIPEA, DCM, room temperature, 97% yield; ii) morpholine, [Pd(PPh$_3$)$_4$], THF, room temperature, 80% yield; iii) morpholine, [Pd(PPh$_3$)$_4$], THF, room temperature, 33% yield; iv) 1 M NaOH, Fmoc-Cl, THF, 88% yield; v) BTSA, DIPEA, Fmoc-Cl, DCM, room temperature, 60% yield. Reprinted with permission of S. Sforza et al *Eur. JOC* 2003 Copyright © John Wiley and Sons 2003**

A novel method for synthesis of a 2D-chiral box PNA with a minimal protection strategy and exploiting Fmoc-based solid phase synthesis was thus developed. For this synthesis, a novel reductive amination by hydrogen transfer mediated by cyclometalated iridium complex was applied[16]. As a test model the synthesis of PNA probe of KRAS exon 2 G12D mutation, the most relevant for clinical diagnosis, was chosen. In this mutation, a cytosine is replaced by a thymine, resulting in a change of amino acid from glycine to aspartic acid. The two adjacent nucleobases are a cytosine and an adenine, so the protected nucleobases of such type have been synthesized (carboxymethyl thymine is commercially available).

**Synthesis of C2-modified PNA backbone**

The most used procedure for synthesizing a modified PNA-backbone is that described in Chapter 3 for the 5L-lysine backbone, and involve the use of protected 2-amino aldehyde that reacts with an amino acid (protected) giving a reductive amination reaction. If the target backbone has a chiral center is in position 5, the aldehyde is a derivative of the chiral amino acid and should react with glycine, whereas in the synthesis of C2 modified PNA backbone, glycinal is used as aldehyde while a chiral amino acid is added for the reductive amination. In 2010, Wang and collaborators[17] developed an efficient reductive amination reaction by hydrogen transfer. This reaction exploits an iridium (III) catalyst, and formic acid as reductive agent that is oxidized to $CO_2$. It is used in combination with DIPEA/formic acid eutectic mixture (formic acid: DIPEA 5:2). Authors proposed an ionic pathway, in which an Ir - H hydride is transferred to a protonated imine without coordination of the C = N moiety to the metal; the scope of the reaction is wide, and reductive amination with both ketones and aldehydes was performed. Reaction with different types of amino groups, including those of unprotected amino acids was also reported. One major advantage of this procedure is that, unlike reductive aminations carried out with hydrides such as $NaBH_3CN$ or $NaBH(OAc)_3$ , double alkylation of the amino group is strongly disfavored, thus leading to high yields of the monoalkylated product.

In our case this reaction was performed using Fmoc-glycinal, obtained as previously reported[18], and D-lysine or D-arginine, with only the side chain protected respectively with Boc and Pbf groups. The reaction was carried out under different conditions, the final conditions optimized for lysine (that can be

applied also for arginine) are the following, and optimized procedures are reported in the experimental part.

- Solvent and temperature: absolute ethanol or dry methanol at 40°C. At this temperature ethanol can dissolve the very polar zwitterionic protected amino acid, which is commercially available. The excess of the amino acid is easy to remove by aqueous washings. Higher temperatures promote the formation of the doubly alkylated side product. For arginine derivatives, better yields have been obtained with MeOH, but the work up of the reaction was more laborious (see experimental part).
- Equivalents of reactants: despite the steric hindrance of side chain of amino acids, the dialkylated product can still be present.
  In an attempt to prevent this side reaction an excess of the amino acid was used in the case of the arginine backbone, for which reactions showed lower yields. The excess of amino acids used could be recovered at the end of the reaction by aqueous washing, because product (and eventually unreacted aldehyde stayed in the organic phase).
- Amount of eutectic reducing-mixture FA-DIPEA 5:2: the right proportion of this mixture is 5 equivalents of formic acid with respect to amino acid. Adding an excess of this solution can reach to unwanted formylation of the secondary amine. This could be due to dismutation of formic acid that produce a small amount of formaldehyde, and this rapidly reacts giving the methylated product.
- Time: the correct timing for this reductive amination is overnight. In eight working hours, the reaction is not complete while more time than overnight does not give better yields but can promote formation of side-products such as di-alkylation and methylation.
- Quantity of iridium catalyst: 0.1 equivalents of iridium catalyst were employed and with more catalyst, the yields were not increased.
- Work-up. In the case of lysine, if the reaction is carried out in absolute ethanol, the product precipitates as a white solid, and can be recovered in pure form by simple filtration. The arginine backbone, on the contrary, does not precipitate in the reaction environment, but following several precipitation cycles using different solvents it can be separated

from reactants without using chromatography, which is unpractical since these molecules are zwitterions.

The general scheme of this reaction is shown in Figure 4.14, typical yields goes from 40 to 60%. These yields are in the same range of the standard reductive amination reaction, but especially in the lysine case, this reaction is simpler and less hazardous than that using $NaBH_3CN$. This catalyzed reductive amination was also tested for creation of C5 modified backbones derived from arginine and lysine PNA backbones, but revealed to be ineffective due to the low solubility of glycine in alcohols.

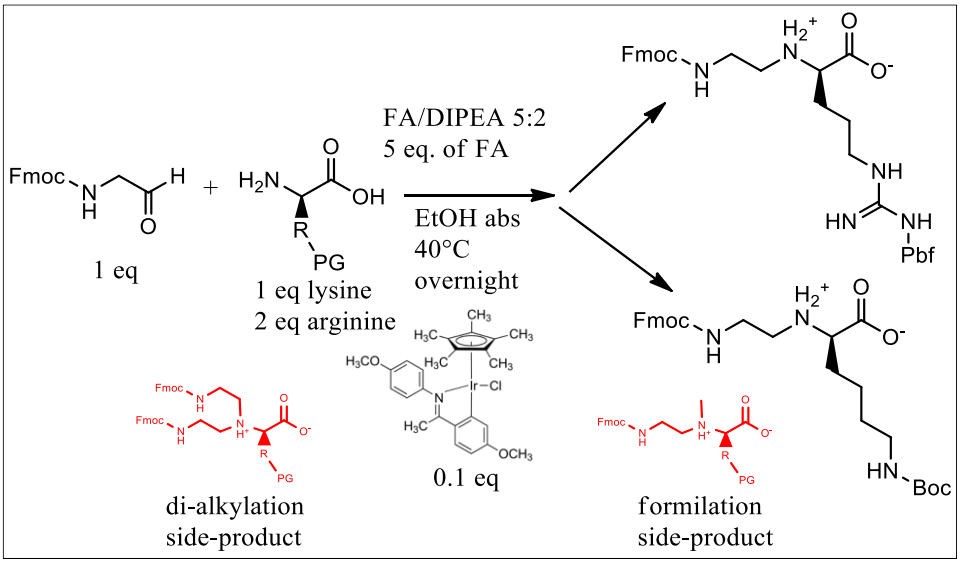


**Figure 4.14: reaction scheme of reductive amination by transfer hydrogenation mediated by iridium catalyst: Chloro(5-methoxy-2-{1-[(4-methoxyphenyl)imino-N]ethyl}phenyl-C)(1,2,3,4,5-pentamethylcyclopentadienyl)iridium(III). The principal sub-products are colored in red.**

### Synthesis of protected nucleobases

For the synthesis of the selected chiral box PNA (Figure 4.15), the syntheses of carboxymethyl Boc-protected nucleobases were also necessary.

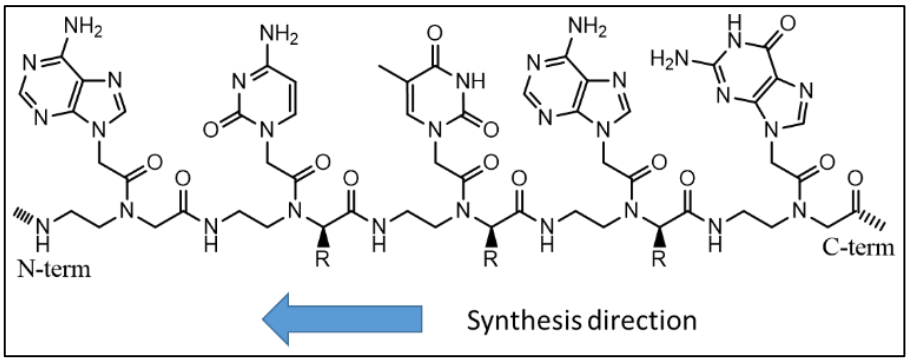


**Figure 4.15: scheme of chiral box PNA of KRAS exon 2 G12D sequence.**

Thymine-1-acetic acid is a commercial compound, while modified cytosine and adenine have to be synthesized. Adenine was synthesized following a literature procedure[19], while for cytosine the procedure was slightly modified. The two synthetic approach are shown in figure 4.16.

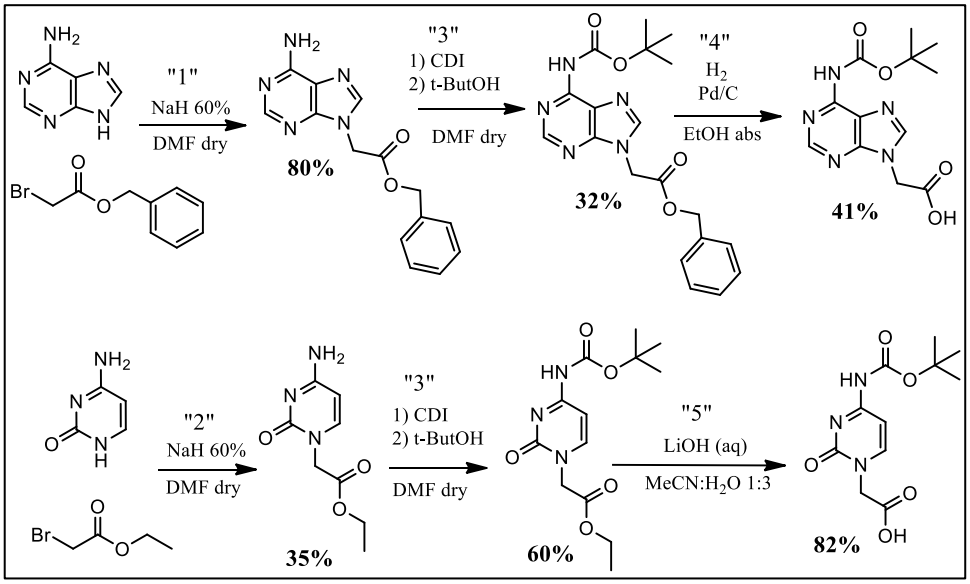


**Figure 4.16: synthetic strategy for derivatives of adenine and cytosine. Reaction 3 (Boc-protection) was the same for both molecules.**

Reactions 1 and 2 were performed similarly, the only change was the bromoacetate ester used. This type of reaction was performed in dry DMF,

using NaH as base; the yields of this reaction can be increased waiting at least one hour after addition of sodium hydride. This reaction is controlled by a slight excess of NaH (1.2 equivalents) that should not deprotonate 6-amino group in adenine, and a slight excess of bromoacetate (1.1 equivalents). Double alkylation occurs when using a larger excess of these reagents. Reaction 3 is a Boc-protection and it was obtained by using CDI (carbonyl di-imidazole) for formation of isocyanate that can be further attacked by tert-butanol, giving the desired product. This reaction was conducted in dry DMF and required a higher temperature for adenine. The heterocyclic amines are not very reactive, so it is not necessary to add a nucleobase in a solution of CDI (usually this is the correct way to perform this reaction, because it avoids self-attack on activated isocyanate). Reaction mechanism of this Boc-protection is shown in Figure 4.17. We chose a different strategy for cytosine because we wonted to avoid reaction 4, which is hydrogenation with Pd/C catalysis, substituting it by reaction 5: a basic hydrolysis in water. This latter reaction is advantageous because product usually precipitates and can be therefore easily recovered. We attempted this strategy also for adenine but precipitation was not possible, leading to a more difficult separation procedure.

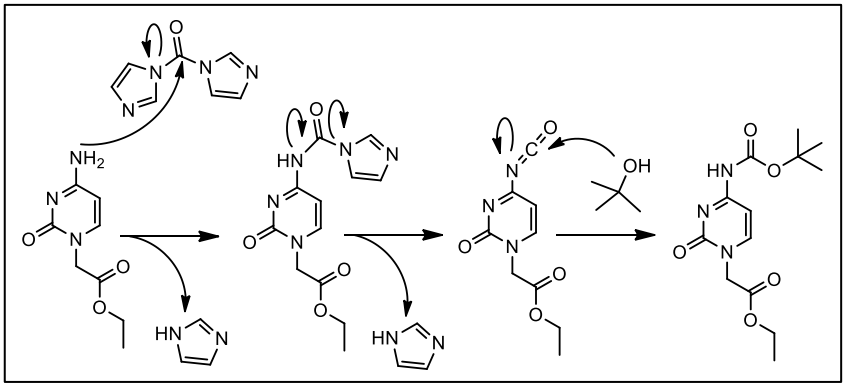

**Figure 4.17: Boc-protection mechanism via CDI activation. Ethyl cytosine-1-acetate (1 eq), carbonyl diimidazole (1.6 eq) in dry DMF 2.5 h at room temperature. Then, t-BuOH (5 eq) 1.5 h at 80°C.**

### "Chiral Box" PNA synthesis

The synthesis of the PNA using the N3-unprotected backbones was then performed. As a preliminary study, we tested how to couple minimal protected monomer without side reactions such as guanidine side product derived by

reaction of the uronium based coupling agents (see Figure 4.18) or attack of a second monomer on the free secondary amino group.

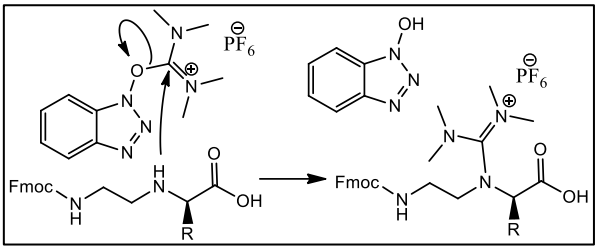


**Figure 4.18: Formation of guanidine side product, in this case possible at activation stage. Usually, with protected amines, this side reaction can be occur only if activation time is not properly long or there is an excess of uronium salt.**

The first tests were performed using HBTU, COMU and PyBOP as activating agents. Modified monomers are zwitterions and thus scarcely soluble; after the formation of activating mixture (5 equivalents of activator and monomer, 10 equivalents of DIPEA in dry DMF) a sonication for 1 minute was necessary to disperse the reagents and start the reaction. We found that for having good conversion rate two consecutive couplings of 30 minutes are necessary. One of the activators, PyBOP have been shown to form O4 -phosphonium compounds with the nucleobase guanine[20], leading to 6-amine-substituted purine products (Figure 4.19).

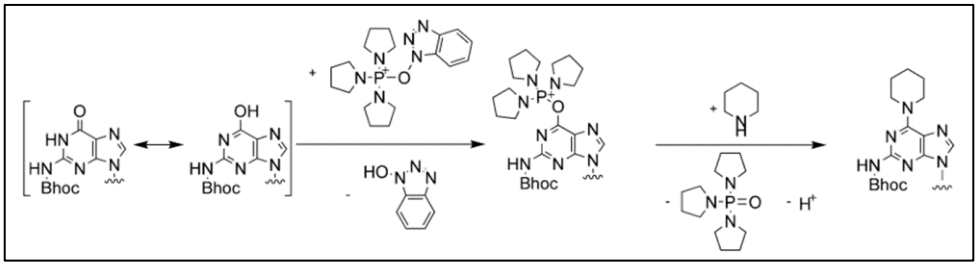


**Figure 4.19: Side reaction of PyBOP activator, the second side product is obtained if deprotection with piperidine is performed after the addition of the monomer.**

We could evaluate this effect because the four monomer precedent to chiral box region represent all the type of nucleobases. UPLC-MS data obtained for the introduction of the first lysine based submonomer are shown in Figure 4.20.

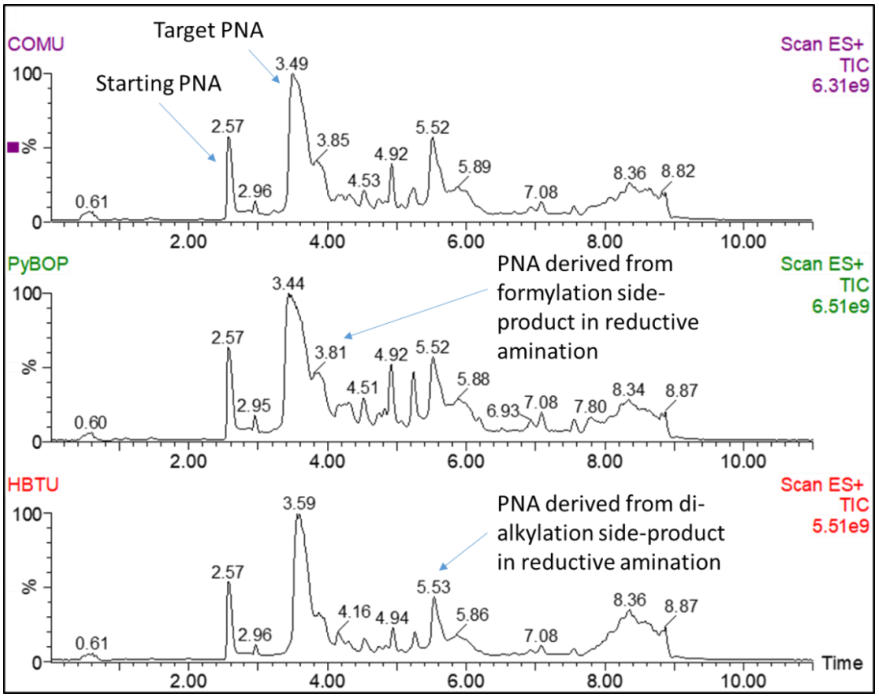


**Figure 4.20: Chromatograms of first tests of backbone coupling using different coupling agents (as indicated). All reactions were performed in the same conditions: 5 eq of activator and backbone, 10 eq of DIPEA. Duration 30 minutes, two times repeated. Resulting chromatograms are identical.**

Surprisingly, negative side products of PyBOP and HBTU were not present, probably because the steric hindrance of the secondary amine in C2-modified backbones is high. Unwanted reactions can be a more severe problem when using C5-modified chiral backbones, since the N3-nitrogen should in this case be more accessible and lead to both reaction with coupling agents and acylation by a second activated monomer. Indeed, test performed using submonomer synthesis of C5-modified backbones showed that in this case HBTU can form guanidine side product (data not shown).

In order to rule out the presence of guanylated products, the PyBOP coupling agent was used in the first syntheses of a ‘chiral box’ PNA following the minimal protection strategy; C2-modified backbones derived from D-lysine and D-arginine were used. The generic scheme of synthesis of the chiral box part of the PNA is shown in Figure 4.21.

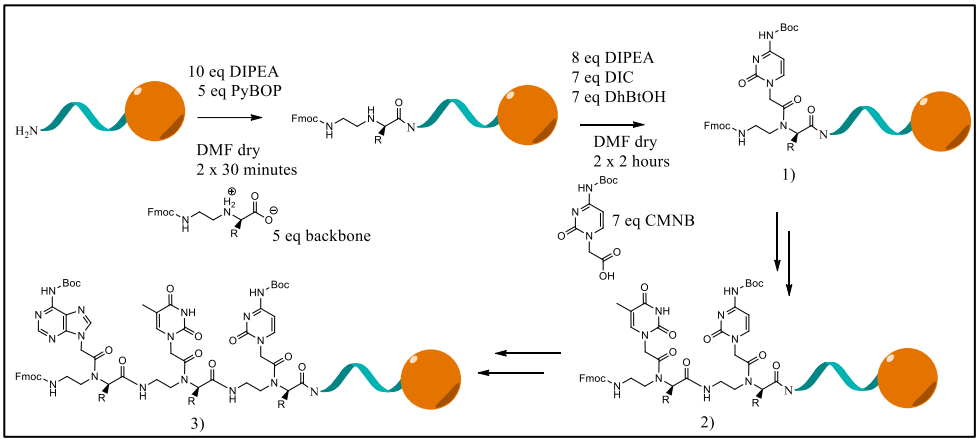


**Figure 4.21: scheme for minimal protective submonomer synthesis in solid phase. PNA identity was check for both lysine and arginine derivatives at point 1, 2 and 3, therefore after each nucleobase coupling.**

The introduction of the backbone involves activation step and coupling. For activation 5 equivalents of both backbone and PyBOP were dissolved separately in 250 µL of dry DMF. Then PyBOP was added to the backbone and both were sonicated at 40°C for about one minute. Especially for lysine backbone the dissolution of such backbone is difficult, so in this case even after the addition of 10 equivalents of DIPEA another sonication step in a heated bath was performed for about one minute. Final step of activation is a stirring for one minute on the stirrer; at this point, usually, the solution changes color. The first coupling was performed for 30 minutes, immediately after that, another coupling of 30 minutes was performed using same amounts of reactant opportunely prepared at the moment. After the backbone addition, it is possible to perform directly the coupling with carboxymethylnucleobase. The chosen nucleobase (7 eq) have to been activated for 15 minutes within DIC (N,N′-Diisopropylcarbodiimide) and DhBtOH (3-Hydroxy-1,2,3-benzotriazin-4(3H)-one) both in 7 equivalents excess.

After introduction of each monomer, the synthesis was checked in UPLC-MS. Especially for coupling of modified cytosine but also for adenine, additional reactions have been performed, due to the steric hindrance on the secondary amino group. The successful activation can be monitored by color changes: turning on of yellow color for cytosine and thymine, and green for adenine. It was found an addition of 8 equivalents of DIPEA during secondary amine coupling allows to reduce activation times, which is rather slow (15 minutes under standard conditions).

The results obtained by systematical UPLC-MS control of lysine and arginine chiral box are shown in Figure 4.22 and 4.23 respectively.

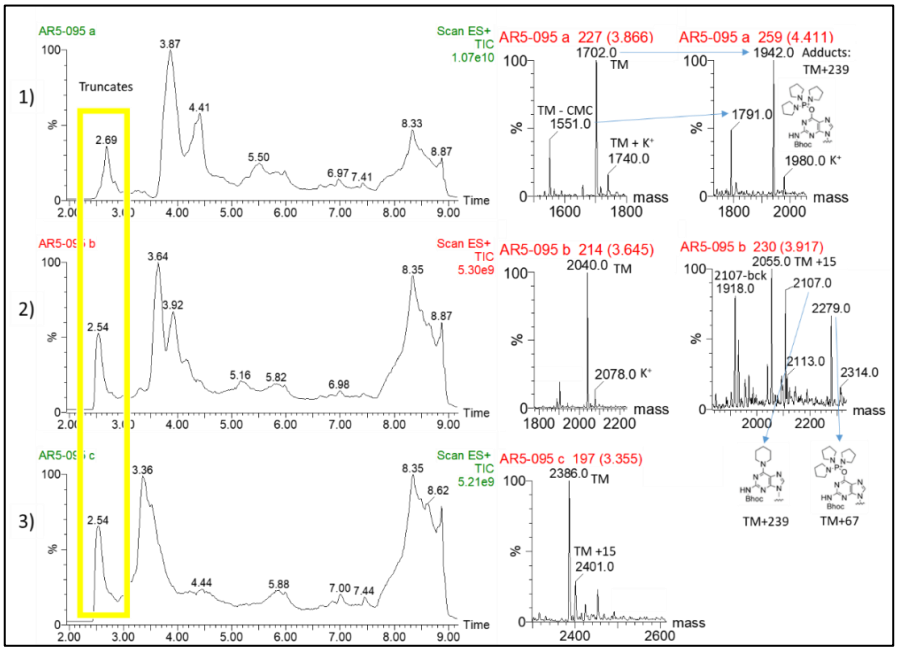


**Figure 4.22: chromatograms and reconstructed spectra acquired after synthesis of each monomer of lysine based chiral box. 1) Chromatogram of control step after addition of carboxymethyl cytosine (CMC). Three main peaks present: 2.69' truncated sequences, 3.87' target PNA (1702) and PNA without CMC (1551), 4.41' O4 –phosphonium adducts at target PNA (1942) and target PNA-CMC (1791). 2) Chromatogram of control step after addition of carboxymethyl thymine (CMT). Three main peaks present: 2.54' truncated sequences, 3.64' target PNA (2040), 3.92' target PNA + 15 uma (2055), O4 –phosphonium adducts at target PNA (2279), pyridine substitution in position 4 of guanine (2107) and latter PNA without backbone (CMT truncated, 1918). 3) Chromatogram of control step after addition of carboxymethyl adenine (CMA). Two main peaks present: 2.54' truncated sequences, 3.36' target PNA (2386) and target PNA + 15 uma (2401).**

The main problems from the synthesis of D-Lys derived chiral box are:

1. appearance of PyBOP coupling side products, that were not present in the test reaction. These products seem to be unstable as they are not present in the last step of chiral box synthesis, probably due to hydrolysis in the washing steps with non-anhydrous solvents.
2. Poor reactivity of the secondary amine to the nucleobase coupling. For this reason, coupling with CMC was repeated four times, while coupling with CMA was repeated twice. This problem is the same in the present synthesis and in the previous submonomeric strategy, as this is the most challenging step in the entire synthesis.
3. Presence of a methylated side product, impossible to be purified. This is avoidable by checking the presence of methylated products in the backbone, and eventually better purifying this.

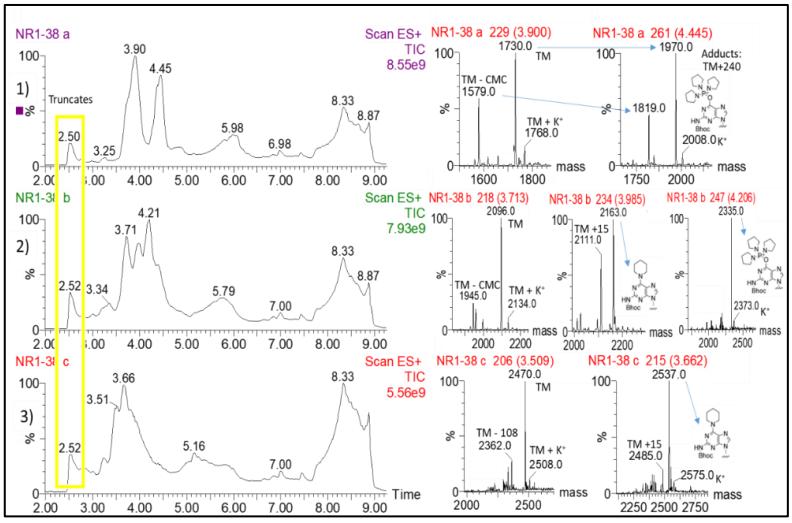


**Figure 4.23: chromatograms and reconstructed spectra acquired after synthesis of each monomer of arginine based chiral box. 1) Chromatogram of control step after addition of carboxymethyl cytosine (CMC). Three main peaks present: 2.50' truncated sequences (TS), 3.90' target PNA (1730) and PNA without CMC (1579), 4.45' O4 –phosphonium adducts at target PNA (1970) and target PNA-CMC (1819). 2) Chromatogram of control step after addition of carboxymethyl thymine (CMT). Four main peaks present: 2.52' TS, 3.71' target PNA (2096), target PNA without CMC (1945), 3.99' pyridine substitution in position 4 of guanine (2163), target PNA + 15 uma (2111), 4.21' O4 –phosphonium adducts at target PNA (2335). 3) Chromatogram of control step after addition of carboxymethyl adenine (CMA). Three main peaks present: 2.52' TS, 3.51' target PNA (2470) and target PNA - 108 (2362), 3.66' pyridine substitution in position 4 of guanine (2537) and target PNA + 15 uma (2485).**

For the synthesis of D-arginine based chiral box the problems emerged were:

1. the N3 secondary amine has in this case a very low reactivity and some unreacted backbone is present even after several treatments with different CMNBs.
2. PyBOP side product are present and differently from lysine chiral box, the corresponding sub-products are persistent.
3. The presence of a methylated side product was also visible in this case, and it was not possible to separate it from the main product in the UPLC chromatogram.

After the synthesis of the 'chiral box', the two PNA sequences have been completed following the standard procedure, and then PNAs were cleaved from the resins. Purification of lysine chiral box (Lys-CB) PNA was easy because it was relatively pure. Arginine chiral box (Arg-CB) PNA showed, besides the peak from target PNA, one of the piperidine complex. Fortunately, standard gradient in HPLC purification was enough to separate the two PNAs. Figure 4.24 shows the HPLC chromatogram of arginine chiral box PNA.

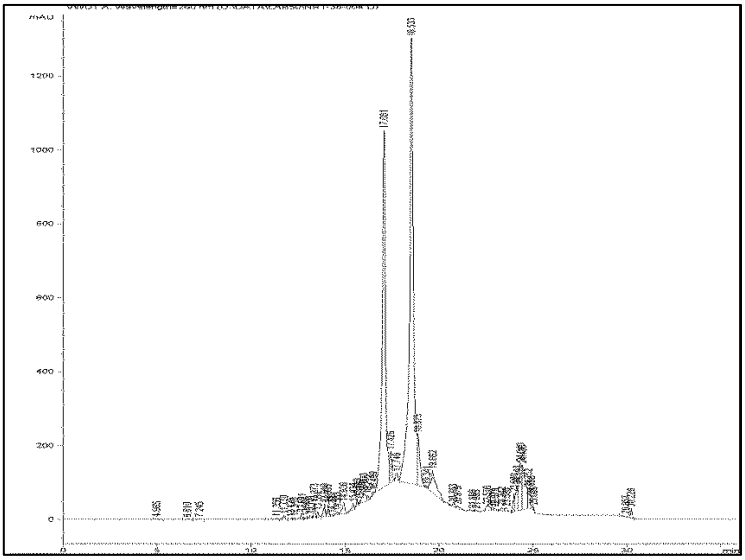

**Figure 4.24: HPLC purification chromatogram of arginine chiral box PNA. Peak at 17.1' is target PNA, piperidine derivative is eluted at 18.5'.**

Overall yield of Arg-CB PNA that is 4%, while Lys-CB PNA it was 5%. These very poor yields are probably due to side reaction caused by PyBOP and poor reactivity of 2D backbones; an amount of growing chains were capped by standard acetylation capping or by CMNB that reacts on primary amine.
Performances of PNAs were tested by measuring with circular dichroism their Tm versus full match DNA (mutated) and mismatched DNA (wild type). Table 4.7 summarize the results obtained:

**Table 4.7: table for comparison of melting temperatures.**

| | NOT MODIFIED | Lys CHIRAL BOX | Arg CHIRAL BOX |
|---|---|---|---|
| FM DNA | 76.7±0.9 | 72.4±0.8 | 73±2 |
| MM DNA | 62.6±0.6 | 56.7±0.8 | 58.0±0.9 |
| difference [°C] | 14.5 | 15.7 | 15 |

We found that differences in the melting temperatures of the WT vs mutated DNA were not significantly different from each other. Both chiral box PNA show a decreased affinity both for full match and mis match DNA sequences, but the decrease of affinity is similar for both types of DNAs. In order to check what can cause this marked decreased of affinity for target sequence, enantiomeric analysis in gas chromatography (GC) have been performed, following an approach early developed in our research group[13]. In order to have both enantiomers of the backbone a L-Lys 2D backbone was synthesized following the same procedure described above. The enantiomeric backbones were Fmoc-deprotected, and then a mixture of TFA and trifluoroacetic anhydride was added in order to obtain cyclization and trifluoroacetylation. The piperazine-2-ones derivatives obtained could then be detected in GC analysis, monitoring specific ions. The same analysis could then be performed on the complete PNA (Lys Chiral Box), by digesting it with HCl 6M at 100°C overnight to obtain the backbone and then using the same derivatization procedure described above. A scheme of these reactions is in Figure 4.25.

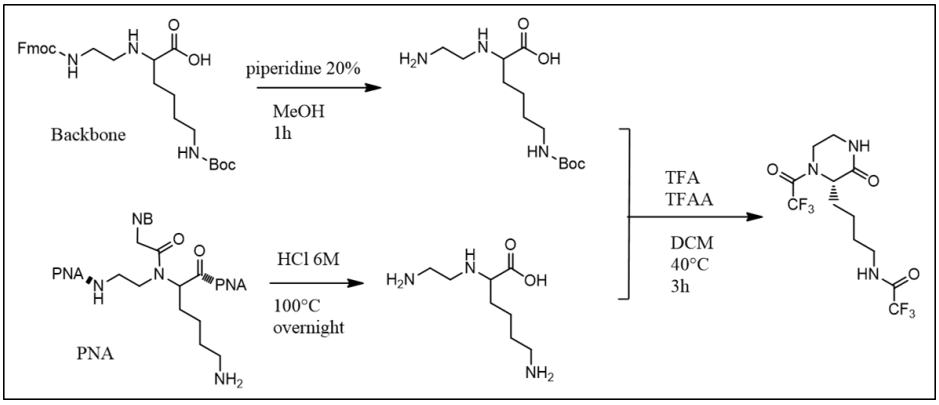


**Figure 4.25: Derivatization scheme for backbone and PNA.**

GC analysis was performed in collaboration with Prof. Federica Bianchi and co-workers, with D, L, D+L enantiomers and digested PNA. Results (Figure 4.1.26) show that backbones from iridium-catalyzed reductive amination are enantiomerically pure (results not shown here are in appendix 7.2), while for the PNA complete racemization was observed. The D enantiomer has a retention time of 45.72', while L enantiomers have a retention time of 50.02'. Their respective percentage in the PNA lysate were 52% and 48% (enantiomeric excess of 4%).

Other tests were performed in order to know the critical step in racemization process. Firstly, PyBOP coupling was investigated by formation of diastereomer and subsequent HPLC analysis. D and L Fmoc-backbones were activated and coupled with H-(L)Leu-OtBu using PyBOP as activator. Exploiting Fmoc group absorption, HPLC purification was performed, and collected peak were analyzed at ESI-MS for correct identification. As shown in figure 4.27, only one type of diastereomer is formed for each coupling, therefore racemization due to PyBOP coupling can be ruled out.

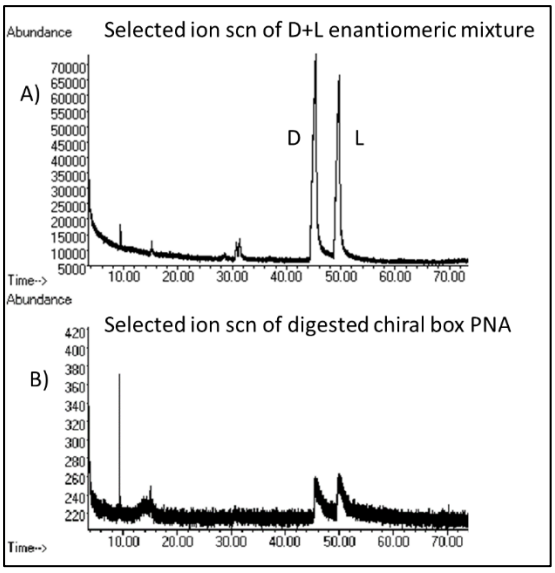


**Figure 4.26: A) GC chromatogram of enantiomeric mixture, B) GC chromatogram of digested PNA**

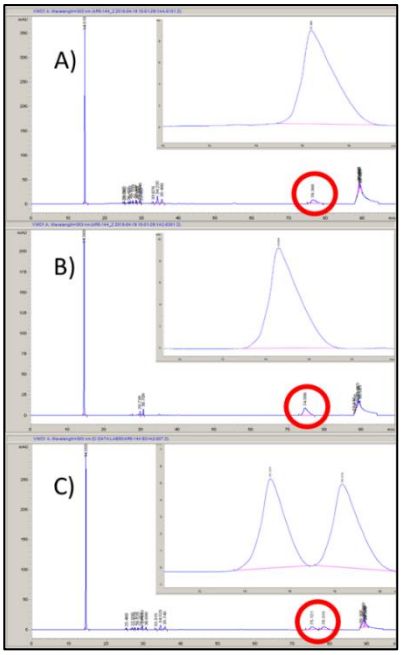


**Figure 4.27: HPLC chromatogram of A) D+L diastereomer, B) L+L diastereomer, C) diastereomeric mixture.**

Two other reactions can be considered for the racemization: the coupling of carboxymethyl nucleobase or the Fmoc deprotection of the monomer in SPS (which have two electron withdrawing groups and an electron withdrawing nucleobase ring). To investigate these reactions, a short PNA segment corresponding to the first part of the chiral box PNA was synthesized and on this a D-Lys based backbone was linked and subjected to different treatments. The following tests were performed:

A) The D-Lys backbone was inserted with the PyBOP coupling, followed by six Fmoc deprotection treatments; the PNA obtained was cleaved from the resin, digested, and subjected to the derivatization procedure for GC analysis.

B) The D-Lys backbone was inserted with the PyBOP coupling, then it was reacted with carboxymethyl thymine (CMT) using only one equivalent of DIPEA during coupling, followed by six Fmoc deprotection treatment, cleavage, digestion, and preparation of GC sample.

The results obtained, showed in Figure 4.28, indicate that even after six treatment with 20% of piperidine, neglectable racemization occurs. In particular, L enantiomer area percentage respect to the total area is 4% for test A and 2% for test B with a respective enantiomeric excess of 92% and 96%.

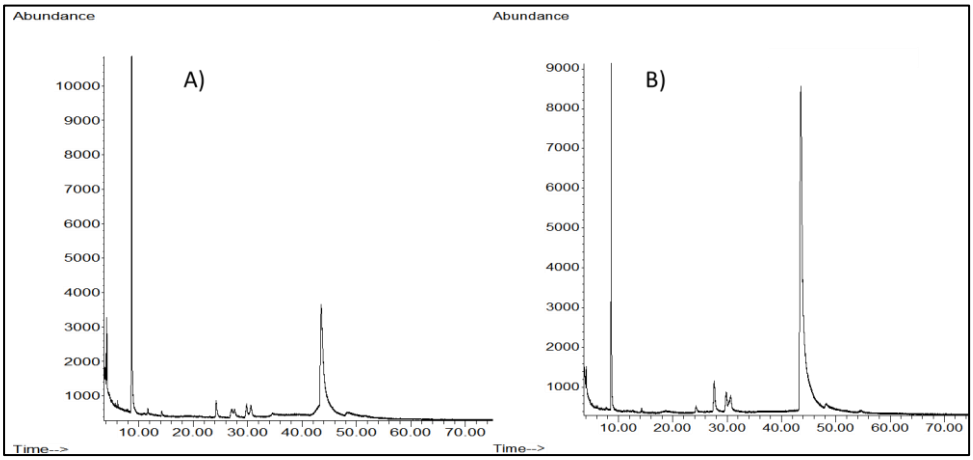


**Figure 4.28: Chiral GC analysis in selected ion scan modality, both sample A) backbone, B) monomer shows a great majority of D-enantiomer while the amount of L-enantiomer (little peak at about 50 minutes) is neglectable. A-chromatogram: D enantiomer rt 43.49', area 1632063; L enantiomer rt 48.24', area 60332. B-chromatogram: D enantiomer rt 43.56', area 3480540; L enantiomer rt 48.24', area 58767.**

The lack of racemization observed in these tests is somehow puzzling in view of the results obtained for the D-Lys PNA. Very little racemization is observed during all the steps leading to incorporation of a new C2-modifed PNA monomer. However, in the test only one equivalent of tertiary amine was used during the CMT coupling, whereas in the PNA synthesis an excess of 8 equivalents was used. This is a possible source of racemization, especially if these conditions are used repeatedly, as in the synthesis of the chiral box.

Following this reviewed strategy, a complete PNA was synthesized, complementary to G12D mutation and with lysine-based chiral box. After synthesis, this PNA was digested and functionalized as previously described, and GC-analysis was performed, showing an enantiomeric excess of 93% of D enantiomer. Similar enantiomeric excesses were found exploiting HBTU and COMU as activators for submonomer coupling of other two chiral box sequences (truncated immediately after chiral box for time deadline). Results are shown in Figure 4.29.

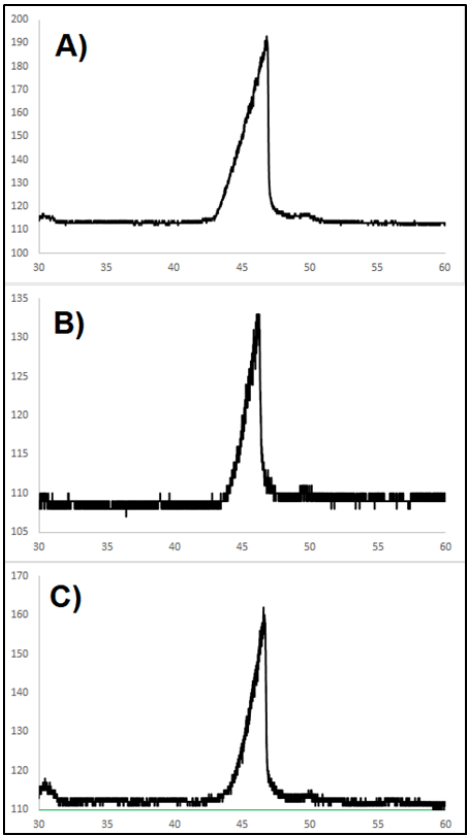


**Figure 4.29: Chiral GC analysis in selected ion scan modality, intensity versus time chromatograms. A) complete PNA with lysine-based CB, PyBOP as coupling reagent, B) PNA with CB without other further bases, HBTU as coupling agent, C) PNA with CB without other further bases, COMU as coupling agent. High enantiomeric excess of D-enantiomer, while the L-enantiomer is the peak at about 50 minutes.**

## Conclusion

A complete set of PNA probes for detection of both genomic DNA and micro RNA have been synthesized. Probes for KRAS and NRAS detection have shown an average good selectivity, while for certain cases there is the possibility of insufficient selectivity. Though surface immobilization strategy tested in sensing devices was by formation of amide bond, other possible alternatives were studied and were shown to be amenable as well. Anti-miR probes have shown a good sensitivity and selectivity, and the best geometry for the assay, which involves an enzymatic polyadenylation, is that of T-shaped PNA.

A new submonomer minimal-protection strategy for synthesis of C2 chiral box PNAs has been developed. First efforts have been done in order to test a reductive amination by hydrogen transfer, catalyzed by Ir(III), and this reaction shows similar yields by easier procedure with respect to standard reductive amination for lysine derivatives, while for arginine derivatives yields are lower. The synthesized backbones were successfully added to a growing chain of PNA avoiding protection of secondary amine, using PyBOP instead of HBTU as coupling agent. After this step carboxymethylnucleobases (CMNs) opportunely protected were coupled, initially with DIC, DhBtOH and DIPEA.

By optimization of the methodologies, the desired high enantiomeric excess has been obtained, for a complete PNA synthesis, exploiting PyBOP as coupling agent. Other appropriate additives could be HBTU and COMU, because using these reagents for the ‘chiral box’ steps of synthesis in preliminary tests, showed an enantiomeric excess similar to that obtained with PyBOP. Future efforts could be directed in developing automatic synthesis of this type of PNA and test the minimal-protected submonomer strategy with 5-L backbones.

## 4.2 EXPERIMENTAL SECTION

General materials and equipment can be seen in Experimental Section of Chapter 3. In addition, NMR JEOL 600MHz ECZ600R was also employed.

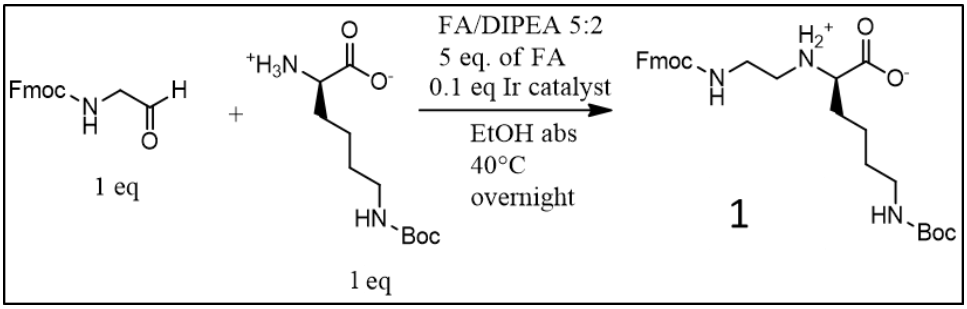


**$N^{\alpha}$-(Fmoc-2-aminoethyl)-$N^{\omega}$-Boc-R-lysine (1):** in a round-bottom flask Fmoc-Gly-H (1 eq) and H-Lys(Boc)-OH were suspended in absolute EtOH. Eutectic mixture Formic Acid/DIPEA 5:2 (5 equivalents of formic acid) and a spatula tip of iridium catalyst (about 0.1 equivalents) were added, and calcium chloride valve was used for protecting the reaction mixture from moisture. Temperature was raised to 40°C, in order to solubilize reagents and the reaction was stirred overnight. The next day a white solid (the product) was precipitated, the reaction was cooled in ice bath and the precipitate was filtered on Buchner and washed with cold ethanol (61% yield). (Yields vary from 40 to 61%).
TLC (Partridge: tBu-OH/EtOH/$H_2O$/AcOH 6:2:1:1) Rf = 0.57

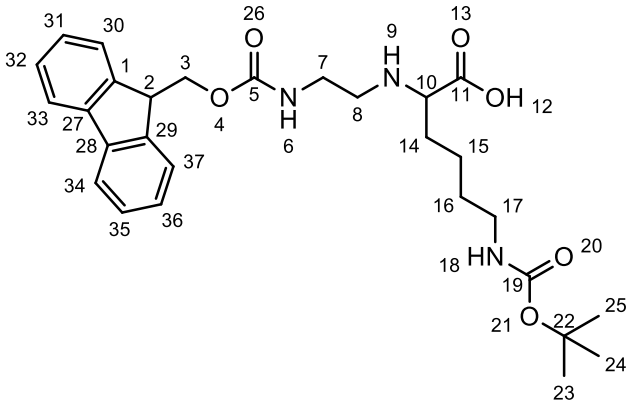

$^{1}$H NMR (600 MHz, DMSO) δ 7.85 (d, *J* = 7.5 Hz, 2H) **H33 H34**, 7.64 (d, *J* = 7.4 Hz, 2H) **H30 H37**, 7.37 (t, *J* = 7.4 Hz, 2H) **H32 H35**, 7.30 (dd, *J* = 15.3, 7.7 Hz, 2H) **H31 H36**, 6.71 (s, 1H) **H6**, 4.28 (d, *J* = 6.9 Hz, 2H) **H3**, 4.18 (t, *J* = 6.7 Hz, 1H) **H2**, 3.14 (d, *J* = 6.2 Hz, 2H) **H17**, 3.06 (t, *J* = 5.9 Hz, 1H) **H10**, 2.87 – 2.81 (m, 2H) **H7**, 2.77 – 2.71 (m, 1H) **H14'**, 2.66 (dt, *J* = 12.4, 6.3 Hz, 1H) **H14''**, 1.54 (d, *J* = 5.7 Hz, 2H) **H8**, 1.32 (s, 9H) **H23 H24 H25**, 1.30 (d, *J* = 7.4 Hz, 2H) **H16**, 1.27 – 1.20 (m, 2H) **H15**. (Figure A9 Appendix)

**H18** signal is under **H31** and **H36** signals (COSY). (Figure A10 Appendix)

$^{13}$C NMR (151 MHz, DMSO) δ 156.96 **C11**, 156.72 **C5**, 156.10 **C19**, 144.43 **C1 C29**, 141.29 **C27 C28**, 128.13 **C32 C35**, 127.60 **C31 C36**, 125.64 **C30 C37**, 120.62 **C33 C34**, 77.85 **C22**, 65.96 **C10**, 62.02 **C3**, 47.29 **C2**, 47.04 **C8**, 31.49 **C14**, 29.94 **C16**, 28.67 **C23 C24 C25**, 23.07 **C15**. (Figure A11 Appendix)
**C7** and **C17** are under DMSO signal; in DEPT spectra (Figure A12 Appendix) two negative peaks are visible in this zone.

MS (ESI, MeOH) m/z calcd for $[C_{28}H_{37}N_3O_6]$: 511.268, found 512.4 $[M+H]^+$, 1023.9 $[2M+H]^+$. (Figure A13 Appendix)

HR-MS (LTQ-Orbitrap, MeOH) m/z calcd for $[C_{28}H_{37}N_3O_6]$: 511.26824, found 510.25986 $[C_{28}H_{36}N_3O_6]^+$. (Figure A14 Appendix)

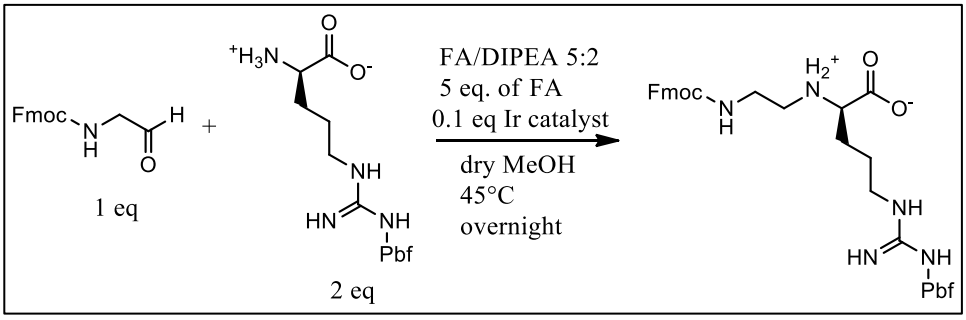


**N$^{\alpha}$-(Fmoc-2-aminoethyl)-N$^{\omega}$-Pbf-R-arginine (2):** in a round-bottom flask Fmoc-Gly-H (200 mg, 0.71 mmol, 1 eq) and H-Arg(Pbf)-OH (608 mg, 1.42 mmol, 2 eq) were suspended in 10 mL of dry MeOH. The mixture was stirred and a spatula tip of iridium catalyst was added. After the addition, the temperature was raised to 45°C, then the reducing agent was added (0.720 mL of FA/DIPEA 5:2, 19 eq of FA). The reaction was let stirring at 45°C overnight.

After a TLC check, solvent was evaporated and the residue was dissolved in EtOAc and placed in a separating funnel, where arginine was removed by 4 extractions with 15 mL of water. The organic phase was treated with anhydrous sodium sulfate to remove water, then filtered, and hexane was added until a white powder was formed. The precipitated product was collected by centrifugation (5' at 5000 rpm), the supernatant was collected and a new addition of hexane was performed. This iterative procedure continued until no further precipitation of the product was observed. Yield 24%.
TLC (Partridge: tBu-OH/EtOH/$H_2O$/AcOH 6:2:1:1) Rf =0.60

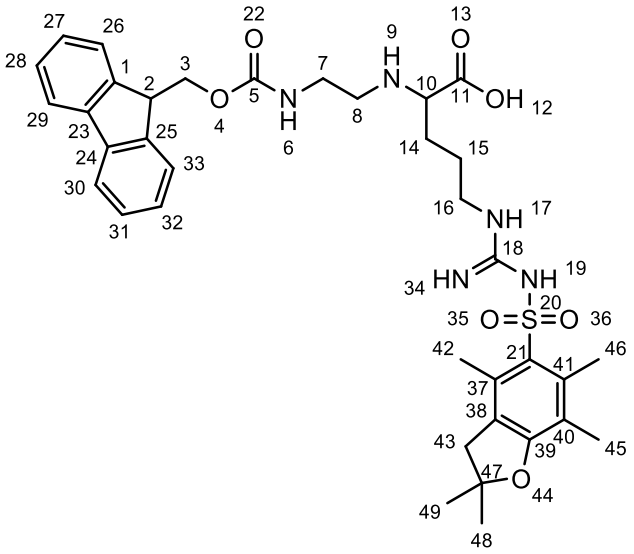

$^{1}$H NMR (400 MHz, DMSO) δ 77.89 (d, J = 7.3 Hz, 2H) **H29 H30**, 7.68 (d, J = 7.1 Hz, 2H) **H26 H33**, 7.45 - 7.37 (m, 3H) **H28 H31 H6**, 7.33 (t, J = 7.1 Hz, 2H) **H27 H32**, 7.22 (s, 1H) **H9**, 6.65 (s, 1H) **H17**, 4.33 (d, J = 6.5 Hz, 2H) **H3**, 4.23 (t, J = 6.3 Hz, 1H) **H2**, 3.20 (s, 3H) **H7 H10**, 3.04 (s, 2H) **H8**, 2.95 (s, 2H) **H43**, 2.85 - 2.63 (m, 2H) **H16**, 2.43 (s, 3H) **H42**, 2., 2.00 (s, 3H) **H45**, 1.59 (s, 2H) **H14**, 1.48 (s, 2H) **H15**, 1.40 (s, 6H) **H48 H49**, **H46** is under DMSO signal. (Figure A15 Appendix)

COSY Spectra (Figure A16 Appendix)

$^{13}$C NMR (101 MHz, DMSO) δ 171.87 **C11**, 157.88 **C39**, 156.71 **C18**, 156.64 **C5**, 144.32 **C1 C25**, 141.22 **C23 C24**, 137.72 **C21**, 134.76 **C38**, 131.87 **C40**, 128.09 **C29 C30**, 127.54 **C28 C31**, 125.57 **C27 C32**, 124.78 **C41**, 120.60 **C26 C33**, 116.72 **C37**, 86.74 **C47**, 65.91 **C3**, 61.58 **C10**, 56.31 **C8**, 47.17 **C2**, 46.52 **C7**, 42.94 **C43**,

38.61 **C16**, 31.16 **C14**, 28.77 **C48 C49**, 27.75 **C15,** 19.43 **C46**, 18.07 **C45**, 12.75 **C42**. (Figure A17 Appendix)

HSQC Spectra (Figure A18 Appendix)
MS (ESI, MeOH) m/z calcd for $[C_{36}H_{45}N_5O_7S]$: 691.304, found 692.3 $[M+H]^+$, 1387.7 $[2M+H]^+$. (Figure A19 Appendix)

HR-MS (LTQ-Orbitrap, MeOH) m/z calcd for $[C_{36}H_{45}N_5O_7S]$: 691.30397, found 690.30 $[C_{36}H_{44}N_5O_7S]^+$. (Figure A20 Appendix)

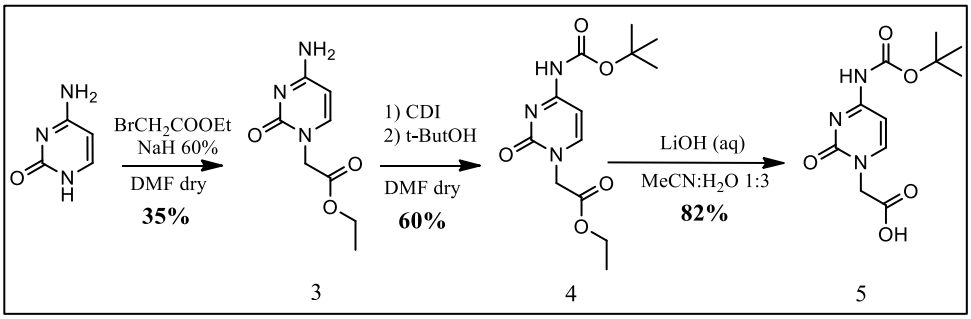


**Ethyl cytosine-1-acetate (3):** in a round-bottom fask, cytosine (1.969 g, 17.72 mmol, 1 eq) was suspended in 30mL of dry and purged DMF, under nitrogen atmosphere and under stirring. NaH was added in three portions (3x 0.287 g, 3x 7.09 mmol, 3x 0.4 eq) and the solution became pale white. The reaction mixture was let stirring for 2.5 h at room temperature, and then ethyl 2-bromoacetate was added in two portions dropwise (2.3 mL, 19.85 mmol, 1.1 eq), the first portion at room temperature, the second at 0°C. The color turned orange and the reaction was let stirring overnight. Work up was performed by adding AcOH (12.2 mL, 0.21 mol, 12 eq) under vigorous magnetic stirring. Solvent was evaporated under high vacuum and the crude mixture was purified with two separations with chromatographic flash column (eluent AcOEt/MeOH 7:3). The pure product was obtained with 35% yield.
TLC (AcOEt/MeOH 8:2) Rf =0.26

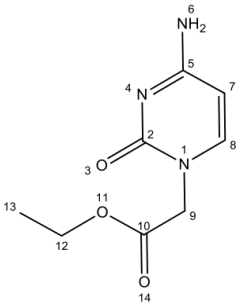


$^{1}$H NMR (400 MHz, DMSO) δ 7.55 (d, J = 7.2 Hz, 1H) **H8**, 7.12 (d, J = 42.0 Hz, 2H) **H6**, 5.69 (d, J = 7.2 Hz, 1H) **H7**, 4.43 (s, 2H) **H9**, 4.12 (q, J = 7.1 Hz, 2H) **H12**, 1.20 (t, J = 7.1 Hz, 3H) **H13**. (Figure A21 Appendix)

$^{13}$C NMR (101 MHz, DMSO) δ 169.22 **C10**, 166.82 **C5**, 156.23 **C2**, 146.79 **C8**, 93.98 **C7**, 61.24 **C12**, 50.40 **C9**, 14.51 **C13.** (Figure A22 Appendix)

MS (ESI(+), MeOH) m/z calcd for $[C_8H_{11}N_3O_3]$: 197.080, found 198.1 $[M+H]^+$, 395.2 [dymer]$^+$. (Figure A23 Appendix)

HR-MS (LTQ-Orbitrap, MeOH) m/z calcd for $[C_8H_{11}N_3O_3]$: 197.08004, found 198.08732 $[C_8H_{12}N_3O_3]^+$, 220.06926 $[C_8H_{11}O_3N_3Na]^+$. (Figure A24 Appendix)

**Ethyl (4-N-(t-Butoxycarbonyl)cytosine)-1-acetate (4):** compound **(3)** (1.223 g, 4.11 mmol, 1 eq) was dissolved in 26 mL of dry and purged DMF. CDI (1.068 g, 6.59 mmol, 1.6 eq) was added under magnetic stirring at room temperature, and reaction, which became brownish, was let stirring 2.5 h. After a TLC check, anhydrous t-BuOH (dried on 3Å sieves) was added (2 mL, 20.59 mmol, 5 eq), and the temperature was raised at 80°C for 1.5 h. After that, reaction was left stirring overnight at room temperature. After a control TLC, the reaction was quenched by addition of MeOH (334 µL, 8.23 mmol, 2 eq) for 5 minutes under vigorous magnetic stirring. Then, solvent was evaporated under high vacuum and brownish oil obtained was dissolved in 20 mL of EtOAc and washed with a saturated $KHSO_4$ aqueous solution (4 x 20 mL). Organic phase was dried on $Na_2SO_4$, filtered on cotton, dried with rotavapor and under high vacuum. The crude mixture was purified with a flash chromatographic column (eluent EtOAc/ MeOH 8:2). Yield 60%.
TLC (AcOEt/MeOH 8:2) Rf=0.60

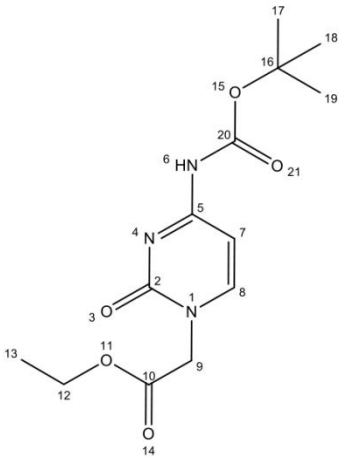


$^1$H NMR (400 MHz, MeOD) δ 7.93 (d, J = 7.3 Hz, 1H) **H8**, 7.30 (d, J = 7.3 Hz, 1H) **H7**, 4.66 (s, 2H) **H9**, 4.25 (q, J = 7.1 Hz, 2H) **H12**, 1.55 (s, 9H) **H17 H18 H19**, 1.30 (t, J = 7.1 Hz, 3H) **H13**. (Figure A25 Appendix)

$^{13}$C NMR (101 MHz, MeOD) δ 167.86 **C10**, 164.36 **C5**, 157.17 **C2**, 152.04 **C20**, 149.48 **C8**, 95.43 **C7**, 81.76 **C16**, 61.51 **C12**, 50.80 **C9**, 26.92 **C17 C18 C19**, 12.99 **C13**. (Figure A26 Appendix)

UPLC-MS (ESI(+), MeOH): tr=4.19, m/z calculated for [$C_{13}H_{19}N_3O_5$]: 297.132, found: 298.2 [M+H]$^+$, 242.17 [M-tBut]$^+$, 595.5 [dymer]$^+$. (Figure A27-A28 Appendix)

HRMS (LTQ-ORBITRAP, MeOH): m/z calculated for [$C_{13}H_{19}N_3O_5$]: 297.13247, found: 298.13975 [$C_{13}H_{20}N_3O_5$], 320.12169 [$C_{13}H_{19}N_3O_5Na$]. (Figure A29 Appendix)

**4-N-(t-Butoxycarbonyl)cytosine)-1-acetic acid (5):** compound **(4)** (0.417 g, 9.82 mmol, 1 eq) was inserted in a 50 mL round-bottom flask and dissolved in a mixture of $H_2O$ (4 mL), MeOH (12 mL) and ACN (12 mL). LiOH· $H_2O$ (0.453 g, 10.80 mmol, 1.1 eq) was dissolved in 4.3 mL of water into a vial; after sonication the basic solution was added to compound **(4)**; a precipitate was immediately formed and the solution became pale yellow. Reaction was monitored every 5 minutes by TLC and, after 10 minutes, the reaction was complete. Quenching was performed by addition of HCl 1M dropwise (about 10 mL) until the pH (measured with pHmeter) drop down to 3-3.5. After that the reaction flask was put in refrigerator for 2.5 h, then the precipitate was filtered on Buchner and washed with cold water. The product was dried under high vacuum and the remaining reaction solution was kept at low temperature to promote an additional precipitation. Yield 82%.
TLC (AcOEt/MeOH 9:1) Rf product=0.00

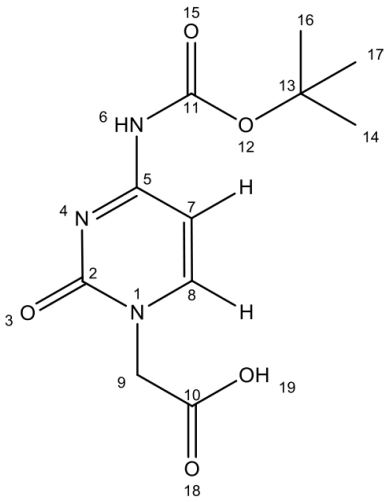

$^{1}$H NMR (300 MHz, DMSO) δ 10.33 (s, 1H) **H19**, 7.99 (d, J = 7.3 Hz, 1H) **H8**, 6.99 (d, J = 7.3 Hz, 1H) **H7**, 4.51 (s, 2H) **H9**, 3.34 (s, 1H) **H6**, 1.46 (s, 9H) **H16 H17 H14**. (Figure A30 Appendix)

$^{13}$C NMR (101 MHz, DMSO) δ 169.87 **C10**, 163.91 **C5**, 155.57 **C2**, 152.60 **C11**, 150.53 **C8**, 94.53 **C7**, 81.46 **C13**, 50.93 **C9**, 28.25 **C14 C16 C17**. (Figure A31 Appendix)

UPLC-MS (ESI(+), MeOH): tr=3.53, m/z calculated for [$C_{11}H_{15}N_3O_5$]: 269.101, found:270.2 $[M+H]^+$, 214.1 $[TM\text{-}tBu]^+$, 539.3 $[dymer]^+$. (Figure A32-A33 Appendix)

HRMS (LTQ-ORBITRAP, MeOH): m/z calculated for [$C_{11}H_{15}N_3O_5$]: 269.10117 found: 268.0938 [$C_{11}H_{14}N_5O_3$]. (Figure A34 Appendix)

**PNA synthesis**

The following solutions were used:

| Solutions for Fmoc-synthesis | | Proportion |
|---|---|---|
| Capping resin | Ac2O/NMP | 1:1 |
| Deprotection | Piperidina/DMF | 1:4 |
| Capping | Ac2O/DIPEA/NMP | 5:6:89 |
| Cleavage | TFA/m-cresol | 9:1 |
| DIPEA wash | DIPEA/DMF | 5:95 |

Fmoc protocol was composed by the following steps. a) Deprotection 2x8'; b) DCM wash; c) DMF Wash; d) Kaiser test (1') (positive); e) Coupling 1x30' (activation for 2'; Activation solution: 5 eq of monomer and activator, 10 eq of DIPEA in dry DMF); f) DMF Wash; g) Kaiser test (1') (negative);h) Capping 2x1' ; i) DMF Wash; l) DIPEA 5% 2x2' ; m) DMF Wash; n) DCM Wash

All PNA sequences without modification were synthesized by automatic synthesizer Syro I. In the automated synthesis protocol for this instrument there is no activation step and coupling reaction are repeated twice with 3 equivalents of monomer, coupling agent and 6 equivalents of DIPEA, while 5% DIPEA washing step is not present. The N-term modification with groups such as the AEEA spacer and other linkers was performed manually. The SPDP spacer was added in 10 equivalent excess, with an overnight coupling.

The following spacers/terminal groups were used at the end of PNA sequences

1. O: [2-(2-(Fmoc-amino)ethoxy)ethoxy]acetic acid (AEEA)

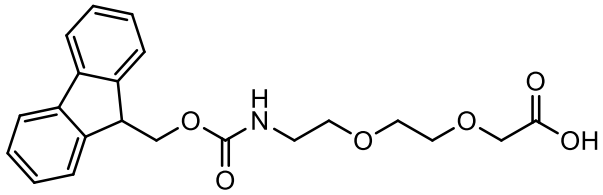

1. Azide: 2-azidoacetic acid

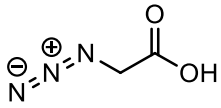

2. SPDP-dPEG$_4$: 3-{2-[2-(2-{2-[3-(Pyridin-2-yldisulfanyl)-propionylamino]-ethoxy}- ethoxy)-ethoxy]-ethoxy}-propionic acid

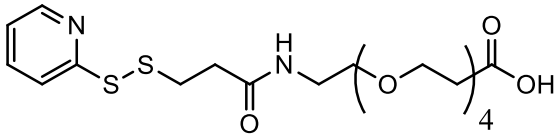

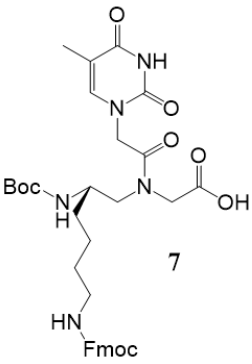

**Modified monomer for T-shaped PNA.**

*Synthesis of C5-modified probes (T-shaped)*

PNA probes for miR detections were automatically synthesized in case of N-term and C-term attack side, while Boc-strategy (see chapter 3) was used for T-shaped probes, using monomer 7 depicted in figure.

*Synthesis of C-terminal-modified probes*

In the case of C-terminal probes, the first amino acid loaded was Fmoc-Lys(Dde). The sequence was grown using using standard peptide synthesizer protocol, while further modifications were carried out manually. These modifications included deprotection and acetylation of

N-terminus followed by deprotection of Lys side chain from Dde protection using 1.2 mL of NMP/DMF 5:1 solution with hydroxylamine chlorohydrate (3M) and imidazole (2.2 M) for 3 h. Upon deprotection, the attachment of first spacer was carried out using double higher concentration of spacer activated with HBTU/DIPEA and repeating this treatment twice for 30 minutes The attachment of second spacer was performed with less difficulty with standard conditions for Fmoc synthesis. Finally, the Fmoc group was removed, and the PNA was cleaved from the resin with a TFA/m-cresol 9-:1 cocktail. The resin was covered with this cleavage solution and after 1 hour the solution was filtered and collected, this procedure was repeated to ensure complete cleavage.
The PNA was purified by HPLC and characterized by UPLC-ESI/MS and UV/Vis techniques.

*Synthesis of C2-modified probes (chiral box)*
The first 4 PNA monomers were introduced using the procedures described above for Fmoc-synthesis. The following steps were then performed for the synthesis of the "chiral box" segment: a)Fmoc deprotection 2x8min; b) DCM wash; c) DMF wash; d) Kaiser test (1 min, positive); e) coupling with the unprotected submonomer (**1** or **2**) 2x30min (activation for 2 min; Activation solution: 5 eq of submonomer and 5 eq of different activator, 10 eq of DIPEA in dry DMF); f) DMF wash; g) coupling with the carboxymethylnucleobase (CMNB 2x2h (activation with 7 eq of CMNB, 7 eq DIC and 7 eq DhBtOH, 1 eq of DIPEA in dry DMF for 15min; h) DMF wash; i) DCM wash.
These steps were repeated for all the three chiral monomers. Check of the reaction outcome was performed after each cycle (submonomer+nucleobase) by treatment of a small portion of resin with the cleavage solution, followed by precipitation and UPLC-MS analysis.
The PNA sequence was then completed using standard unmodified Fmoc (Bhoc) monomers as described above.

Concentrations of PNA-solutions were measured by measuring absorbance in the function of wavelength by Thermo Scientific Evolution 260 BIO spectrophotometer. The values at 260 and 400 nm were extracted and together with calculated molar absorptivity (ε), scale of synthesis, solution dilution (for UV/Vis measurements) and PNA solution volume, determined solution concentration and reaction yield.

AR4-9 WT: H-OO-CTA CGC CAC CAG CT-$NH_2$ KRAS Ex2 WT
yield 11%. Rt : 2.72; ε (260 nm): 127900
UPLC-ESI-MS characterization: m/z calcd 4064.0 [M]: 1017.1 $[M+4H]^{4+}$, 813.8 $[M+5H]^{5+}$, 678.3 $[M+6H]^{6+}$, 581.6 $[M+7H]^{7+}$, 509.0 $[M+8H]^{8+}$. (Figure A35 Appendix)

AR4-9 G12D: H-OO-CTA CGC CAT CAG CT-$NH_2$ KRAS Ex2 G12D
yield 8.3%. Rt : 2.78; ε (260 nm): 129900
UPLC-ESI-MS characterization: m/z calcd 4078.0 [M]: 1020.7 $[M+4H]^{4+}$, 816.9 $[M+5H]^{5+}$, 680.9 $[M+6H]^{6+}$, 583.7 $[M+7H]^{7+}$, 510.9 $[M+8H]^{8+}$. (Figure A36 Appendix)

AR4-10 WT: $N_3$-OO-CTA CGC CAC CAG CT-$NH_2$ KRAS Ex2 WT
yield 17%. Rt : 2.92; ε (260 nm): 127900
UPLC-ESI-MS characterization: m/z calcd 4147.1 [M]: 1383.3 $[M+3H]^{3+}$, 1037.5 $[M+4H]^{4+}$, 830.4 $[M+5H]^{5+}$, 692.1 $[M+6H]^{6+}$, 593.3 $[M+7H]^{7+}$. (Figure A37 Appendix)

AR4-10 G12D: $N_3$-OO-CTA CGC CAT CAG CT-$NH_2$ KRAS Ex2 G12D
yield 23%. Rt : 2.99; ε (260 nm): 129900 $cm^{-1}$ $M^{-1}$
UPLC-ESI-MS characterization: m/z calcd 4162.1 [M]: 1388.4 $[M+3H]^{3+}$, 1041.5 $[M+4H]^{4+}$, 833.4 $[M+5H]^{5+}$, 694.6 $[M+6H]^{6+}$, 595.5 $[M+7H]^{7+}$. (Figure A38 Appendix)

AR4-11 WT: SPDP-$dPEG_4$-CTA CGC CAC CAG CT-$NH_2$ KRAS Ex2 WT
yield 22%. Rt : 3.33; ε (260 nm): 127900 $cm^{-1}$ $M^{-1}$
UPLC-ESI-MS characterization: m/z calcd 4218.3 [M]: 1055.4 $[M+4H]^{4+}$, 844.6 $[M+5H]^{5+}$, 703.9 $[M+6H]^{6+}$, 603.6 $[M+7H]^{7+}$, 528.2 $[M+8H]^{8+}$. (Figure A39 Appendix)

AR4-11 G12D: SPDP-$dPEG_4$-CTA CGC CAT CAG CT-$NH_2$ KRAS Ex2 G12D
yield 19%. Rt : 3.36; ε (260 nm): 129900 $cm^{-1}$ $M^{-1}$

UPLC-ESI-MS characterization: m/z calcd 4233.3 [M]: 1059.3 $[M+4H]^{4+}$, 847.7 $[M+5H]^{5+}$, 706.4 $[M+6H]^{6+}$, 605.7 $[M+7H]^{7+}$, 530.1 $[M+8H]^{8+}$. (Figure A40 Appendix)

AR5-004: Ac-AAC CCC ATC AGA GAA AGT-Lys(O-O-$NH_2$)-$NH_2$
PNA for miR221 4 mismatch
yield 2.8%. Rt : 2.95; ε (260 nm): 194900 $cm^{-1}$ $M^{-1}$
UPLC-ESI-MS characterization: m/z calcd 5342.3 [M]: 1070.1 $[M+5H]^{5+}$, 891.6 $[M+6H]^{6+}$, 764.4 $[M+7H]^{7+}$, 669.0 $[M+8H]^{8+}$, 594.8 $[M+9H]^{9+}$, 535.4 $[M+10H]^{10+}$. (Figure A41 Appendix)

AR4-67: H-OO-GTA GCC AGA TGT AGC T-$NH_2$
PNA anti miR 222-2
yield 17%. Rt : 3.68; ε (260 nm): 167500 $cm^{-1}$ $M^{-1}$
UPLC-ESI-MS characterization: m/z calcd 4740.6 [M]: 1185.9 $[M+4H]^{4+}$,949.0 $[M+5H]^{5+}$, 791.1 $[M+6H]^{6+}$, 678.2 $[M+7H]^{7+}$, 593.6 $[M+8H]^{8+}$, 527.7 $[M+9H]^{9+}$. (Figure A42 Appendix)

AR4-68: H- OO-CCA TCT TTA CCA GAC AGT -$NH_2$
PNA anti miR 141-2
yield 28%. Rt : 3.63; ε (260 nm): 174500 $cm^{-1}$ $M^{-1}$
UPLC-ESI-MS characterization: m/z calcd 5162.1 [M]: 1033.6 $[M+5H]^{5+}$, 861.3 $[M+6H]^{6+}$, 738.3 $[M+7H]^{7+}$, 646.3 $[M+8H]^{8+}$, 574.5 $[M+9H]^{9+}$, 517.2 $[M+10H]^{10+}$. (Figure A43 Appendix)

AR4-69: H- OO- AAT CCC ACC AGA GAA AGT -$NH_2$
PNA anti miR 221 4MM
yield 8.9%. Rt : 3.51; ε (260 nm): 194900 $cm^{-1}$ $M^{-1}$
UPLC-ESI-MS characterization: m/z calcd 5229.1 [M]: 1047.0 $[M+5H]^{5+}$, 872.6 $[M+6H]^{6+}$, 748.1 $[M+7H]^{7+}$, 654.7 $[M+8H]^{8+}$, 582.1 $[M+9H]^{9+}$, 524.0 $[M+10H]^{10+}$. (Figure A44 Appendix)

AR4-40: H- OO- CCA GCA GAC AAT GTA GCT -$NH_2$
PNA anti miR 221-2 N-term
yield 6.2%. Rt : 6.50; ε (260 nm): 187800 $cm^{-1}$ $M^{-1}$

UPLC-ESI-MS characterization: m/z calcd 5236.1 [M]: 1048.1 $[M+5H]^{5+}$, 873.7 $[M+6H]^{6+}$, 749.1 $[M+7H]^{7+}$, 655.5 $[M+8H]^{8+}$, 582.8 $[M+9H]^{9+}$. (Figure A45 Appendix)

AR4-41: $N_3$- OO- CCA GCA GAC AAT GTA GCT -$NH_2$
PNA anti miR 221-2 N-term azide
yield 3.3%. Rt : 6.90; ε (260 nm): 187800 $cm^{-1}$ $M^{-1}$
UPLC-ESI-MS characterization: m/z calcd 5319.0 [M]: 133.8 $[M+4H]^{4+}$, 1064.9 $[M+5H]^{5+}$, 887.6 $[M+6H]^{6+}$, 760.8 $[M+7H]^{7+}$, 665.9 $[M+8H]^{8+}$. (Figure A46 Appendix)

AR4-42: SPDP-$dPEG_4$- CCA GCA GAC AAT GTA GCT -$NH_2$
PNA anti miR 221-2 N-term thiol
yield 14%. Rt : 7.80; ε (260 nm): 187800 $cm^{-1}$ $M^{-1}$
UPLC-ESI-MS characterization: m/z calcd 5390.4 [M]: 1079.0 $[M+5H]^{5+}$, 899.4 $[M+6H]^{6+}$, 771.1 $[M+7H]^{7+}$, 674.8 $[M+8H]^{8+}$, 600.0 $[M+9H]^{9+}$, 540.0 $[M+10H]^{10+}$. (Figure A47 Appendix)

AR4-43: Ac-CCA GCA GAC AAT*(OO- $NH_2$) GTA GCT -$NH_2$
PNA anti miR 221-4 T shaped
yield 16%. Rt : 7.80; ε (260 nm): 187800 $cm^{-1}$ $M^{-1}$
UPLC-ESI-MS characterization: m/z calcd 5349.3 [M]: 1338.4 $[M+4H]^{4+}$,1070.8 $[M+5H]^{5+}$, 892.5 $[M+6H]^{6+}$, 765.2 $[M+7H]^{7+}$, 699.7 $[M+8H]^{8+}$, 595.5 $[M+9H]^{9+}$. (Figure A48 Appendix)

AR5-095: H-CTA CGC CAT CAG CT-$NH_2$
PNA sequence KRAS Ex2 G12D Chiral Box D-Lys
yield 5%. Rt : 2.45; ε (260 nm): 129900 $cm^{-1}$ $M^{-1}$
UPLC-ESI-MS characterization: m/z calcd 4002.0 [M]: m/z 1335.1 $[M+3H]^{3+}$, 1001.4 $[M+4H]^{4+}$, 801.3 $[M+5H]^{5+}$, 668.1 $[M+6H]^{6+}$, 572.6 $[M+7H]^{7+}$ , 501.2 $[M+8H]^{8+}$. (Figure A49 Appendix)

NR1-38: H-CTA CGC CAT CAG CT-$NH_2$
PNA sequence KRAS Ex2 G12D Chiral Box D-Arg
yield 4%. Rt : 2.57; ε (260 nm): 129900 $cm^{-1}$ $M^{-1}$

UPLC-ESI-MS characterization: m/z calcd 4002.0 [M]: m/z 876.3 $[M+5H]^{5+}$, 730.3 $[M+6H]^{6+}$, 626.1 $[M+7H]^{7+}$, 548.0 $[M+8H]^{8+}$. (Figure A50 Appendix)

**FORMATION OF DIASTEREOMERIC DIMERS FOR OPTICAL PURITY ASSESSMENT**

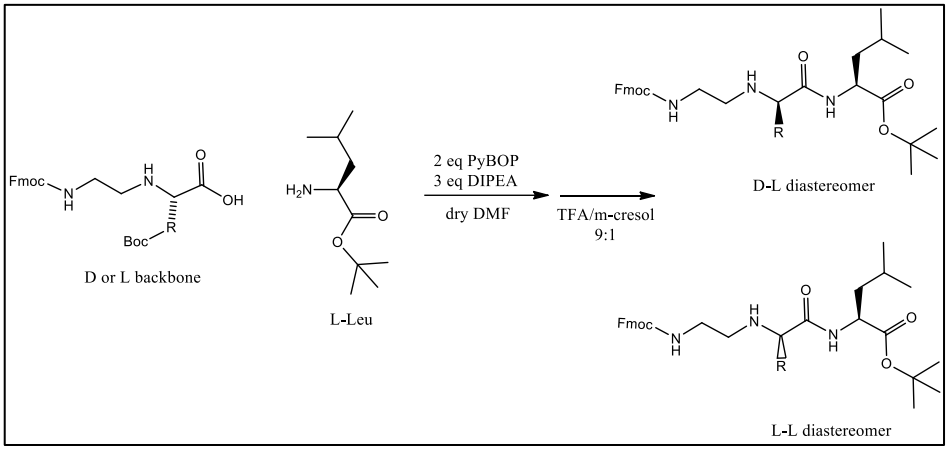


**PNA-(Lys)-backbone-Leu dimer**: in a round-bottom flask $N^{\alpha}$-(Fmoc-2-aminoethyl)-$N^{\omega}$-Boc-R-lysin or L-lysine (20 mg, 39 µmol, 1 eq) was dissolved in 5 mL of dry and purged DMF. H-Leu-OtBu·HCl (8.7 mg, 39 µmol, 1 eq) and subsequently, PyBOP (40 mg, 78 µmol, 2 eq) and DIPEA (20 µL, 120 µmol, 3eq) were added. The reaction was let stirring at room temperature for 4 hours; TLC confirmed that the coupling was complete. Solvent was dried under high vacuum and residue was dissolved in 5mL of EtOAc and extracted with brine (2x25 mL) and saturated solution of $KHSO_4$ (2x25 mL). The organic phase was dried with anhydrous $Na_2SO_4$ and filtered. To this solution, an equal amount of TFA/m-cresol was added and the reaction mixture was let stirring for 30'. After Boc deprotection (ninhydrin check), the solution was dried and re-dissolved in 3 mL of methanol. An UPLC-MS analysis was performed (data not reported) and as main product was found to be the target molecule (m/z= 581.4). TLC (EtOAc) Rf product= 0.16.

Three backbones were employed: one from D-lysine derived from standard reductive amination (batch C), the other two were D (batch A) and L-lysine (batch B) derivatives and have been synthesized with the new method above described.

**HPLC ANALYSIS**

The diasteromers obtained in the previous reaction were analyzed by HPLC using UV detector. After the Boc deprotections these diastereomers were very apolar, therefore after an initial step in gradient the chromatographic run was performed in isocratic conditions, column at 40°C, flow rate 4 mL/min, UV-detector λ=303 nm, eluent A: water 0.1% TFA, eluent B: MeCN 0.1% TFA.

| Time [min] | 0 | 5 | 25 | 84 | 85 | 90 | 91 | 99 |
|---|---|---|---|---|---|---|---|---|
| % eluent B | 0 | 0 | 33.3 | 33.3 | 100 | 100 | 0 | 0 |

Products from batches A and C showed the same $t_r$ D-L = 75', while products from batch B exhibit a $t_r$ L-L = 78'. When A+ B or C+ B chromatographic runs were performed, two peaks were observed (3 replicates).

The peaks of the diastereomeric products were collected and their identity was confirmed by UPLC-MS analysis. An example of ESI spectrum of the collected chromatographic peak, target molecule have m/z of 581.4.

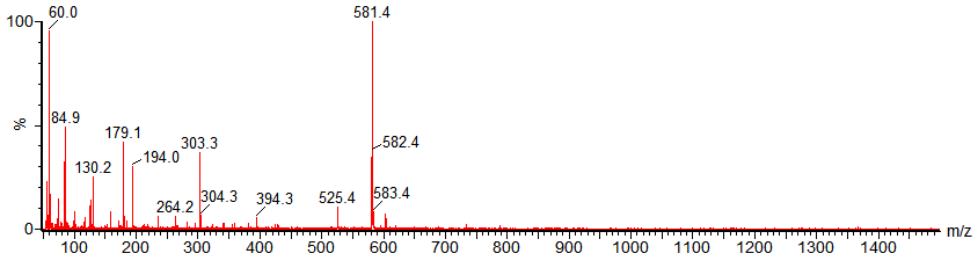


Derivatization procedure for enantiomeric analysis.

1. Lysine derivative backbones were Fmoc-deprotected by dissolution in a solution containing 20% piperidine in methanol. Reaction was stirred for about 50 minutes and then solvent was removed under low pressure. The crude mixture was suspended in EtOAc and centrifuged at 5000 rpm for five minutes. The supernatant was eliminated and solid residue was re-suspended twice. In the last suspension, an EtOAc/EtOH 9:1 mixture was used; the final solid was the deprotected backbone (checked with TLC spot: disappearing of the fluorescence,

strong ninhydrin response). After that it was important to dissolve the solid obtained in TFA, promoting Boc deprotection and primary nitrogen protonation before step 3.

2. Chiral PNA (10 nmol in 200 µL of aqueous solution) was put in a test tube with emery neck and a slight excess (0.3 mL) of HCl 37% was added. Temperature was raised to 100 °C and hydrolysis reaction was let to occur at this temperature overnight. Solvents were then removed under nitrogen flux.
3. Both backbones and hydrolyzed PNAs were treated with trifluoroacetic anhydride (TFAA) in excess (about 2 mL), and temperature was raised to 40°C. Formation of piperazine-2-one derivative was carried out for at least 3 h. After that, solvent was removed under nitrogen flux and residue was dissolved in 1mL of EtOAc.

GC-MS analyses were performed using a HP 6890 Series Plus gas chromatograph (Agilent Technologies, Palo Alto, CA) equipped with a MSD 5973 mass spectrometer (Agilent Technologies). Chromatographic separation was performed on a 25 m × 0.25 mm, df 0.12 µm CP-ChirasilVal capillary column (Agilent Technologies), using the following chromatographic conditions:

Full-scan method (m/z: 45 - 200), used for backbones:

| | |
|---|---|
| Injector Temperature | 230 °C |
| Modality | **Split 10** |
| Flow rate | **1.2 mL/min** |
| Solvent delay | **3.5 min** |
| Column Temperature | **190 °C for 90 min** |

SIM method (m/z: 140, 167, 196), used for PNAs:

| | |
|---|---|
| Injector Temperature | 230 °C |
| Modality | **Split 10** |
| Flow rate | **1.2 mL/min** |
| Solvent delay | **3.5 min** |
| Column Temperature | **190 °C for 100 min** |

The following GC analysis were performed: a) L+D Lys submonomers (Figure A51 Appendix); b) D-Lys submonomer (Figure A52 Appendix); c) L-Lys submonomer (Figure A53 Appendix); d) D-Lys “chiral box” PNA hydrolysate (Figure A54 Appendix); e) D-Lys PNA racemization test A described at page 151 (Figure A55 Appendix); D-Lys PNA racemization test B described at page 151 (Figure A56 Appendix).

Bibliography:


1. Crowley E, Di Nicolantonio F, Loupakis F, Bardelli A. Liquid biopsy: monitoring cancer-genetics in the blood. *Nat Rev Clin Oncol*. 2013;10(8):472-484.
2. Toiyama Y, Okugawa Y, Fleshman J, Richard Boland C, Goel A. MicroRNAs as potential liquid biopsy biomarkers in colorectal cancer: A systematic review. *Biochim Biophys Acta - Rev Cancer*. May 2018.
3. Heitzer E, Ulz P, Geigl JB. Circulating tumor DNA as a liquid biopsy for cancer. *Clin Chem*. 2015;61(1):112-123.
4. Gasparini G, Buttitta F, D'Andrea MR, et al. Optimizing Single Agent Panitumumab Therapy in Pre-Treated Advanced Colorectal Cancer. *Neoplasia*. 2014;16(9):751-756.
5. Pu X, Huang G, Guo H, et al. Circulating miR-221 directly amplified from plasma is a potential diagnostic and prognostic marker of colorectal cancer and is correlated with p53 expression. *J Gastroenterol Hepatol*. 2010;25(10):1674-1680.
6. Cheng H, Zhang L, Cogdell DE, et al. Circulating Plasma MiR-141 Is a Novel Biomarker for Metastatic Colon Cancer and Predicts Poor Prognosis. Navarro A, ed. *PLoS One*. 2011;6(3):e17745.
7. Gao Y, Feng B, Han S, et al. The Roles of MicroRNA-141 in Human Cancers: From Diagnosis to Treatment. Cell Physiol Biochem. 2016;38(2):427-448.
8. Manicardi A, Fabbri E, Tedeschi T, et al. Cellular Uptakes, Biostabilities and Anti-miR-210 Activities of Chiral Arginine-PNAs in Leukaemic K562 Cells. *ChemBioChem*. 2012;13(9):1327-1337.
9. Corradini R, Sforza S, Tedeschi T, Totsingan F, Manicardi A, Marchelli R. Peptide Nucleic Acids with a Structurally Biased Backbone. Updated Review and Emerging Challenges. Current topics in medicinal chemistry,2011; 11(12), 1535-1554.
10. Corradini R, Feriotto G, Sforza S, Marchelli R, Gambari R. Enhanced recognition of cystic fibrosis W1282X DNA point mutation by chiral peptide nucleic acid probes by a surface plasmon resonance biosensor. *J Mol Recognit*. 2004;17(1):76-84.
11. Manicardi A, Calabretta A, Bencivenni M, et al. Affinity and selectivity of C2- and C5-substituted "chiral-box" PNA in solution and on microarrays. *Chirality*. 2010;22(1E):E161-E172.
12. Tedeschi T, Chiari M, Galaverna G, et al. Detection of the R553X DNA single point mutation related to cystic fibrosis by a "chiral box" D-lysine-peptide nucleic acid probe by capillary electrophoresis. *Electrophoresis*. 2005;26(22):4310-4316.
13. Tedeschi T, Corradini R, Marchelli R, Pushl A, Nielsen PE. Racemization of chiral PNAs during solid-phase synthesis: Effect of the coupling conditions on enantiomeric purity. *Tetrahedron Asymmetry*. 2002;13(15):1629-1636.

14. Manicardi A, Fabbri E, Tedeschi T, et al. Cellular Uptakes, Biostabilities and Anti-miR-210 Activities of Chiral Arginine-PNAs in Leukaemic K562 Cells. *ChemBioChem*. 2012;13(9):1327-1337.
15. Sforza S, Tedeschi T, Corradini R, Ciavardelli D, Dossena A, Marchelli R. Fast, Solid-Phase Synthesis of Chiral Peptide Nucleic Acids with a High Optical Purity by a Submonomeric Strategy. *European J Org Chem*. 2003;2003(6):1056-1063.
16. Lei Q, Wei Y, Talwar D, Wang C, Xue D, Xiao J. Fast Reductive Amination by Transfer Hydrogenation “on Water.” *Chem - A Eur J*. 2013;19(12):4021-4029.
17. Wang C, Pettman A, Basca J, Xiao J. A Versatile Catalyst for Reductive Amination by Transfer Hydrogenation. *Angew Chemie Int Ed*. 2010;49(41):7548-7552.
18. Organica C, Corradini PR, Accetta A. Università degli Studi di Parma Molecular Engineering of PNA Using Modified Uracil Derivatives and Porphyrins. 2010.
19. Pothukanuri S, Pianowski Z, Winssinger N. Expanding the scope and orthogonality of PNA synthesis. *European J Org Chem*. 2008;(18):3141-3148.
20. Pritz S, Wolf Y, Klemm C, Bienert M. Modification of guanine residues in PNA-synthesis by PyBOP. *Tetrahedron Lett*. 2006;47(33):5893-5896.
21. Juan Jose Díaz-Mochón, Laurent Bialy and, Bradley M. Full Orthogonality between Dde and Fmoc: The Direct Synthesis of PNA−Peptide Conjugates. 2004.

# 5- PNAS FOR AMPEROMETRIC GENOSENSOR DEVELOPMENT


## Abstract:

In this Chapter, the synthesis of PNA probes for amperometric genosensor will be discussed. For this purpose, PNA modified probes were designed for a sandwich assay in which a biotinylated signaling probe of PNA binds in solution to a long trait of target DNA and this complex is further hybridized by a capture PNA probe linked on the sensor's surface. These probes were shown to be effective in the detection of oligonucleotides, as well as in the ultrasensitive detection of genomic DNA. A general scheme of the genosensing is shown in Figure 5.1.


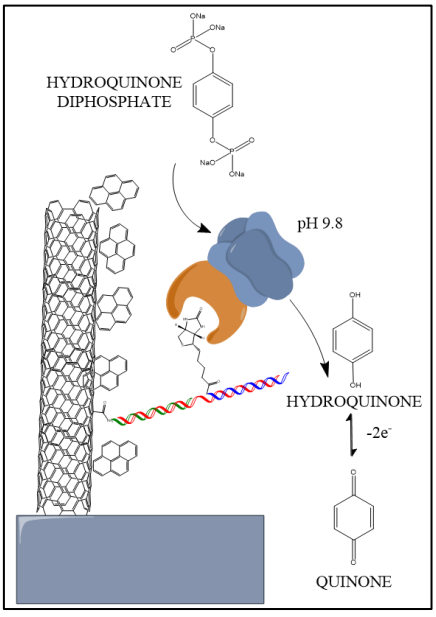


**Figure 5.1: Scheme of amperometric genosensing on carbon nanotubes support. PNA capture probe (green) is linked to the surface and blocking with pyrene is performed. After hybridization in solution between target DNA (red) and PNA signaling probe (blue), this complex is added dropwise on the electrode. The addition of streptavidin-alkaline phosphatase conjugate and the enzymatic substrate (hydroquinone diphosphate) lead to the electroactive specie hydroquinone that is oxidized to quinone by voltage application.**

## 5.0 INTRODUCTION

A voltammetric analysis is a technique in which current is measured in a potential gradient. The potential is scanned in order to obtain non-spontaneous reactions at the working electrode. This electrode can act as anode in case of oxidation, cathode if a reduction is performed. Usually, it is constituted of noble metals such as gold, silver, platinum or conductive nanomaterials like glassy carbon and carbon nanotubes.
In this technique, other two electrodes are present; firstly there is a counter electrode, which is the source of current in the electrochemical cell and for this reason needs a large area. The current is measured between counter- and working-electrodes and this current has positive sign if electrons are withdrawn by counter electrode (oxidation process). A third, reference, electrode is used for measuring the potential difference with the working electrode. One of the most used, well-known reference electrodes is made of Ag/AgCl. Only in dynamic voltammetry the solution is stirred, otherwise the migration of charged molecules to the opposite sign electrode has to be avoided and for this reason inert ions are usually added in excess. Analytes should arrive in proximity of the working electrode through diffusion and be captured by a recognition molecule placed onto its surface. If a linear scan of potential is performed (linear sweep voltammetry) not only the faradic current is measured, which is the current derived by redox processes, but also the capacitive current, derived from double electric layers formed in proximity of the electrode surface. This double layer act like a condenser, which can store charges. Capacitive current decrease exponentially in time, therefore adding impulse to the linear scan ramp and subtracting current immediately before the current after the impulse, the capacitive current can be neglected. In this case the only component measured is the faradic current that is proportional to the amount of sample oxidized or reduced. This technique is called differential pulse voltammetry (DPV) and it is one of the most used, because the signal/noise ratio is very high. Another important and diagnostic technique is cyclic voltammetry (CV), which is performed by positive and subsequent negative ramp of potential. If the process is reversible two peaks are present (oxidation and reduction) and the reversibility of the electrochemical reaction can be evaluated by the symmetry of these peaks.
Cost-effective platforms for voltammetric sensing are screen-printed electrodes: these are disposable chips where electrodes are printed on a ceramic support. Some companies, such as DropSens provide these

electrodes with different types of materials as electrodic surface, among them gold, glassy carbon and carbon nanotubes have been used in the measurements connected with the present work. A scheme of a typical screen printed electrode is showed in Figure 5.2.
The carbon nanotubes are allotropic form of carbon which have cylindrical shape with a width of approximately 2 nm. Single-Walled Carbon nanotubes (SWCNTs), with a single cylindrical shape, have been developed, and Multi-Walled Carbon Nanotubes (MWCNTs) where multiple cylinder are concentrically disposed are available and used for different purposes. When carbon nanotubes are deposited onto screen printed chips, an enhancement of the electrochemical signal is obtained[1]. This is partially due to an increased surface that can be modified with receptor by exploiting carboxylic moieties at the edges of cylinders.

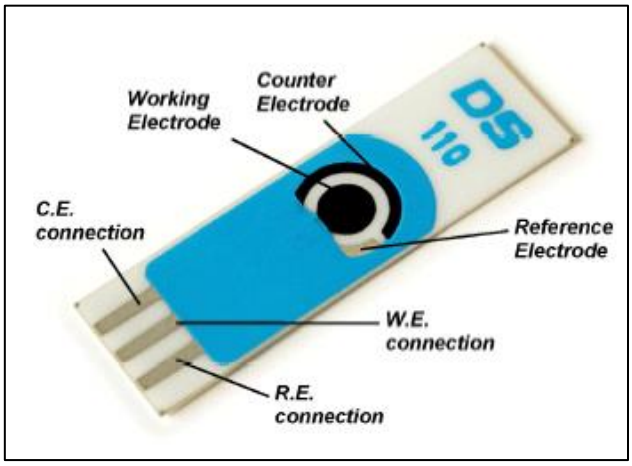


**Figure 5.2: Configuration of a DropSens screen-printed electrode.**

Many methods have been developed for different type of analytes using this platform, spanning from proteins to nucleic acids and from biomedical tests to food analysis.
We wanted to explore the potentiality of PNA probes in this technology, especially in respect to the possibility to adopt a PCR-free detection. As a test system, we choose the sequence of DNA inserted in transgenic soy (Soy-RR, Roundup Ready), for which suitable certified materials are available. These modified soybeans have been genetically engineered for becoming resistant to glyphosate herbicide, which kills other plants that can subtract resources to

soybean. Glyphosate interferes with the synthesis of amino acids like tyrosine, tryptophan and phenylalanine, these aromatic amino acids are synthesized by the enzyme 5-enolpyruvylshikimate-3-phosphate synthase (EPSPS). RR soybeans have been modified by a plasmid with a trait of DNA from *Agrobacterium tumefaciens* coding for a glyphosate resistant version of EPSPS enzyme and other genome part from other organism in order to enhance the activity of this gene. Regulation EC 1829/2003, allows for Europe a threshold level in food of genetic modified organisms (GMOs) of 0.9%, if the food contains more than this percentage of GMOs derived material it must be labelled as containing GM product. Detection methods are aimed at recognition of DNA traits or resistant type of protein. Most used methods are PCR-based while for protein detection ELISA and strip kit are available[2]. Manzanares-Palenzuela and collaborators[3] developed a multiplex electrochemical platform for detection of characteristic trait of Soy RR DNA. This assay was based on biotinylated capture probes that can bind to streptavidin-coated magnetic beads; meanwhile target DNA and differently labelled signaling probes were hybridized. After that, this partial duplex was placed in contact with derivatized magnetic beads and measurement phase was performed on screen printed electrodes surface. This developed sensing strategy was able to detect 0.9% of transgenic soy in wild type soy, so a useful analysis allowing to enforce European regulation.

The aim of this work was to synthesize the probes for the development of a DPV analysis, able to detect specific DNA in real matrices, namely to detect a trait of soy RR genome at level required by the European Union or below. For achieving this result, PNA probes have been used as bio-recognition elements and screen printed electrodes have been used as cheap but effective sensing platform. The entire work was carried out in collaboration with the Prof. M. Giannetto's group at University of Parma and in particular in close collaboration with Dr. Simone Fortunati who performed all the electrochemical studies.

In order to produce an amperometic signal, the hybridization of PNA probes with the target DNA should produce a change in the electrochemical properties of the surface layer. This is possible if the interaction is coupled with the capture of an electrochemical active species either free or linked to a secondary (reporter) probe. In previous work we focused on a competitive assay in which PNA reporter probe was labelled with a redox moiety such as ferrocene, using a gold electrode. For this methodology, PNA bearing a ferrocene moiety were synthesized.

The detection scheme (Figure 5.3) was designed using competitive binding, in which a pre-hybridized capture probe-reporter probe complex could be displaced if target DNA was added at the assay causing a decrease of the amperometric signal. Short reporter probes labeled with ferrocene were used. The sensor substrate was micro-structured gold, which was previously modified by creation of a self-assembled monolayer.

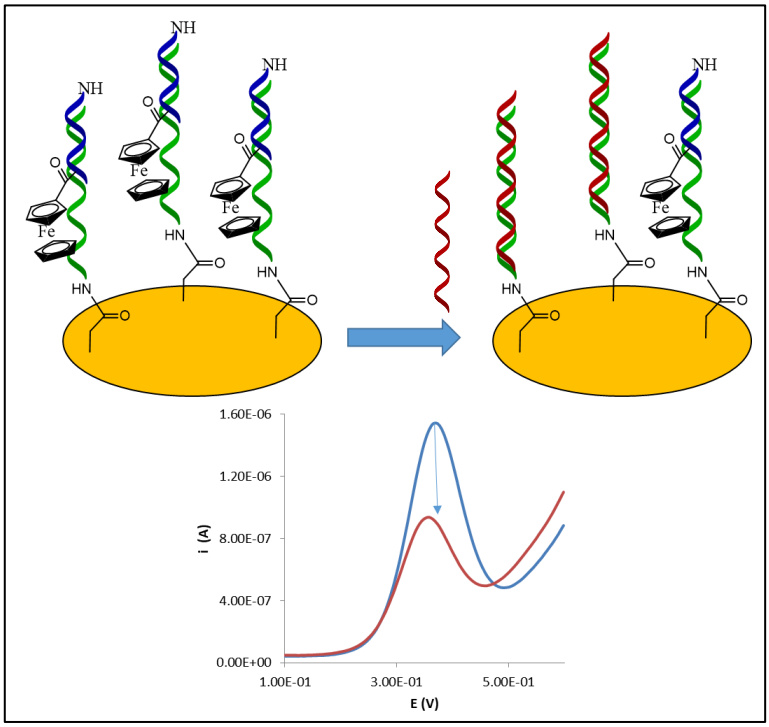


**Figure 5.3: first attempt of genosensing on screen-printed electrodes. PNA capture probe (green) is initially hybridized with shorter PNA reporter probe (blue), ferrocene labelled. After DNA (red) addition the signal of ferrocene oxidation drop down, voltammogram, from blue line to red line.**

The synthesis of the PNA probes containing the ferrocene unit was particularly challenging, as shown in my master thesis. Different length of reporter probe was tested, from 4 to 8 nucleobases. In order to have a reliable blank signal, the longest sequence was chosen, which exhibit high Tm with capture probe but lower than CP PNA:DNA target.

The first problem of this system was the degradation of the ferrocene moiety, probably due to the acidic condition used for the cleavage of the PNA from the resin. Not all the Reporter probes were therefore redox active.
The self-assembled monolayer on the electrode was constituted by mercapto undecanoic acid, and coupling reaction with free terminal amine of PNA were used for surface functionalization. Ethanolamine capping was performed in order to avoid unwanted coupling with reporter probes and for reducing non-specific adsorption of PNAs. The PNA-ferrocene was found to be non-reducible after the first voltammetric oxidation. This made it impossible to repeat the voltammetric cycle in order to test bank and sample (after the addition of DNA) on the same electrode. Different electrodic substrates were tested, in particular AuNPs on glassy carbon, streptavidin modified glassy carbon (a specific biotinylated capture probe was synthesized for this type of electrodes), glassy carbon and carbon nanotubes, without significantly improving the results. The weakness of the PNA:PNA duplexes when short reporter probes were used and the sensitivity of the competitive test to changes in environmental conditions might be the source of these reproducibility problems.
In order to avoid these problems, a sandwich approach was developed in the present work. In this configuration a secondary probe (hereinafter call signaling probe) was synthesized for maximizing interaction with target DNA, which was elongated from 20 to 45-mer.

## 5.1 RESULTS AND DISCUSSION

For the above mentioned sandwich approach an enzyme-based detection was used, in which the electroactive species was produced by alkaline phosphatase-streptavidin conjugate, captured on the surface by means of a biotinylated secondary signaling probe. In this case, the advantage compared to the competitive scheme was that the length of both PNA capture probe and the PNA signaling probe could be increased, making the DNA binding more performant. In this configuration, it is also possible to perform hybridization reaction between target DNA and signaling probe in solution, prior to hybridization with the PNA capture probe on the electrode, thus making it more effective in terms of kinetics and of compatibility with different conditions. Glassy carbon and carbon nanotubes electrodes were used, while for the first type a preliminary functionalization inducing the formation of carboxylic acid moieties by voltammetric oxidation is necessary, for this is not necessary since

they have carboxylic groups at the edges of tubes and this treatment can be avoided. A standard coupling with PNA capture probe was performed exploiting EDC-NHS chemistry.
The advantage of this type of derivatization is principally due to the fact that the receptor is directly bound to the electrode surface, without any other "passivation" layer such as SAM. Moreover, carbon nanotubes have a three dimensional shape and the amount of loaded capture probe can be increased[4].
The main problem of these types of electrodes was the high unspecific binding, in particular on glassy carbon electrodes[5]. Carbon nanotubes were used as final system, since these showed better performances because they increase electron transfer reaction between redox species and the electrode[6].

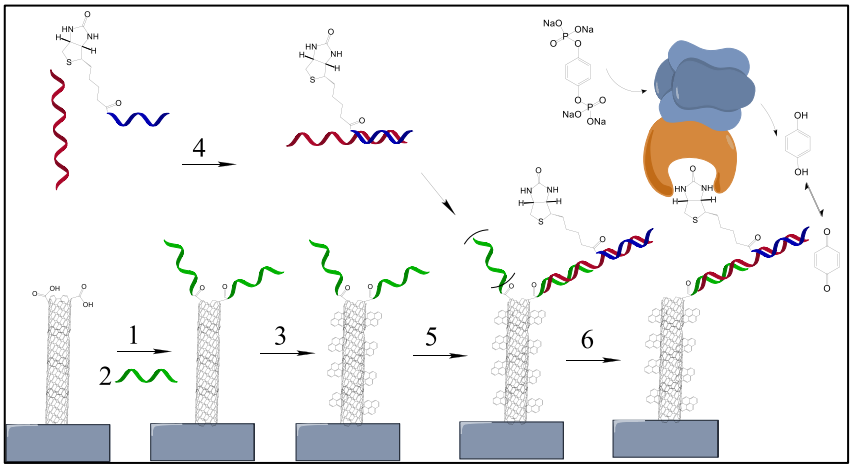


**Scheme 5.2: Functionalization of the electrode and amperometric detection. 1) EDC-NHS activation, 2) PNA CP coupling, 3) blocking with pyrene, 4) PNA SP/DNA hybridization, 5) hybridization of free DNA trait with PNA CP, 6) enzymatic detection by first adding of enzyme conjugate and then substrate; the species produced is electroactive and is then oxidized by the electrode.**

The design and synthesis of the PNA capture probe (CP) and signaling probe (SP) were performed to be adapted to this scheme. 20mer PNA probes were chosen, for increasing the stability of their hybrids with target DNA and eventually for allowing them to interact with double stranded genomic DNA.
The target sequence was chosen as a part of the Roundup-Ready soy, for which standard reference materials are available. Capture probe sequence was chosen according to previous studies in which PNA probes were used in combination of microarray technology, SPR or optical fibers sensors; the same

region was targeted, but with a longer probe. Compared to these previous works, a PNA signaling probe was chosen instead of a DNA one, in order to further stabilize the resulting sandwich. Between CP and SP regions of hybridization, 5 free nucleotides were left in order to allow streptavidin linking. Figure 5.3 shows the chosen regions of the genome; since this is a guanine-poor region it could also facilitate the PNA synthesis.

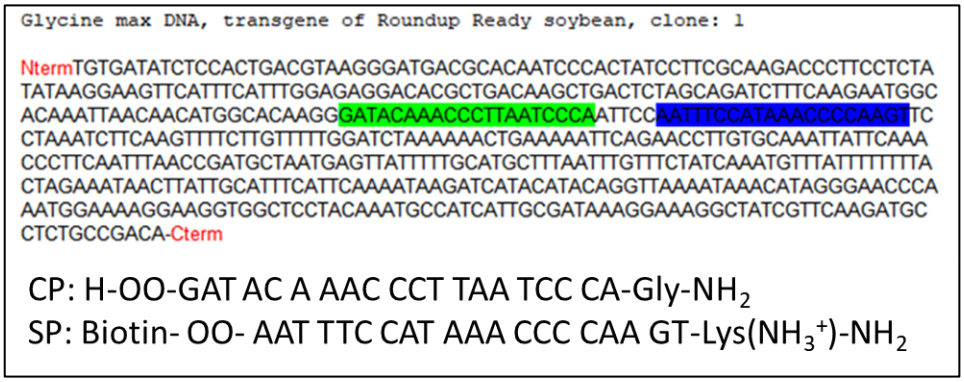


**Figure 5.3: Gene of SoyRR, the CP region is highlighted in green, while SP region is in blue, CP and SP are also explicitly shown.**

The capture probe was synthesized following a standard Fmoc-based synthesis, exploiting two spacers “O” that are [2-(2-(Fmoc-amino) ethoxy) ethoxy] acetic acid for allowing a sufficient distance to the sensor surface. The signaling probe was also synthesized with Fmoc-strategy, and at the beginning of the sequence a lysine was inserted, in order to enhance the solubility and increase the interactions with double stranded DNA helix. At the N-term of SP, after two spacer units, a biotin molecule was added exploiting the natural carboxylic acid present in this molecule.

The two PNAs probes were purified using reversed phase semi-preparative HPLC and their identity was checked at UPLC-MS analyzer. Interestingly, in the HPLC chromatogram, SP showed two peaks both corresponding to the product mass (Figure 5.4). That can be caused by a self-pairing of the sequence as shown in Figure 5.5.

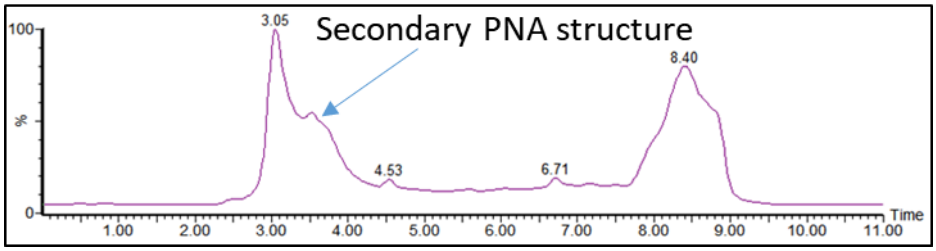


**Figure 5.4: chromatogram of SP with two peak of the target PNA.**

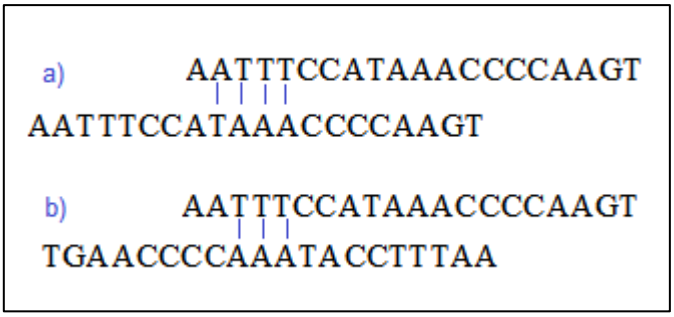


**Figure 5.5: a) parallel self-pairing, b) anti-parallel self-pairing of the capture probe.**

In order to measure the affinity of CP for the complementary oligomer DNA in solution, melting temperatures were measured. In Table 5.1 differences between 15-mer CP and 20-mer CP were evaluated. Five monomers increased the stability of the complex of about 8°C. Melting temperatures graphs obtained at UV-Vis spectrophotometer are shown in Figure 5.6.

**Table 5.1: Comparison of melting temperatures between target DNA and capture probes of 15-mer and 20-mer.**

| | Melting [°C] | Annealing [°C] | Δ |
|---|---|---|---|
| CP 15mer-DNA FM | 67.1 | 64.9 | 0 ; 0 |
| CP 20mer-DNA FM | 74.7 | 73.1 | +7.6 ; +8.2 |

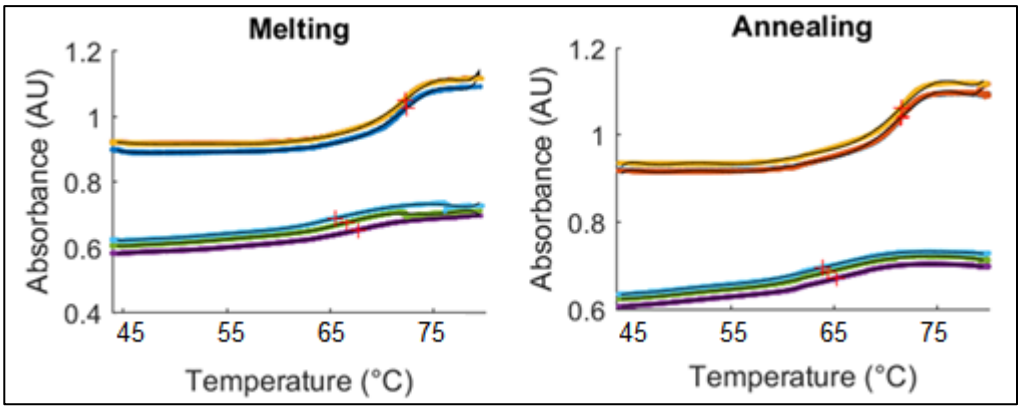


**Figure 5.6: Melting temperature profile obtained for 20-mer CP (above) and 15-mer CP (below). Both DNA and PNA were at 5 µM concentration in PBS solution at pH 7.**

Both Tm of 15 and 20-mer CP are good for hybridization with target DNA, but since the capture probe is bound to the surface, the hybridization kinetic is slow. Moreover, the trait of DNA that have to hybridize is more hindered because it is partially hybridized with signaling probe. Therefore, an higher Tm is advisable for enhancing the hybridization.

The set-up and optimization of the amperometric sensor were the subject of a parallel PhD thesis work (Simone Fortunati PhD thesis) and thus only the major results will be summarized here. Further details will be given in the corresponding PhD thesis.
The coupling reaction between carboxylic acid on carbon nanotubes and amines of PNA was performed in aqueous environment, following an EDC-NHS strategy, which is depicted in Figure 5.7.

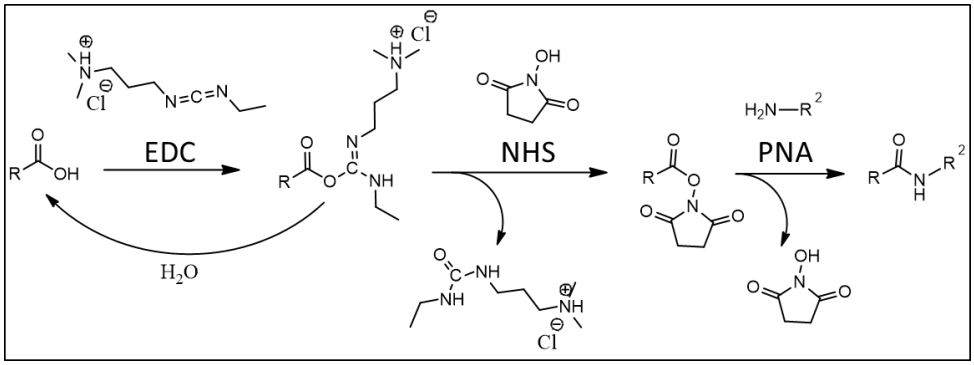


**Figure 5.7: EDC-NHS mediated coupling between carboxylic acids on carbon nanotubes and PNA probes.**

EDC (N-(3-Dimethylaminopropyl)-N'-ethylcar-bodiimide · HCl) is a water soluble carbodiimide developed for fast and effective activation for couplings in aqueous solutions, NHS (N-Hydroxysuccinimide) is an additive that can form stable active ester in acqueous solution and avoid hydrolysis of EDC-mediated active ester. Formation of active ester was carried out at pH 5, in MES buffer (2-(N-morpholino) ethanesulfonic acid). Since NHS esters have a half-life of 4-5 hours at pH 7, 1 hour at pH 8 and only10 minutes at pH 8.6 an acidic condition have been chosen for the NHS active ester formation, while coupling with capture probes has been performed under basic conditions for having neutral amine (carbonate buffer, pH 9)[7].

The final tests were performed by hybridization of the target DNA with the biotinylated signaling probe in solution, followed by hybridization with the capture probe on the electrode. These sandwiches were then used to capture alkaline phosphatase-streptavidin conjugate. The enzyme catalyzes the transformation of a masked substrate hydroquinone diphosphate (HQDP) into an electroactive hydroxyquinone, which was oxidized by the electrode.

After optimization of conditions, and most importantly the treatment of the electrodes for eliminating unspecific interactions, the results were very good in terms of sensitivity and selectivity. As an example, the signals obtained with oligonucleotides full-match, singly mismatched and scrambled are reported in figure 5.8

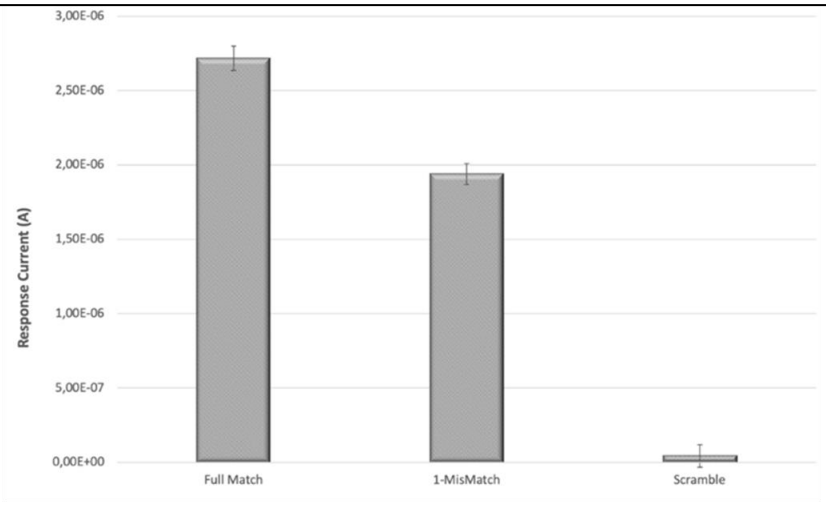


Full match (FM) DNA:
5'-ACT TGG GGT TTA TGG AAA TTG GAA TTG GGA TTA AGG GTT TGT ATC-3'.
Single mismatch (1-MM) DNA:
5'-ACT TGG GGT TTA TGG AAA TTG GAA TTG GGA TTA AG**T** GTT TGT ATC-3'.
Scramble DNA (SCR):
5'-ACT TGG GGT TTA TGG AAA TTG GAA T**GG TTA GAA TTG TGT GTA TGC**-3'.

**Figure 5.8: Selectivity of the genosensor towards 1-mis match (1-MM) and scrambled (SCR) sequences, as from comparison with full match (FM) DNA at a concentration of 10 nM Means and standard deviation (n=3) are reported. Sequences of DNA used are listed.**

The limit of detection (LOD) of the biosensor was 71 pM and the limit of quantitation (LOQ) 256 pM. The same system was used to detect Roundup Ready soy DNA without previous amplification, and it was shown to be able to discriminate between 0%, 1% and 10% content of transgenic soy in flour (results not shown). A detailed description of the procedures and analytical data are reported in a manuscript submitted for publication and will be the subject of a subsequent PhD thesis.

**Conclusion**

The PNA probes synthesized have shown great affinity with target DNA and quite unexpectedly selectivity, for such long sequences. The detection limit obtained is at the same level of similar genosensor, while the applicability to real sample is remarkable. In this application a key-role is played by PNA that can avoid self-pairing of the double stranded, genomic DNA. Further improvements of this systems could be the use of magnetic beads that make the hybridization between CP and DNA more similar to a bulk process and test this sensory system in other complex matrices such as blood.

## 5.2 EXPERIMENTAL PROCEDURE

General materials and equipment can be seen in Experimental Section of Chapter 3; if not specified reagents and solvents have been purchased from Sigma Aldrich.
Double-distilled and deionized water purified with a Milli-Q system was used for the preparation of the buffered solutions.

A major part of PNAs synthesis was performed by an automatic synthesizer Biotage Syro I in 2.5 mL polypropylene reactors. PNAs were synthesized on Chemmatrix Rink Amide resin, pre-loaded with Fmoc-Glycine for CP PNA and Fmoc-Lysine for SP PNA. The latter has a positive amino-acid for enhancing attractive electrostatic forces between SP PNA and negatively-charged DNA, helping SP in strand invasion reaction in the double helix of genomic DNA, during annealing procedure.

PNAs were synthesized in 5 µmol scale, automatically from the 1st to the 15th monomer for CP, from the 1st to the 20th monomer for SP. For automatic synthesis PNA monomers and HBTU were dissolved in dry DMF at concentration respectively of 0.1 M and 0.47 M; DIPEA was dissolved in dry DMF 0.40 M. After swelling in dichloromethane (DCM) it was followed a cyclic procedure: a) deprotection with 20% piperidine in DMF, (2 times, 8 minutes), b) coupling with PNA monomer (5 equivalents), HBTU (5 equivalents), DIPEA (10 equivalents) in dry DMF (2 subsequent coupling reaction, 30 minute as reaction time each), c) capping with acetic anhydride/DIPEA in dry DMF respectively 5:6:95, (2 times, 1 minute).

After the synthesis of the PNA segment, terminal monomers and spacers “O” for CP and biotin for SP were added in polypropylene reactors for solid phase synthesis following Fmoc protocol: a) deprotection with 20% piperidine in DMF, (2 times, 8 minutes), b) coupling with PNA monomer, spacer or biotin (10 equivalents at c = 0.05 M), HBTU (10 equivalents at c = 0.05 M ), DIPEA (20 equivalents, c = 0.1M) in dry DMF (2 min activation followed by 40 minute as reaction time), c) capping with acetic anhydride/DIPEA in dry DMF respectively 5:6:95, (2 times, 1 minute), d) washing with DIPEA 20% in DMF for remove traces of acetic anhydride (2 times, 2 minutes).

Both PNAs were cleaved from resins using a 10% m-cresol solution in TFA; after this treatment PNAs were precipitated in ethyl ether. After removal of the ether, PNAs were dissolved in water and purified in reversed phase HPLC. PNAs identity and purity were checked using UPLC-MS. Finally, PNAs were quantified at UV-Vis spectrometer, at 260 nm of wavelength: CP ε = 201900 $M^{-1}$ $cm^{-1}$, SP ε= 203900 $M^{-1}$ $cm^{-1}$.

CP: H-OO-GAT ACA AAC CCT TAA TCC CA-Gly-$NH_2$
yield 5.3%
Chromatogram, tr= 2.78'.Mass spectrum, multicharged ions: m/z 1137.29 $[M+5H]^{5+}$, 947.89 $[M+6H]^{6+}$, 812.68 $[M+7H]^{7+}$, 711.09 $[M+8H]^{8+}$, 632.32 $[M+9H]^{9+}$, 569.14 $[M+10H]^{10+}$, 517.57 $[M+11H]^{11+}$, 474.43 $[M+12H]^{12+}$. Reconstructed spectrum, m/z calculated 5681.60, found 5682.0 (TM). (Figure A57 Appendix)

SP: Biotin- OO- AAT TTC CAT AAA CCC CAA GT-Lys($NH_3$+)-$NH_2$
yield 5.2%
Chromatogram, tr= 3.05'. Mass spectrum, multicharged ions: m/z z1200 $[M+5H]^{5+}$, 1000 $[M+6H]^{6+}$, 857 $[M+7H]^{7+}$, 750 $[M+8H]^{8+}$, 667 $[M+9H]^{9+}$, 601 $[M+10H]^{10+}$. Same multicharged for the TM-Lys. Reconstructed spectrum, m/z calculated 5994.04, found 5995.0 (TM), 5866.0 (TM-Lys). (Figure A58 Appendix)

The procedure for functionalization of electrodes is briefly reported, these activities were carried out principally by Simone Fortunati, in the research group of Prof. Marco Giannetto.

- Activation of carboxylic acid on CNTs and CP coupling

The carboxylic function of SWCNTs were activated by incubation of 50 µL of 0.2 M EDC and 0.05 M NHS in MES buffer for 1h at room temperature. After removal of the solution by rinsing with water, 50 µL of 500nM CP in carbonated buffer was incubated for 2h at room temperature, after which unreacted species were removed by rinsing with water. In order to prevent non-specific interaction of probes with the electrode substrates, a blocking step was performed by depositing 50 µL of 500 nM pyrene in DMSO. The SPEs surface were then washed with DMSO followed by water.

Bibliography:


1. Giannetto M, Bianchi MV, Mattarozzi M, Careri M. Competitive amperometric immunosensor for determination of p53 protein in urine with carbon nanotubes/gold nanoparticles screen-printed electrodes: A potential rapid and noninvasive screening tool for early diagnosis of urinary tract carcinoma. *Anal Chim Acta*. 2017;991:133-141.
2. Dong W, Yang L, Shen K, et al. GMDD: a database of GMO detection methods. *BMC Bioinformatics*. 2008;9(1):260.
3. Manzanares-Palenzuela CL, de-los-Santos-Álvarez N, Lobo-Castañón MJ, López-Ruiz B. Multiplex electrochemical DNA platform for femtomolar-level quantification of genetically modified soybean. *Biosens Bioelectron*. 2015;68:259-265.
4. Yang W, Ratinac KR, Ringer SP, Thordarson P, Gooding JJ, Braet F. Carbon Nanomaterials in Biosensors: Should You Use Nanotubes or Graphene? *Angew Chemie Int Ed*. 2010;49(12):2114-2138.
5. Umadevi D, Sastry GN. Quantum Mechanical Study of Physisorption of Nucleobases on Carbon Materials: Graphene versus Carbon Nanotubes. *J Phys Chem Lett*. 2011;2(13):1572-1576.
6. Reta N, Saint CP, Michelmore A, Prieto-Simon B, Voelcker NH. Nanostructured Electrochemical Biosensors for Label-Free Detection of Water- and Food-Borne Pathogens. *ACS Appl Mater Interfaces*. 2018;10(7):6055-6072.
7. Grabarek Z, Gergely J. Zero-length crosslinking procedure with the use of active esters. *Anal Biochem*. 1990;185(1):131-135.

# 6- DEVELOPING OF NEW ADVANCED BIOSENSOR SYSTEMS


## Abstract:

New sensing platforms based on both electronic and optical advanced technologies have been developed using a well-established ligand-protein interaction as model system, in order to easily set-up and verify the transduction system. Detection of DNA through PNA-DNA interactions is the ultimate goal of this research, but in these first studies aimed at testing the chemical tools and detection schemes, the biotin-streptavidin interaction was used (Figure 6.1). In this chapter we describe the results obtained by this approach in the tests performed on r-GO-FET (reduced-Graphene Oxide-Field Effect Transistor) during a secondment period at Austrian Institute of Technology, under the supervision of Prof. Wolfgang Knoll. Moreover, the development of a novel type of hollow core photonic crystal fibers for biosensing is described. This last project was carried on with Prof. Annamaria Cucinotta (UniPR, engineer department) and Prof. Luca Vincetti (UniMoRe, engineer department).


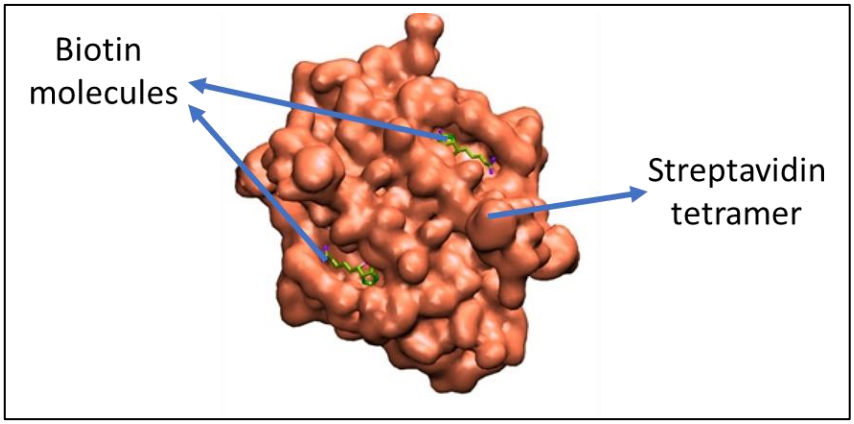


**Figure 6.1: Biotin-streptavidin interaction, derived from XRD data in PDB from D.E. Hyre et al, (2006) Protein Sci.**15: **459-467, graphically modified by ViewerLite 50.**

## 6.0 rGO-FET

As mentioned in chapter 1, field effect transistors (FETs) are electronic devices in which a current passes through a semiconductor from source to drain electrodes and it is tuned by a gate electrode; organic-FETs use π-conjugated molecules as semiconductors. The FETs can be used as sensing devices if a receptor or a probe molecule is placed either on the semiconductor or on the gate surface. The sensing abilities is provided by bio-receptor and even a slight change in terms of current should be detected as a result of the capture of the analyte[1]; this is therefore potentially an intrinsic label-free technique. Two configurations of FET have been mainly developed: EGO-FET (Electrolyte Gated Organic Field Effect Transistor Figure 6.2 A and B) and BGO-FET (Back Gated Organic Field Effect Transistor Figure 6.2 B).

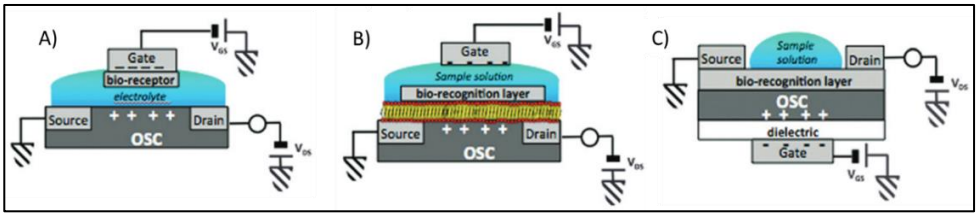


**Figure 6.2: Main types of organic FET. A) Electrolyte Gated Organic Field Effect Transistor; B) Electrolyte Gated Organic Field Effect Transistor with a double membrane of phospholipids for prevent the doping of the semiconductor; C) Back Gated Organic Field Effect Transistor. Adapted with the permission of L. Torsi et al. Chem. Soc. Rev., 2013, Copyright © 2013 Royal Society of Chemistry.**

In the EGO-FET configurations a Debye-Helmoltz double layer is formed (Figure 6.3). A perturbation in this capacitive layer caused by analyte-receptor interaction, produce a signal due to current variation between source and gate electrodes, and this signal is stronger if the solution used has low ionic strength or the analyte is a polyelectrolyte (for example DNA). The sensing molecule can be placed on the semiconductor or on the gate electrode. Figure 6.2 B shows a recent example using a biotinylated phospholipid bilayer for detection of streptavidin[2]. The phospholipid bilayer prevents the doping of the semiconductor with charges and the sensing of streptavidin is increased even in high ionic-strength solution. Alternatively (Figure 6.2 A), the gate electrode, which is usually made of gold, can be modified in order to link a bio-recognition

molecule. In this way, it was possible to e.g. obtain the enantiomeric sensing of carvone[3].

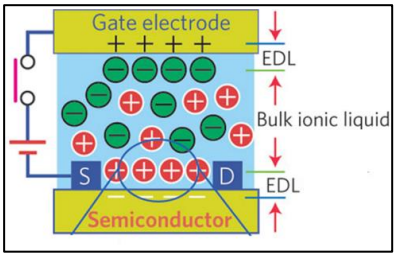


**Figure 6.3: Formation of Debye-Helmoltz double layer. EDL= electric double layer.**

In back-gated FET there is no formation of charge double layers, here the signal is generated as difference in circulating current between source and drain electrodes, and this process is gate mediated. The reliability of these sensors is higher in comparison with EGO-FET, because the signal is not affected by solution properties. An example is DNA detection on a pentacene film as semi-conductive materials[4].

As organic semi-conductor material, graphene could be ideal, because it is a zero-band gap semiconductor and its band gap can be modified by surface modifications. Graphene used in FET devices can be produced by chemical vapor deposition (CVD), or exfoliation of graphite and graphite oxide (GO). The last one is the cheapest method to produce graphene oxide, which can then be reduced chemically or thermally, in order to obtain graphene-like material. In fact the carboxylic, alcoholic and epoxy groups presented by GO, which are absent in CVD graphene that shows a perfect honeycomb structure, create defects that lower the material performances. Reduction of defect should however not be complete, in order to promote a faster heterogeneous electron transport in the electrochemistry of $sp^2$ carbons that occurs mainly at the edges and defects of the graphene sheet[5]. Another important aspect to consider for genosensing applications is that aromatic groups, as well as the nucleobases present in both PNA and DNA, can interact with GO and reduced GO, thus producing unspecific binding[6].

In a joint project in collaboration with Prof. Wolfgang Knoll's bio-sensing group in Vienna, we aimed at developing a liquid gated field effect transistor which uses reduced graphene oxide as semi conductive material. Different kinds of reduction strategy were evaluated and the sensing was performed by modification of the graphene surface as shown in Figure 6.4. Experiments were conducted, under the supervision of Doct. Johannes Bintinger, in flow cells

designed from commercially available chips with interdigitated gold electrodes. Interdigitating electrodes have the aim to increase surface contact area from source to drain electrodes and therefore increase the signal.

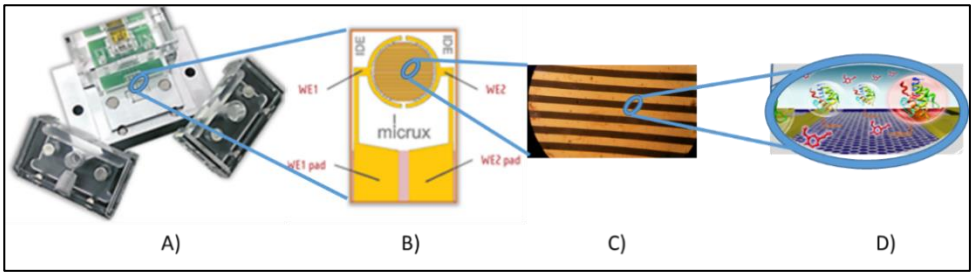


**Figure 6.4: A) flow cell used in experiments, B) commercial chip with interdigitated gold electrodes, C) glass surface between electrodes that were modified with reduced graphene oxide, D) schematic example of bio-sensing.**

## 6.1 RESULTS AND DISCUSSION

In order to develop appropriate FET sensor formats, several steps for the modification of interdigitated electrodes have been tested, in order to create a reliable and robust functionalization, which shows low resistivity, a clear sign of the reduction of graphene oxide. A commercially available micuX chip was used as substrate with standard dimensions: 10 x 6 x 0.75 mm, substrate: glass, electrochemical cell: 3.5 mm Ø, electrode material: gold, number of feet: 120 pairs, thickness 50/150 nm.
The glass surface between interdigitated electrodes was silanized with APTES ((3-Aminopropyl)triethoxysilane) and annealed. After that, Hummers graphene oxide, (i.e. GO obtained by potassium permanaganate treatment of a solution of graphite, sulfuric acid and sodium nitrate) was added at 12.5 µg/mL concentration and reduction was carried out thermally at 200 °C under vacuum for 2 hours and/or chemically by hydrazine. This procedure was carried out by pipetting 1 mL of reducing agent at the edge of a glass Petri dish, with chips inside; the Petri dish was hermetically closed and placed in an oven at 80°C overnight, allowing gaseous hydrazine to perform the reduction. Hydrazine, though more hazardous, showed better performances; other kinds of graphene oxides led to worse results in terms of transistor behavior or final resistance

(which should be below 100 Ω). Other examples of functionalization that do not lead to a transistor behavior are shown in Appendix, Figure A59 and A60.
The obtained surface was characterized with Atomic Force Microscope (AFM) by Prof. Mesquida in order to evaluate the coverage of the surface and the presence of multilayers (Figure 6.5). Results showed that most of the area is covered mainly by a single layer of graphene, as monitored from thickness variation on the surface, therefore the concentration of graphene oxide used was appropriate for the fabrication process.

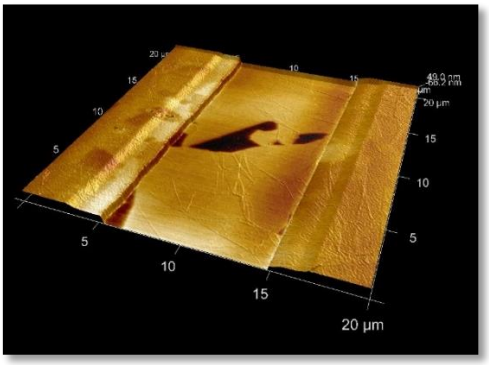


**Figure 6.5: AFM analysis of MicuX chip used for FET fabrication, the area between source and drain electrodes was selected. The black areas show an unmodified glass surface while relief areas are borders of two overlapping graphene flakes. Source and drain electrodes are at the edge of the channel.**

At this stage of functionalization transistor behavior vas evaluated measuring the current between source and drain electrodes at different voltages applied at the gate (Id/Vg curve) and how the current source-drain vary in time at fixed potential (Id/t curve). An example of this test is shown in Figure 6.6.

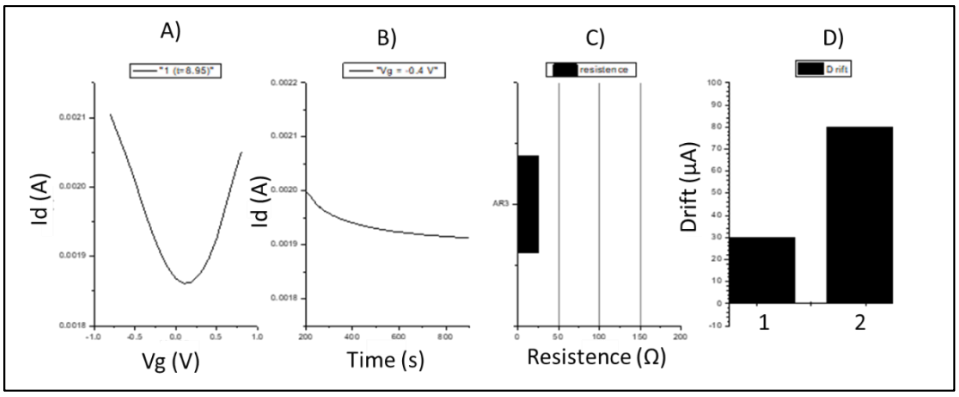


**Figure 6.6: A) Id/Vg curve of reduced graphene oxide modified chip showing a typical graphene transistor behavior, where electrons have the same mobility of electron holes. B) Id/t curve, the drift of the signal is due to the formation of the Debye-Helmotz double layer. C) resistance of the chip. D) drift in terms of current from the measure at 200 s (1) and at 500 and 800 s (2) after the flow start.**

After the addition of graphene, a functionalization with sensing molecules, such as PNA and biotin, has been performed. The main strategy tested exploit a π-π stacking of pyrene acetic acid (or it N-hydroxysuccinimidyl ester) or pyrene methylamine to the graphene surface followed by a coupling with amine PNA and biotin, respectively. Secondary strategies tested involve the direct linking of pyrene modified PNA. A scheme of functionalization steps is presented in Figure 6.7.

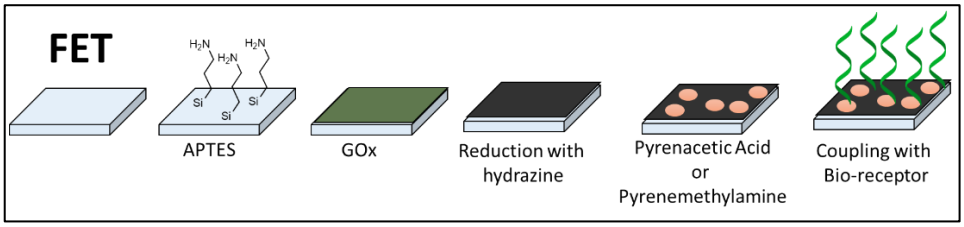


**Figure 6.7: FET fabrication, the Id/Vg curve after PNA or biotin addition change in terms of current and Dirac point voltage.**

After the functionalization with sensing molecules, such as biotin or PNA, G-FETs continues to shows transistor behavior, as shown in Figure 6.8.

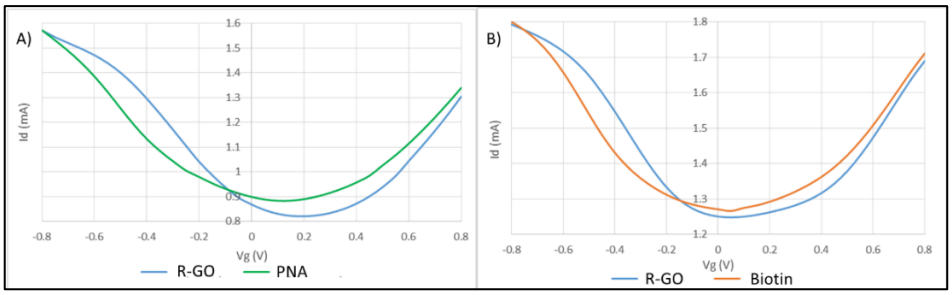


**Figure 6.8: variation of the Id/Vg curve before functionalization (blue curves) after the functionalization with A) pyrenacetic acid, activation with EDC-NHS, coupling with PNA; B) pyrene methylamine, activated biotin.**

Sensing of DNA and streptavidin was attempted firstly in static configuration: an Id/Vg curve was measured before and after the addition of the analyte by drop-casting. The flow cell used was similar to the ones showed in Figure 6.4 A), with a silver wire as gate electrode.

Measurements showed lack of reproducibility of this sensing format. Two summary Figures 6.9 show that, differently from what expected, the signal changes were not proportional to the DNA or streptavidin concentration. In particular, the current at Dirac point and its voltage are higher than values of graphene-modified chips, previously registered. Probably, the eventual specific signal is covered by unspecific effects deriving from the contact of the FET with the measuring electrolyte solution. Moreover, a test for unspecificity was conducted when DNA was added on the graphene surface, without functionalization with bio-receptors.

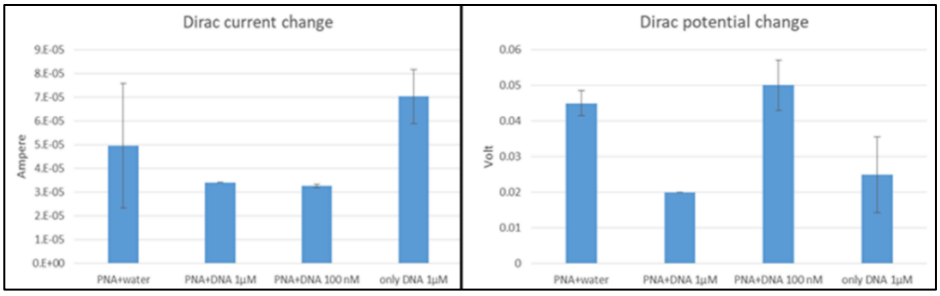


**Figure 6.9: evaluation of difference before and after analyte addition in terms of shift of the Dirac point in static measurement similar to that showed in Figure 6.8. Current changes are measured in the same diagram but on the Y axis, while potential changes are measured on X axis in Id/Vg diagram. Last measurement in both histogram graphs are the unspecific binding-control.**

In order to test the system in a dynamic environment and to understand kinetics aspects, an “in-flow” analysis was performed, but no step in current was observed (except drift) after injection of both DNA on the PNA-modified sensor, or of streptavidin on the biotin modified one, as shown in Figure 6.10. The successful functionalization with bio-receptors of the graphene surface with the method used was however confirmed by XPS analysis, showed later.

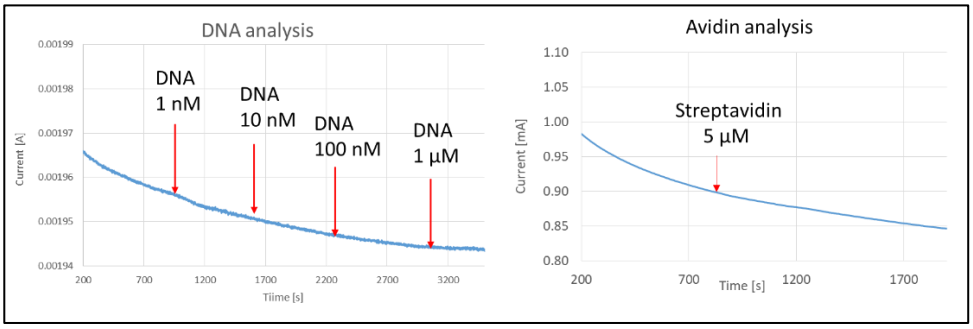


**Figure 6.10: Id/t analysis of modified rGO-FET with bio-receptors PNA (left) and biotin (right). No signals were detected after each injection.**

Therefore, it was not clear if the main problem is derived from surface architecture or G-FET configuration. In order to clarify this aspect, the analyses of ligand-surface processes were performed also on a SPR (Surface Plasmon Resonance) platform. A similar system to that obtained on the G-FET surface was built on a gold surface. SPR chips were fabricated starting from glass slides, opportunely treated and cut at the right dimension for fitting in a shadow mask. A chemical vapour deposition (CVD) of chromium (2 nm) and gold (about 50 nm) was performed. On this approximatively flat gold surface a self-assembled monolayer of cysteamine was formed, in order to provide amine functional groups. Graphene oxide was added by drop casting and reduced overnight with hydrazine. After this treatment, the pyrene-based linker was added and corresponding bio-sensing molecule was coupled (Figure 6.11).

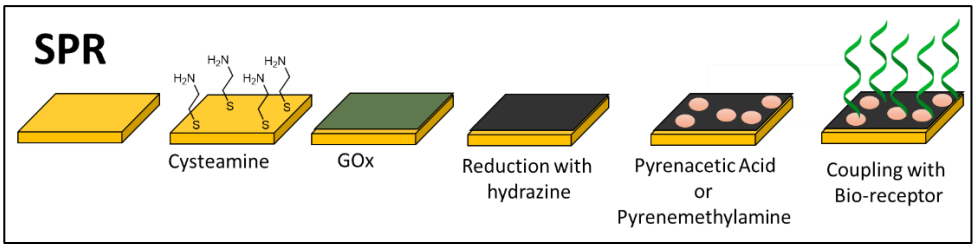


**Figure 6.11: Functionalization of gold surface for SPR sensing.**

Experiments were performed in flow, using a Kretschmann configuration SPR, equipped with laser beam at wavelength of λ = 633 nm. A preliminary scan was performed for choosing the best angle for the measurement (minimum of the reflected light). For each analysis a calibration with a solution of 2% of ethylene glycol was performed. By injection of DNA on PNA-modified chip only minimal signals were detected, comparable to the unspecific signal obtained with non-complementary DNA. Figure 6.12 shows the attachment of PNA probe to active ester moiety of pyreneacetic acid and subsequently DNA sensing with a minimal change of the baseline. A more pronounced signal was obtained when an N-term pyrene-modified PNA was added, as shown in Figure 6.13. After an initial fast increase of the refractive index of the surface due to both π-π stacking of pyrenes and unspecific nucleobase interactions, the washing step with buffer cleaved the PNA molecules with weaker interactions with graphene but the net variation was positive. However, also in this case, the DNA sensing was minimal and not different from unspecific effects.

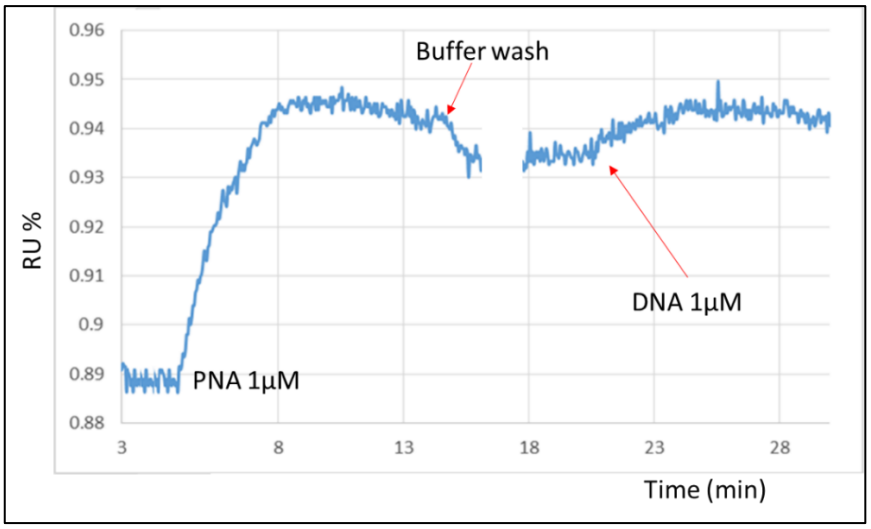


**Figure 6.12: SPR dynamic measurement of PNA functionalization in carbonate buffer at pH 9 and, after the white break, the addition of DNA in PBS buffer at pH 7 that lead to a minimal signal, similar to unspecific binding. The second part of the graph have been re-scaled for a better comparison: the baseline was shifted to compensate change from carbonate buffer at pH 9 (deposition) to PBS buffer at pH 7 (hybridization).**

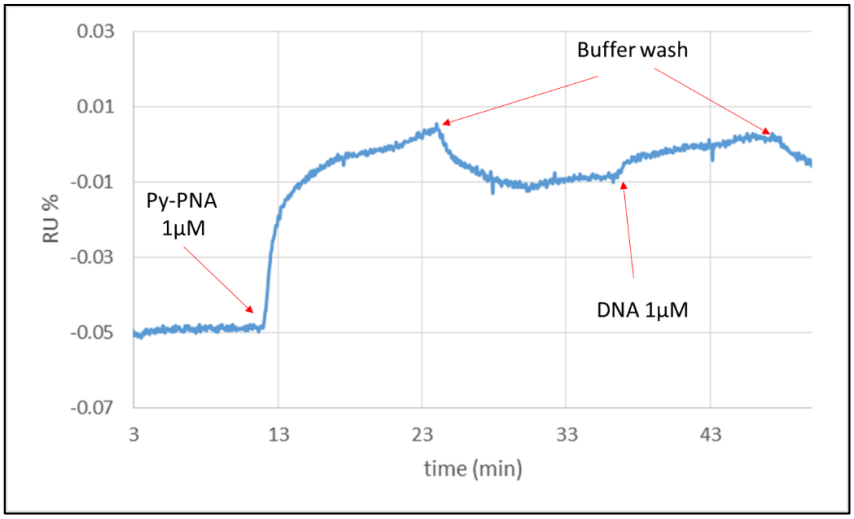


**Figure 6.13: SPR dynamic measurement of Py-PNA deposition. After that DNA sensing lead a minimal signal that after buffer wash tends to disappear. Both pert of the experiments were carried on in PBS buffer at pH 7.**

In the case of streptavidin injection on the biotin-modified PNA, the signal was higher and reliable, while using the same solutions for functionalization and sensing, G-FET showed no response. Figure 6.14 shows the output of the streptavidin binding on SPR.

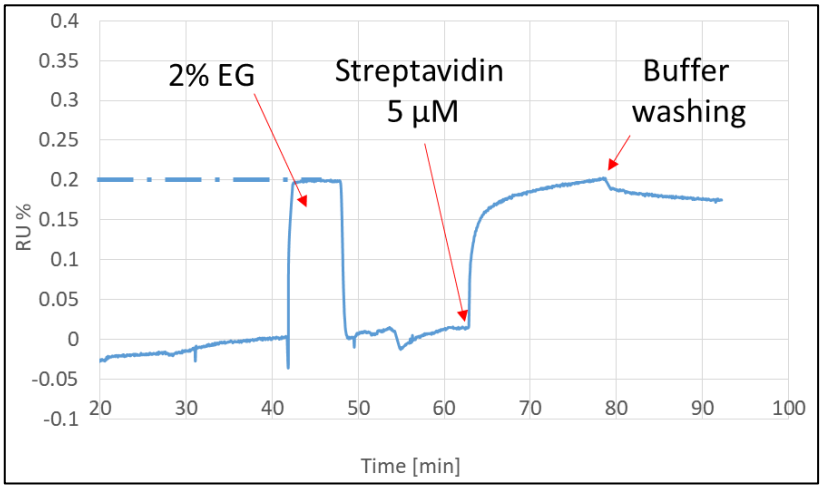


**Figure 6.14: sensogram of Streptavidin biosensing. 2% of ethylene glycol was used for calibrate the Refractive Units percentage at 0.2%.**

A further analysis was performed to find out if the pyrene acetic acid / PNA functionalization was effective or the cause of the lack of signal in DNA detection could be due to incorrect functionalization. X-Ray Photoemission Spectroscopy (XPS) was performed on an SPR chip prepared for DNA sensing by drop-casting: the whole surface was covered by a layer of cysteamine and graphene, while only the central part has been functionalized by pyrenecarboxylic acid and coupled with PNA. A comparison between PNA-functionalized and non-functionalized zones was performed. Results showed that the amount of atoms present in PNA chain was increased, in particular typical signals revealing the presence of the amide bond were detected, as visible in Figure 6.15, while the spectra used for quantification are reported in Figure 6.16, where regions used for quantification are shown in blue.

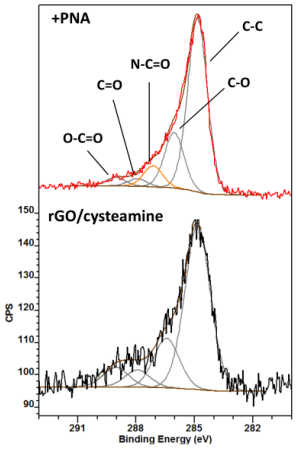


**Figure 6.15: XPS C 1s detail spectra of regions in- and outside of the area where PNA was deposited. All spectra have been normalized to their strongest signals.**

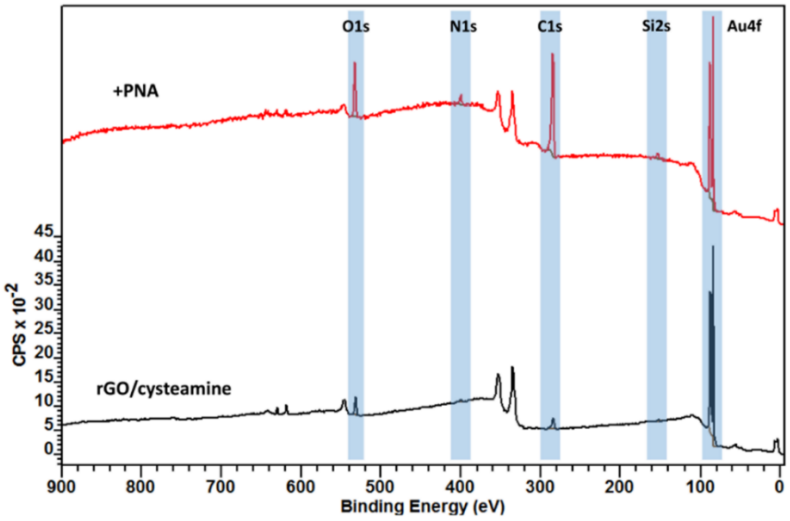


| | Component (at%) | | | | |
|---|---|---|---|---|---|
| Sample | C-C | C-O | O=C-N | C=O | O-C=O |
| PNAlinker_outside | 65.2 | 19.8 | | 7.0 | 8.0 |
| PNAlinker_inside | 65.1 | 20.9 | 7.9 | 2.9 | 3.2 |

**Figure 6.16: XPS analysis of SPR-graphene modified chip inside the PNA functionalization zone and outside this zone, where only cysteamine and graphene are present. All spectra have been normalized to their strongest signals.**

## Conclusion

In conclusion of this first part of validation of sensing, has been demonstrated that the configuration of rGO-FET first tested does not presently allow sensing using either Id/Vg or Id/t curves. One possible explanation is that the electron transfer property of produced reduced graphene oxide are not as good as expected and the signal from bio-sensitive layer is covered by the effects of solution changes on the graphene. If further experiments will confirm this hypothesis, source and drain electrodes have to been fully covered by organic semiconductor material and the sensing molecule should be placed on the gate electrode. Another possible approach is substitution of rGO with chemical vapor deposited graphene or carbon nanotubes, which enhance electron transfer, as seen in chapter 5. The preliminary results of this work confirmed however that is possible to perform deposit a biosensing layer on reduced graphene oxide using non-covalent stacking pyrene-graphene interactions at least in the case of biotin-streptavidin assay with SPR detection. Further work is needed to correctly transduce these interactions on the graphene-FET system.

## 6.2 MICROSTRUCTURED OPTICAL FIBERS FOR SENSING

A recent methodology for sensing was developed in our laboratory for the first time and is based on Photonics Crystal Fibers (PCFs). These are a novel type of optical fiber that exploit properties of photonic crystals and confine light in hollow cores. Such materials are structured with periodic variation of dielectric constant that affect electromagnetic light wave, thus defining allowed and forbidden energy bands. Only certain photons with precise wavelengths can propagate in this medium and are called modes; group of modes forms bands, while closer wavelengths that cannot propagate form band gaps. These band gaps can also be seen as results of multiple destructive interference, because a property of these materials is low-loss-waveguiding and no other mechanism of signal attenuation should occur in a properly built or functionalized PCF. PCFs are characterized by air holes running along the length of the fiber, which can be infiltrated with solutions of biological compounds. If the inner surface is modified with a bio-receptor such as PNA probe, ligand or antibody, the captured biological marker can increase the surface thickness and therefore change bands and band gap distribution. If the variation of thickness is sufficiently high, the fiber can act as a label-free sensor for different types of bioanalytes such as DNA, proteins or even cells. In previous works, micro structured optical fibers with a Bragg grating have been used for genosensing[7]; genomic DNA was detected but gold nanoparticle amplification was necessary. In another work[8], several detection mechanism have been compared; this comparison is showed in Figure 6.17. In the developed optical fiber sensory system, cladding modes (some possible propagating modes, like core modes) are greatly confined inside the silica and thus are strongly affected by possible layers, giving to sensor a very high sensitivity and, therefore, the possibility to detection without amplification of the signal. A preliminary, theoretical work have been done to demonstrate the possibility of sensing DNA exploiting PNA-modified fibers[9]. In this work, inhibited coupling-guiding hollow fibers have been tested directly with streptavidin-biotin system, in order to better appreciate the efficiency of the derivatization procedure and the sensitivity of detection through the capture of a large protein molecule, since the lower changes expected for the DNA oligonucleotides might be not optimal during the system set-up.
Two types of fibers were tested: with 8 and 9 hollow tubes named respectively type A and type B. Their section can be seen in Figure 6.18.

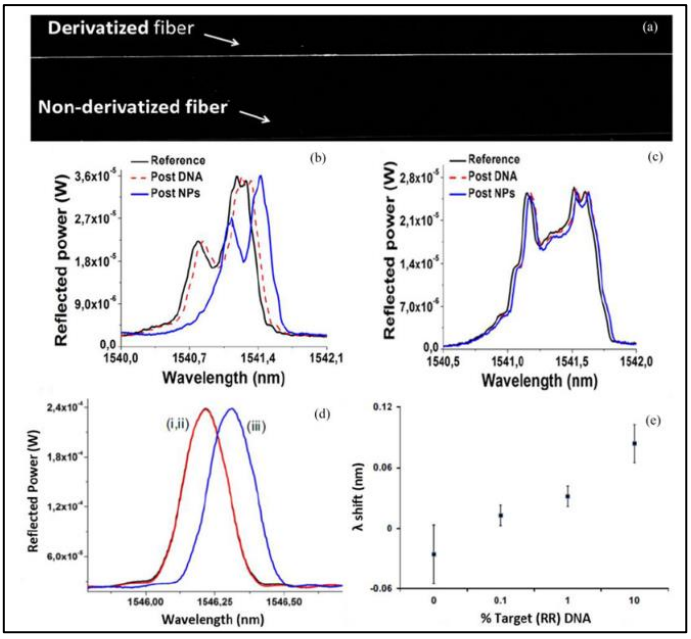


**Figure 6.17: (a) Fluorescence image of PNA-modified and unmodified fibers after infiltration of fluorescent DNA; (b) shift in the high order band induced by infiltration of target sample; (c) shift in the high order band induced by infiltration of non-target sample; (d) wavelength shift in the reflection mode obtained for the LMA10-PNA fibers (i) before(blackline), (ii) after DNA(redline), and (iii) after ON-AuNPs infiltration (blue line),using10%GMO DNA sample; (e) optical shifts obtained using DNA at the same concentration but with different GMO% (vertical bars represent standard deviation). Reprinted with permission from M. Barozzi et al. *Journal of Lightwave Technology,* 2017, Copyright © 2017, OSA.**

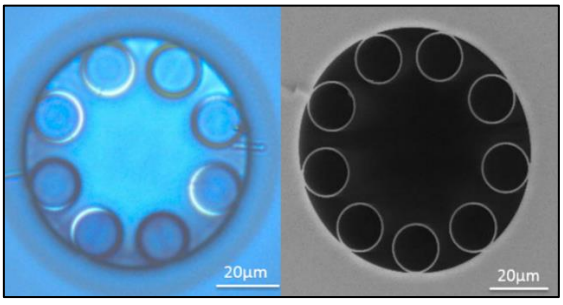


**Figure 6.18: The two types of fiber have an outer diameter of 260 µm, and the claddings are composed of eight (fiber A, left) and nine (fiber B, right) circularly arranged silica tubes, respectively, forming tubular lattice. In fiber A, the inner core diameter is $D_{co}$ = 39 µm, the thickness of the silica tubes is about $t_{si}$ = 610 nm. In fiber B, the inner core diameter is $D_{co}$ = 44 µm, the thickness of the silica tubes is about $t_{si}$ = 725 nm.**

## 6.3 RESULTS AND DISCUSSION

For streptavidin sensing, the inner surface of the optical fibers have to been proper functionalized with biotin, and biotin can be coupled with APTES amino moieties after silanization of glass, that can be promoted by acid treatment.
The experimental set-up is depicted in Figure 6.19. Nitrogen flux apparatus for functionalization and argon flux apparatus for drying are both showed.

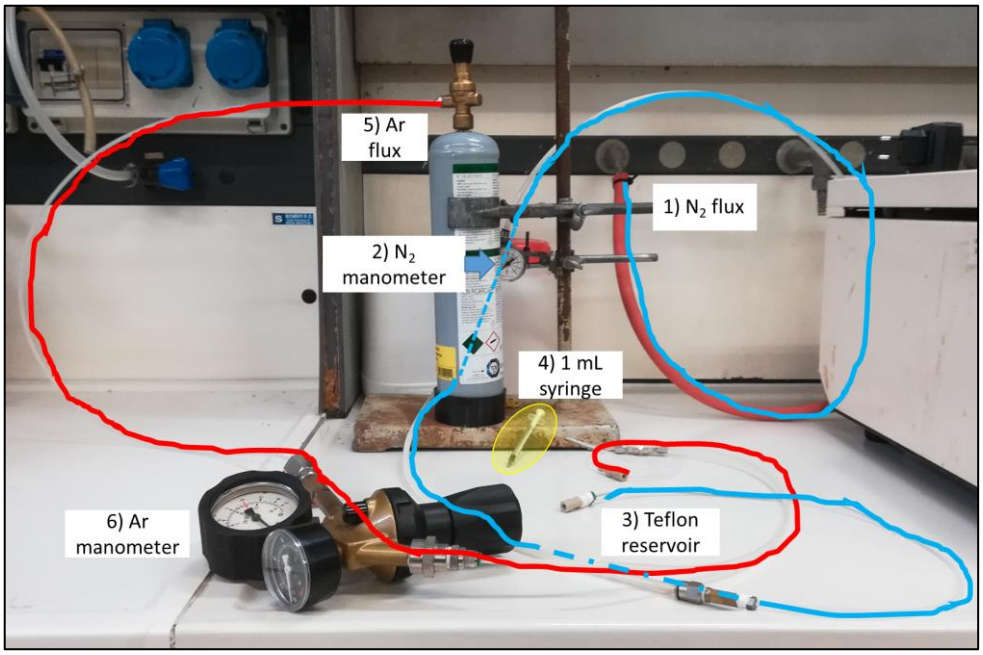


**Figure 6.19: experimental set-up for fibers infiltration 1) nitrogen flux, 2) manometer (2 atm), 3) Teflon reservoir of solvents, 4) syringe; and for fiber drying 5) argon gas cylinder, 6) manometer (4 atm). Red lines indicate the argon-high pressure line, blue lines indicate nitrogen low-pression line alternatively used for infiltration.**

All the reagents and analyte solutions were infiltrated into the fibers using an in-house made liquid handling apparatus, in which a nitrogen flux was connected to a Teflon tube acting as reservoir, and this was coupled with the fiber through an HPLC-type joint with two ferrules. The reservoir was filled with the reagents and then pressure was applied. Pressure as high as 2 atm was necessary to properly infiltrate the fiber without deposition of material. The

fibers were dried under argon flux provided by a gas cylinder; for this purpose 4 atm of pressure have been reached.
Three functionalization step were performed to create the sensing fiber: cleaning of the surface and acid activation with a 1:1 MeOH/HCl solution, APTES functionalization and biotin coupling in aqueous solution, exploiting the EDC-NHS activation strategy. A proper washing of the fiber has to follow all of these steps, for the first two an ethanol wash is enough while for biotin coupling a long aqueous wash is recommended. After streptavidin sensing, a further aqueous wash was required, in order to eliminate all the unspecifically bound proteins. The infiltrating system requires almost one hour for the infiltration of about 500µL of solution, so the coupling time was equal to the infiltration time. The inner volume of 1 meter long fiber is very limited, 8 µL, so every time a large excess of solution was used.
The critical steps of this procedure have been shown to be APTES functionalization and biotin coupling. For the first one we have used a 1:20 dilution in absolute ethanol (therefore 5% v/v solution) and we observed that a multi-layer is formed. Probably this is due to retaining of aqueous solution in the fiber derived from previous treatment (HCl 37% 1:1 MeOH and wash with 96% EtOH). The inner surface of the fiber was therefore less homogenous, leading a possible loss in sensibility. A second, well known, side effect is the formation of a silane cap at the end of the fiber that has to be cut off, losing few centimeters. Biotin coupling was conducted in carbonate buffer, at pH 9. In order to have a very fast activation, we shook the eppendorf in which all reactant were dissolved for 5 minutes only, since the active ester is prone to water hydrolysis. Immediately after the brief activation, the coupling solution was injected. Coupling in DMF was avoided due to the difficulty to completely eliminate this high-boiling solvent from the fiber. Another problem incurred during the coupling reaction was the obstruction of the fiber, which was avoided by a preliminary filtering of the solutions and long water washing to remove not only unwanted reactants, but also possible salts precipitated from the buffer. Following these precautions allowed to avoid obstruction of the fiber.
In the sensing experiment 0.1 mg/mL streptavidin solution in PBS (for miming physiological conditions) have been used, with two hours of infiltration for a total amount of 500 µL. Fibers were then washed with water to eliminate the excess of streptavidin and let dry by flushing nitrogen or argon for at least 2 hours. Measurements were performed by Dr. Fabio Giovanardi, using the instrumentation available in Prof. Annamaria Cucinotta's laboratory in the Department of Engineering and Architecture, University of Parma. A scheme of

the optical set-up is shown in Fig. 6.20. As source, a supercontinuum white light source was used. The output beam emitted by the source was coupled into a 25 cm long piece of fiber through a system of lenses. The fiber output beam was sent to an infrared camera to record the near field profile for monitoring the right fiber excitation or to an optical spectrum analyzer, with a resolution bandwidth of 1 nm in order to measure the output transmission spectrum.

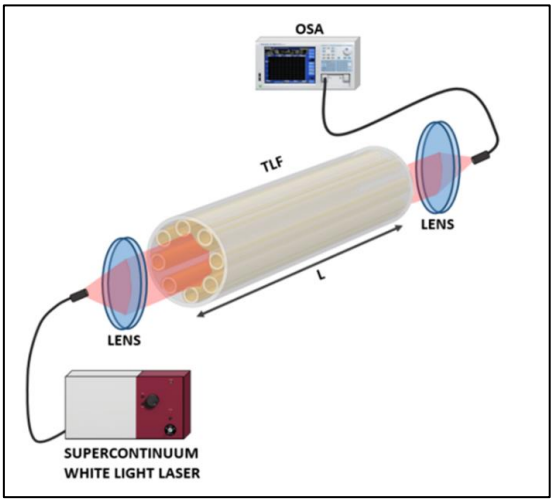


**Figure 6.20: Reading set-up: after a supercontinuum white light laser, a lens system is used to focus the beam inside a short fragment of the Tube Lattice Fiber (TLF), at the end another lens system focus the beam to Optical Spectrum Analyzer (OSA).**

The shape of streptavidin is well known by crystallographic data[10], with a size estimated around 6 nm (Figure 6.21); thus, the expected increase in the organic layer is in this order of magnitude. The equation used for the calculation of the bio-layer thickness ($t_{ly}$) take in account several parameters such as the Δλ measured (caused by the change in the allowed modes frequency), the wavelength of the measure and refractive indexes of the fiber and the organic layer. These two last parameters can be seen as rather identical in the wavelength interval considered[11,12] and therefore been approximated. The final equation is Eq. 1:

$$t_{ly} = \frac{\Delta\lambda t_{si}}{2\lambda}$$

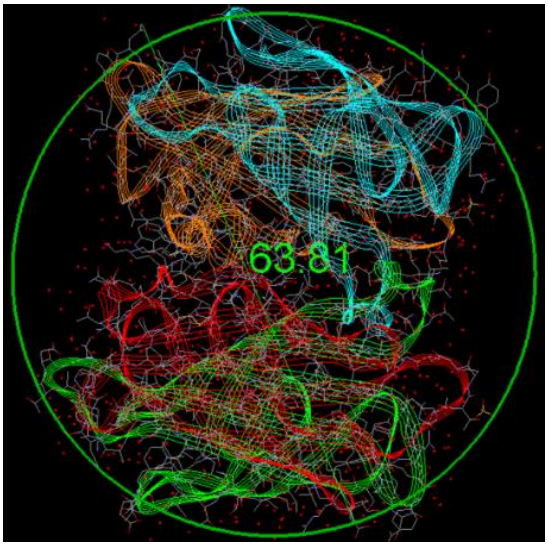


**Figure 6.21: Image of XRD structure of streptavidin obtained by T. Kawato and coworkers, modified by ViewerLite 50. The streptavidin appear as tetramer (each subunit is differently colored) and the whole protein can be circumscribed by a 6.4 nm circle, which is the approximate thickness of the protein.**

Figure 6.22 and Figure 6.23 compare the transmission spectra normalized to the source spectrum respectively for fiber A and B of the functionalization with biotin (blue) and streptavidin (red). In Figure 6.3.4, the redshift of the low wavelength edge of the transmission spectrum is about 24 nm, while in the high wavelength it seems that the shift is not present or, in any case, not relevant. According with Eq. 1, the lower wavelength shift observed correspond to layer thicknesses of 6.9 nm, similar to what expected for the dimensions of streptavidin inferred from X-Ray data. For fiber B (Figure 6.3.5), three different stumps were considered. The shifts are present both in the lower and higher edges and are about 13 nm and 16 nm respectively. Therefore, on the lower wavelength front the corresponding layer thicknesses is 7.3 nm while for the higher wavelength front the thickness result of 7.8 nm.

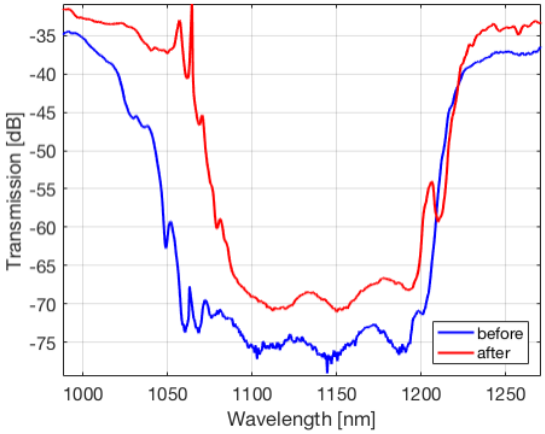


**Figure 6.22: Experimental transmission spectra of a piece of fiber A, 25cm long, before (blue) and after (red) infiltration with streptavidin solution.**

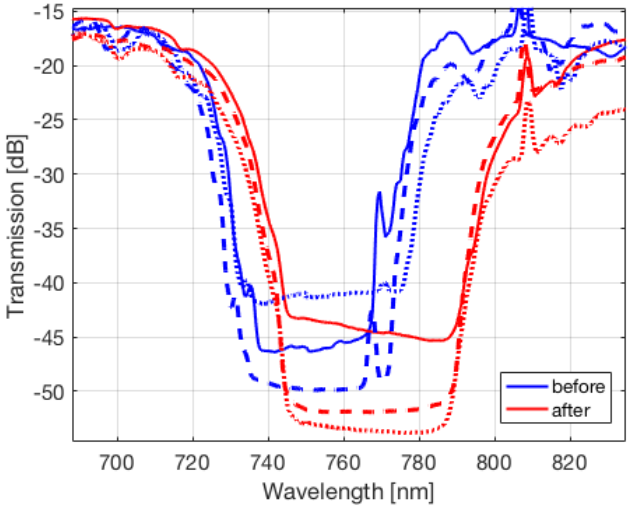


**Figure 6.23: Experimental transmission spectra of a piece of fiber B, 25cm long, before (blue) and after (red) streptavidin solution infiltration. Different line styles correspond to different fiber pieces.**

**Conclusion**

According to these results, these hollow core fibers can be used as sensing platform. Presently, fiber A results are less clear since the shift is only seen on one side of the forbidden mode band, while for fiber B the entire band was clearly shifted. Nevertheless, a variation in the mean band position was observed in both cases consistent with the deposition of a protein layer on the inner surfaces. Further studies should be performed in order to determine if this novel sensory platform can be used for biosensing in a quantitative way, and in particular, for genosensing exploiting PNA as capture probes. These results have been reported in a paper accepted for publication in Journal of Lightwave technology.

## 6.4 EXPERIMENTAL PROCEDURE G-FET

Resistance of the fabricated devices was measured for a check of graphene-oxide reduction quality using a Fluke Multimeter "87 V True RMS Multimeter". Electrical measurements were performed by means of a probe station (Keithley 4200). A silver-silver chloride reference electrode was used to operate the FET device in liquid gate configuration.
SPR instrument was home-made and exploit the attenuated total reflection (ATR) method in Kretschmann configuration, with a laser beam at wavelength of λ = 633 nm with its intensity modulated by a chopper was coupled to a 90° prism made of LASFN9 glass.
All solvents and reagents were purchased from Sigma Aldrich, AFM and XPS analysis were performed in TU Wien, PNAs used have been characterized in Chapter 4, in particular PNA complementary to gene K-RAS WT and G12D were used. Microelectrodes with interdigitated gold array were purchased from MicruX. Hummer's graphene oxide was synthesized by University of Bayreuth.

- FET-chip fabrication:

Microelectrodes were cleaned by submerging in a glass beaker with absolute EtOH, sonicated for 2 min, rinsed again with absolute EtOH, blow dried with compressed air and put into plastic Petri dishes. For attachment of graphene oxide, the surface of the microelectrodes was functionalized with a 2 % APTES solution prepared in absolute EtOH (15 mL EtOH, 0.3 mL APTES). APTES had to be handled under argon to avoid exposure to oxygen. The solution was poured over the chips in the plastic Petri dish and incubated in ambient conditions for 1 hour to allow the formation of a self-assembled monolayer. Subsequently, the electrodes were rinsed with absolute EtOH to remove excess of APTES and carefully blow dried with compressed air. The chips had been put into a glass Petri dish and annealed in an oven at 120 °C for 1.5 hours.
Hummer's graphene oxide was present as 1 mg/mL suspended powder in deionized water. This suspension was diluted 1:80 in distilled water inside a 1.5 mL eppendorf, and an eventual centrifugation at 3000 rpm for 5 minutes could be performed for separate agglomerates. This suspension was applied to the array area of chips by drop-casting of 25 µL, after one hour in which intermolecular bonds were formed, the excess of graphene was rinsed off with gently water rinsing and carefully air-dried.

Chemical reduction was performed by placing chips in the middle of a glass Petri dish and pipetting 1 mL of hydrazine at the edge of the dish. Hydrazine had to be carefully handled. The dish was closed by wrapping scotch tape and put in an under-hood oven at 80°C overnight. After reduction, chips were rinsed with distilled water and gently blow dried. If a thermal reduction is desired, chips could be placed in glass Petri dish in a pre-heated oven at 200°C for 2 hours. Finally, chips were stored under vacuum, in desiccators.

- Functionalization of chips:

A 2.5 µM solution in THF of pyrenacetic acid, pyrenemethylamine or PBSE (1-pyrenebutanoic acid succinimidyl ester) was formed in a glass vial and 15 µL of this solution was drop-casted onto the sensor surface and let dry under fume hood. After the evaporation, another 15 µL aliquot was added and let dry. Chips were gently rinsed with THF and let dry. In case of PBSE functionalization the amino terminal PNA could be directly added and let react for 2 hours in a basic buffer such as carbonate buffer (see chapter 5). If pyrenacetic acid was deposited, an activation of the carboxylic acid was performed with 0.1 M EDC and 0.2 M NHS solution in water or ethanol for one hour and then coupling with amino PNA or amino biotin in basic buffer for 2 hours was performed. Pyrenemethylamine was used for biotin, in this case the activation with 0.1 M EDC and 0.2 M NHS in water was performed with biotin for 15 minutes under stirring, and then, the active ester of biotin was opportunely diluted in basic buffer for the coupling reaction of 2h. These described methods have been the most used but several tests were performed varying times, solvents or equivalents of reactant in order to find the best combination.

- FET measurements:

Measurements were performed using a self-built software named Lua Script, developed at AIT. The chip was placed in the flow cell and this was carefully closed. Tubes were connected to a solvent reservoir and the flux was adjusted with peristaltic pump. For Id/Vg (static) measurement parameters have been usually set as follows: V gate start -0.8 V, V gate end +0.8 V, V gate step 0.01 V, I drain max 0.01 A. In Id/t measurement the V gate have been varied several times but the most used was -0.4 V, with an I drain max of 0.01 A.

- SPR chip fabrication:

Glass slides were cut about 2 cm long and sonicated in 1% Hellmanex™ solution in water for 15 minutes. The slides were then washed with water and EtOH and carefully blow-dried avoiding dust contamination, and put in a gold evaporator machine, under an appropriate shadow mask. Vacuum was inducted in the metal evaporation chamber containing a chromium bar to which a voltage was applied to make it melt and evaporate. A quartz crystal microbalance was used for monitoring the thickness of the metal layer deposited (about 2 nm). Then, the potential was applied to a gold bar and a deposition of about 50 nm of gold was performed. Chips were stored under argon until use. For derivatization, chips were immersed in 0.2M thiol solution in order to form a self assembled monolayer. Cysteamine, mercaptopropionic acid and mercaptoundecanoic acid /mercaptoundecanol were tested as SAM forming molecules. The obtained chip was optically tested at SPR in order to determine the quality of the gold: thickness, roughness and purity (sharp SPR signals are preferable for best sensing). For SAM bearing a carboxylic acid terminal, an activation with EDC 0.1 M and NHS 0.2 M, in water, 1h, was performed before the addition of PNA in basic buffer. After that, eventually unreacted active ester were capped by ethanolamine in basic buffer. Cysteamine SAM was used for coupling with active ester of biotin (15 minutes of activation in water, then dilution in basic buffer and coupling 2h) or as platform for graphene oxide functionalization. This last functionalization was performed as for FET, exploiting the fact that some bonds can be formed between amines of cysteamine and lower face of graphene oxide, similarly to what happens with APTES in FET functionalization.
SPR static measurement was performed by varying angle of incident light. For dry chips the variation was from 20 to 65 degree, while for wet chips the total reflective angle shift and the angle was varied from 45 to 65 degrees. In the latter case, the angle of maximum slope before the plasmon was chosen for kinetic measurement as showed in Figure 6.24. For measurement in flow, the apparatus was connected with a solvent tank and flow was controlled by a peristaltic pump. A silicon, homemade flow chamber was placed on the chip surface.

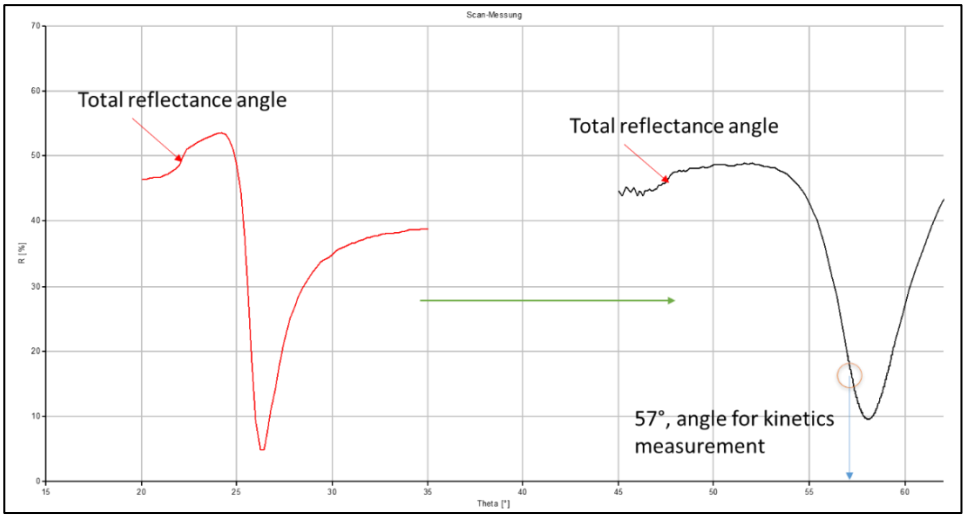


**Figure 6.24: Static SPR measurement on dry chip (red) and wet chip (black). The same surface is shown in both configuration: not only the plamon angle changes, but also the shape of the peak.**

## 6.5 EXPERIMENTAL PROCEDURE OPTICAL FIBERS

Chemical reactants and solvents have been purchased from Sigma Aldrich; MilliQ water was employed in washing steps and in buffer preparation. A handmade infiltration setup was employed for fibers functionalization, while for reading supercontinuum white light source SuperK COMPACT was employed.
The layer on the fiber surfaces has been obtained by infiltrating liquid solutions of reagents induced by a nitrogen overpressure (2 atm).
After an initial cleaning and activation with HCl/Methanol 1:1, followed by an ethanol washing, a solution of (3-aminopropyl) triethoxysilane (APTES, 5% in absolute ethanol) was infiltrated to obtain amino groups on the fiber inner surface. After that another ethanol rinsing was performed. Biotin, 5 mM, was then activated using *N*-(3-Dimethylaminopropyl)-*N'*-ethylcarbodiimide hydrochloride (EDC) and *N*-Hydroxysuccinimide (NHS) 0.25 M both, in a buffered aqueous solution (carbonate buffer, 100 mM, pH 9) and passed through the fiber for 2 hours. The hollow core fiber was then washed with distilled water; the resulting functional fiber was then used for the sensing experiments. In these, a solution of streptavidin in PBS buffer was used, which was passed through the fiber for 2 hours. The fiber was then washed with distilled water and dried using nitrogen. All the above mentioned liquids were filtered on a polytetrafluoroethylene (PTFE) filter, with pore size of 0.45µm, to avoid clogging of the fiber channels. Finally, a 0.1 mg/mL solution of streptavidin in phosphate buffered saline (PBS) was employed for bio-sensing. Excess of streptavidin was washed away with distilled water and fibers were carefully dried with nitrogen flux.
Fabio Giovanardi performed measurement of fibers and elaborated the data.

Bibliography:


1. Torsi L, Magliulo M, Manoli K, Palazzo G. Organic field-effect transistor sensors: a tutorial review. *Chem Soc Rev*. 2013;42(22):8612.
2. Magliulo M, Mallardi A, Mulla MY, et al. Electrolyte-Gated Organic Field-Effect Transistor Sensors Based on Supported Biotinylated Phospholipid Bilayer. *Adv Mater*. 2013;25(14):2090-2094.
3. Mulla MY, Tuccori E, Magliulo M, et al. Capacitance-modulated transistor detects odorant binding protein chiral interactions. *Nat Commun*. 2015;6(1):6010.
4. Stoliar P, Bystrenova E, Quiroga SD, et al. DNA adsorption measured with ultra-thin film organic field effect transistors. *Biosens Bioelectron*. 2009;24(9):2935-2938.
5. Pumera M. Graphene in biosensing. *Mater Today*. 2011;14(7-8):308-315.
6. Vovusha H, Sanyal S, Sanyal B. Interaction of Nucleobases and Aromatic Amino Acids with Graphene Oxide and Graphene Flakes. *J Phys Chem Lett*. 2013;4(21):3710-3718.
7. Bertucci A, Manicardi A, Candiani A, et al. Detection of unamplified genomic DNA by a PNA-based microstructured optical fiber (MOF) Bragg-grating optofluidic system. *Biosens Bioelectron*. 2015;63:248-254.
8. Candiani A, Manicardi A, Cucinotta A, et al. Optical Fiber Sensors for Label-Free DNA Detection. *J Light Technol Vol 35, Issue 16, pp 3461-3472*. 2017;35(16):3461-3472.
9. Giovanardi F, Cucinotta A, Vincetti L. Inhibited coupling guiding hollow fibers for label-free DNA detection. *Opt Express*. 2017;25(21):26215.
10. Kawato T, Mizohata E, Meshizuka T, et al. Crystal structure of streptavidin mutant with low immunogenicity. *J Biosci Bioeng*. 2015;119(6):642-647.
11. Vörös J. The density and refractive index of adsorbing protein layers. *Biophys J*. 2004;87(1):553-561.
12. Oudshoorn RGC, Kooyman RPH, Greve J. Refractive index and layer thickness of an adsorbing protein as reporters of monolayer formation. *Thin Solid Films*. 1996;284-285:836-840.

# 7- APPENDIX

## 7.1 APPENDIX CHAPTER 3

**NMR spectra:**

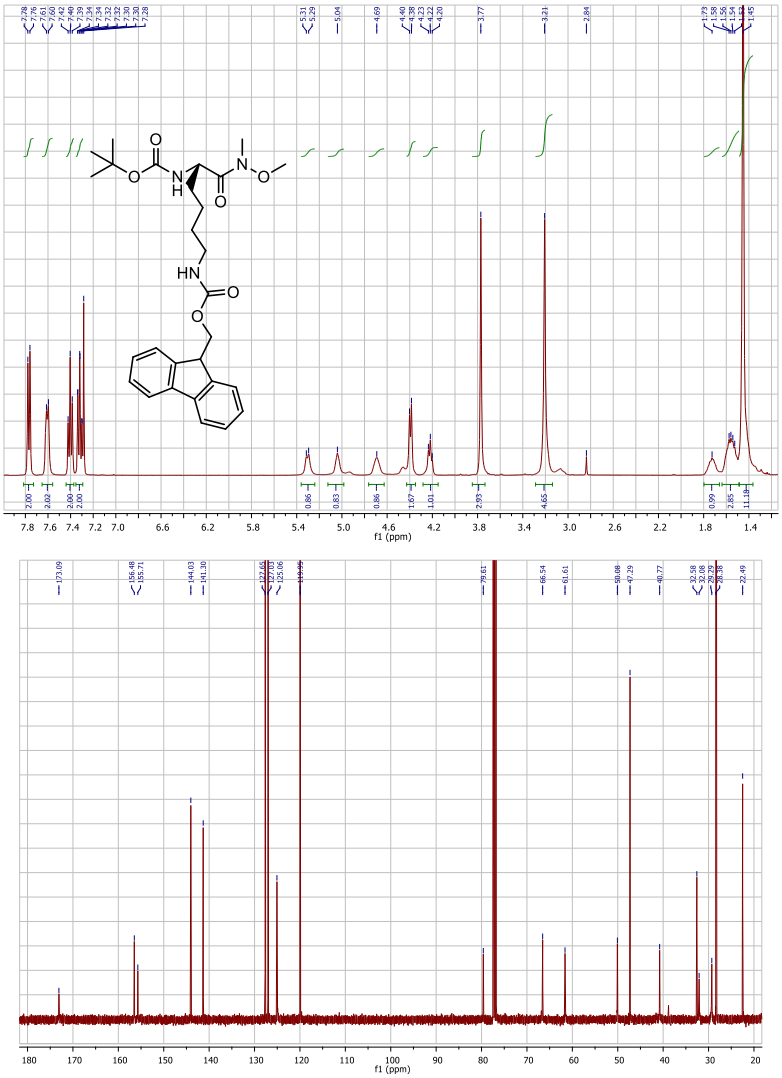


**Figure A1: 1H-NMR and 13C-NMR of compound s1.**

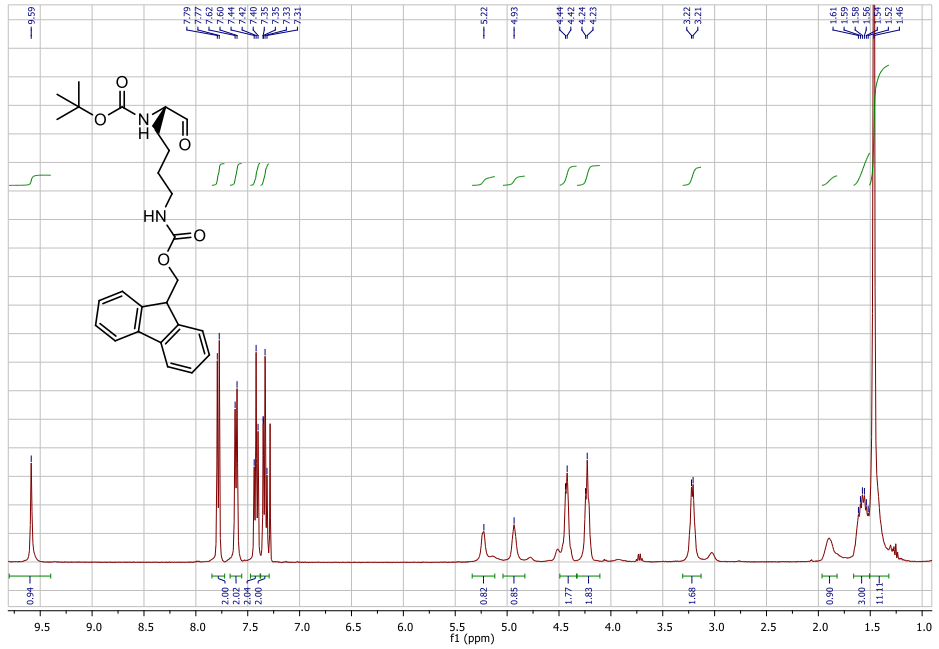
9.59
7.79
7.77
7.62
7.60
7.44
7.42
7.40
7.35
7.33
7.31
5.22
4.93
4.44
4.42
4.34
4.23
3.22
3.21
1.61
1.59
1.58
1.56
1.52
1.46
0.94
2.00
2.02
2.04
2.00
0.82
0.85
1.77
1.83
1.68
0.90
3.00
11.11
f1 (ppm)

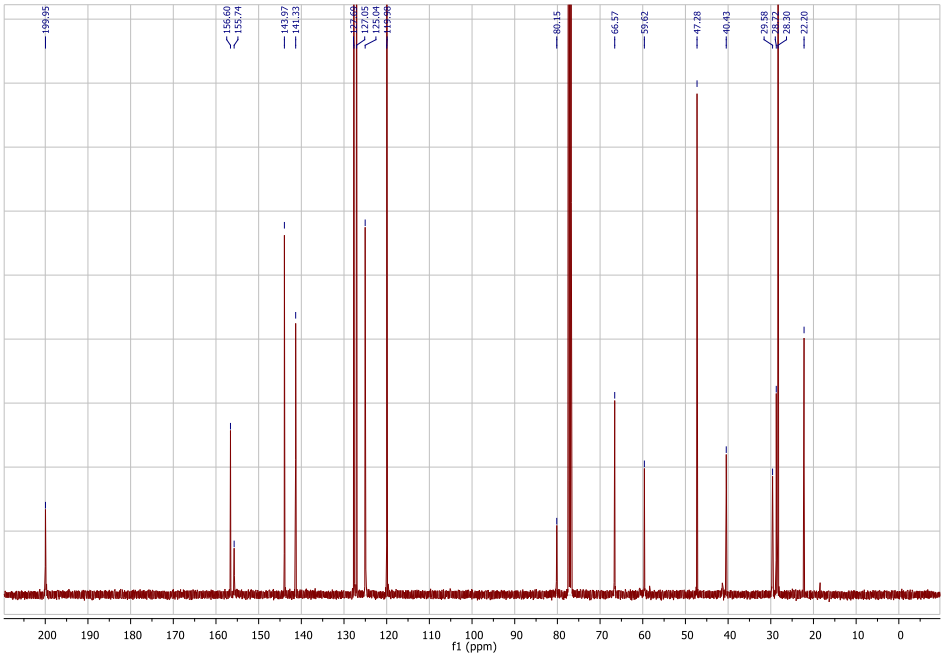
199.95
156.60
155.74
143.97
141.33
127.68
127.05
125.04
119.98
80.15
66.57
59.62
47.28
40.43
29.58
28.72
28.30
22.20
f1 (ppm)

**Figure A2: 1H-NMR and 13C-NMR of compound s2.**

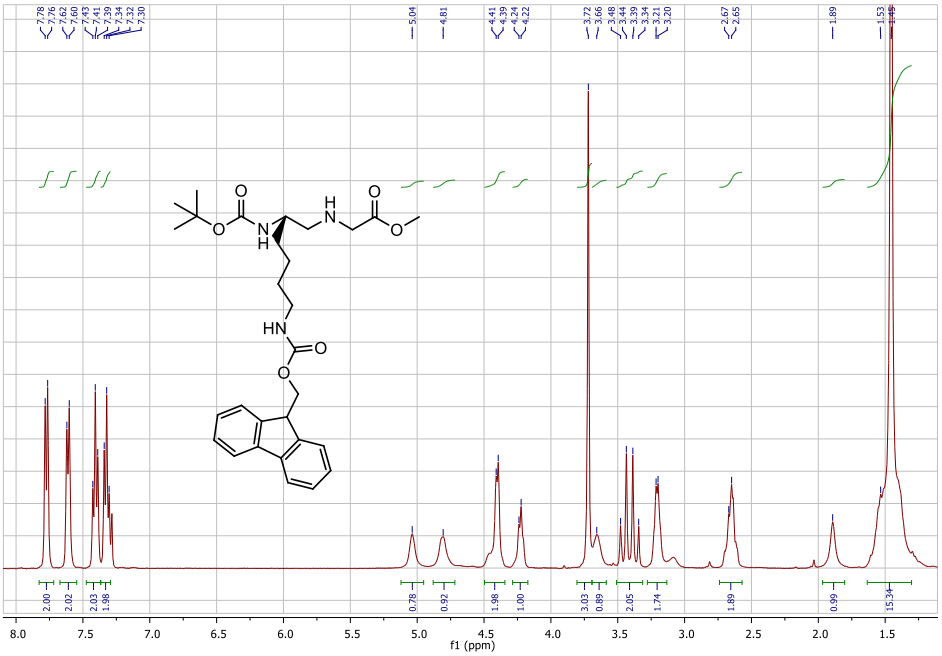


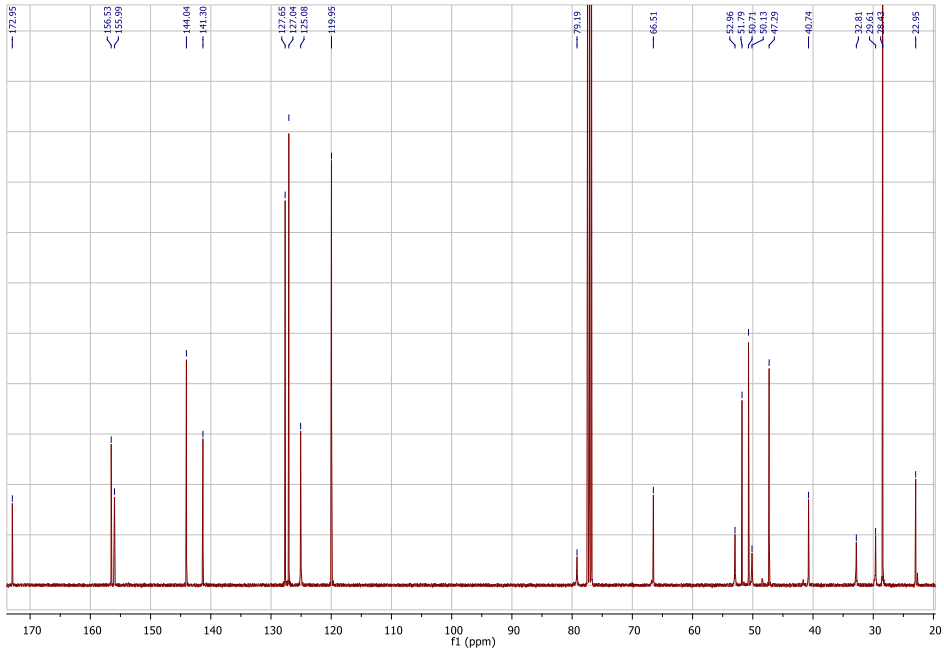


**Figure A3: 1H-NMR and 13C-NMR of compound s3.**

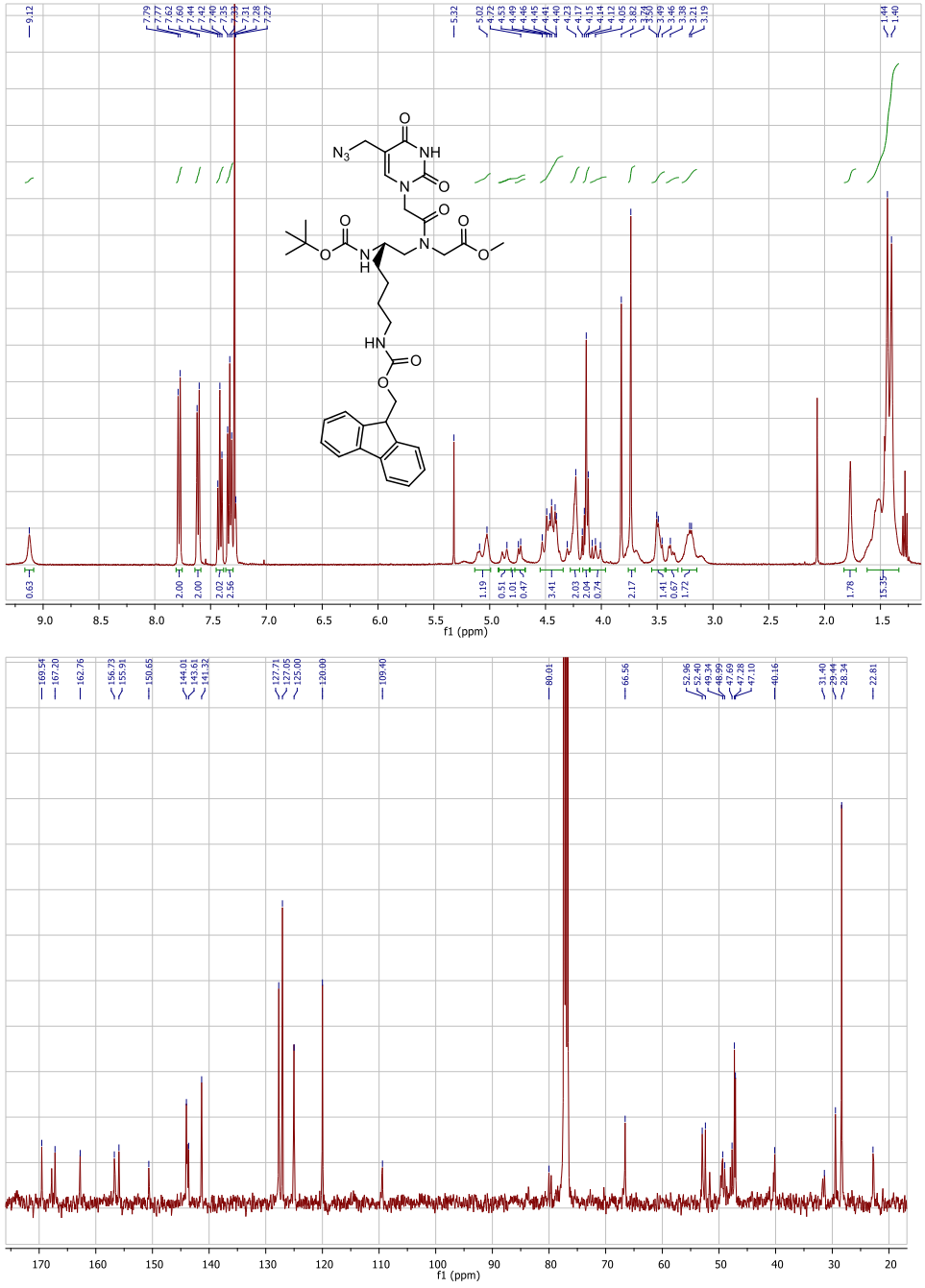


**Figure A4: 1H-NMR and 13C-NMR of compound s4.**

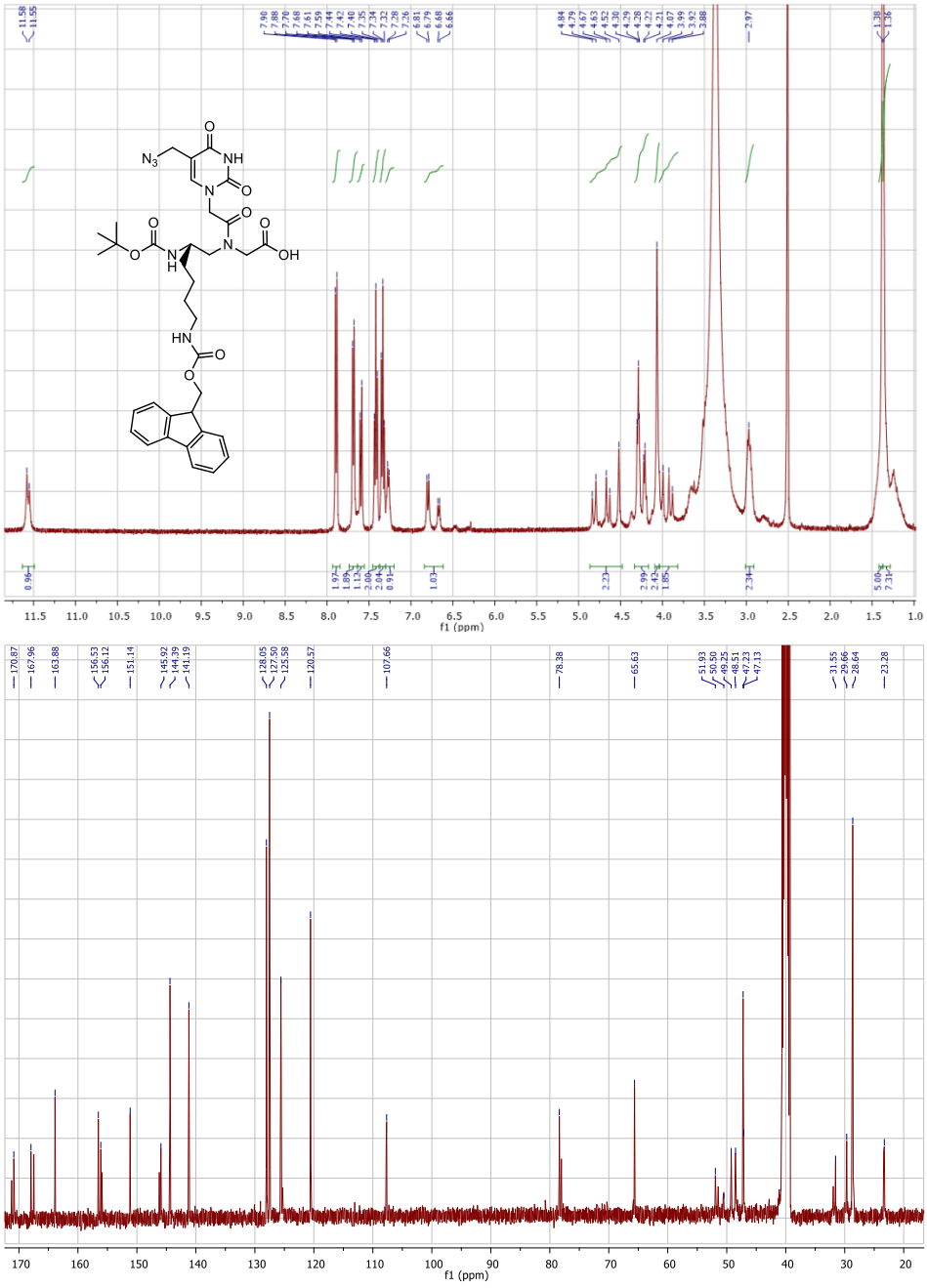

**Figure A5: 1H-NMR and 13C-NMR of compound 1: the modified-monomer.**

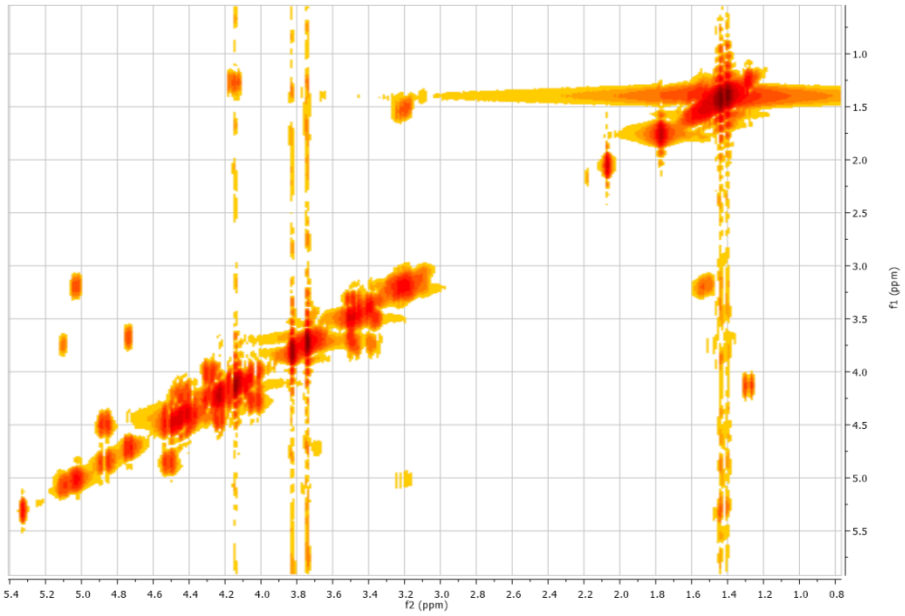


**Figure A6: GCOSY of compound 1 for the identification of proton signals under water peak.**

## PNA characterization

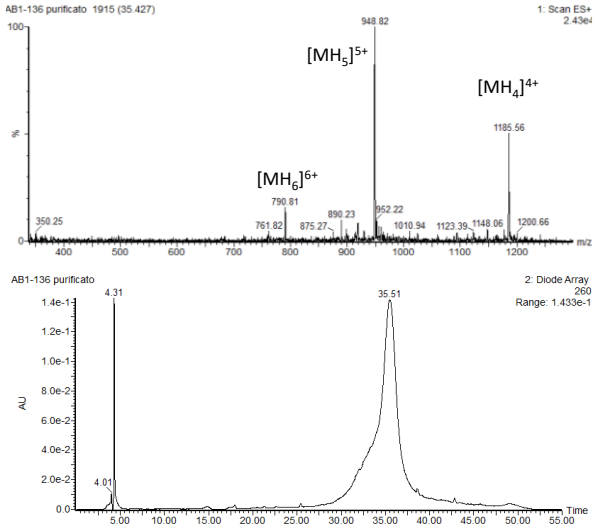

**Figure A7:** HPLC-DAD-MS **chromatogram** of **purified PNA 5**. HPLC-UV at 260 nm trace (bottom), MS spectrum of the corresponding peak at 35.5 min (top).

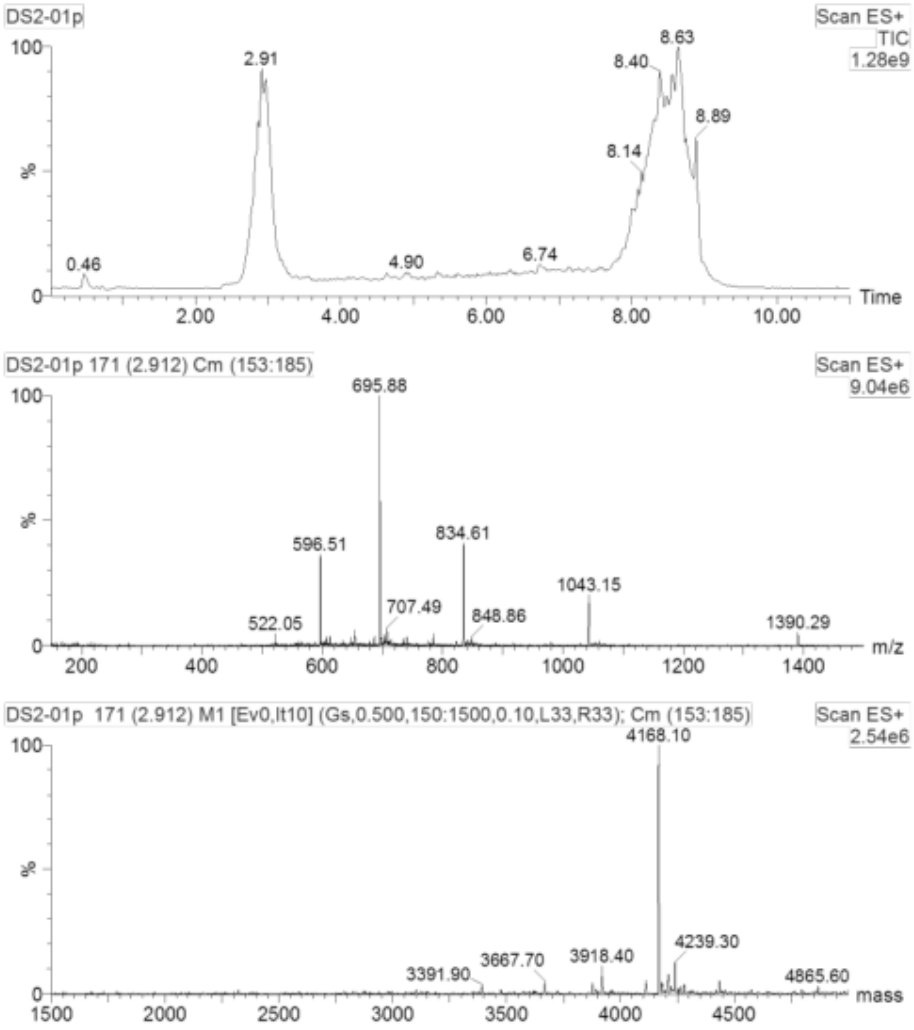


**Figure A8: UPLC-MS of PNA 6. UPLC-MS trace (top), MS spectrum of the corresponding peak at 2.91 min (center) and mathematical deconvolution of the multicharged signals (bottom).**

## 7.2 APPENDIX CHAPTER 4

**Lysine derivative backbone:**

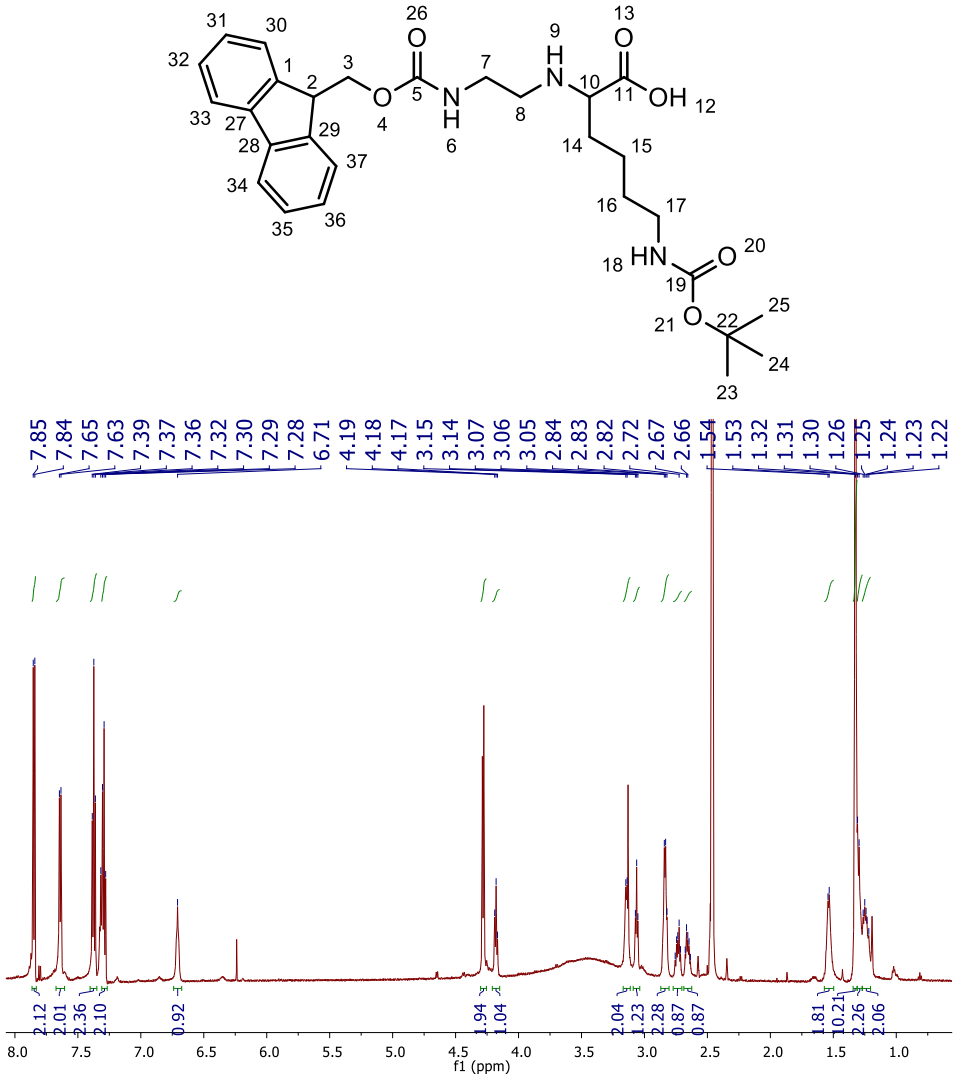


**Figure A9: 1H-NMR spectrum of compound (1)**

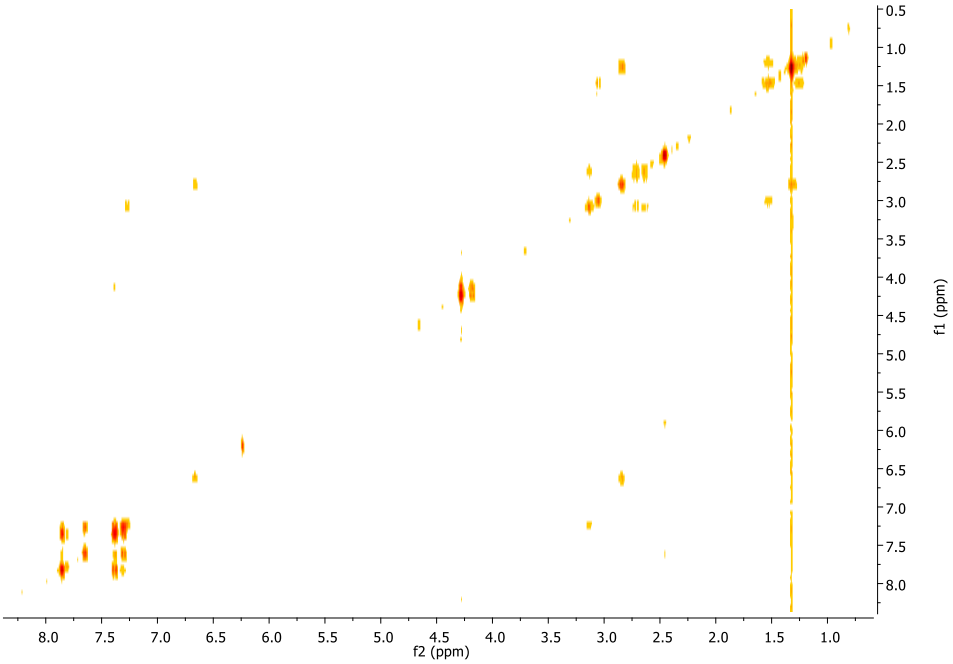


**Figure A10: COSY spectrum of compound (1)**

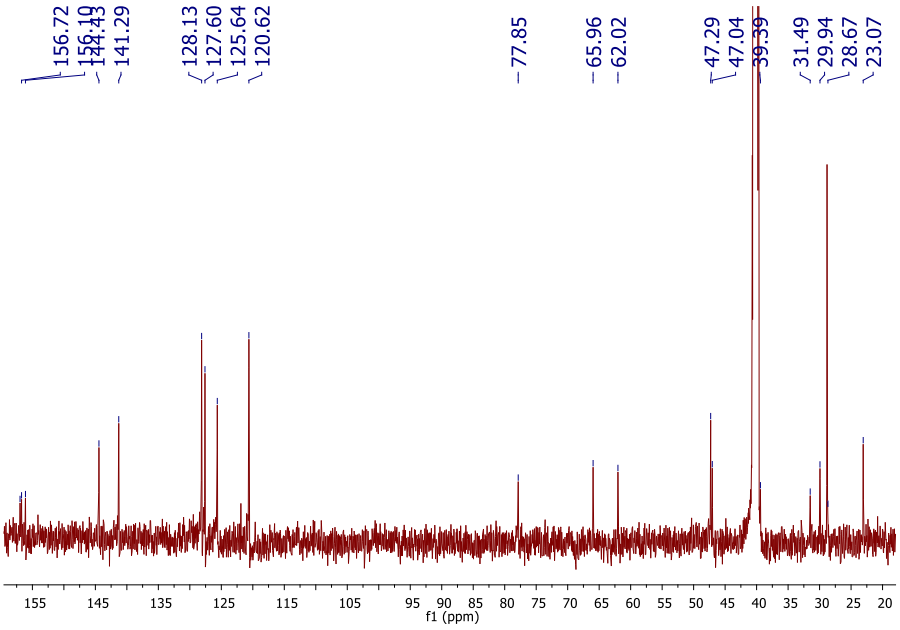

**Figure A11: 13C-NMR spectrum of compound (1)**

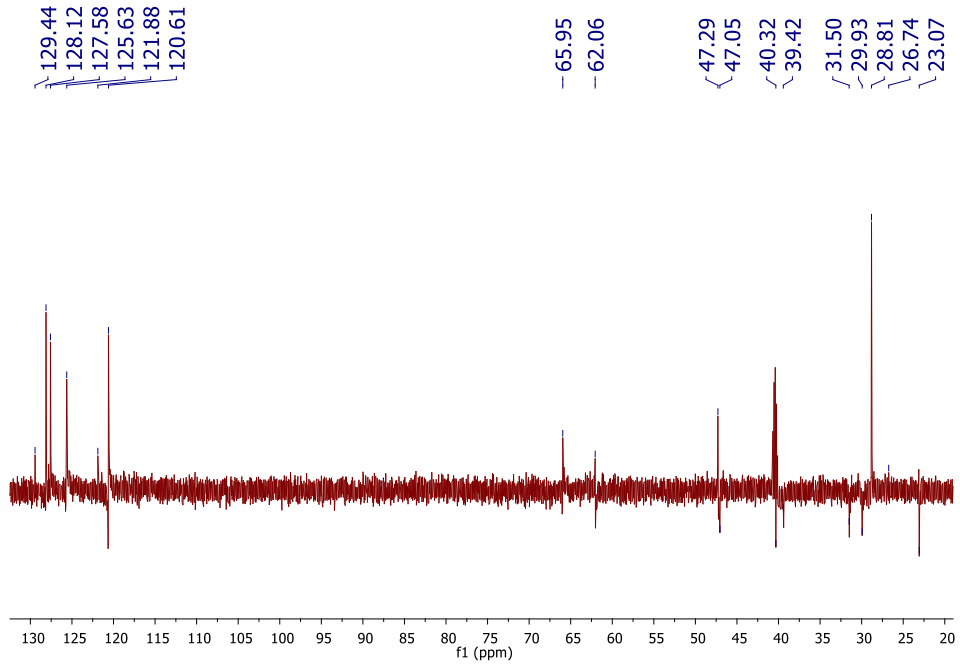


**Figure A12: DEPT 135 spectrum of compound (1)**

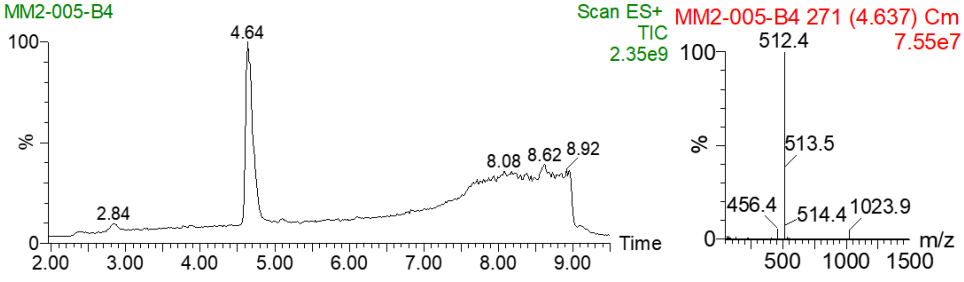


**Figure A13: Chromatogram and ESI (+) spectrum of compound (1)**

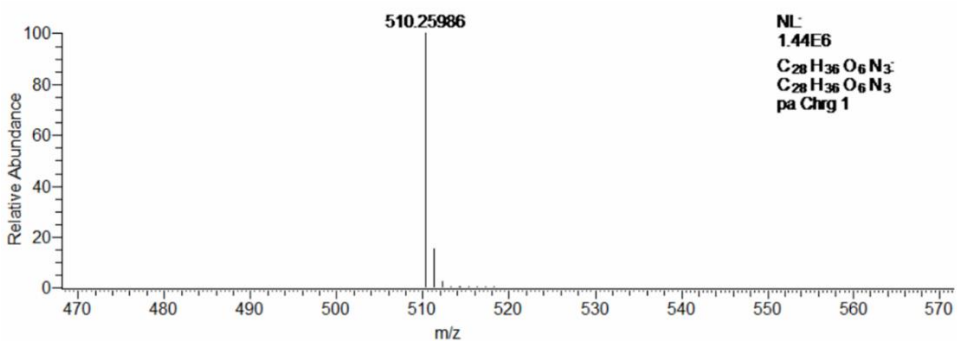


**Figure A14: HRMS LTQ-ORBITRAP spectrum of compound (1)**

**Arginine derivative backbone**

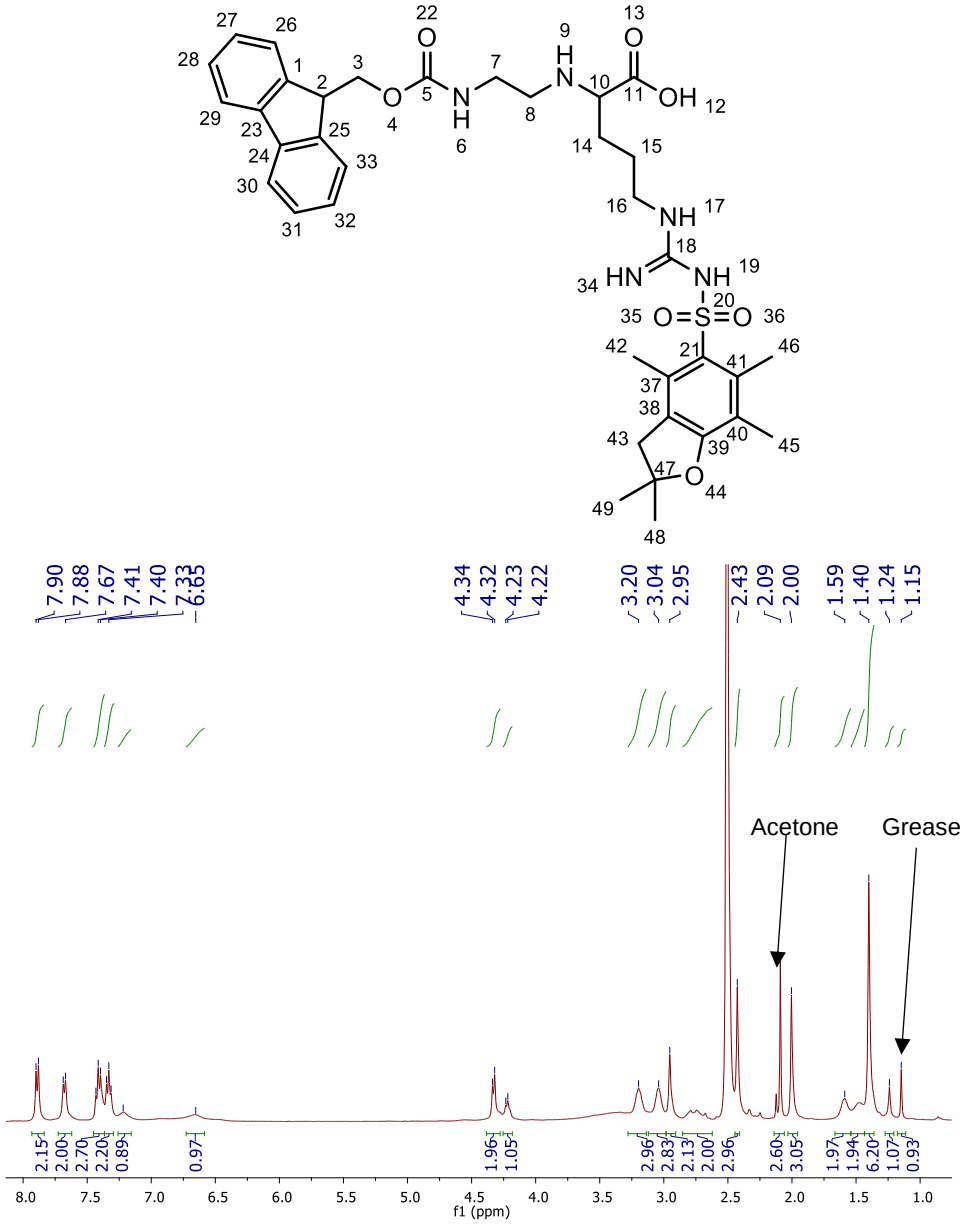


**Figure A15: 1H-NMR spectrum of compound (2)**

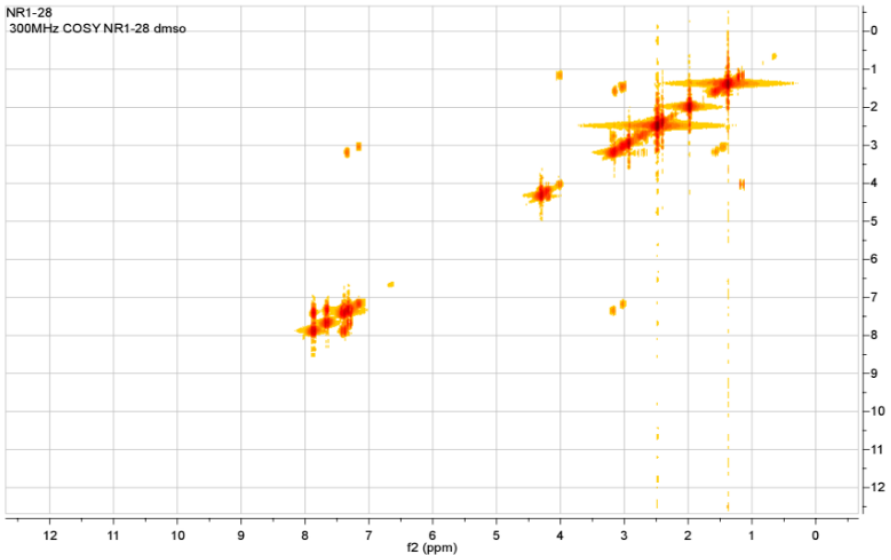


**Figure A16: COSY spectrum of compound (2)**

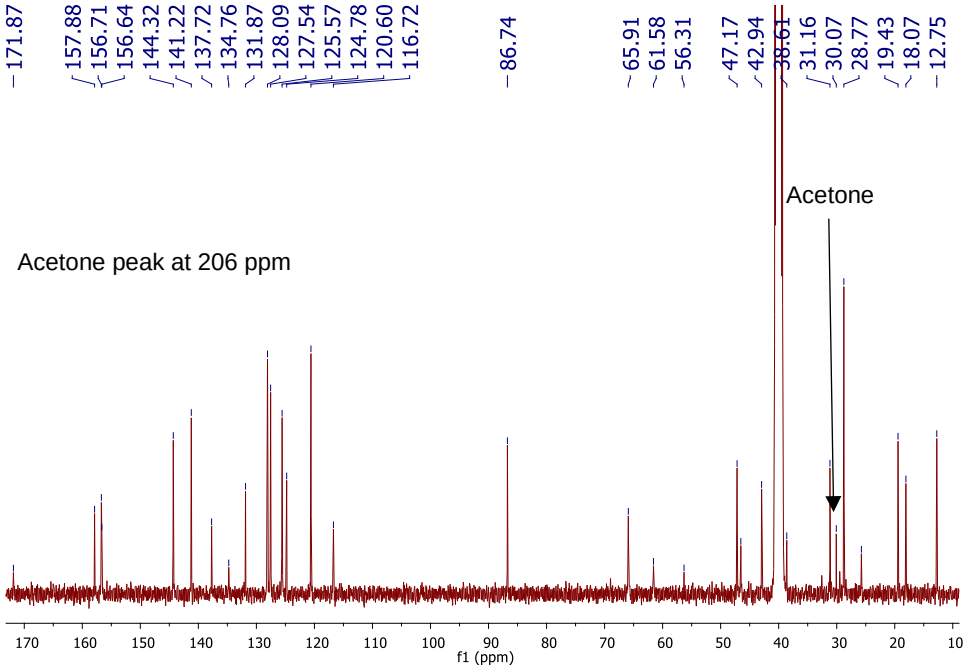


**Figura A17: 13C-NMR spectrum of compound (2)**

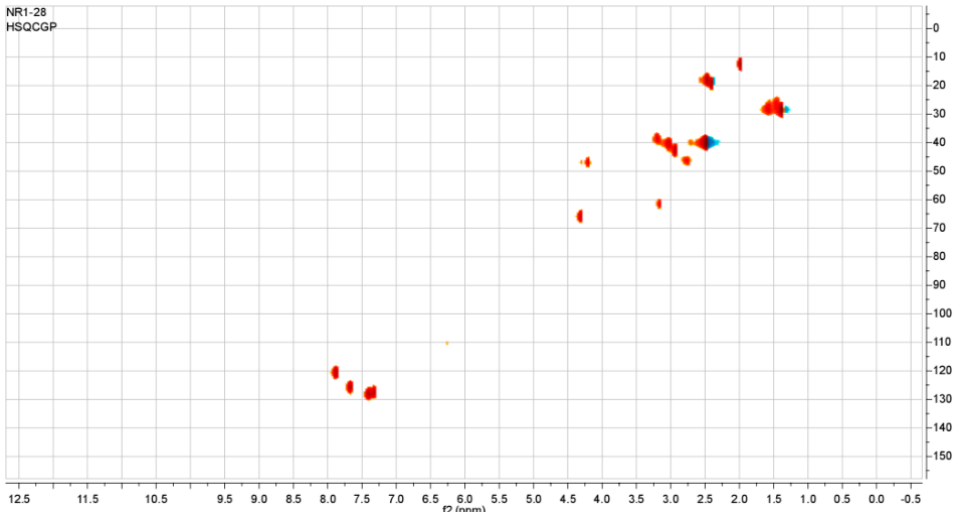


**Figure A.18: HSQC spectrum of compound (2)**

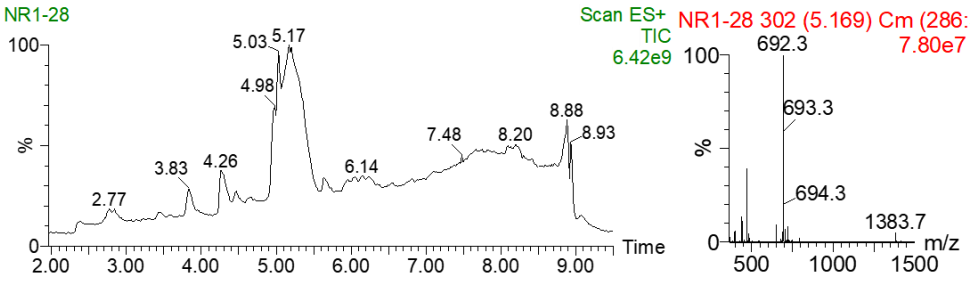


**Figure A19: Chromatogram and ESI (+) spectrum of compound (2)**

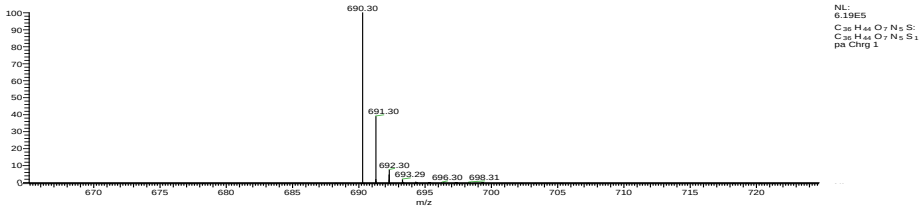


**Figure A20: HRMS LTQ-ORBITRAP spectrum of compound (2)**

**Carboxy methyl cytosine:**

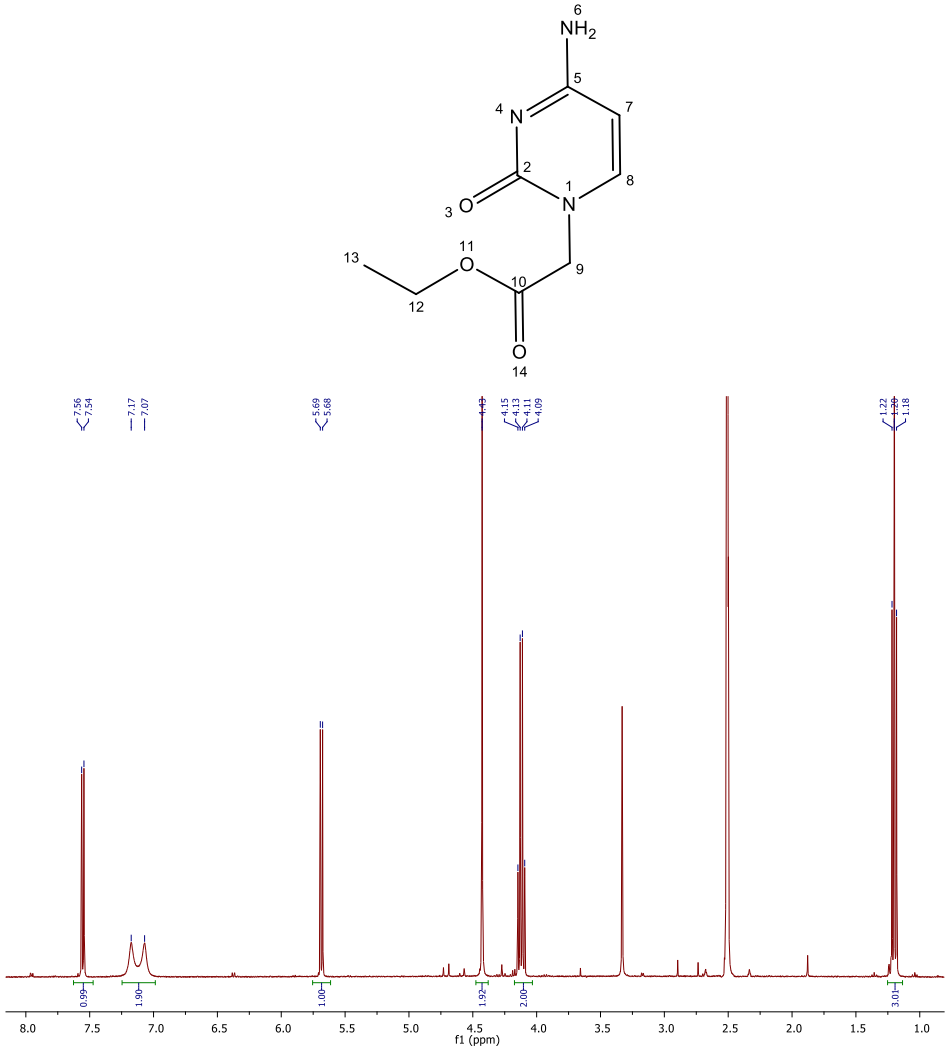


**Figure A21: 1H-NMR spectrum of compound (3)**

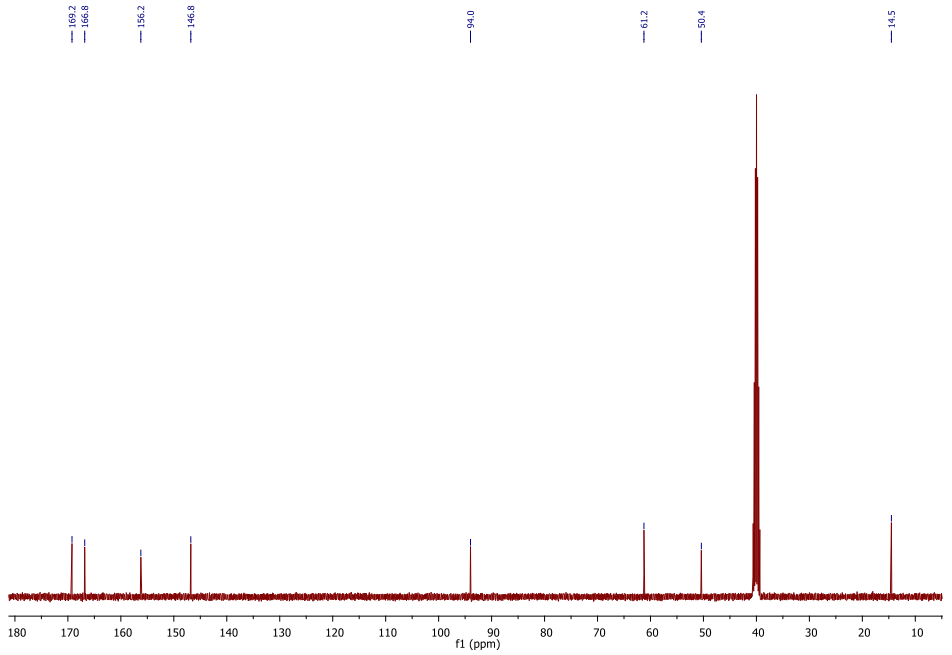


**Figure A22: 13C-NMR spectrum of compound (3)**

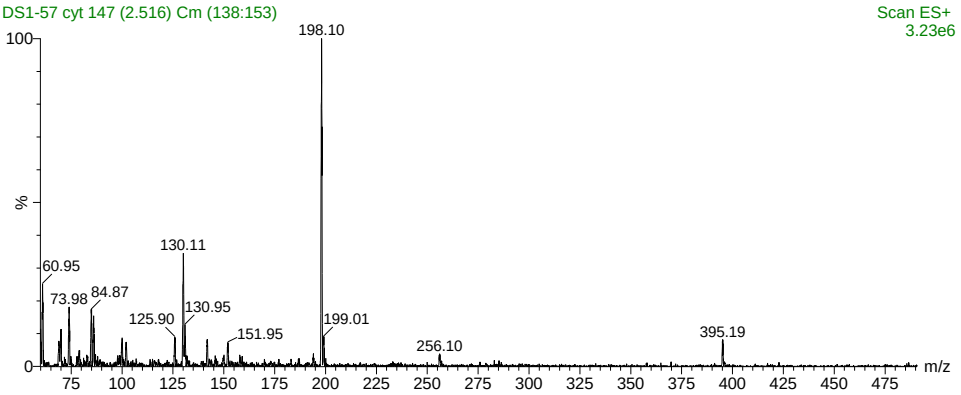


**Figure A23: ESI (+) spectrum of compound (3)**

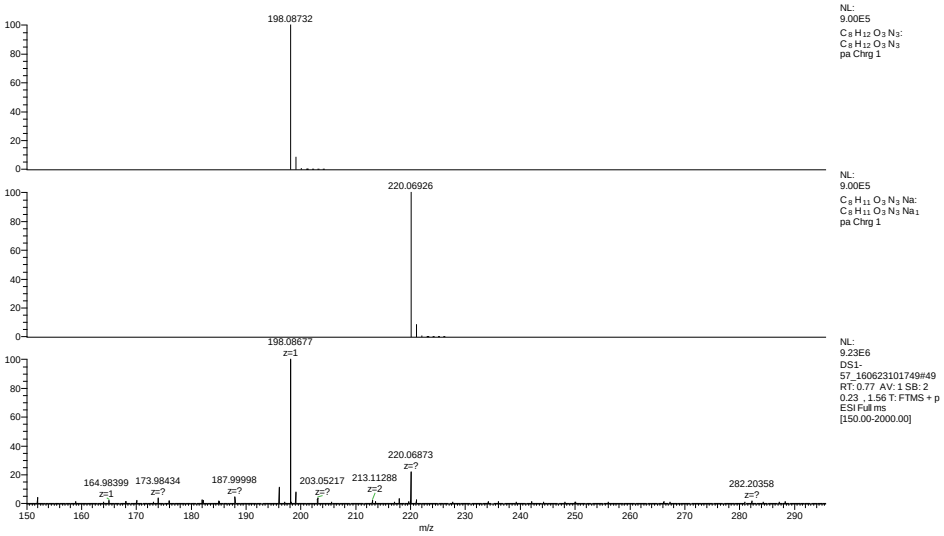


**Figure A24: HRMS LTQ-ORBITRAP spectrum of compound (3)**

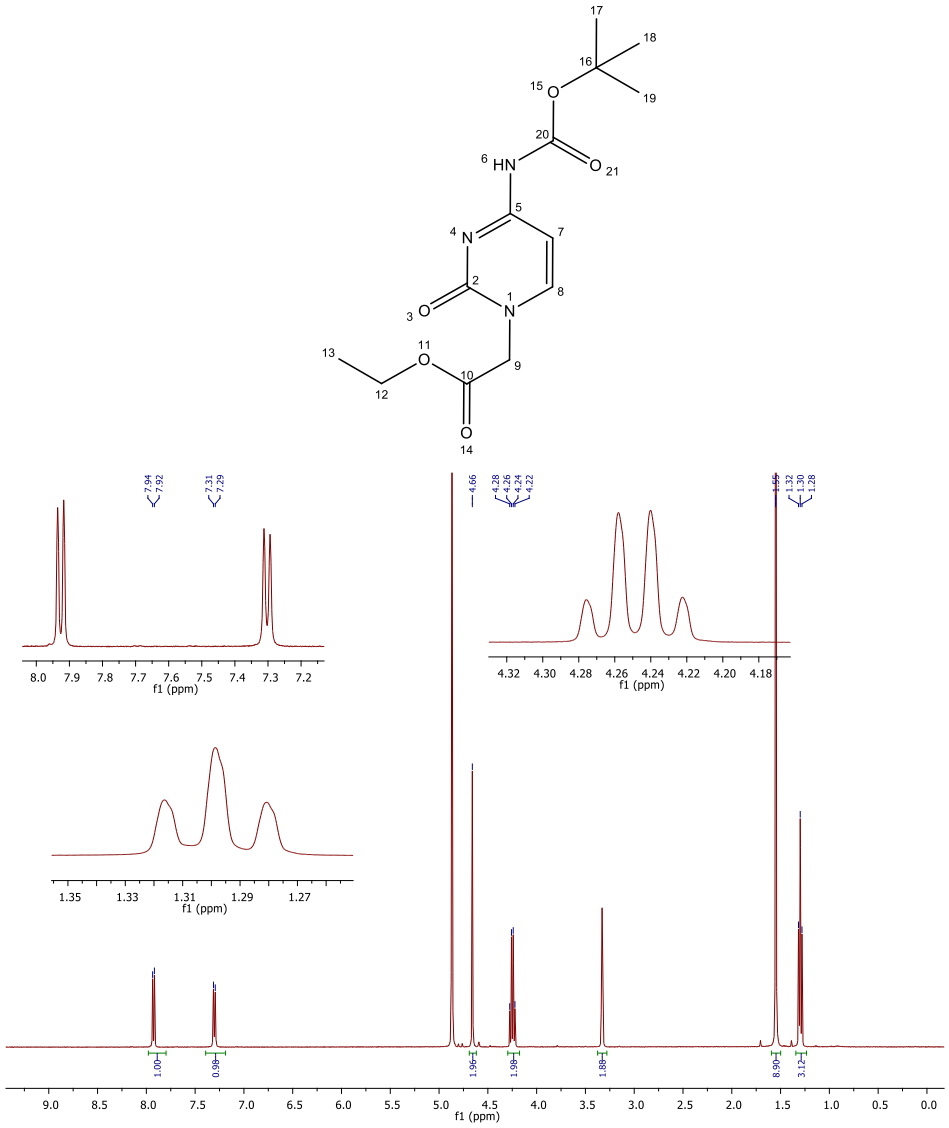


**Figure A25: 1H-NMR spectrum of compound (4)**

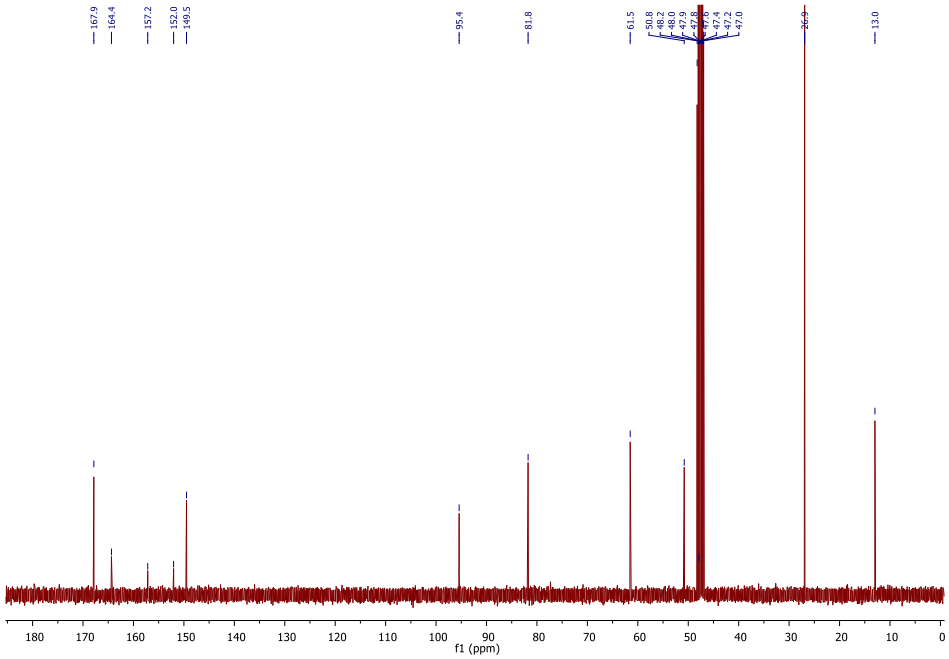


**Figure A26: 13C-NMR spectrum of compound (4)**

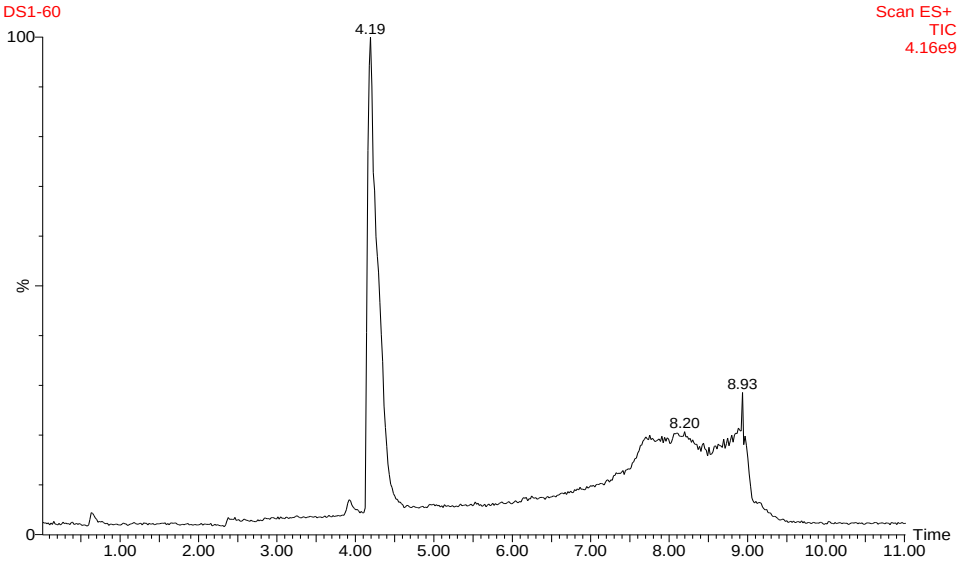


**Figure A27: UPLC Chromatogram of compound (4).**

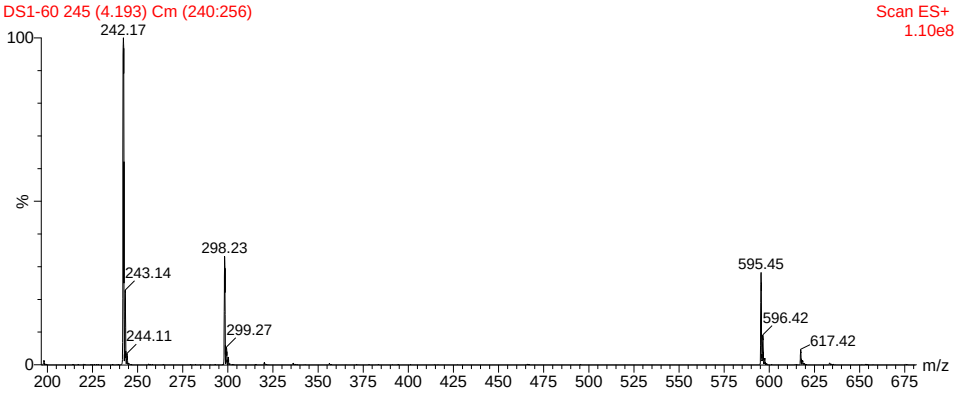


**Figure A28: ESI (+) spectrum of compound (4)**

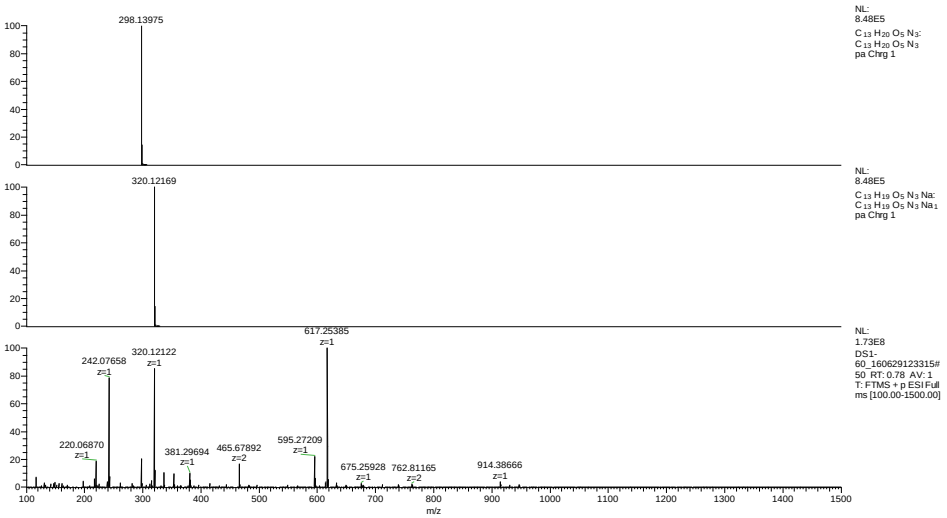


**Figure A29: HRMS LTQ-ORBITRAP spectrum of compound (4)**

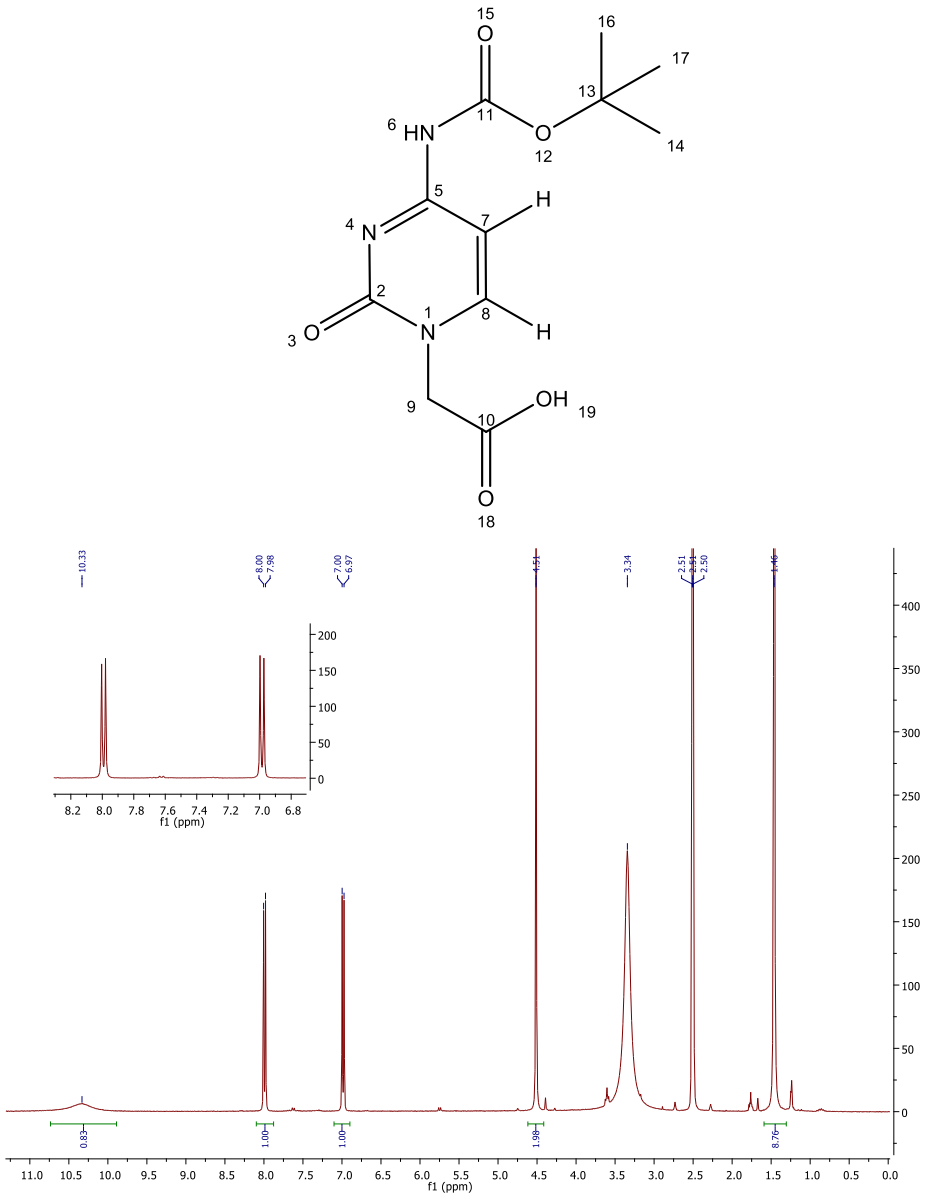


**Figure A30: 1H-NMR spectrum of compound (5)**

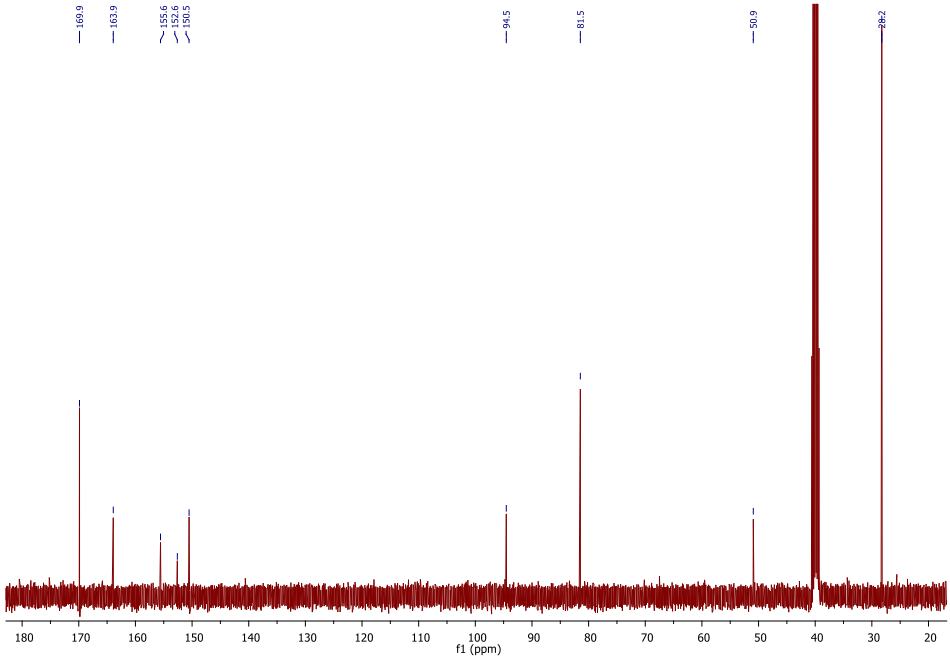


**Figure A31: 13C-NMR spectrum of compound (5)**

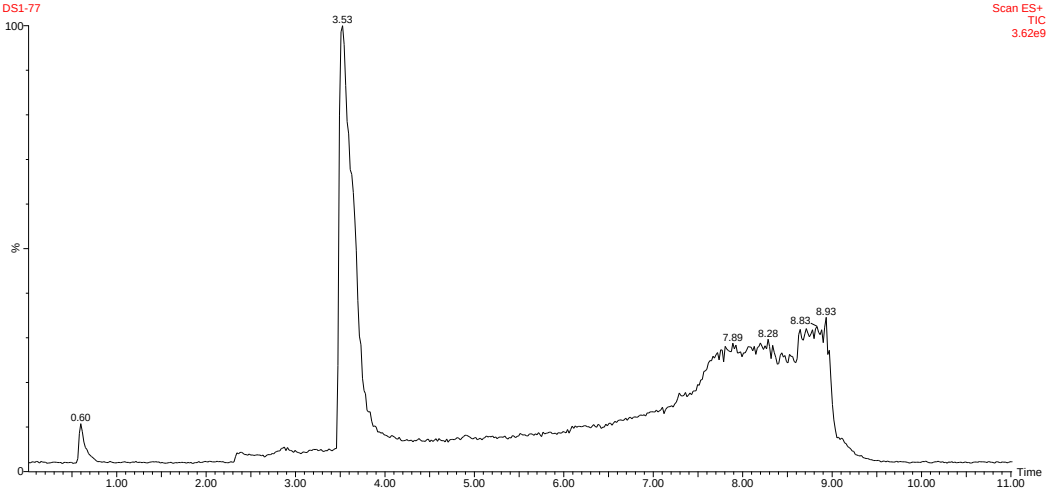


**Figure A32: UPLC Chromatogram of compound (5).**

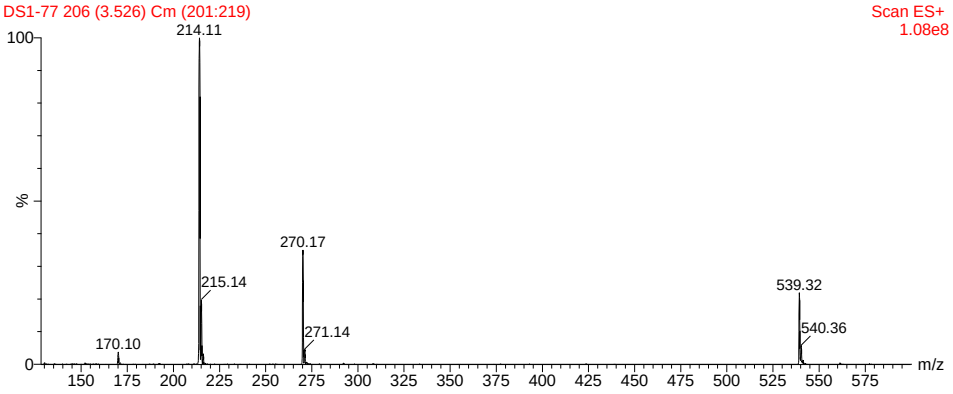


**Figure A33: ESI (+) spectrum of compound (5)**

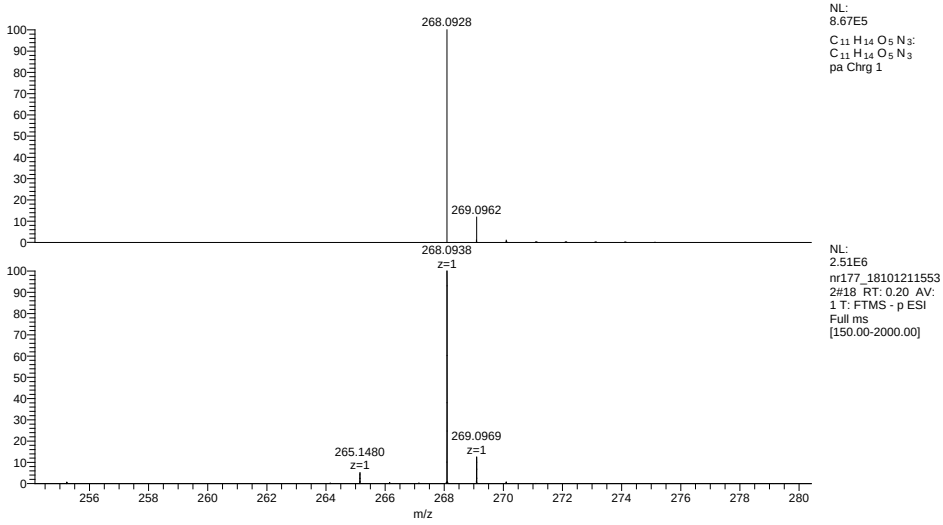


**Figure A34: HRMS LTQ-ORBITRAP spectrum of compound (5)**

## PNA characterization :

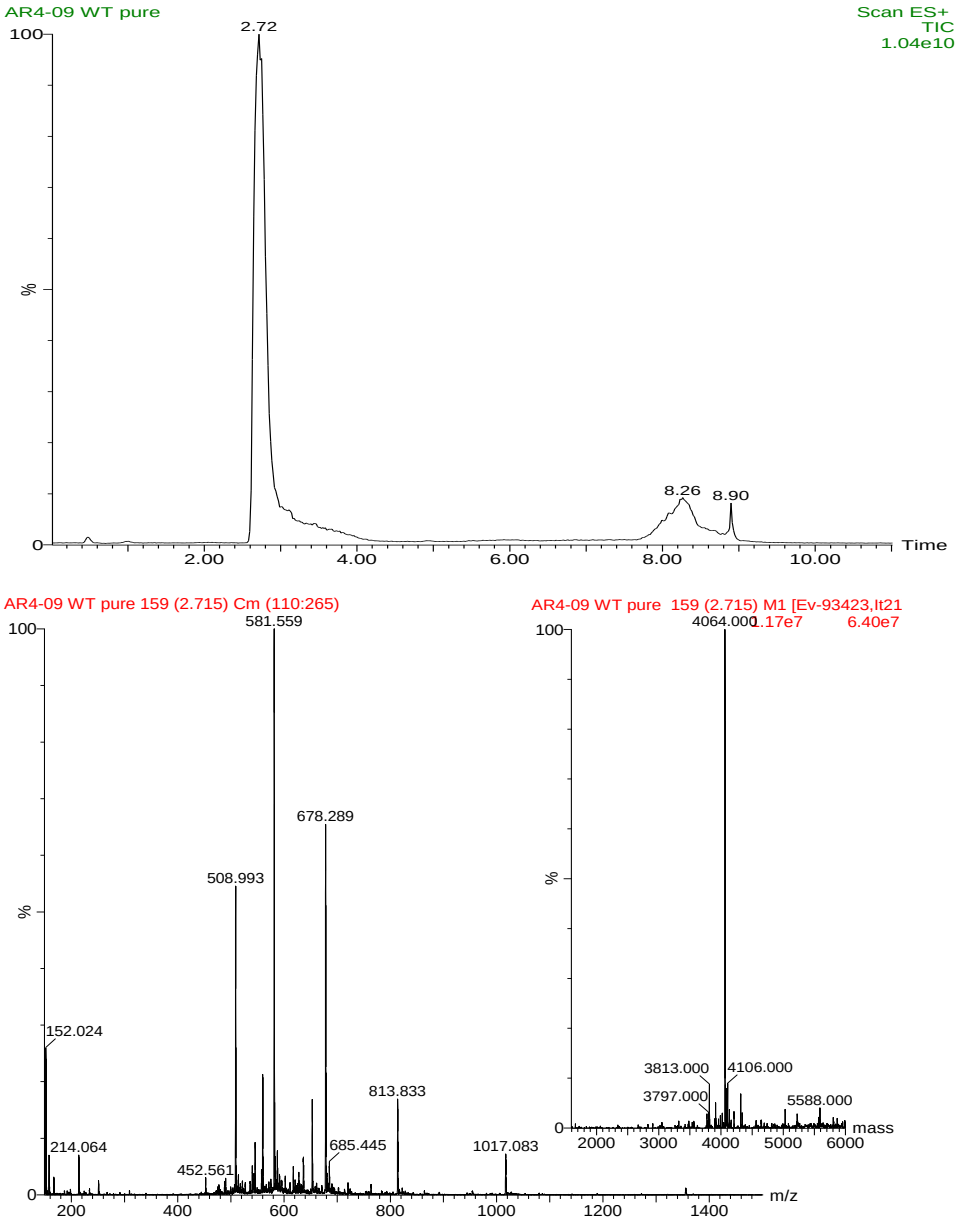


**Figure A35: UPLC-MS of AR4-09 WT. Chromatogram, mass spectra and deconvoluted spectra in the insert.**

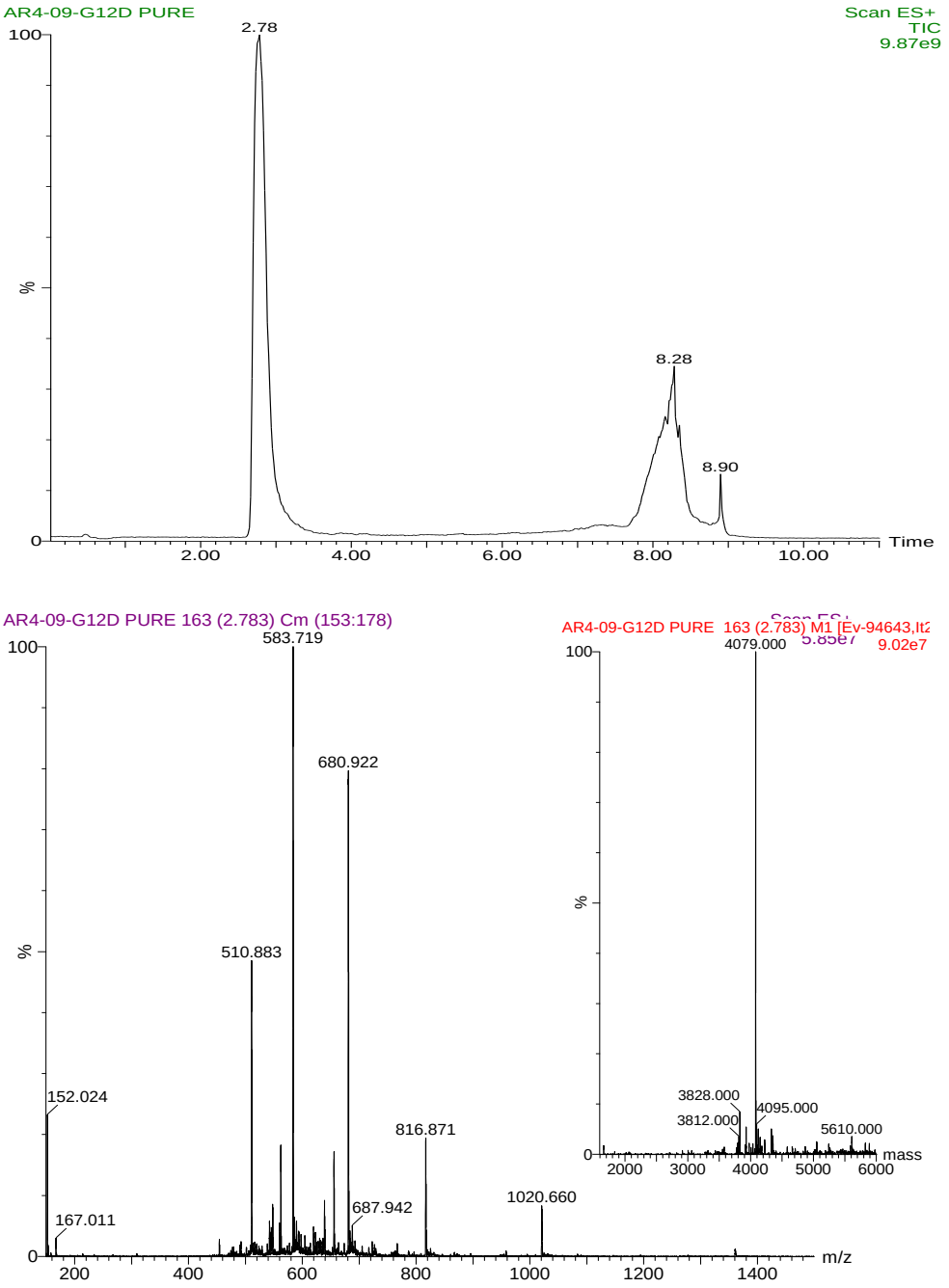


**Figure A36: UPLC-MS of AR4-09 G12D. Chromatogram, mass spectra and deconvoluted spectra in the insert.**

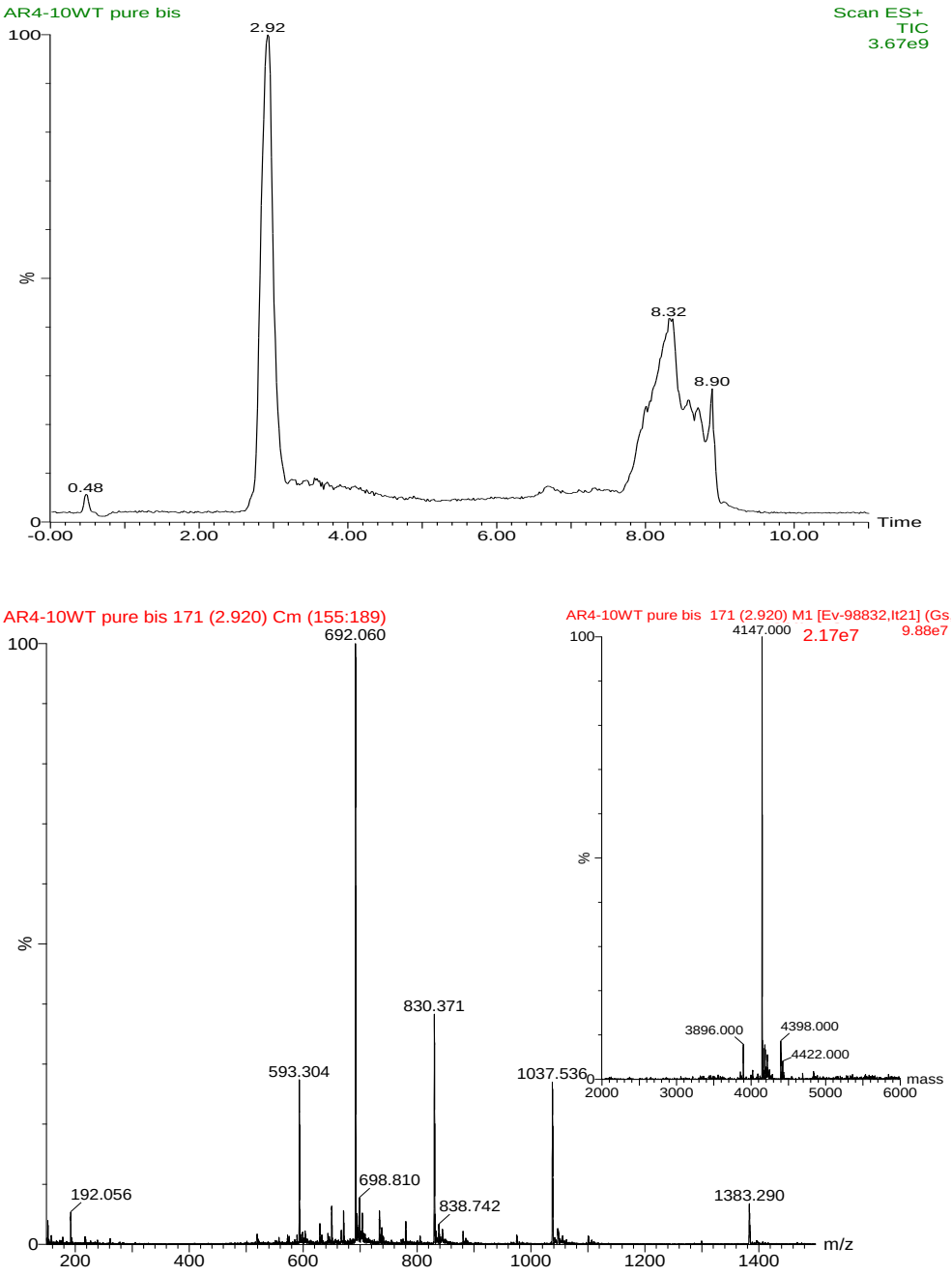


**Figure A37: UPLC-MS of AR4-10 WT. Chromatogram, mass spectra and deconvoluted spectra in the insert.**

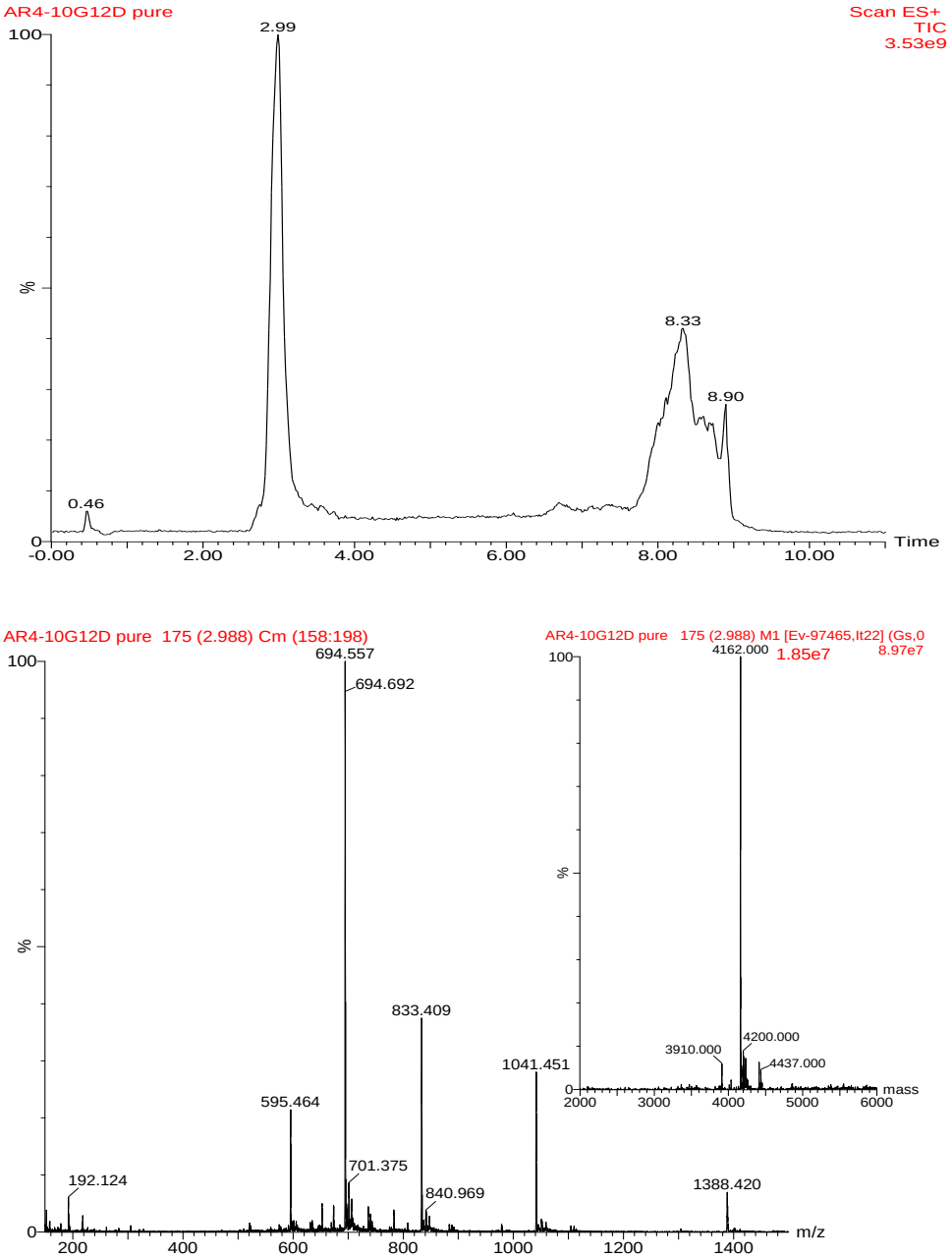


**Figure A38: UPLC-MS of AR4-10 G12D. Chromatogram, mass spectra and deconvoluted spectra in the insert.**

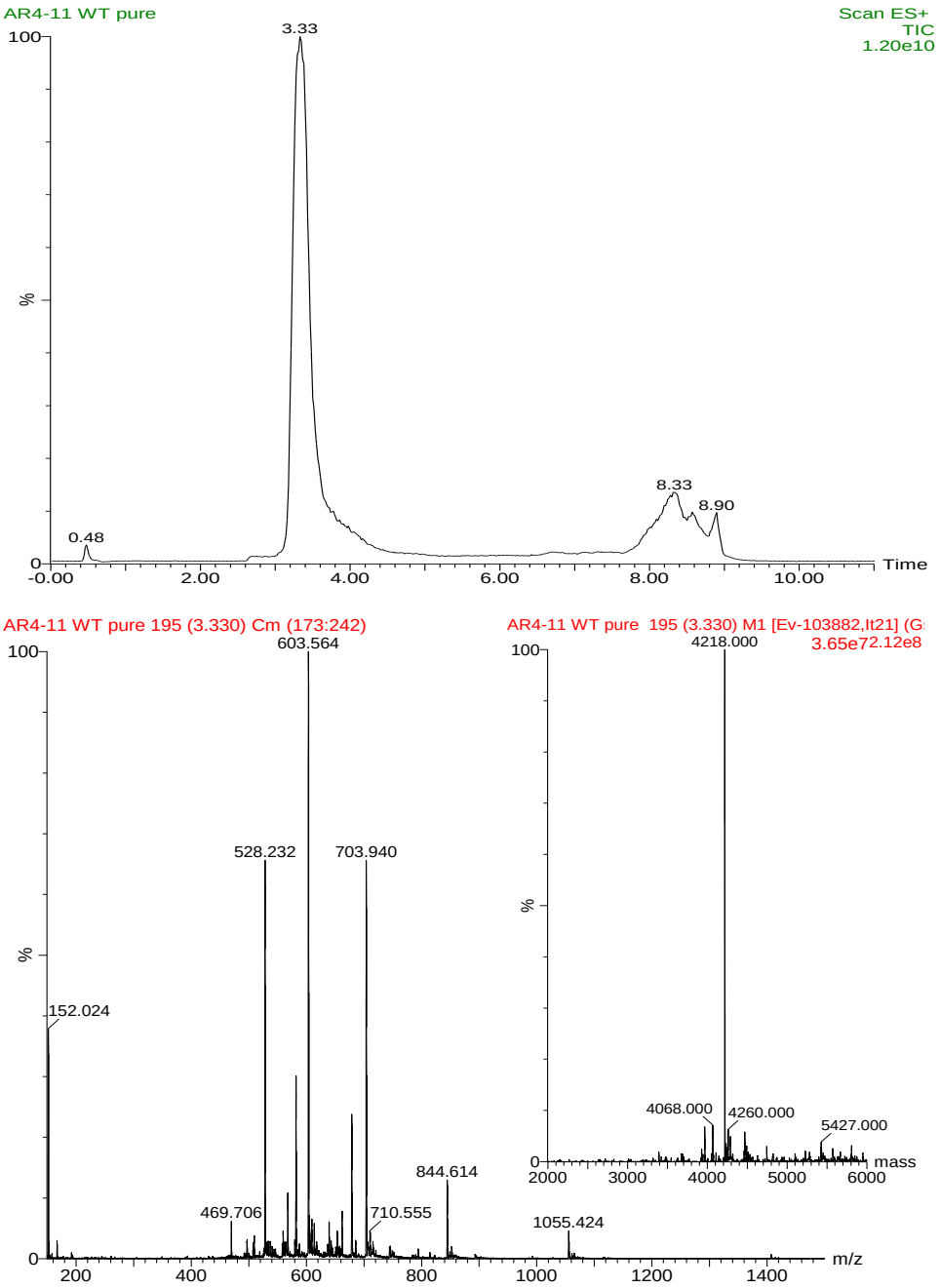


**Figure A39: UPLC-MS of AR4-11 WT. Chromatogram, mass spectra and deconvoluted spectra in the insert.**

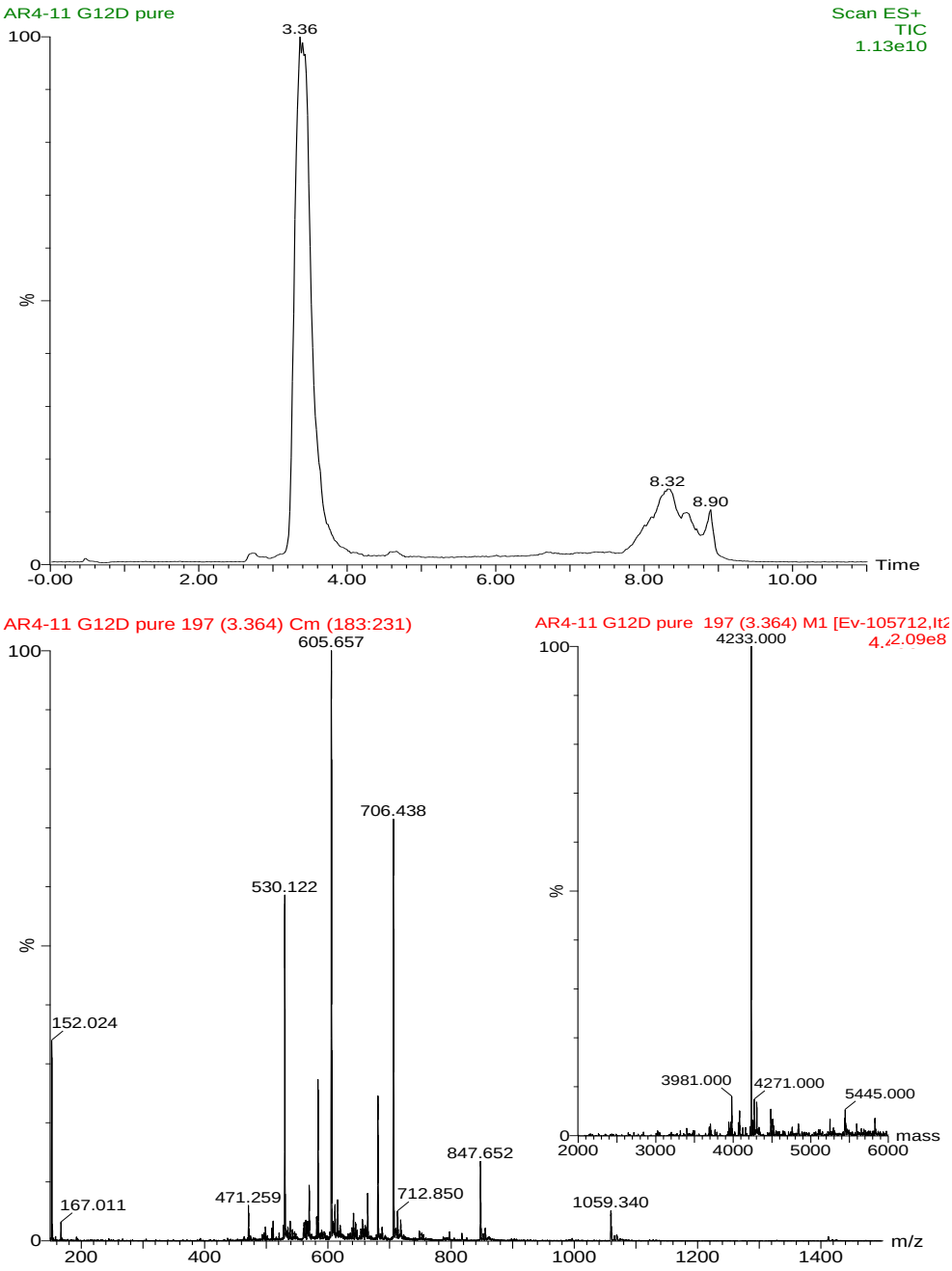


**Figure A40: UPLC-MS of AR4-11 G12D. Chromatogram, mass spectra and deconvoluted spectra in the insert.**

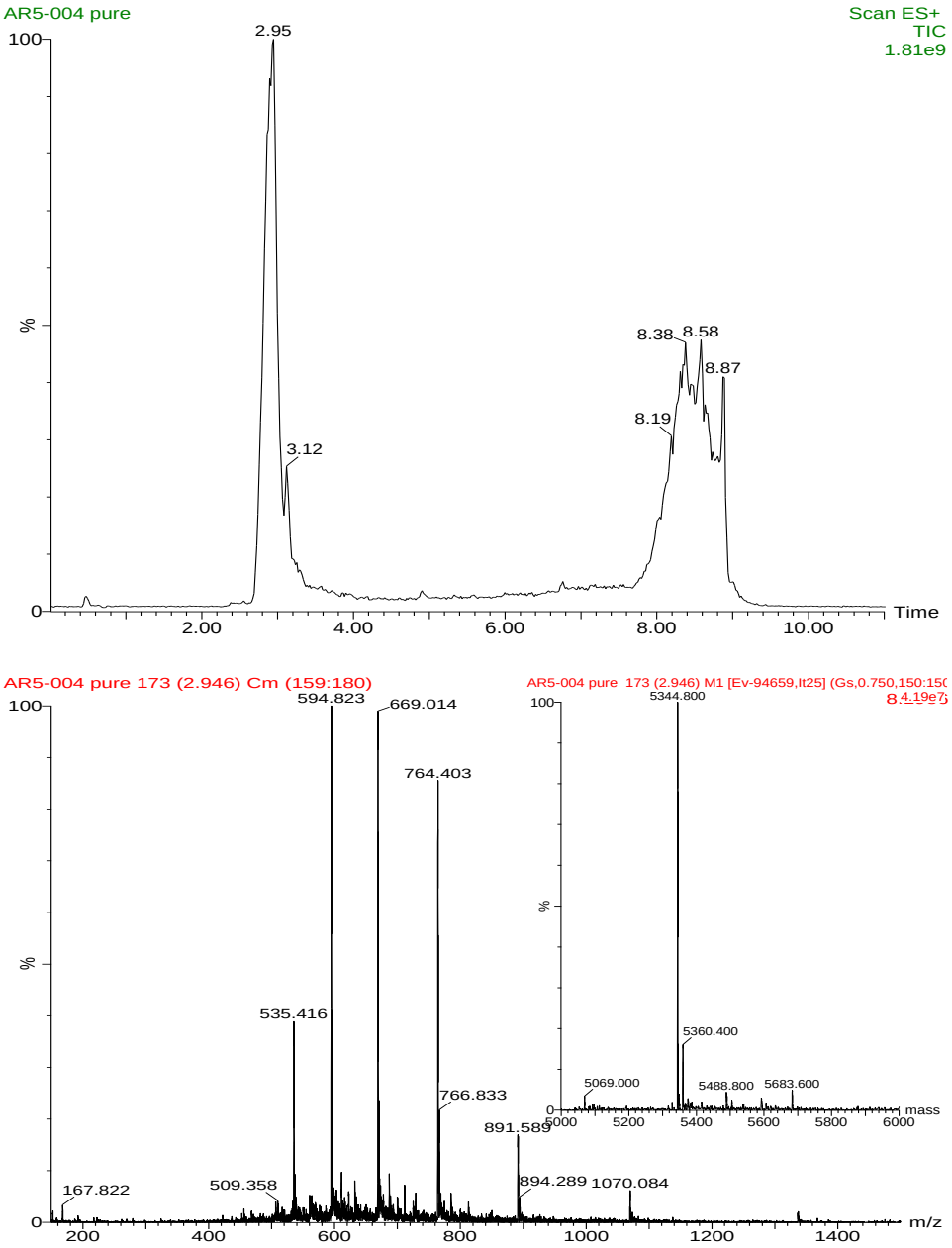


**Figure A41: UPLC-MS of AR5-004. Chromatogram, mass spectra and deconvoluted spectra in the insert.**

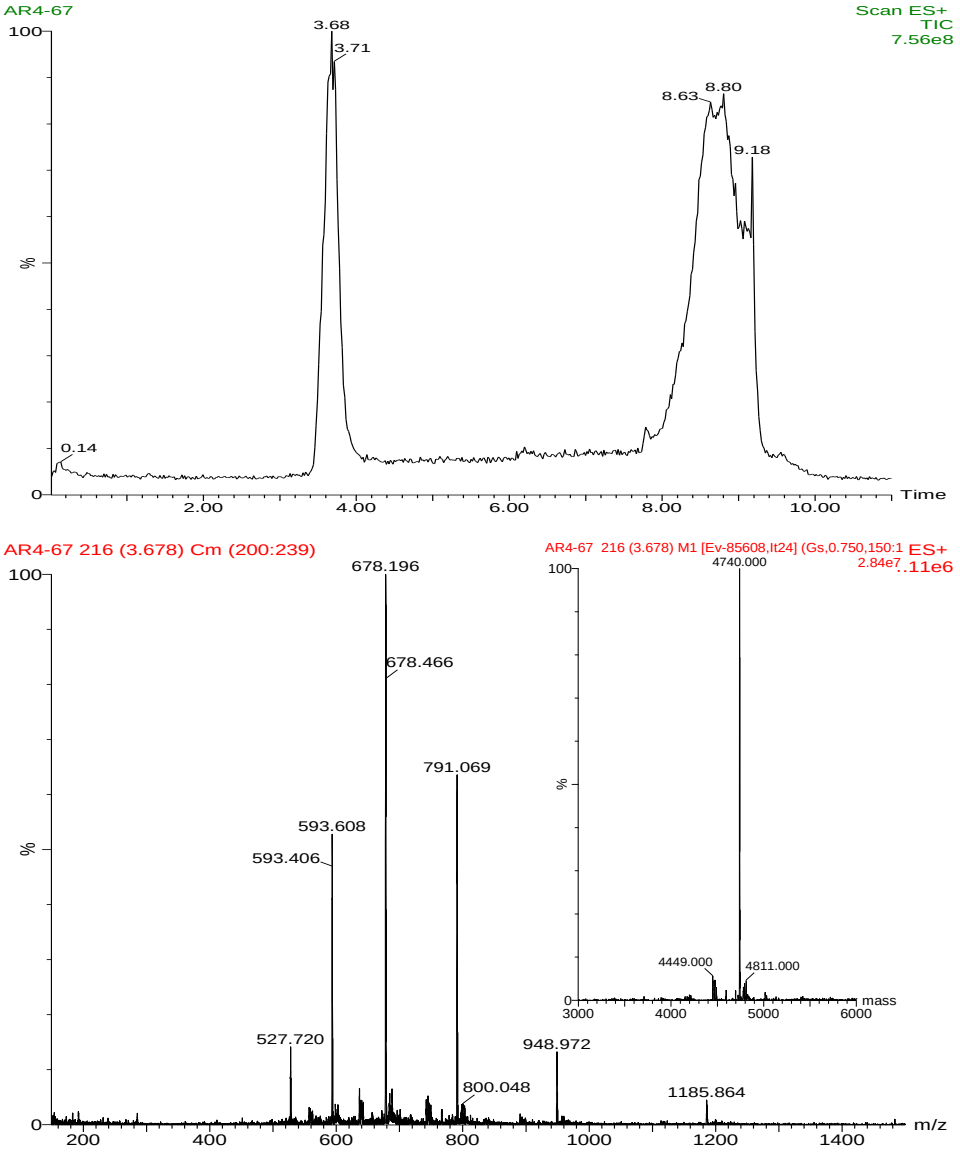


**Figure A42: UPLC-MS of AR4-67. Chromatogram, mass spectra and deconvoluted spectra in the insert.**

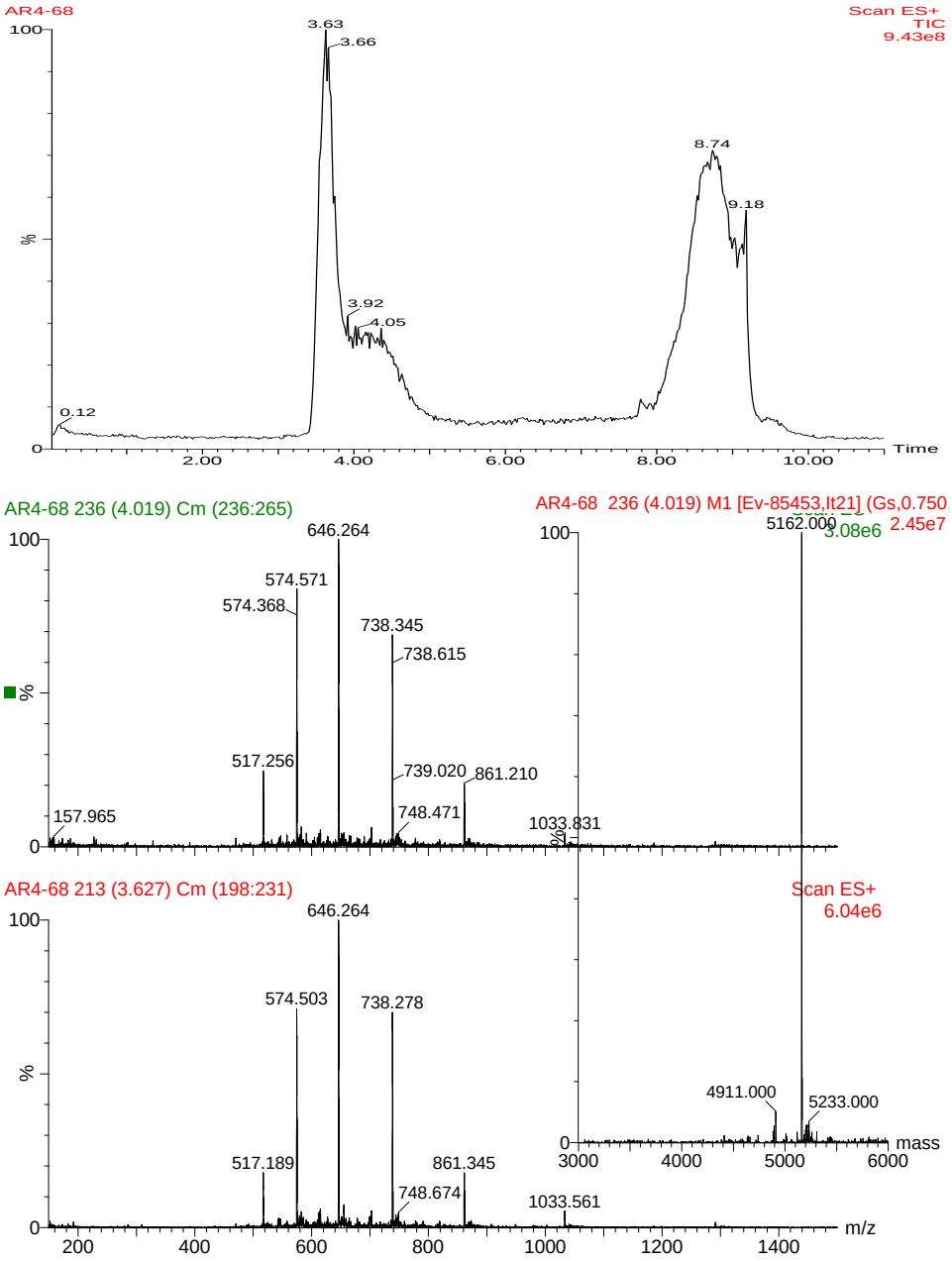


**Figure A43: UPLC-MS of AR4-68. Chromatogram, mass spectra and deconvoluted spectra in the insert.**

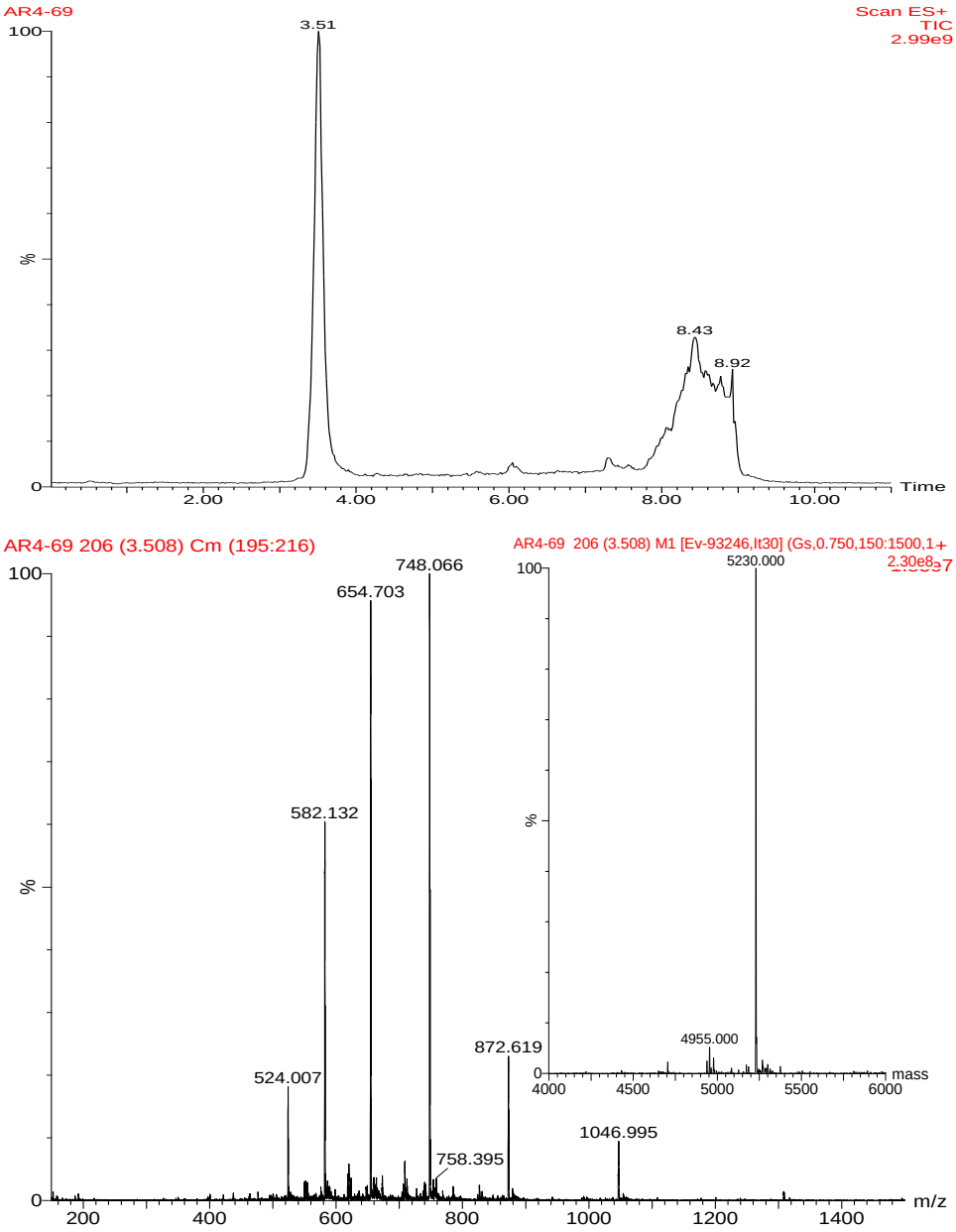


**Figure A44: UPLC-MS of AR4-69. Chromatogram, mass spectra and deconvoluted spectra in the insert.**

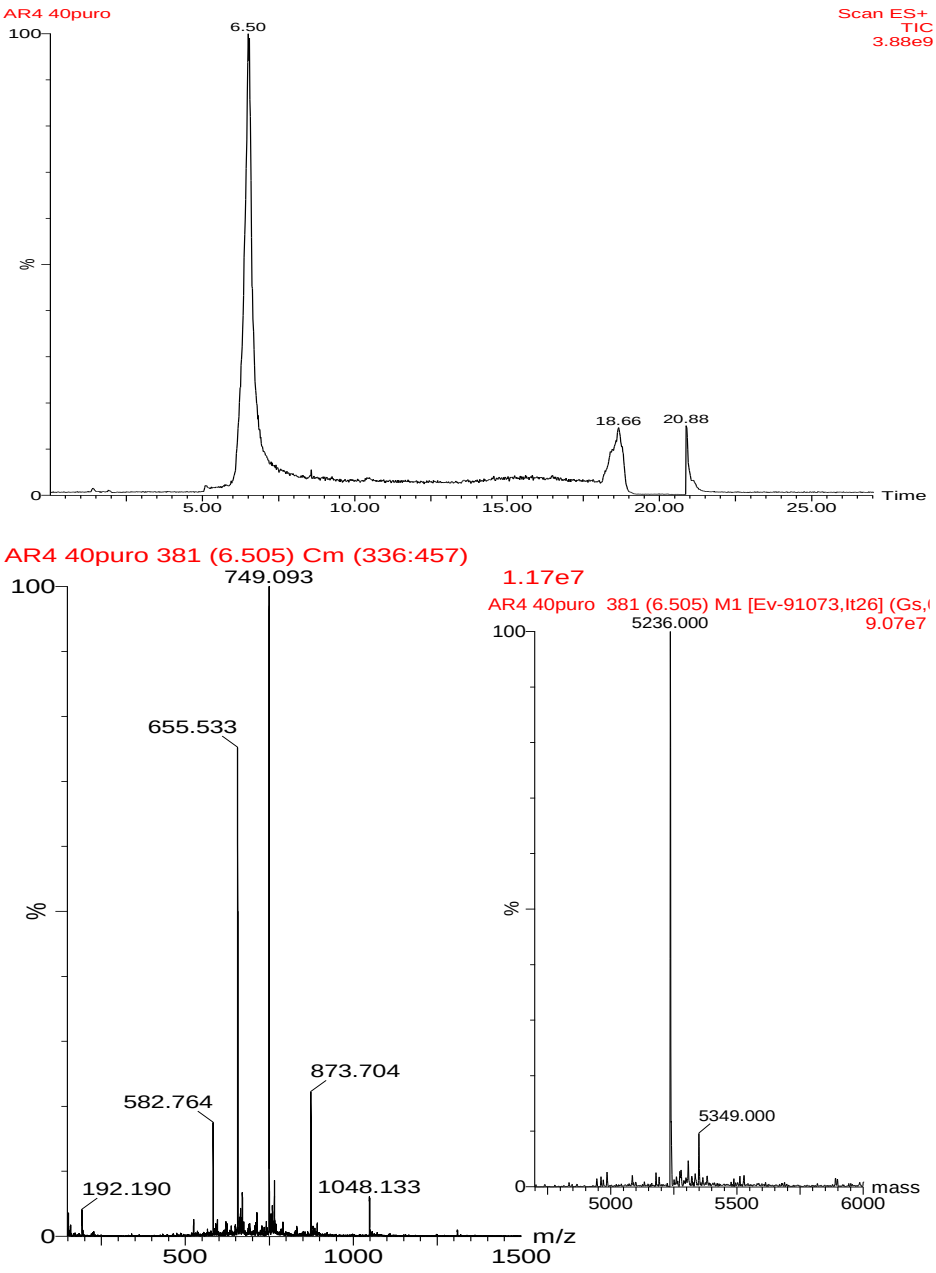


**Figure A45: UPLC-MS of AR4-40. Chromatogram, mass spectra and deconvoluted spectra in the insert.**

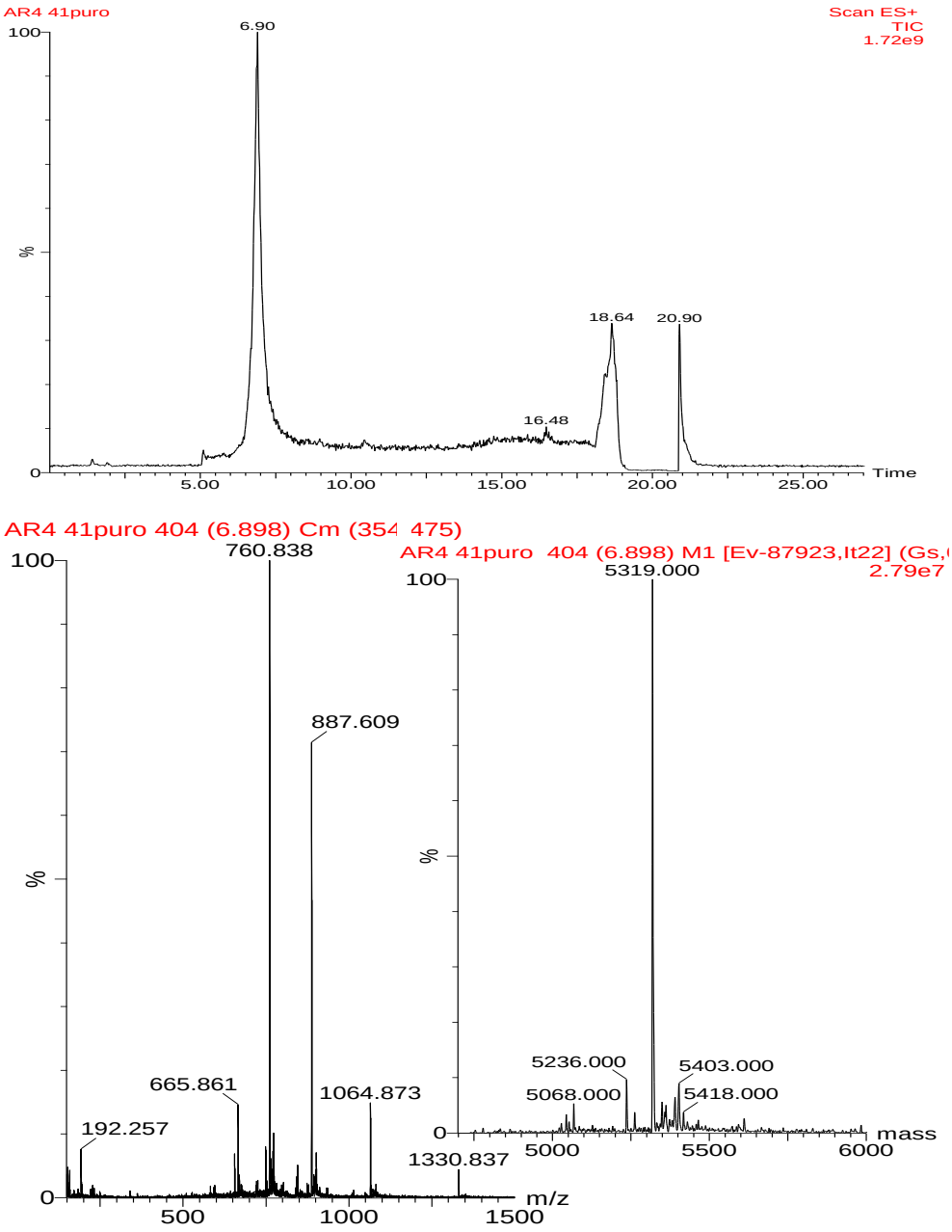


**Figure A46: UPLC-MS of AR4-41. Chromatogram, mass spectra and deconvoluted spectra in the insert.**

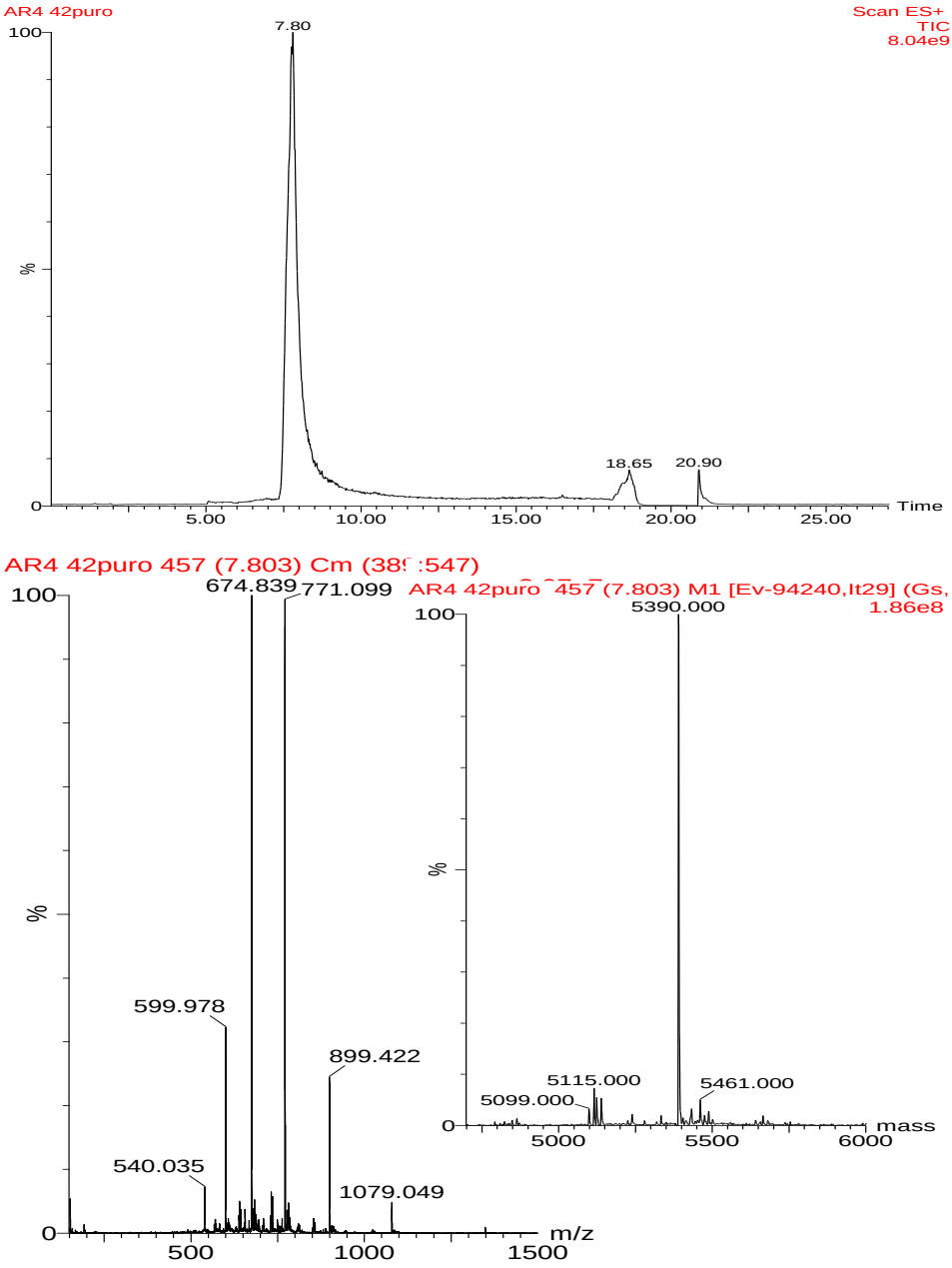


**Figure A47: UPLC-MS of AR4-42. Chromatogram, mass spectra and deconvoluted spectra in the insert.**

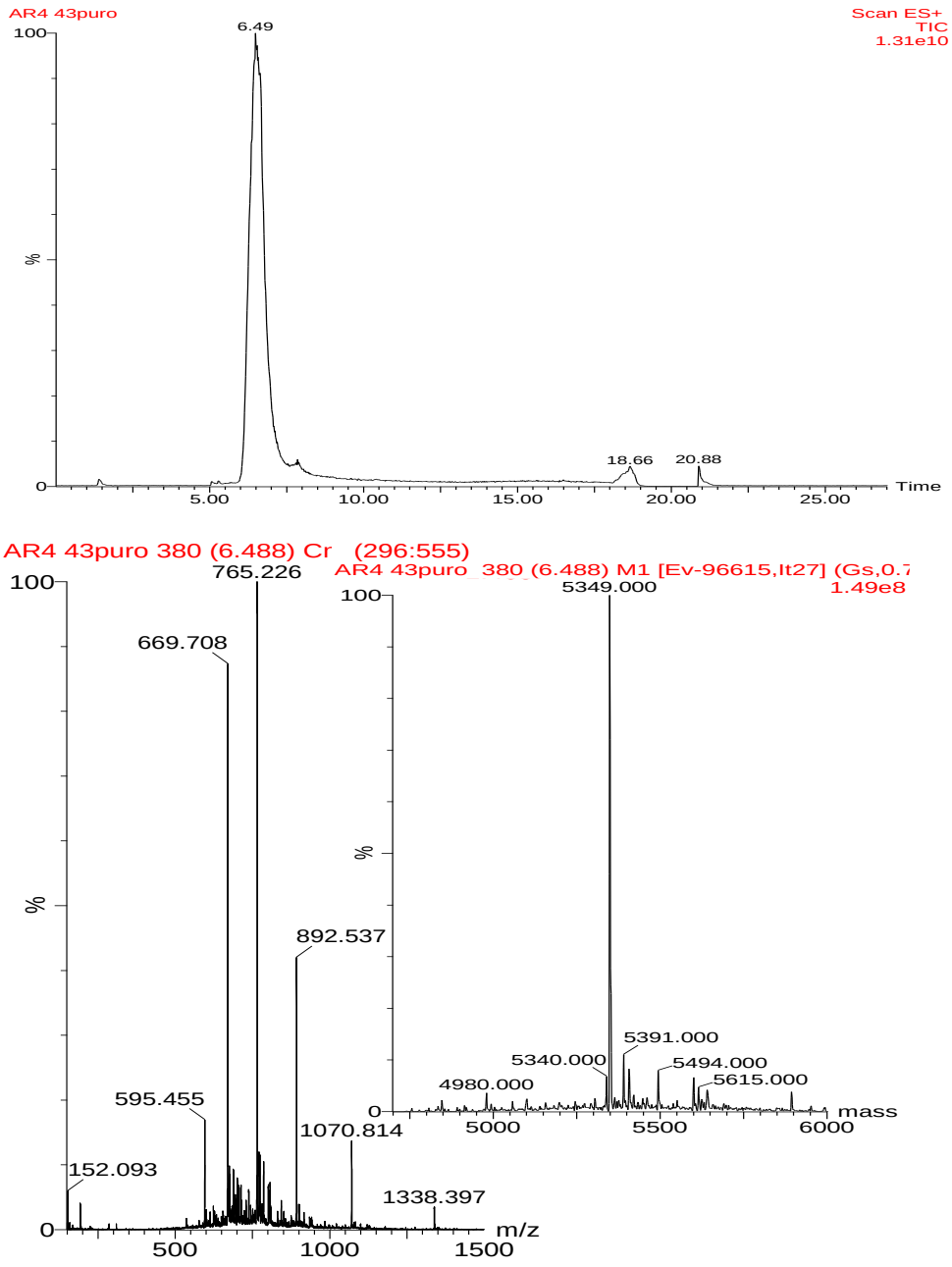


**Figure A48: UPLC-MS of AR4-43. Chromatogram, mass spectra and deconvoluted spectra in the insert.**

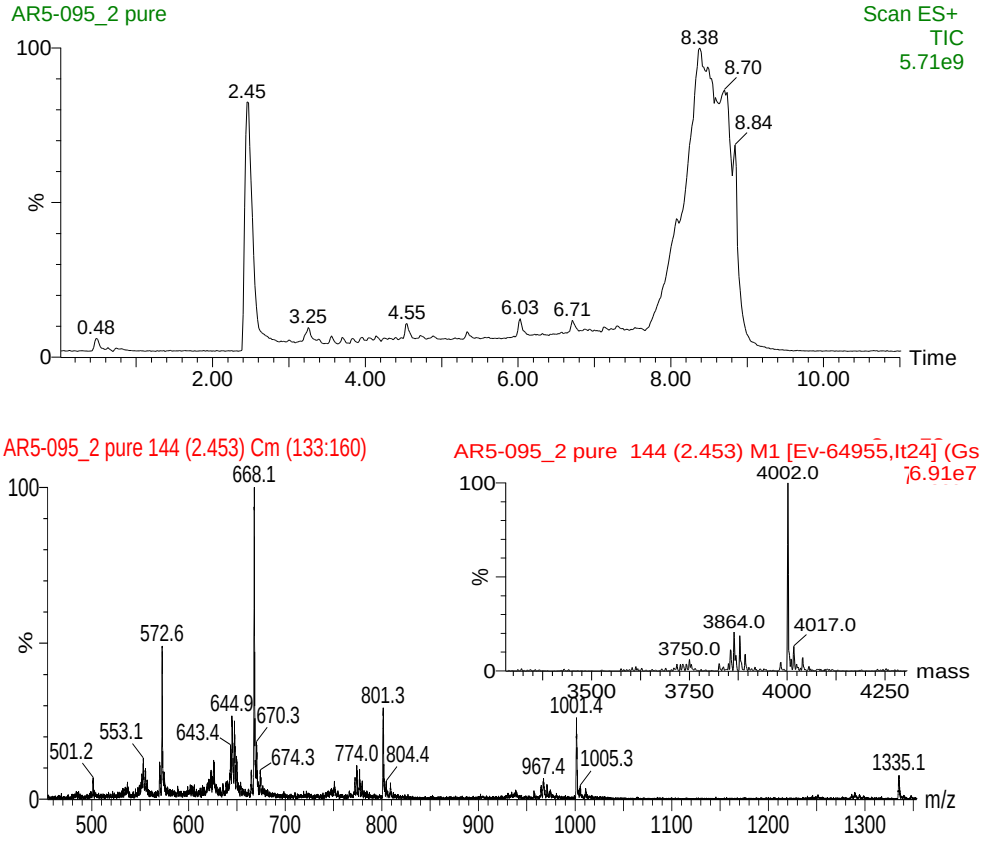


**Figure A49: UPLC-MS of AR5-095. Chromatogram, mass spectra and deconvoluted spectra in the insert.**

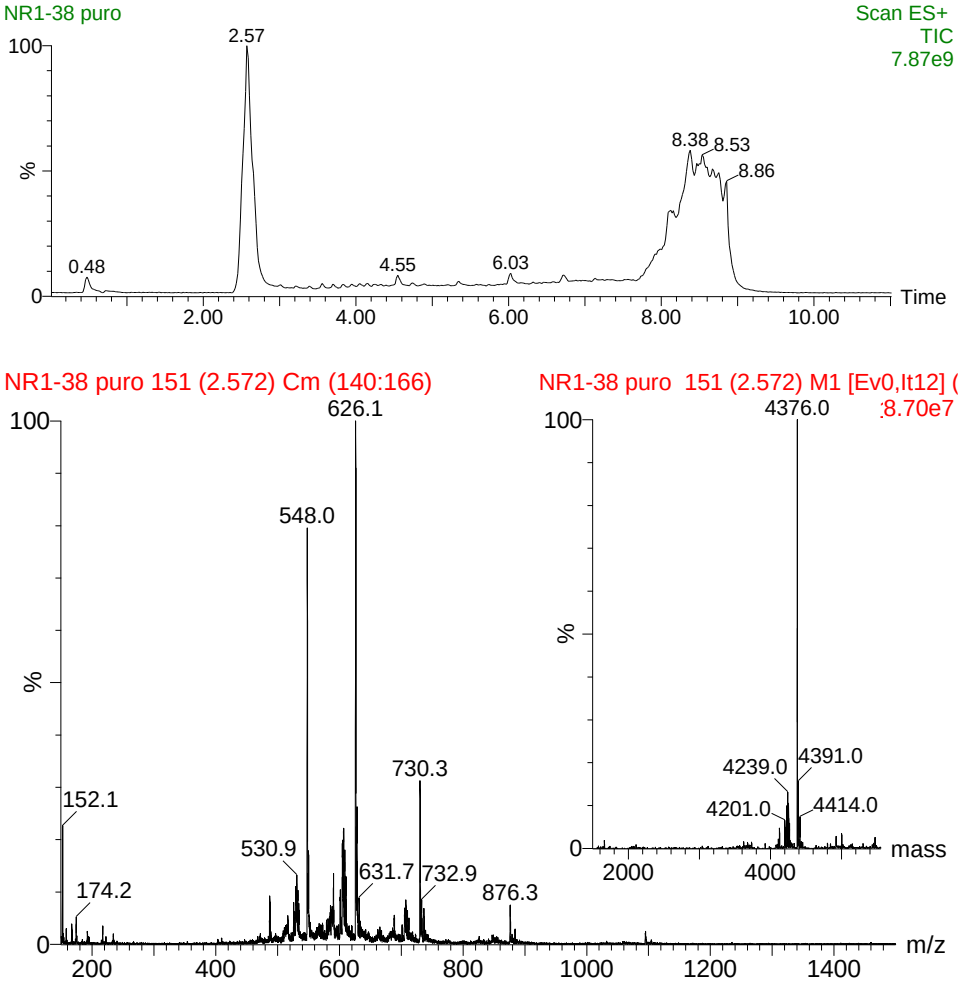


**Figure A50: UPLC-MS of NR1-38. Chromatogram, mass spectra and deconvoluted spectra in the insert.**

## GC-MS Chromatograms

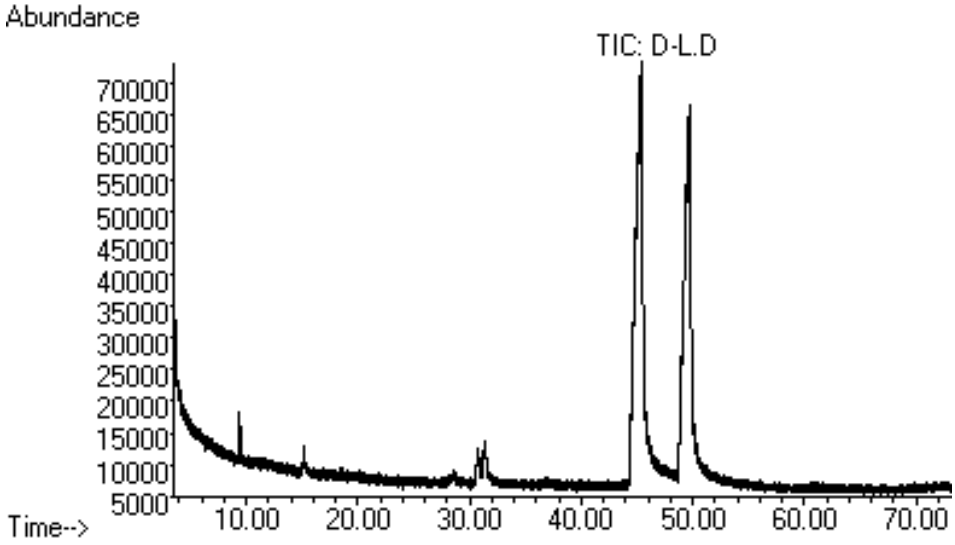


**Figure A51: GC-MS (full scan) of D+L backbones sample.**

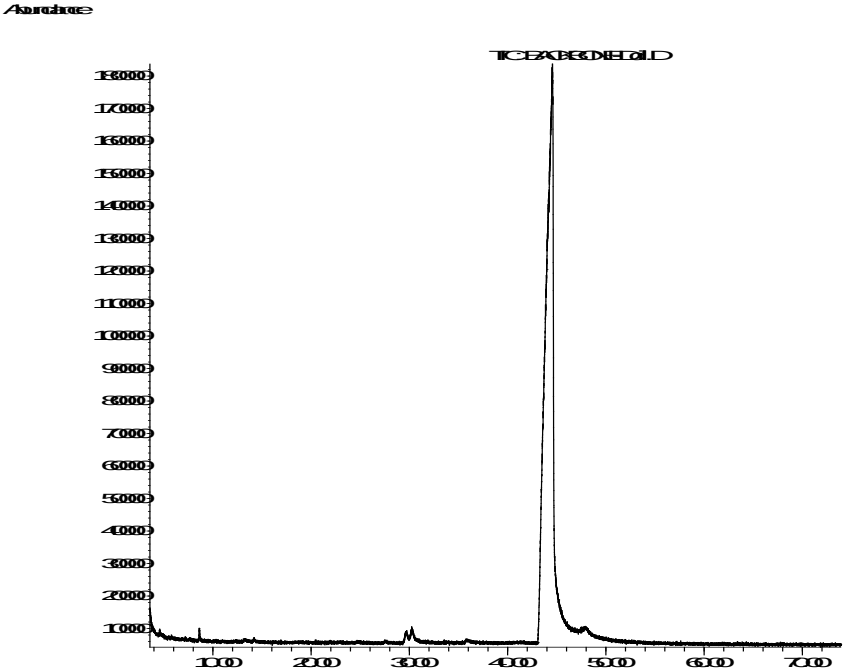

**Figure A52: GC-MS (full scan) of enantiomer D sample.**

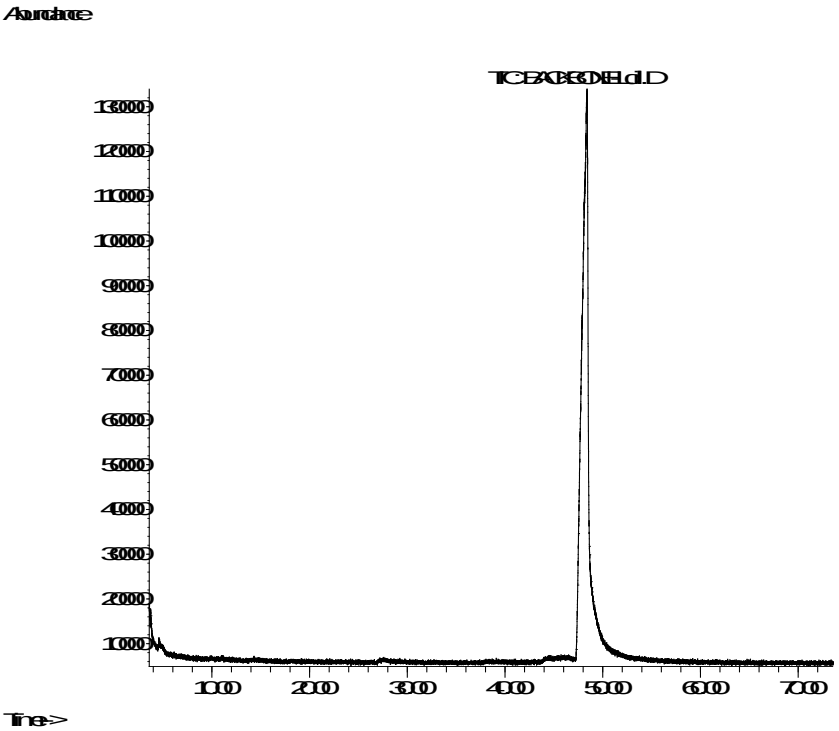

**Figure A53: GC-MS (full scan) of enantiomer L sample.**

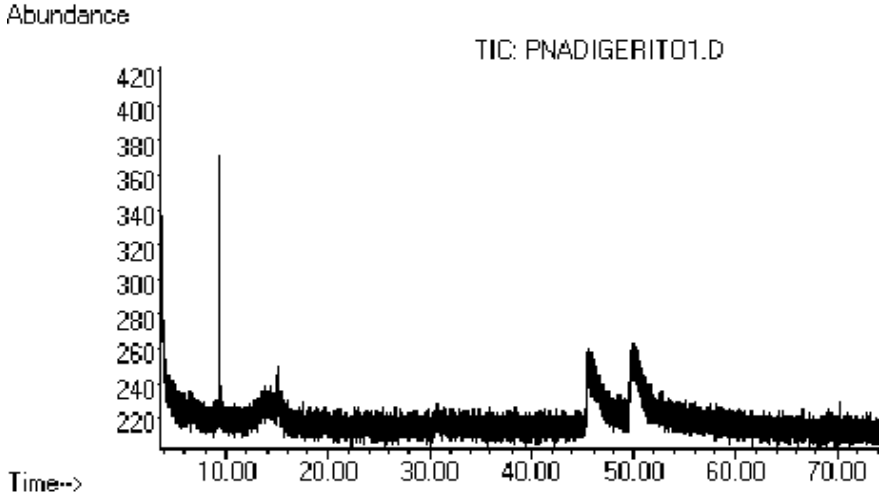


**Figure A54: GC-MS (selected ion monitoring) of digested PNA.**

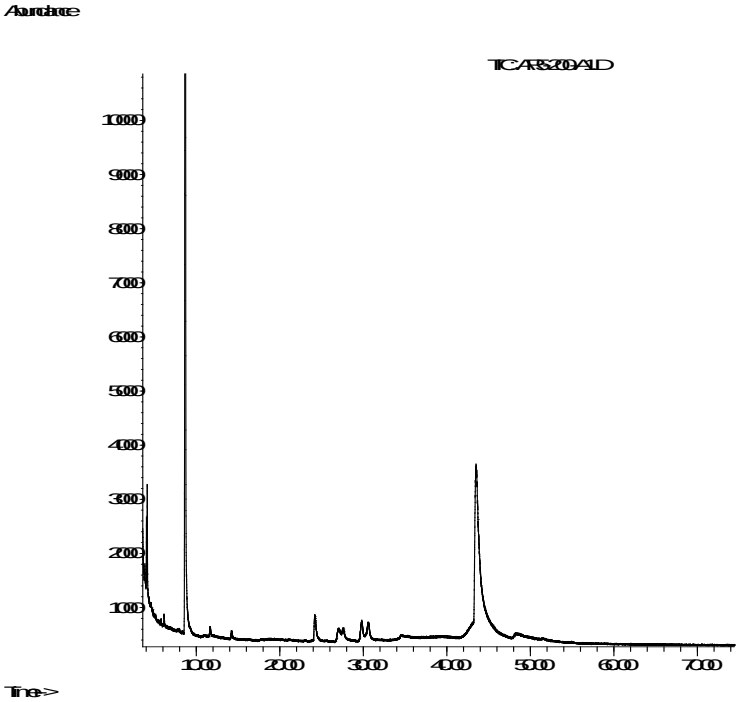


**Figure A55: GC-MS (selected ion monitoring) of digested PNA AR5-200 A.**

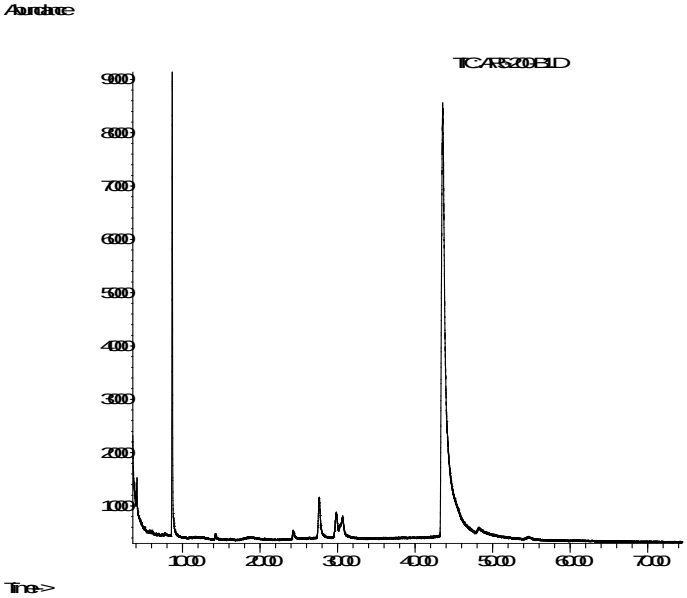


**Figure A56: GC-MS (selected ion monitoring) of digested PNA AR5-200 B.**

## 7.3 APPENDIX CHAPTER 5

**PNA characterization:**

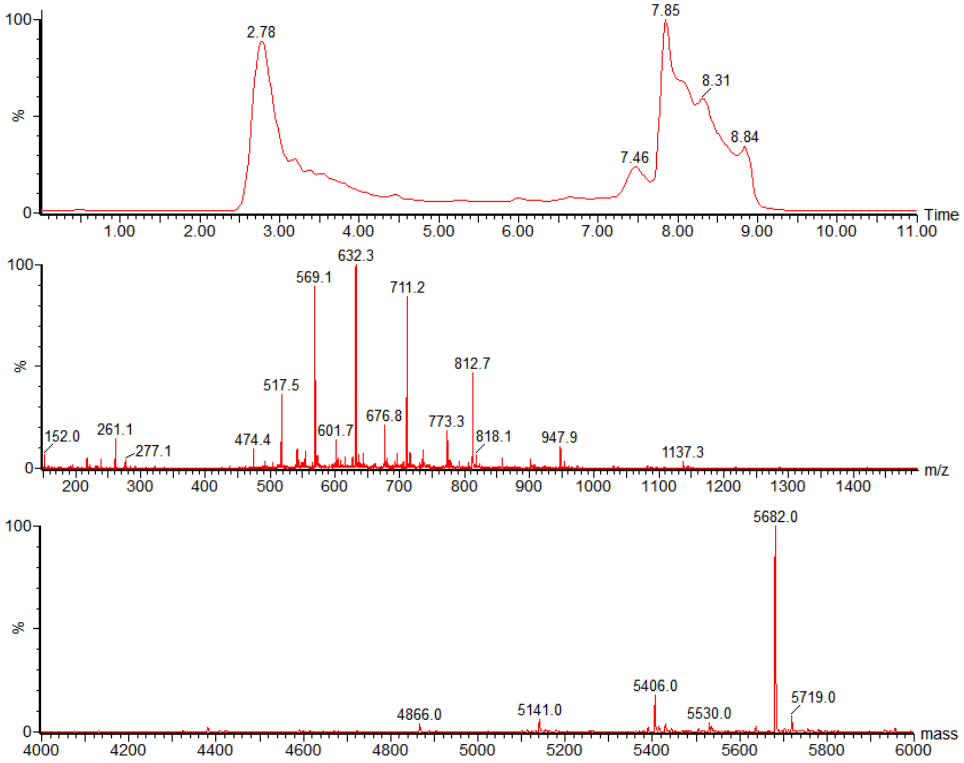


**Figure A57: Chromatogram, mass spectrum and reconstructed mw of PNA CP.**

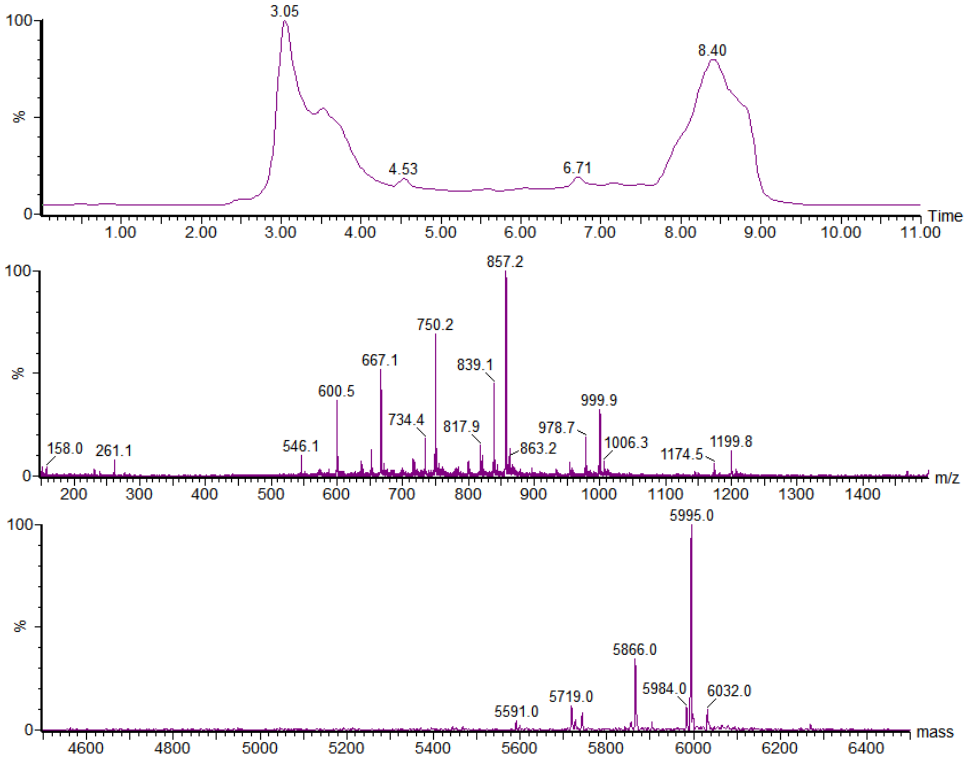


**Figure A58: Chromatogram, mass spectrum and reconstructed mw of PNA SP.**

## 7.4 APPENDIX CHAPTER 6

### Id/Vg curves of not working chips:

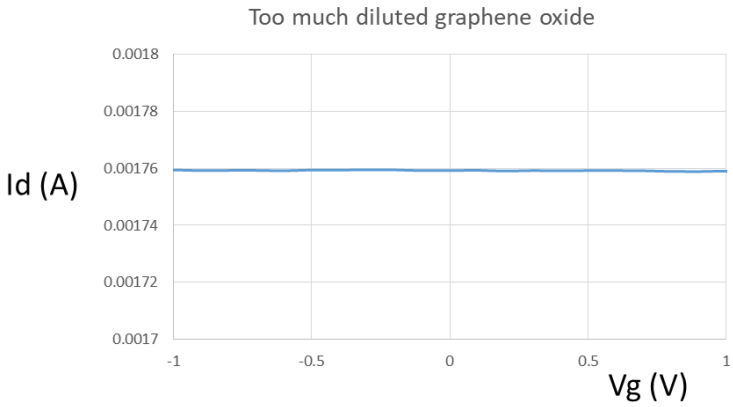


**Figure A59: chip functionalized with 6.25 µg/mL graphene oxide does not show transistor behavior. In this case, the amount of graphene is not enough for cover entirely the source-drain distance and thus these electrodes are not communicant.**

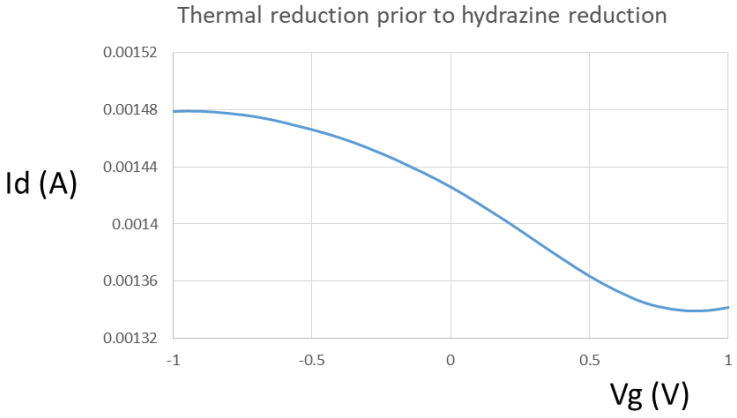


**Figure A60: this chip was annealed before the reduction with hydrazine and does not show transistor behavior.**

**Acknowledgements**

I would like to thanks Prof. Roberto Corradini for giving me the opportunity to became a PhD student and improve my skills as chemist, in the interesting field of PNA. He was always ready to listen and help me when I was in laboratory trouble. I wish to Roberto all the best for his career and scientific discover.
I would like to acknowledge Prof. Wolfgang Knoll for hosting me in Austrian Institute of Technology for six month, and for have thought me enthusiasm in research activity.
Thanks to Prof. Marco Giannetto, for his help and funny moments during PhD; our joint projects are going to been published soon and I am very proud of our efforts.
Thanks to Professors Vincetti and Cucinotta for introducing me in a quite new field, I have discovered that interacts with people with different backgrounds is often difficult, I have to practice a lot.
Finally, to what concern Professors, I would like to thanks all our collaborators in ULTRAPLACAD project, especially Prof. Giuseppe Spoto and Prof. Jurriaan Huskens.

For what concern post-docs, I would like to thanks the person who introduce me in chemistry lab: Dott. Alex Manicardi. During PhD I had several occasion to taught bachelor students and I understood how it is difficult to fully guide a person meanwhile you have to continue your work, so thanks a lot Alex! Other guides at the beginning of my route were Dott. Sasa Korom (congratulation for your marriage!), Dott. Alessandro Bertucci and Dott. Massimiliano Donato Verona, thanks for your advices and encouragements.
Thanks to Dott. Johannes Bintinger, the post-doc that followed me at AIT, always kind and understanding.

For what concern my colleagues, I would like to thanks them all for their help when I was sad, their companionship and for being the best medicine for all troubles: Ema (I am still waiting your painting!), Martina (I leave my beautiful rack to you…), Simone, Mergh, Fra, Mary, briscola masters Spez and Nick, Anna, Orso, Chiara, Vero, Pacio&Chiara, Tiziana, Francesco (best scientist I have ever met), Barbara (thanks for the help with the UPLC-ESI!), Davide, Stefano, Mag, Rispo, Bea, Fede, Andre Monica, Gius, Luke (the force is strong in this man), Marta, Stefania, my nerd friends: Jack, Gio, Silvia, Nico, Fed (my fume hood mate, how many bad adventures??) and his girlfriend Greta. Also

friends that I have met in Vienna: Juan (thanks for taught me SPR, you will be a great professor, otherwise you have a nice plan B…) Stefan, Simone, Seba, Hulan, Nestor (unbeatable team at badminton) and Greca, Valeriia, Paolo, Shabnam, Patrick, Vanessa, Tadija, Agnes, Daria, Jeannette and Andreas. Also thanks to Jacopo Movilli, the man who received most of my PNAs.

For finishing acknowledgement I would like to switch in Italian.

Cari amici, vi ringrazio tanto per il vostro sostegno e l'allegria che mi regalate tutte le volte che sono in vostra compagnia. Per gli amici ex-karateki Gian, Bene, Bonna, Bruno e Sere faccio un inchino e dico:"Oss!". Grazie a Diego, che trova sempre un po' di tempo per scambiare quattro chiacchiere. Un ringraziamento speciale agli amici di una vita Ricky, Torri, Jonus e Walter, che fa parte anche della mia compagnia di amici del venerdì/sabato sera, insieme ad Anto, Jenny, Davide, Carlo e Robby. Rimarrete sempre nel mio cuore e quello che sono è anche grazie a voi.

Grazie a Moni, che mi rincuora sempre quando le cose vanno male e mi fa sentire importante ogni giorno.

Un grazie immenso alla mia famiglia, zii e cugini e nonni, anche se alcuni non ci sono più in questo momento il loro ricordo vivrà sempre in me e i loro insegnamenti continueranno a guidarmi.
Infine il grazie più grande di tutti: ai miei genitori, che mi hanno cresciuto con tutto l'amore che un figlio può desiderare, che è il vero segreto del "successo". Spero un giorno di poter ricambiare anche in parte tutto l'impegno che hanno messo per crescermi e istruirmi.

Un abbraccio forte a tutti!!!